NOTE TO USERS

uOttawa

L'Université canadienne
Canada's university

FACULTÉ DES ÉTUDES SUPÉRIEURES ET POSTOCTORALES

uOttawa

L'Université canadienne
Canada's university

FACULTY OF GRADUATE AND POSDOCTORAL STUDIES

Iana Tsandev
AUTEUR DE LA THÈSE / AUTHOR OF THESIS

M.Sc. (Physics)
GRADE / DEGREE

Department of Physics
FACULTÉ, ÉCOLE, DÉPARTEMENT / FACULTY, SCHOOL, DEPARTMENT

Numerical Study of the Factors Affecting the Cycling of Iron, Sulfur and Phosphorus in Lake Sediments

TITRE DE LA THÈSE / TITLE OF THESIS

I. L'Heureux
DIRECTEUR (DIRECTRICE) DE LA THÈSE / THESIS SUPERVISOR

D. Rancourt
CO-DIRECTEUR (CO-DIRECTRICE) DE LA THÈSE / THESIS CO-SUPERVISOR

EXAMINATEURS (EXAMINATRICES) DE LA THÈSE / THESIS EXAMINERS

B. Joos

R. Hodgson

P. Watson

Gary W. Slater
LE DOYEN DE LA FACULTÉ DES ÉTUDES SUPÉRIEURES ET POSTDOCTORALES /
DEAN OF THE FACULTY OF GRADUATE AND POSTDOCORAL STUDIES

Numerical Study of the Factors Affecting the Cycling of Iron, Sulfur and Phosphorus in Lake Sediments

Iana Tsandev

Thesis submitted to the
Faculty of Graduate and Postdoctoral Studies
In partial fulfilment of the requirements
for the MSc degree in Physics

Department of Physics
Faculty of Science
University of Ottawa

Your file Votre référence
ISBN: 0-494-11434-7
Our file Notre référence
ISBN: 0-494-11434-7

Numerical study of factors affecting the cycling of iron, sulfur and phosphorus in lake sediments

In recent years, reaction transport models have gained importance in the study of diagenesis, which describes the chemical, biological and physical processes that take place in sediments. This project reports on factors influencing chemical profiles in lake sediments through an exploration of a generic reaction transport model which includes representations of the major reactions involved in the cycling of iron, sulfur and phosphorus. We have performed a global sensitivity analysis examining the steady state effects of physical, kinetic and thermodynamic factors on the magnitude, shape and burial concentrations of chemical profiles of iron, sulfur and phosphorus-bearing species. The environmental conditions were varied within a broad range typical of lake sediments. The exploration demonstrates the importance of the nature of boundary conditions (i.e. characteristics of the water column) and their coupling to the water column dynamics. The study additionally points to some chemical mechanisms such as precipitation of vivianite and scavenging of vivianite by sulfide having a dominant influence on the depth profiles of chemical species. Investigation also shows the importance of physical transport processes such as bioturbation near the sediment water interface and sedimentation velocity. Additionally, the distribution of reaction rates with depth and their role in shaping the profiles of chemical concentrations under typical environmental conditions were investigated.

Étude Numérique des Facteurs qui Influencent le Cycle du Fer, du Soufre et du Phosphore dans les Sédiments Lacustres

Dans les années récentes, des modèles de réaction et transport ont accrû en importance dans l'étude de la diagenèse qui décrit les processus chimiques, physiques et biologiques dans les sédiments. Ce projet rend compte des facteurs qui influencent les profils chimiques dans les sédiments des lacs par le bilan exploratoire d'un modèle générique de réactions et transport qui inclut les réactions majeures décrivant les cycles biogéochimiques du fer, du soufre et du phosphore. On a fait une analyse de sensitivité globale afin d'examiner les effets (dans l'état stationnaire) des facteurs physiques, cinétiques et thermodynamiques sur l'ampleur et la forme des profils des espèces chimiques contenant du fer, du phosphore et du soufre ainsi que sur les taux d'enfouissement. Les conditions environnementales furent variées sur une gamme de valeurs typiques pour les sédiments lacustres. Notre exploration démontre l'importance des conditions limites (donc les caractéristiques de la colonne d'eau) et leur couplage à la dynamique de la colonne d'eau sur les profils chimiques. Nous rapportons également que certaines réactions, comme la précipitation de vivianite et la dissolution de vivianite par le sulfure d'hydrogène, ont une influence importante sur les distributions des espèces chimiques. On démontre aussi l'importance des processus de transport physiques comme la bioturbation près de la surface du sédiment et la vitesse de sédimentation. Additionnellement, on discute la distribution des taux de réaction en profondeur

et leur rôle dans l'établissement des profils des espèces chimiques, sous des conditions environnementales typiques.

Statement of originality

Parts of this thesis incorporate the outcome of research undertaken in collaboration with Dr. Sergei Katsev as part of a research project under the supervision of Professors Ivan L'Heureux and Denis Rancourt. The collaboration relates to the generation of data as detailed in the beginning of Chapter 4 of the thesis. The work is based on a software model developed by the LSSE group at the University of Ottawa, with the participation of Dr. Ivan L'Heureux, Dr. Sergei Katsev, Benoit Valiron, Louise Vaillancourt, and myself.

I certify that, with the above qualification, this thesis, and the research to which it refers, i.e. all analysis and conclusions reported, are the product of my own work, and that any ideas or quotations from the work of other people, published or otherwise, are acknowledged in accordance with the standard referencing practice. I acknowledge the helpful guidance and support of my supervisors, Professors Denis Rancourt and Ivan L'Heureux.

The publication by Katsev et. al. (submitted) referenced in this thesis and for which I am a co-author, is a separate work, whose findings are not reported in this thesis. My contribution to that work was in parameter selection, data generation and in discussions as to the interpretation of the results. However, that work is not pertinent to the understanding of this thesis.

Table of Contents:

List of Tables and Figures:

List of symbols:

Alk_c – Carbonate alkalinity
CH4 – Methane : CH_4
cm_{PW} – centimeters of porewater
cm_{DS} – centimeters of dry sediment
cm_{sed} – centimeters of total sediment
FeCO3 – Siderite-calcite : $Fe_xCa_{(1-x)}CO_3$
FeOH3 – Iron oxyhydroxide (ferrihydrite) : $Fe(OH)_3$
FeS – Iron mononsulfide
FeS2 – Pyrite : FeS_2
g_{DS} – grams of dry sediment
MoL – Method of lines
O2 – Oxygen : O_2
ODE – ordinary differential equation
OM – Organic matter
PDE – Partial differential equation
pH – Acidity
φ – porosity = cm^3_{PW}/ cm^3_{sed}
RF – Response function; single value representing a feature of a chemical profile
ρ – grain density of sediment = g_{DS}/ cm^3_{DS}
SIA – Sequential iterative approach
SNIA – Sequential non-iterative approach
SO4 – Sulfate : SO_4
SWI – Sediment water interface
TC – Total aqueous carbon: $[H_2CO_3] + [HCO_3^-] + [CO_3^{2-}]$
TS – Total aqueous sulfur: $[H_2S] + [HS^-]$
Viv – Vivianite : $Fe_3(PO_4)_2$
VODE – An initial value ODE solver (code)
W – Total alkalinity
Z1 – Dissolved and adsorbed iron
ZP – Dissolved and adsorbed phosphate

Introduction

"Controlling the adverse effects of chemicals on the environment requires an understanding of how chemicals behave in the natural world".[1] Investigation of the inner workings of our environment is paramount, firstly in order to increase our knowledge of the world we live in and also for the usefulness of such information in helping maintain homeostasis of the environment in the face of anthropogenic interferences induced by civilization. In the field of sedimentary deposits, the study of the group of processes which occur in sediments is termed diagenesis. As such, diagenesis describes the physical transport, chemical transformations and biological processes occurring in sediments. Much of the study in this field is based on experimental study of real sediments. These studies have yielded a great deal of understanding about what processes occur in sediments, as illustrated in the first chapter. In recent years, however, numerical techniques have gained prominence due to their ability to provide mechanistic explanations to observed geochemical phenomena thus furthering the conceptual understanding of sediment diagenesis. Additionally, modeling allows the exploration of a variety of inputs corresponding to a wide range of environmental conditions for which measurements are difficult or impossible to acquire.

---

[1] McKay Donald, PhD, P.Eng., "Model Behaviour", Engineering Dimensions, p.47-49, 2003.

Early diagenesis refers specifically to the processes occurring in the top centimeters of sediments which corresponds to the last 100 – 1000 years. Fundamental concepts in early sedimentary diagenesis for aqueous systems are summarized by the work of Berner (1980) who represented different diagenetic processes mathematically, such as physical transport processes (diffusion, advection, bioturbation and irrigation) as well as chemical reaction kinetics and precipitation processes, in the framework of reaction transport modeling (RTM). The principle of modeling, across disciplinary fields, is often to describe the time dependence of a variable by solving ordinary or partial differential equations (ODEs or PDEs respectively). For early diagenesis, Berner illustrated how the sum of all processes affecting the evolution of one chemical species in space and time can be described as a partial differential equation for the species concentration. Based on such formulations of sedimentary processes, Boudreau (1996a) considered more complex processes, expanded their mathematical description and explored different methods of solving the resulting PDEs (Boudreau 1996a, Boudreau 1996b).

Reactive transport modeling has been applied in a number of diagenetic processes (Van Cappellen et. al. 1993, Boudreau 1996b). Significant work in the field has been performed by Van Cappellen and Wang (1996) who formulated a multi-component model for early diagenesis coupling the redox cycles of iron and manganese. They expressed the oxidation of organic matter (OM), the oxidation of secondary species produced by the OM degradation, as well as precipitation processes, in addition to the transport processes mentioned above, in order to explain sets of collected data. Other modeling studies have been performed in the context of explaining specific aqueous

environments through calibration with experimental data (Omlin et. al 2001, Fossing et. al. 2004, Manning et. al. 1999, Carrigan and Tessier 1988, Curtis 1989, Froelich et. al. 1979, Furrer and Wherli 1996, Manning et. al. 1991, etc.). Further advancements have been made by Meysman (2001) who elaborated on the coupling between the benthic biology and the geochemistry of sediments. More recently, Aguilera et. al. (2005) have constructed a knowledge based RTM for simulating transport and biogeochemistry of subsurface environments.

Despite the advancement of understanding provided by numerical studies and the usefulness of calibrating results to field data, much is still uncertain about the uniqueness of such results. The uniqueness of a particular solution cannot usually be demonstrated beyond doubt. That is, model parameters can be adjusted to corroborate experimentally measured chemical profiles, but the solution is not exclusive of other possible solutions. Often other combinations of parameters can reproduce statistically equivalent results. Therefore pointing to the exact mechanisms responsible for an observed behaviour, known as identifiability, is difficult (Brun et. al. 2001, Beck 1987). Additionally, what may be significant mechanisms in one environment may not be important in others, leading to unwarranted emphasis of some mechanisms, based on the specifics of the conditions of the calibrating environment. In this context, it is useful to explore the parameter space of a model in its full breadth and observe the range of behaviours (Tromp et. al. 1995, Soetaert et. al. 1996). This allows one to point out which parameters (and their corresponding environmental factors) play significant roles in shaping chemical profiles across the parameters' observed ranges of values. Global sensitivity

analysis (Saltelli 1999), which is what such a scan would amount to, is necessary in order to extract what mechanisms or factors have an universal impact on chemical profiles for a wide range of environments.

Also, given the complexity and diversity of lake environments, the breadth of their chemical and biological characteristics and their physical parameter, diagenesis describes a multifaceted system of interacting components. The basic properties and effects of physical mechanisms on chemical profiles can easily be lost in the complex web of interactions that constitutes a "black box". In a system of so many variables, it is useful to take a reductionist approach, striping away redundancies in the chemical and transport processes, in order to look at individual mechanisms in a more isolated setting. This kind of description allows an understanding of the characteristics of the components of the system before observing how they integrate into a larger and more realistic model, with more intricacies and dependencies. Such understanding of the system building blocks and their influences is useful in constructing a qualitative understanding of diagenesis, that can guide both further model development and field and laboratory interpretations.

This project looks at a model of early diagenesis in lake sediments. It uses a global sensitivity analysis to look at the question of identifying which parameters in a generic early diagenetic RTM have influence over the chemical range of variability, as reported in the literature. Therefore we look for universal behaviour across many simulated environments by compiling a large statistical set of numerical results corresponding to these environments. Given the resulting system complexity, as explained earlier, and the size of the data set, statistical methods, outlined later in the thesis, are necessary to

untangle the data. This study focuses on the shape of chemical depth profiles for a variety of species related to the cycles of iron, sulfur and phosphorus. We use factorial analysis along with individual tests to ascertain the role of boundary conditions, transport parameters, reactions rates and other factors on the distribution of chemical species throughout the depth of sediment. This thesis reports on those results and some conclusions which can be drawn from the results.

The text is organized into five chapters. The first chapter introduces a summary of principal and peripheral chemical and physical mechanisms known to occur in lake sediments as reported in the literature. It also introduces the reactions which are incorporated into the model. The second chapter, outlines the general principles used in RTM and some strategies for solving the resulting PDEs. Chapter 3 gives details on the particular model used for this study, as well as the range of variation of its parameters. Chapter 4 describes the systematic scan in parameter space using a factorial analysis (Montgomery 1997) and reports on the emerging important factors. Chapter 5 reports on some further testing, which was motivated by the factorial analysis, aimed at identifying mechanisms responsible for typical profile shapes. Finally some concluding remarks summarize the findings of the thesis.

Chapter 1

Lake Sediment Diagenesis Overview

The following chapter is an introductory-level overview of biogeochemical processes which are believed to occur in lake sediments. It is meant to elucidate what chemical and physical processes that diagenetic models describe. The next chapter will, in turn, outline how partial differential equations (PDEs) describe diagenetic phenomena. This summary is organized by chemical species/groups but is not exhaustive. This text emphasizes a set of reactions deemed important to lacustrine environments in particular. Therefore, it may overlook some significant cycles and/or mechanisms, particularly if they are characteristic of other types of aquatic environments, such as marine sediments (ex: the nitrogen cycle). Additionally, there are many complex reactions in aquatic environments which are traditionally omitted by diagenesis modelers, because they are expected to have little impact on the environment or to have no significant interaction with the environment except in some specific cases (ex: clay minerals, trace metals).

The numerical model used for this thesis includes the minimal set of reactions for the cycles of iron, sulfur and phosphorus, according to present knowledge. The chemical

system studied by our numerical model is referenced throughout in the context of this general narrative. All the reactions included in the model are listed below, in their exact stoichiometric form, where they illustrate the corresponding diagenetic process. Many of the reactions given below will be summarized again, in Chapter 3, within the specifics of the numerical model. However, not all concepts detailed herein are illustrated by reaction expressions. This is because our numerical model is not a comprehensive realization of all realistic lake geochemistry, but rather, as mentioned above, the minimal subset of possible reactions.

1.1 Lake Characteristics

Before trying to define some characteristics of lake environments and the chemical reactions they host, it is important to recognize their diversity (Kalff 2002, Wetzel 1983). Unlike marine systems, which are more stagnant bodies of water, lakes are shallower (Lerman et. al. 1978). Their dynamical response time scale is shorter and they may exhibit greater seasonal variations. This difference is exemplified in the typical mixing times (Kalff 2002) τ_w defined as the ratio of basin volume (m^3) to the average annual water outflow (m^3/yr), which are tens of years for lacustrine environments as opposed to thousands of years for marine systems (Wetzel 1983). This makes describing lakes difficult as they are influenced by many variables such as water depth, surrounding soil and vegetation, mixing effects and many more (Talbot and Allen 1996, Lerman 1978). Lacustrine environments therefore typically exhibit pronounced seasonal variation and various biogeochemical processes from one lake to another, or even within different sites

in the same lake (Talbot and Allen 1996, Lerman 1978). Universal behaviors, are consequently difficult to discern due to the complexity of the ecological lake system.

The following are some important concepts for lakes, as they help in understanding the cycling of nutrients and other chemicals (Wetzel 1983, Langmuir 1997, Lerman 1978). The upper section of a lake's watercolumn is its epilimnion. It is a highly dynamic layer, subjected to wind-induced turbulent mixing and intense biotic activity. The deeper section of the water column, the hypolimnion, depending on lake depth and biota, may have significantly reduced light penetration (Kalff 2002). The temperature of water may vary throughout the depth of a lake. For example in summer the upper layers of lakes are warmer. This temperature difference induces a stratification based on the difference in the water density between the layers (Wetzel 1983, Kalff 2002). The region delineating the warm regions from the cold layers is called the thermocline. Another important characteristic of the water column is its oxygen content[1]. Lakes can have completely oxygenated water columns, but oxygen may also be consumed within a certain water depth and the lake may exhibit an oxygen stratification, with an oxic (oxygen rich) epilimnion and an anoxic (oxygen poor) hypolimnion. The depth delineating these areas is called the oxycline. Some lakes remain permanently in this stratified state; others turn over periodically throughout the year re-oxygenating the water column. This turnover is usually seasonal as it is related to temperature changes which affect the density of water. Thus mixing occurs in transitional seasons such as fall (in the case of summer stratification) or spring (in the case of winter stratification) when water densities of upper

[1] These and other lake characteristics are introduced in a useful website which summarizes them in the context of lake Washington : http://www.ecy.wa.gov/programs/wq/plants/lakes/characteristics.html

and lower layers are equalized making the whole water column subject to wind mixing (Wetzel and Likens 2000).

The nature of the water column has a significant effect on the underlying sediment. The activity of the water column can influence the amount of oxygen getting to the bottom as well as how much material, organic and inorganic, reaches the sediment. Sediments, in turn, affect the chemistry of the water column because material from the mud[2] can re-suspend into the water.

The boundary between the water body and underlying sediment is termed the sediment water interface (SWI). In reality, the SWI is a fluid, poorly defined region of suspended material of increasing density and realistically is best represented by a region of depth with varying porosity. However, for the purposes of our model and this text it will be treated as simple straight line demarking water from mud[2].

1.2 Chemical Processes

The evolution of sediments deposited in aqueous environments is called diagenesis. The term diagenesis refers to the sum of all physical, chemical, and biological processes that take place in sediments (Berner 1970). It describes the transformation of chemical species as they get buried into the mud. In order to qualify or quantify lake sediment behavior it is important to identify what sediment species and which transitional forms are pertinent

[2] Here and henceforth the term mud is used as a synonym for sediment with low permeability. In the context of this text they will be used interchangeably.

to the lake activity. Those considered most important and studied most widely are: organic matter, oxygen, iron, manganese, phosphates, nitrates, sulfides, pH ([H+]), carbonates, trace metals, ammonia, and methane (Katsev et. al. 2004, Wetzel 1983, Langmuir 1997, Lerman 1978, Kalff 2002). Their chemical cycles are intimately linked and one can rarely be described without reference to most of the other species. In particular, iron and sulfur, due to their abundance and high reactivity, are key players in most relevant diagenetic reactions.

1.2.1 Organic matter

Organic matter (OM) is a central participant in biogeochemical cycles, as it is a source of nutrients, such as phosphates and nitrates, that get incorporated into organic material, as well as a source of energy for organisms. OM is a mixture of lipids, carbohydrates, proteins and other biochemicals originating in benthic plants and organisms (Lerman 1978) and, depending on its form, will be more or less resistant to degradation. OM is broken down through reactions which are biologically mediated; that is, degradation occurs through bacterial respiration or fermentation[3]. If oxygen is present, it will be the predominant oxidizing agent according to:

$$(CH_2O)_x(NH_3)_y(H_3PO_4)_z + (x+2y)O_2 \xrightarrow{RO_2} xCO_2 + yHNO_3 + zH_3PO_4 + (x+y)H_2O \quad \textbf{(1.1)}$$

[3] These processes are also called mineralization.

Here the first term on the left hand side represents organic matter. Once oxygen is depleted, a series of alternative electron acceptors may act. They are hierarchically listed in order of competitiveness, which is based on the thermodynamic energy yield of the reaction (see Fig 1.1). However, these reactions are not necessarily mutually exclusive. For example the regions where denitrification and iron reduction occur may overlap depending partly on the availability of material or bacterial populations and species. Once oxygen is depleted, and in the presence of nitrate, organic matter (OM) is oxidized to CO_2 and water

$$(CH_2O)_x(NH_3)_y(H_3PO_4)_z + \frac{4}{5}xNO_3^- \xrightarrow{RNO_3} \frac{x}{5}CO_2 + \frac{4}{5}xHCO_3^- + \frac{2}{5}xN_2 + yNH_3 + zH_3PO_4 + \frac{3}{5}xH_2O \quad \textbf{(1.2)}$$

Manganese or iron oxides can also act as electron acceptors

$$(CH_2O)_x(NH_3)_y(H_3PO_4)_z + 2xMnO_2 + 3xCO_2 + xH_2O \xrightarrow{RMnO_3} 4xHCO_3^- + 2xMn^{2+} + yNH_3 + zH_3PO_4 \quad \textbf{(1.3)}$$

$$(CH_2O)_x(NH_3)_y(H_3PO_4)_z + 4xFe(OH)_3 + 7xCO_2 \xrightarrow{RFe(OH)_3} 8xHCO_3^- + 4xFe^{2+} + yNH_3 + zH_3PO_4 + 3xH_2O \quad \textbf{(1.4)}$$

Sulfate can also oxidize organic matter through the reduction process

$$(CH_2O)_x(NH_3)_y(H_3PO_4)_z + \frac{x}{2}SO_4^{2-} \xrightarrow{RSO_4} xHCO_3^- + \frac{x}{2}H_2S + yNH_3 + zH_3PO_4 \quad \textbf{(1.5)}$$

Finally, if no electron acceptors are present OM simply ferments producing methane gas, a process known as methanogenesis

$$(CH_2O)_x(NH_3)_y(H_3PO_4)_z \xrightarrow{RCH_4} \frac{x}{2}CO_2 + \frac{x}{2}CH_4 + yNH_3 + zH_3PO_4 \cdot \quad \textbf{(1.6)}$$

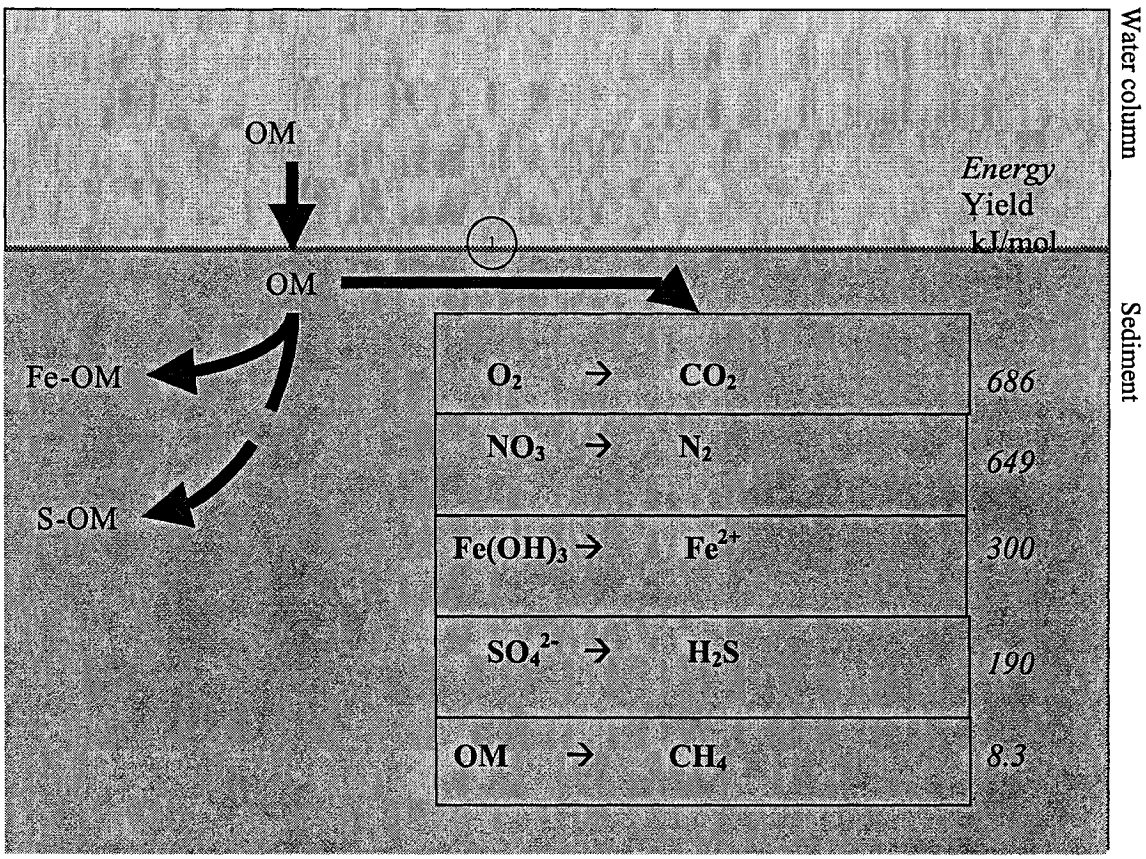

Figure 1.1 – Respiration pathways in sediments. The reactions are listed by hierarchical order with respect to depth: aerobic respiration, followed by denitrification, iron reduction, sulphate reduction, methanogenesis. Organic matter may persist at depth binding sulphur and iron (symbolized by S-OM, F-OM respectively).

Clearly, form the above reactions, the susceptibility of organic matter to degradation will significantly affect the chemistry of sediments. OM which is stable to microbial degradation will carry other chemical species, such as phosphate and nitrate deeper into the sediment, thus affecting their profiles. Additionally, both sulfides (Rudd 1986, King 1982) and iron oxyhydroxides (Laskov et. al. 2002, Santana-Casiano et. al. 2000, Lerman 1995) can complex to organic matter and get buried with it, affecting those profiles as well. Such organic matter complexes are generally more resistant to mineralization reactions.

1.2.2 Oxygen

As pointed out above, oxygen is a very important component of the OM degradation pathways. Its presence enables certain bacterial populations and biota to thrive, since oxygen is essential for the sustenance of many life forms. In fact the majority of O_2 consumption is through the primary respiration reaction (1.1). However, oxygen can also act as an electron acceptor in other reactions and is thus significant because it determines the oxidation states of many chemical species. For example, in the oxic layer of sediment, iron and manganese are favoured in their oxidized valence states (3+ and 4+ respectively). Reduced iron or manganese, whether in solution or adsorbed to a solid, will precipitate as an oxide or oxyhydroxide. Thus manganese oxides (MnO_2) and iron oxyhydroxides (denoted here as ferrihydrite - $Fe(OH)_3$) can exist with various chemical formulas and morphologies.

$$4Fe^{2+} + O_2 + 8HCO_3^- + 2H_2O \xrightarrow{RFeOX} 4Fe(OH)_3 + 8CO_2 \quad , \qquad \textbf{(1.7)}$$

$$4S \equiv Fe^{+} + O_2 + 4HCO_3^- + 6H_2O \xrightarrow{RsurFe} 4S \equiv H^0 + 4Fe(OH)_3 + 4CO_2 \ , \qquad \textbf{(1.8)}$$

$$2Mn^{2+} + O_2 + 4HCO_3^- \xrightarrow{RMnOX} 2MnO_2 + 4CO_2 + 2H_2O \quad , \qquad \textbf{(1.9)}$$

$$2S \equiv Mn^{+} + O_2 + 4HCO_3^- \xrightarrow{RsurMn} 2S \equiv H^0 + 2MnO_2 + 2CO_2 \ . \qquad \textbf{(1.10)}$$

In reactions 8 and 10 the S≡ refers to the solid surface site onto which the ion is adsorbed (the triple line differentiates an adsorptive connection from an ionic or covalent bond). Oxygen will also oxidize sulfide in solution

$$H_2S + 2O_2 + 2HCO_3^- \xrightarrow{RSOX} SO_4^{2-} + 2CO_2 + 2H_2O \ . \qquad \textbf{(1.11)}$$

It can also dissolve some more soluble reduced iron phases such as iron monosulfides,

$$FeS + 2O_2 \xrightarrow{RFeSOX} Fe^{2+} + SO_4^{2-} \ , \qquad \textbf{(1.12)}$$

and in turn re-precipitate the iron as an oxyhydroxide (reaction 1.7). Thus oxygen is an important regulator of the chemistry of other species. If any oxygen is allowed to the bottom of the water column of a lake, as in the case of shallow and mixed lakes, it will

typically get consumed, primarily through respiration, in the top few millimeters of the sediments. Thus sediments are for the most part anaerobic and reducing environments, and the redox reactions listed above are confined to a thin layer at the top of the sediment.

1.2.3 Redox active metals (Fe, Mn)

Iron and manganese are influential elements in lake sediments because of their high reactivity which is due to their flexible valence states and propensity for reduction/oxidation (redox) reactions. Though their behaviors are similar, the more abundant of the two is iron (Loveley 1987). If the water column is oxygenated, iron arrives at the sediment water interface (SWI) in part (though not exclusively) in the form of oxyhydroxides or complexed to organic mater. Once inside the reducing environment of the sediment, iron and manganese oxides are no longer thermodynamically favored. Iron oxyhydroxides are gradually dissolved; however, because the dissolution process is controlled by kinetics, it can be slow: iron oxyhydroxides may persist at significant depth inside certain sediments. Microbial reduction, illustrated by reaction 4 as one of the respiration pathways, is the predominant mechanism for iron reduction, but chemical abiotic reduction has also been identified (Pyzik 1981, Haese 2000), such as sulfide-induced dissolution

$$2Fe(OH)_3 + H_2S + 4CO_2 \xrightarrow{RsFe3} 2Fe^{2+} + S^0 + 4HCO_3^- + 2H_2O \quad . \qquad \textbf{(1.13)}$$

Iron oxide reduction has the effect of releasing ferrous iron (Fe^{2+}) into the porewaters of sediments. The aqueous iron can then diffuse back into the water column to be reoxidized (reaction 1.7). Other anaerobic oxidation pathways have been found (Haese 2000) though these are believed to be less significant contributors to iron oxidation.

The ferrous ion can then react with other surrounding ions to precipitate various iron-bearing solid phases. Combined with sulfide it can form iron monosulfide

$$Fe^{2+} + HCO_3^- + HS^- \xleftrightarrow{RFeS/RFeS'} FeS + CO_2 + H_2O \quad . \qquad \textbf{(1.14)}$$

This is postulated to be the preferential precipitation pathway (Rudd et. al. 1986; Davison et. al. 1985; Hupfer et. al. 1998; Murray 1995), largely due to its fast kinetics. Alternatively, combined with phosphate ions, iron forms iron phosphates such as vivianite:

$$3Fe^{2+} + 2H_3PO_4 + 8H_2O \xleftrightarrow{Rviv/Rviv'} Fe_3(PO_4)_2 * 8H_2O + 6H^+ \quad . \qquad \textbf{(1.15)}$$

For example, combined with carbonate species (and calcium), it can precipitate minerals of the siderite-calcite ($FeCO_3 - CaCO_3$) series

$$xFe^{2+} + (1-x)Ca^{2+} + 2HCO_3^- \xleftrightarrow{RFeCO3/RFeCO3'} Fe_xCa_{1-x}CO_3 + CO_2 + H_2O \; . \qquad \textbf{(1.16)}$$

However, though the above precipitation reactions are thermodynamically possible they may not always significantly occur (Wersin et. al. 1991; Hupfer et. al. 1998; Emerson 1985): the kinetics of the reaction may be too slow.

The previously mentioned iron compounds may also rearrange into other iron-bearing phases. In the presence of sulfide, which is a highly competitive reactant for iron, vivianite can reform into monosulfide

$$Fe_3(PO_4)_2 + 3H_2S \xrightarrow{Rsviv} 3FeS + 2H_3PO_4 \quad . \qquad \textbf{(1.17)}$$

Similarly, siderite can form monosulfide as well

$$FeCO_3 + H_2S \xrightarrow{Rsviv} FeS + CO_2 + H_2O \quad . \qquad \textbf{(1.18)}$$

If it does not precipitate, aqueous iron and manganese may complex to solids (including iron oxides and OM) by adsorption

$$S \equiv H^0 + Fe^{2+} + HCO_3^- \longleftrightarrow S \equiv Fe^+ + CO_2 + H_2O \quad , \qquad \textbf{(1.19)}$$

$$S \equiv H^0 + Mn^{2+} + HCO_3^- \longleftrightarrow S \equiv Mn^+ + CO_2 + H_2O \qquad \textbf{(1.20)}$$

(Van Cappellen and Wang 1996).

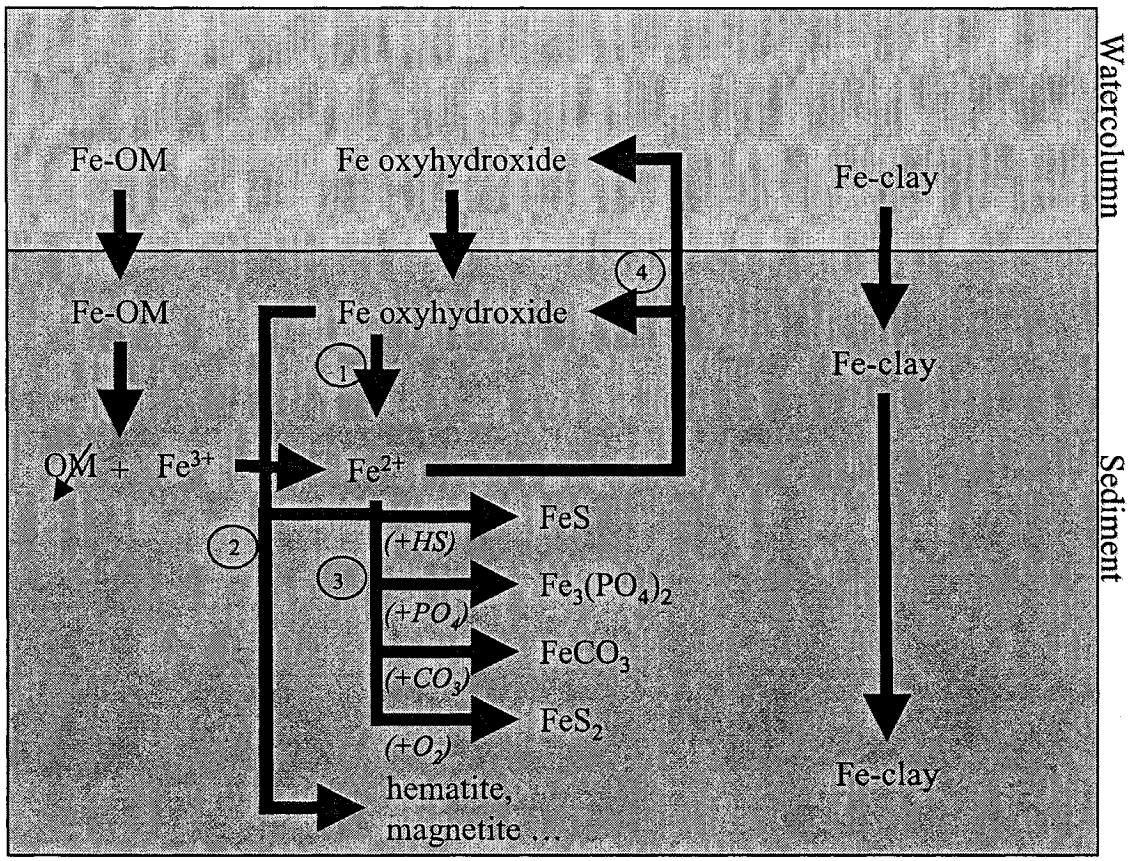

Figure 1.2 - Diagenetic iron transformation pathways in sediment. (1) reductive dissolution, (2) aging, (3) precipitation and (4) oxidation. Fe-OM refers to iron hydroxides complexed to organic matter such as humic substances.

Besides the reactivity of reduced iron detailed previously, ferrihydrite-like oxides which persist inside sediments can rearrange into other more stable phases such as hematite (Fe_2O_3), goethite (α-FeOOH), magnetite (Fe_3O_4), lepidocrocite (γ-FeOOH). The mechanisms are many, from internal bacterially mediated aggregation, to dissolution and re-precipitation, to spin rearrangement (Konhauser 1998, Hansel 2003). Iron monosulfide can also redissolve anoxically through interaction with iron oxides

$$2Fe(OH)_3 + FeS + 6CO_2 \xrightarrow{RFeSFe3} 3Fe^{2+} + S^0 + 6HCO_3^- \quad . \qquad (1.21)$$

Additionally, some iron arrives to the sediment incorporated into clay minerals. This fraction of iron may be buried without transforming. A summary of the diagenetic pathways of iron and iron-bearing compounds is illustrated in Figure 1.2.

1.2.4 Phosphorus

Phosphorus is an essential nutrient for life sustenance. In lakes, phosphates (H_3PO_4) are far less abundant than nitrates (NO_3^-), another major aquatic nutrient; phosphorus is thus most often the growth limiting nutrient. However, in excess abundance, such as that caused by anthropogenic effects, it can lead to eutrophication – a water condition in which high nutrient concentrations stimulate the growth of algae, cutting off sunlight to deeper parts of the lake and leading to a high oxygen consumption.

Phosphorus arrives to the water column and sediment in a variety of fashions, such as dead organic material, run-off, inflow from other lakes, dissolving minerals etc. Organic matter decomposition releases phosphate through any of the mineralisation pathways previously outlined (reactions 1.1,1.2,1.3,1.4,1.5,1.6). In the presence of iron oxides or other minerals, phosphate may adsorb onto the surface of solid phases

$$H_3PO_4 \longleftrightarrow H_3PO_4(ads) \quad . \qquad (1.22)$$

Adsorption is governed by the pH conditions of the water column or sediment porewater, as well as the availability of surface binding sites on minerals as will be seen in the following chapter. Availability of competing ions in the porewater will also play a role in phosphate adsorption. Also, aqueous phosphate can co-precipitate with iron in the form of vivianite as shown in reaction 1.15.

In the presence of sulfide, however, iron phosphate interactions are outcompeted by hydrogen sulfide. Roden and Edmonds (1997) ruled out adsorption competition between phosphate (PO_4^{3-}) and sulfate (SO_4^{2-}) ions. They found that hydrogen sulfide could dissolve both amorphous and crystalline iron-bearing solids (reactions 1.13,1.17,1.18) to form iron sulfides. Thus, in the presence of sulfur, orthophosphate (H_3PO_4) is released into the porewater by the dissolution of phosphate adsorbing or phosphate carrying iron minerals. The phosphorus cycle is outlined in Figure 1.3.

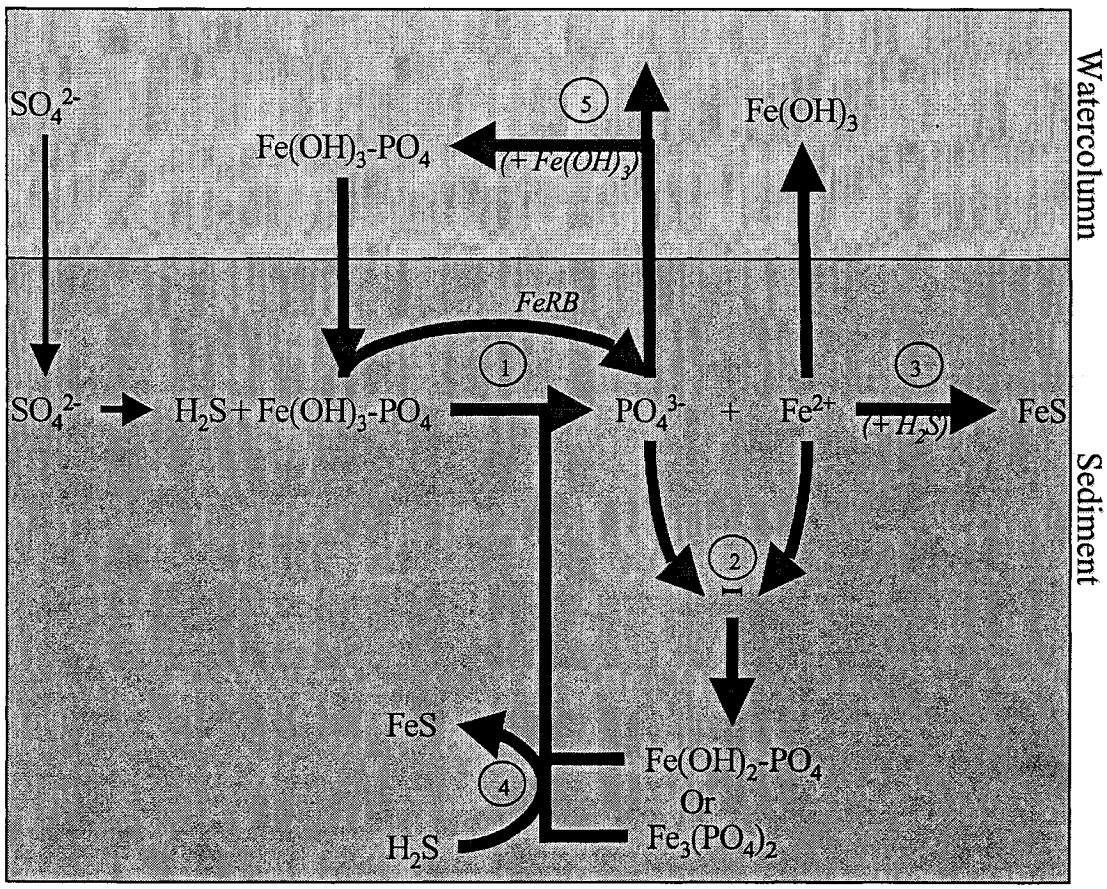

Figure 1.3 - Diagenetic pathways of phosphorus in sediments. The main interactions are (1) reduction of ferric hydoxide phosphate complexes (FeRB designates iron reducing bacteria), (2) re-precipitation of ferrous iron with phosphate, (3) iron sulfide precipitation, (4) redissolution of ferrous phosphate complexes coupled to iron monosulfide precipitation, (5) diffusion of phosphate up to the watercolumn.

Based on Roden and Edmonds (1997)

1.2.5 Sulfur

Sulfur is a very abundant element - the sixth most abundant in biomass (Urban 1994) - a nutrient for microorganisms, and highly reactive in its reduced form. It either arrives to the water column as sulfate (SO_4^{2-}) or is oxidized to that form (reaction 1.11) which is the favored state under oxic conditions. It is relatively inert in its oxidized form, but gets

uptaken by organisms which then die and deposit onto the sediment. In reducing environments, sulfate (SO_4^{2-}) is reduced to sulfide (H_2S) according to reaction 1.5 . Other OM mineralization reactions (1.1,1.2,1.3,1.4,1.6) will also free any sulfide that is complexed to the depositing organic matter (Nedwell 1982). Once H_2S is released into porewater, it will preferentially react with iron or iron-bearing species to form iron monosulfide (Berner 1970; Davison 1993; Banstra 2000; Murray 1995; Hupfer 1998). Reactions 1.14, 1.17 and 1.18 are examples. Through aging, iron monosulfide will then form pyrite (FeS_2):

$$FeS + H_2S \xrightarrow{RFeSHS} FeS_2 + H_2 \ . \qquad \textbf{(1.23)}$$

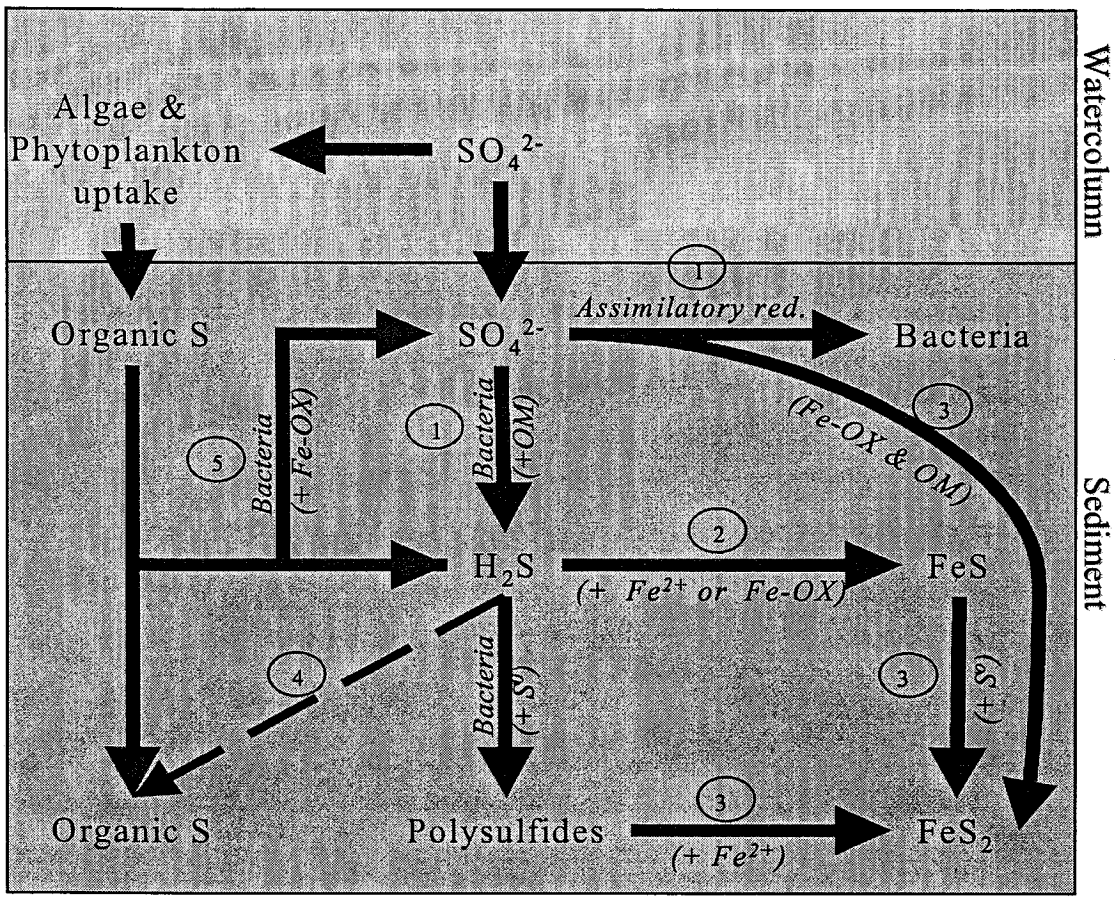

Figure 1.4 - Diagenetic pathways of sulfur in sediment. The main reactions categories are (1) reduction (dissimulatory or assimilatory), (2) iron monosulphide formation, (3) pyrite formation, (4) organo-sulphur compound formation, (5) oxidation of sulphide. All reaction pathways, except reduction and organic complexation, involve iron, and are influenced by the presence of iron due to competition.

There are several other proposed mechanisms for pyrite formation besides R_{FeSHS}, such as direct formation from aqueous iron (Davison 1985) or polysulfides (Urban 1994) or elemental sulfur (Morse 1999). Unreacted sulfide may re-diffuse up to the water column and re-oxidize there (reaction 1.11).

The other notable interaction of sulfide is that with organic matter, particularly in acidified lakes where organo-sulfur compounds form as either carbon-bonded sulfurs (R-C-SH)[4] or sulfate esters ($R\text{-}OSO_3^-$) (Rudd 1986). These complexes are resistant to degradation and help store sulfur and preserve organic matter in the sediment. The sulfur cycle, illustrated here in Figure 1.4, is an important player in the cycles of other elements.

1.2.6 Alkalinity (pH, carbonates)

The acidity/alkalinity of a lake and its associated sediments is a fundamental variable defining the state of the geochemical system. It influences the likelihood and rate of most chemical reactions, complex formations, adsorption and precipitation/dissolution. The acidity of a lake, however, is also a direct result of the reactions taking place as is it defined by the amount of acidic or alkaline species produced or consumed during diagenesis in the sediment. "More precisely, the pH is determined by the extent of dissociation of the dissolved carbonic acid , and other weak acids such as water, whose net negative charge (HCO_3^-, CO_3^{2-}, OH^-) has to balance exactly the net positive charge from the strong mineral bases (Na^+, K^+, Ca^{2+})" (Morel 1993). In dealing with the acidity due to weak acids/bases in natural waters, one deals primarily with the carbonate system because of the high abundance of carbon dioxide (CO_2). CO_2 is generated either by carbonate rock dissolutions (reaction 1.18), diffusion of atmospheric CO_2 into the water column or respiration processes (reactions 1.1,1.2,1.3,1.4,1.5,1.6). The dissociation of carbonic acid ($H_2CO_3 = CO_2 + H_2O$) is described by:

[4] The symbol R refers to an arbitrary carbohydrate chain.

$$CO_2 + H_2O \longleftrightarrow HCO_3^- + H^+$$
$$HCO_3^- \longleftrightarrow CO_3^{2-} + H^+$$

The concentrations of the various carbonate species varies according to the pH (Figure 1.5).

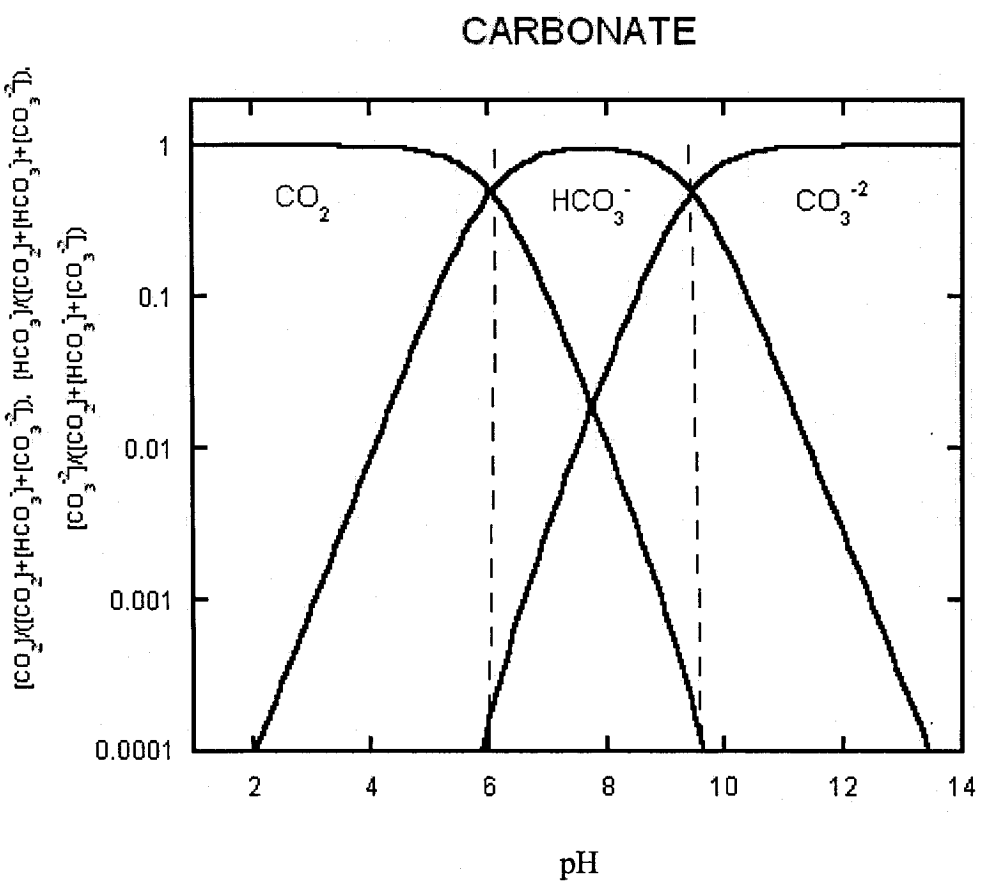

a)

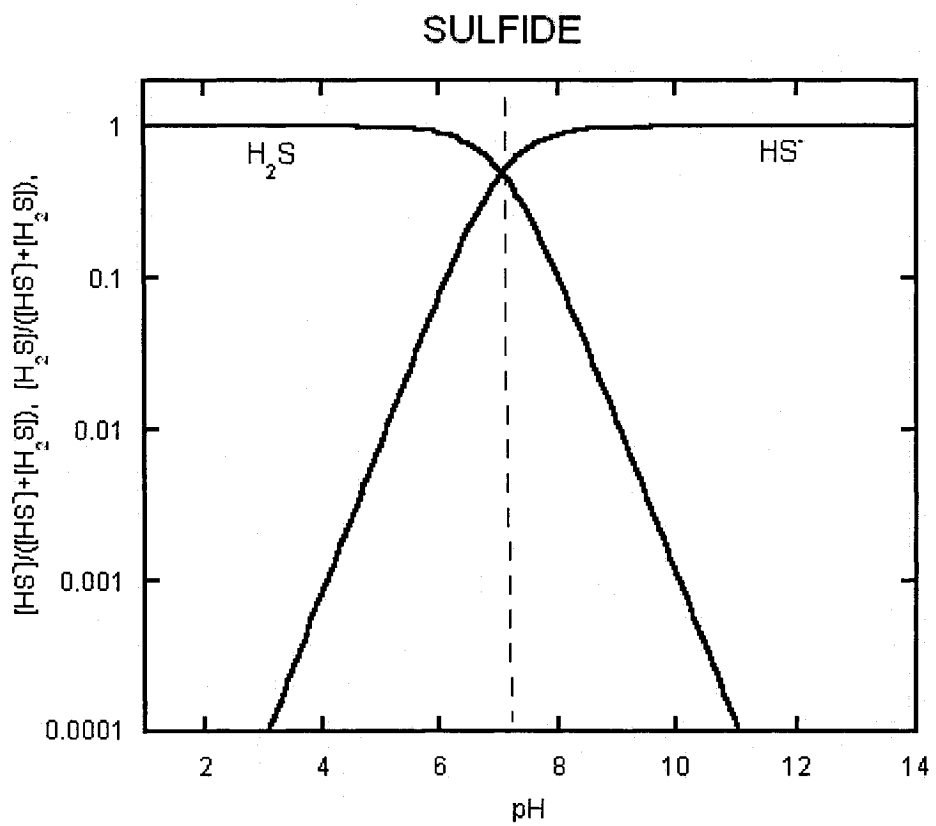

b)

Figure 1.5 Speciation curves for a) carbonate and b) sulfide. Plot of the ratio species/concentration/total carbonate or total sulfide vs. pH at 20^0C. The vertical lines define the pH regimes where a given species dominates over the others.

Other weak acids are silicates, ammonia, phosphates, borates, sulfides, and water itself; for example:

$$H_2S \longleftrightarrow HS^- + H^+$$

$$H_2O \longleftrightarrow OH^- + H^+$$

The pH of pore water is therefore the result of a delicate interplay between input and output of acidic/alkaline species and their ionic dissociations inside the sediment environment.

1.3 Sample Profiles

In order to help orient the reader in the scale, nature and variability of chemical behavior one might observe, some sample profiles, included herein, were extracted from literature to illustrate possible behaviors observed in the natural environment, particularly lake sediments or the like (see Figure 1.6).

These illustrations are, however, not to be taken as an exhaustive set of examples of lake chemistry characteristics. There is tremendous variation in chemical behavior in lake sediments, which a few sample profiles cannot possibly document, and it is difficult to identify typical profiles for that reason. The following, however, can provide a useful idea of expected behavior.

Figure 1.6 - Illustrations of sample chemical profiles of organic matter, iron, sulfur and phosphorus in the sediments of lakes and other dynamic water bodies, as reported in the literature. Please note that the following profiles by no means cover the range of observed behavior in lakes. Chemical species profiles can vary greatly, in both shape and scale, from one environment to the next.

a)

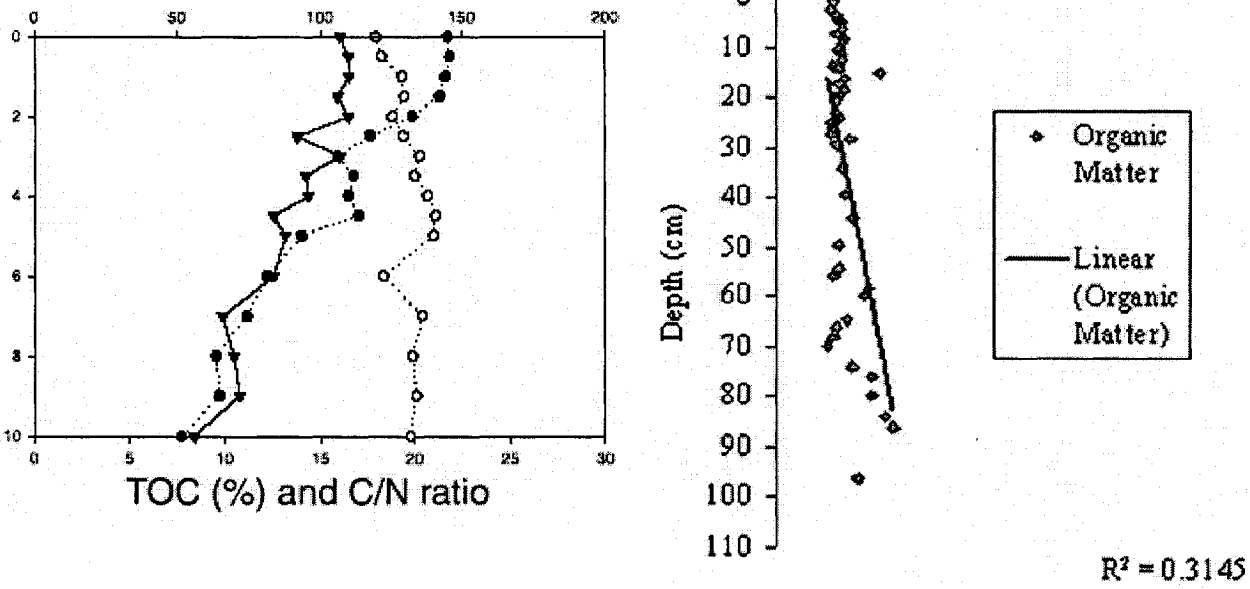

i) ii)

a) Organic matter profiles: i) Total organic carbon concentrations (TOC (%); solid circles with broken line) with depth (Kainz et. al. 2003) and ii) variation of organic matter (by weight percent) with depth (Bharmal and Laurent 2004).

b)

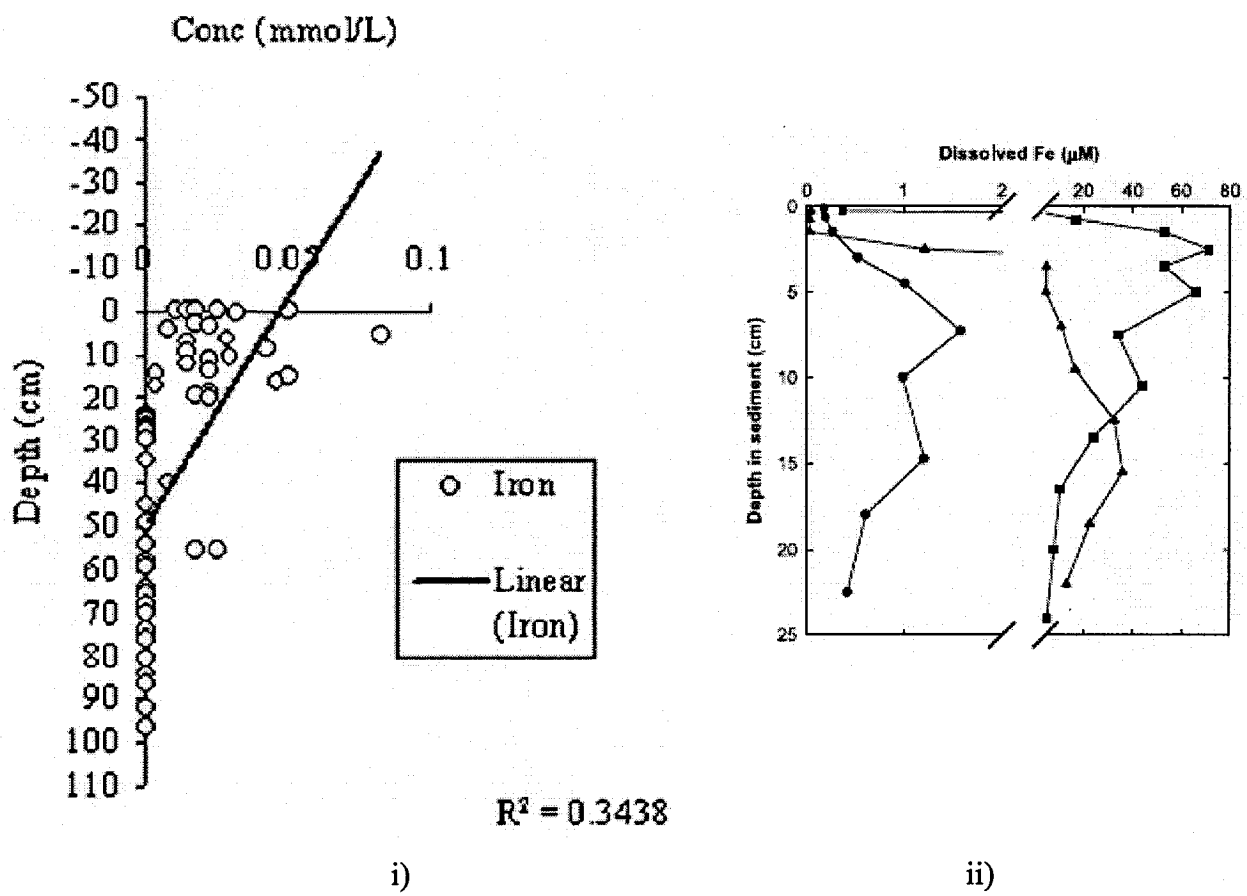

i) ii)

b) Iron profiles: i)Variation of pore water iron with depth (Bharmal and Laurent 2004) and ii) dissolved iron in pore-waters of shelf (Elrod et. al. 2004)

c)

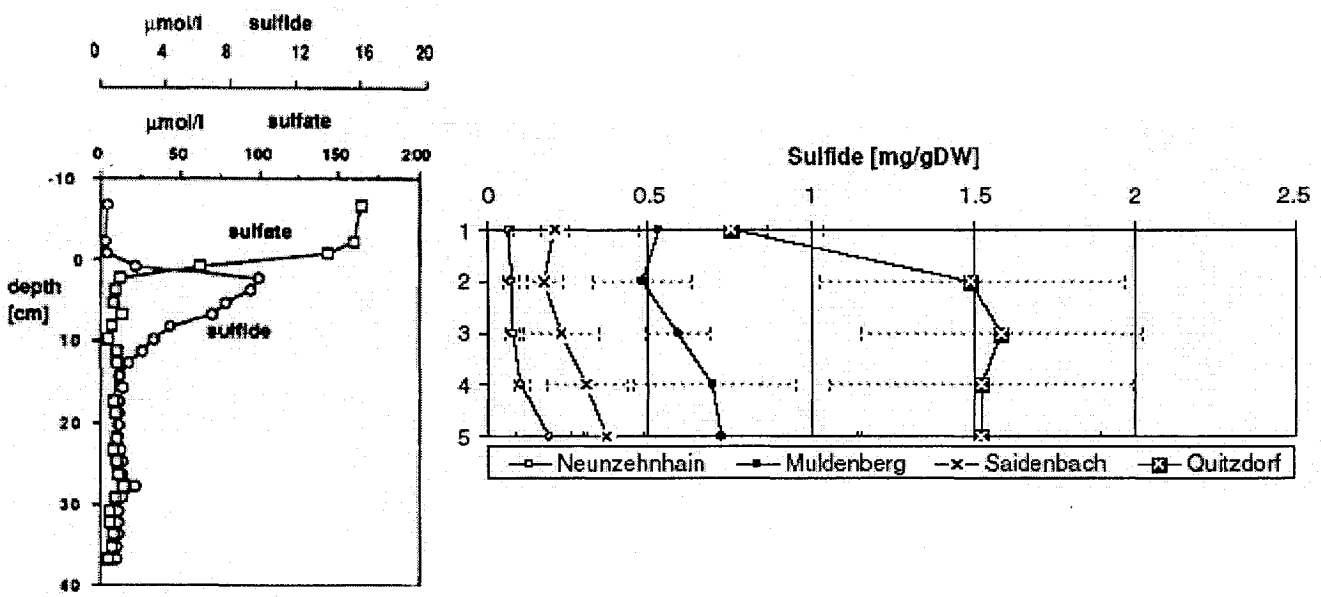

i) ii)

c) Sulfur profiles: i) Sulfate (squares) and sulfide (circles) concentrations with depth (Wersin et. at. 1991) and ii) sulfide concentration in the sediment of a reservoir (Maassen et. al. 2005)

d)

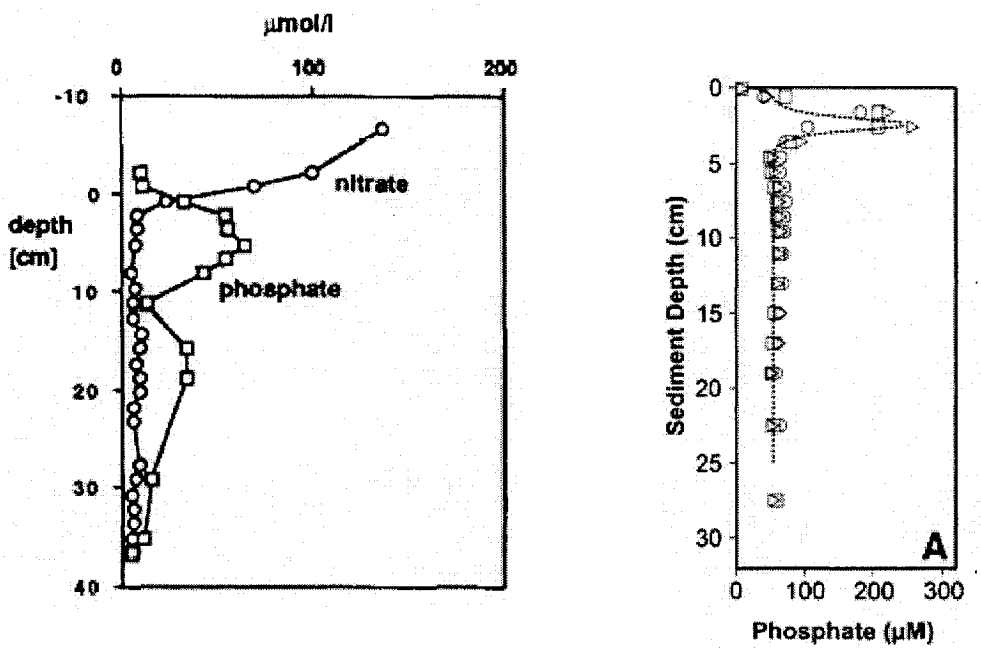

i) ii)

d) Phosphorus profiles: i) Interstitial water concentrations of phosphate (squares) and nitrate (circles) versus depth (Wersin et.al. 1991) and ii) phosphate concentrations in pore water (Schulz and Schulz 2005)

1.4 Transport processes

So far, the discussion was centered on chemical reactions occurring in lake sediments. These as very important as they are the sources/sinks of chemical species, but they do not alone define the depth profiles of chemicals species in lake sediments. Because of gravitational forces, concentration gradients and the presence of biota, much of the chemical distribution inside lake sediments is caused by physical transport which can be grouped into four categories: diffusion, advection, irrigation, bioturbation.

1.4.1 Physical processes

Diffusion is the random movement of particles in solution. Due to the interaction potential between molecules, the net effect of diffusion is that of moving material from an area of high concentration (where many molecular collisions are likely) to an area of low concentration (where the free path of molecules is longer), thus balancing any concentration gradients.

Advection conversely is the directional movement (flow) of material due to an impressed force, such as gravitational pull, hydrological flow, etc. It has the effect of a net flux of material in or out of a volume element. Burial and compaction are examples of directional movement of material (Berner 1980, Boudreau 1996). Burial refers to the movement of a sediment layer relative to the SWI due to new sediment depositing (thus

the SWI moves up). Compaction is due to loss of water caused by the weight of the overlying sediment.

1.4.2 Biological processes

Additional transport is created by biological organisms living in sediments. Bioturbation describes the burrowing, consumption and excretion of material by small organisms. Because such activity causes material to be displaced over small distances inside the sediment, much smaller than the length scales of depth usually considered, such transport is considered essentially local.

However, some bottom dwelling organisms build channels inside sediment that act as conduits. The organisms may actively pump material from one end to the other to supply their needs. This kind of non-local transport, termed irrigation, is over longer distances and thus is treated differently than local biological transport.

In order to describe sediment chemistry and its spatial distribution, one must take into account both the physical transport mechanisms, which distribute material in the mud, as well as the chemical mechanisms which create or destroy (interconvert) chemical material. The first challenge of diagenetic modeling is in describing mathematically the qualitative behavior, overviewed above, in order to quantitatively assess how the sum total of such interactions combine to affect the chemistry of sediments. This is done by expressing the transport and reactions pertinent to a particular chemical species as partial

differential equations and solving those for the dependent variables. The variables are represented by a concentration profile as a function of space inside the sediment. This methodology is outlined in the next chapter.

Chapter 2

Diagenetic Modeling Overview

The following chapter is an introductory level-overview of diagenetic modeling, with the goal of introducing the concepts used in our numerical model. It discusses the various terms in a typical diagenetic equation, their mathematical construction and methods for solving the resulting equations.

The goal of diagenetic modeling is to describe the physical and chemical processes outlined in the previous review chapter. This is done through a mass balance equation, which operates on the conservation of mass principle, that is what accumulates in a sediment elementary volume is the difference between what comes in minus what leaves plus what gets produced minus what gets consumed. In one spatial dimension this differential form of mass conservation is

$$\frac{\partial C_i}{\partial t} = -\frac{\partial F_i}{\partial x} + \sum R_i \quad . \tag{2.1}$$

The left hand side represents the accumulation or depletion of concentration of material C_i defined in appropriate units, as will be shown. The first term on the right hand side refers to

all local physical transport of existing material i (where F_i is flux of material i) in and out and the second term represents source/sink of material i (usually chemical inter-conversions, precipitation/dissolution or radioactive decay). In the case of non-local transport, such as irrigation, an additional descriptive term is required as will be shown later.

2.1 Physical Transport

The physical transport is traditionally defined relative to an adopted reference frame. A common such reference is the sediment water interface (SWI). Four transport phenomena typically considered in diagenesis were described in the previous chapter: advection, diffusion, bioturbation, irrigation.

2.1.1 Advection

Advection is the net movement of material relative to the SWI, due to burial or compaction. Burial refers to the accumulation of new sediment which shifts the SWI reference frame upward resulting in an effective downward transport of the underlying sediment with respect to the SWI. Compaction is due to loss of water caused by compression from the settling overlying sediment (Berner 1980). Solid particles will compress closer together and pore water may get expulsed upward. From this description we see that the advection behaviors of solid and aqueous species need to be described differently. For solid species

$$\left.\frac{\partial((1-\phi)\rho_s C_s)}{\partial t}\right|_{advection} = -\frac{\partial(w(1-\phi)\rho_s C_s)}{\partial x} \quad , \tag{2.2}$$

where w is the velocity of the solid sediment matrix relative to the SWI due to burial and compaction, C_s is in moles per unit mass of dry sediment and ρ_s is the grain density of dry sediment (g/cm^3). For aqueous species

$$\left.\frac{\partial(\phi C_{aq})}{\partial t}\right|_{advection} = -\frac{\partial(v\phi C_{aq})}{\partial x} \quad , \tag{2.3}$$

where v is the velocity of water relative to the SWI and C_{aq} is in number of moles per unit volume of pore water.

One effect of compaction is to change the porosity of sediment with depth, where porosity is defined as

$$\phi = \frac{\text{volume of water pores}}{\text{volume of total sediment}} \quad .$$

Porosity typically diminishes with depth due to compaction. Advection can also be induced by other externally impressed flows (Boudreau 1996a) such as the hydrological flow

caused by pressure gradients, but these are typically disregarded in the context of muddy aquatic sediments where permeability[1] is low.

2.1.1.1 Steady state compaction

In a case where compaction is non-negligible but externally impressed flow can be ignored, the system can be viewed as under steady state compaction. That is, the deposition rate is constant and porosity is constant in time for all fixed depths ($\partial\phi/\partial t = 0$). We can write the general diagenetic equations for total solids

$$\frac{\partial[\rho_s(1-\phi)]}{\partial t} = \frac{\partial\left(D_{ts}\dfrac{\partial[\rho_w(1-\phi)]}{\partial x}\right)}{\partial x} - \frac{\partial[\rho_s(1-\phi)w]}{\partial x} + R_{ts}, \tag{2.4}$$

where the first term on the right hand side expresses the diffusive flux which is outlined later. For total porewater

$$\frac{\partial[\rho_w\phi]}{\partial t} = \frac{\partial\left(D_w\dfrac{\partial[\rho_s\phi]}{\partial x}\right)}{\partial x} - \frac{\partial[\rho_w\phi v]}{\partial x} + R_w. \tag{2.5}$$

Here, $\rho_s(1-\phi)$ expresses the concentration of solids in sediment (mass per unit sediment volume) and $\rho_w\phi$ expresses the concentration of water in pore solution (moles per unit

[1] Permeability: Capability of the soil to allow fluid movement through it.

sediment volume). If we do not concern ourselves with diffusion of total solids or pore solution, which arise mainly from bioturbation, and if we approximate the chemical reaction rates to sum to zero, we are left with the expressions

$$\frac{\partial[\rho_s(1-\phi)]}{\partial t} = -\frac{\partial[\rho_s(1-\phi)w]}{\partial x} \tag{2.6}$$

and

$$\frac{\partial[\rho_w\phi]}{\partial t} = -\frac{\partial[\rho_w\phi v]}{\partial x} \tag{2.7}$$

We can further simplify these expressions by noting that density changes of total solids or total water with depth are very small and the densities of these quantities can be approximated as constant. Therefore

$$\frac{\partial(1-\phi)}{\partial t} = -\frac{\partial[(1-\phi)w]}{\partial x} \tag{2.8}$$

and

$$\frac{\partial(\phi)}{\partial t} = -\frac{\partial(\phi v)}{\partial x}. \tag{2.9}$$

Coming back to the steady state condition ($\partial\phi/\partial t = 0$) initially postulated, we get:

$$0 = \frac{\partial[(1-\phi)w]}{\partial x} \quad , \tag{2.10}$$

$$0 = \frac{\partial(\phi v)}{\partial x} \quad . \tag{2.11}$$

These results imply that the product of porosity and advection are constant with depth, therefore

$$\begin{aligned} &(1-\phi)w = (1-\phi_x)w_x \\ &\therefore w = \frac{(1-\phi_x)}{(1-\phi)}w_x \end{aligned} \tag{2.12}$$

and

$$\begin{aligned} &(\phi)v = (\phi_x)v_x \\ &\therefore v = \frac{\phi_x}{\phi}v_x \end{aligned} \quad . \tag{2.13}$$

Where ϕ_x, w_x and v_x are the known porosity and burial rates at a given depth x. Additionally, when there is no compaction, the porosity can be assumed spatially constant as well. Then v and w are constant and identical to each other ($v = w$) (Berner 1980).

2.1.2 Liquid and solid mixing

As the motion of material due to random motion of particles, diffusion is modeled using Fick's laws. Molecular diffusion considers the rearrangement of atomic constituents of a particular phase (Einstein 1905). Although molecular motion is random, it has the effect of eliminating chemical or electrical potential gradients. This is because "if there are more ions/molecules of a dissolved substance (or even colloids) in one region of fluid, random molecular motions due to collisions between solutes and water molecules will eventually lead to a homogenization" (Boudreau 1996a).

According to Fick's first law of diffusion, the diffusive flux aqueous species is given by

$$F_i = -D_i \phi \frac{\partial C_i}{\partial x} \quad . \tag{2.14}$$

Here we omit the electrical effects due to electric field gradients caused by ions distributed in solution. The net expression for time variance in concentration due to diffusion is therefore

$$\left.\frac{\partial(\phi C_i)}{\partial t}\right|_{diffusion} = \frac{\partial}{\partial x}\left(D_i \phi \frac{\partial C_i}{\partial x}\right) \tag{2.15}$$

for aqueous species. Molecular diffusion is neglected for solid species.

The constant term D_i refers to the molecular diffusion coefficient of a substance. Such constants can be calculated experimentally in the laboratory. In real sediments however, this constant can be affected by several factors. Adsorption onto solids can inhibit diffusion. Temperature can also affect it by changing the molecular speeds, bringing possible seasonal variations to the diffusion constants (Berner 1980, Boudreau 1996a). Also the tortuosity of sediments, the constriction imposed on the molecular path by collisions with solid particles, will also hinder diffusion. Aqueous species travel in the pore water which is distributed in channels and interconnected pockets throughout the sediment. Tortuosity is formally defined as "the length of actual sinuous path (Δl) over a depth interval (Δx) " (Berner 1980)

$$\theta = \frac{\Delta l}{\Delta x} > 1 \qquad \textbf{(2.16)}$$

It has been related to the porosity of sediment empirically several different ways, one of which is (Manheim 1970)

$$\theta^2 = \phi^{1-n} \qquad \textbf{(2.17)}$$

which for $n = 2$ is Archie's law. This is only one of many postulated tortuosity-porosity relations (Boudreau 1996a) some of which are theoretically based and others, such as Archie's law, are empirical models. The diffusive correction for tortuosity is accounted for in the diffusion constant such that

$$D_i = \frac{D_0}{\theta^2} = \frac{D_0}{\phi^{1-n}} \quad . \tag{2.18}$$

Here D_0 denotes the diffusion coefficient in pure water.

Although biological in origin, bioturbation is commonly modeled as another form of diffusion. Bioturbation is the sum of small scale mixing effects brought on by crawling, burrowing or ingesting/excreting of sediment by biological organisms. Given the unpredictability and complexity of the process, the strategy of treating it as a random mixing, like diffusion, is appropriate. In the context of so called intraphase mixing[2] (Boudreau 1996a) bioturbation can be described by the following relation

$$\left.\frac{\partial(\phi C_i)}{\partial t}\right|_{Bioturbation} = \frac{\partial}{\partial x}\left(D_B \phi \frac{\partial C_i}{\partial x}\right) \quad , \tag{2.19}$$

for aqueous species and

$$\left.\frac{\partial((1-\phi)C_i)}{\partial t}\right|_{Bioturbation} = \frac{\partial}{\partial x}\left(D_B(1-\phi)\frac{\partial C_i}{\partial x}\right). \tag{2.20}$$

for solid species. D_B is the bioturbation diffusion coefficient and can be space and time dependent.

[2] When solids and fluids are not mixed together, thus porosity gradients remain the same.

2.1.3 Irrigation

Irrigation is one biological mixing process considered separately. It describes the flushing of channels in the sediment with overlaying water (Berner 1980). This transport process differs from generic bioturbation. It describes a directional flow (from the SWI to a depth in the sediment) and the length scales over which material is transported are larger, thus it cannot be considered as a local transport process like bioturbation.

For a dissolved species, it is commonly expressed as

$$\left.\frac{d(\phi C_i)}{dt}\right|_{irrigation} = -\alpha(x)\phi(C_i - C_{SWI}), \tag{2.21}$$

where the expression for the irrigation coefficient α, follows from a burrow tube model (Aller 1982) of two coaxial cylinders, one representing the burial tube and the other the sediment. The irrigation coefficient is given by (the derivation is presently omitted)

$$\alpha(x) = \frac{2Dr_1}{(r_2^2 - r_1^2)(\bar{r}(x) - r_1)} \quad . \tag{2.22}$$

Here r_1 is the radius of the inner cylinder, which contains overlying water , r_2 is the outer cylinder radius, $\bar{r}$ the radial distance at which the concentration is the mean concentration in a radial slice of sediment. In practice $\alpha(x)$ is chosen as an empirical function.

2.2 Chemical Reactions

The reactions detailed in the previous chapter must also be accounted for when modeling the time evolution of lake sediments. Adding chemical reactions to the mass balance equation, however, adds complexity to the problem, as these terms tend to introduce coupling between the chemical species and are often non-linear depending on their stoichiometry. There are a few concepts describing chemical reactions, namely homogeneous vs. heterogeneous reactions, reversible vs. irreversible reactions and fast vs. slow reactions.

Homogeneous reactions are those which occur inside a single phase of sediment (such as acid base reactions). Ones which occur at phase boundaries such as precipitation and adsorption reaction are considered heterogeneous, though they are modeled as quasi-homogeneous (Boudreau 1996a). The distinction between fast and slow reactions can be made based on the reaction rate time scale compared to other time scales such as transport. Reactions occurring on time scales comparable or longer than transport processes are treated with a full kinetic description. On the other hand, fast reactions are controlled by the transport of species to and from the reaction site. Such reactions can be considered reversible, in local chemical equilibrium, and are treated thermodynamically (Meysman 2001).

The "chemistry" occurring in lake sediments can be delineated as four separate mechanisms: local equilibrium (fast and reversible) and kinetic (slow) chemical reactions, precipitation/dissolution and adsorption/de-sorption.

2.2.1 Local equilibrium and kinetic reactions

Consider the generic binary reaction

$$aA + bB \xleftrightarrow{K_f / K_r} cC + dD$$

In the case when the reaction is one directional (irreversible), and setting activity coefficients[3] to 1, its rate can be expressed as

$$\left.\frac{dC}{dt}\right|_{reaction} = cR_f = ck_f[A]^a[B]^b \tag{2.23}$$

Where [] denotes concentration. In the case when the reaction is reversible

$$\left.\frac{dC}{dt}\right|_{reaction} = cR_{net} = c(R_f - R_r) = c\left\{k_f[A]^a[B]^b - k_r[C]^c[D]^d\right\} \tag{2.24}$$

[3] The activity coefficient γ is a factor which corrects for non-ideal behavior, such as ion interaction in solution. It is affected by parameters such as temperature and ionic composition of the solution. γ is defined as the ratio of activity to the concentration. The activity, A, in turn is equivalent to the chemical potential μ through the relation $\mu = k_B T \cdot \log A$, where T is temperature and k_B is Boltzmann's constant.

For very fast reversible reactions (equilibrium reactions) the net rate is effectively zero since the reaction will proceed instantaneously to balance reactant concentrations

$$R_{net} = 0$$
$$\therefore \frac{k_f}{k_r} = K_{eq} = \frac{[C]^c[D]^d}{[A]^a[B]^b} \tag{2.25}$$

Most chemical reactions can be expressed using such rate or equilibrium constants (k_f, k_r, K_{eq}). One notable exception is the degradation of organic matter which is an example of a decaying process. A conventional way of describing it is using so called Monod kinetics (Boudreau 1996a)

$$\left.\frac{d[OM]}{dt}\right|_{reaction} = -k_{OM}[OM]\frac{[Ox]}{K^{Ox}+[Ox]}\ , \tag{2.26}$$

where $[Ox]$ is the concentration of oxidizing agent. Here K^{ox}, the saturation constant, is defined as the concentration of oxidant when the reaction has reached half its maximum rate. This form is appropriate if there was only one OM degradation pathway. In the presence of multiple electron acceptors however (R_{O2}, R_{NO3}, $R_{Fe(OH)3}$, R_{SO4}, R_{CH4}), the term is expressed slightly differently. There is inhibition from preferential electron acceptors on subsequent oxidizing agents which must be reflected in the reaction rates. This is achieved, for example, by the incorporation of an inhibition term (Boudreau 1996a, van Capellen 1996).

$$\left.\frac{d[OM]}{dt}\right|_{oxidant\ i} = -k_{OM}[OM]\frac{[Ox_i]}{K_i^{Ox}+[Ox_i]}\prod_{j<i}\frac{K_j^{inh}}{K_j^{inh}+[Ox_j]} \tag{2.27}$$

Here the degradation rate due to each electron acceptor is multiplied by inhibition terms (with constants K^{inh}) from those other oxidizers which are thermodynamically more favorable. Thus oxygen does not have any inhibition terms, while sulfate reduction has inhibition multipliers from all other oxidation reactions. For methanogenesis the probablility of reaction is simply 1 minus the probabilities of all other OM degradation reactions.

2.2.2 Precipitation

Precipitation, or crystal growth, is a complex process. In order for crystals to grow, small template particles must form first through a process called nucleation. When impurities act as nuclei the process is heterogeneous and when proper crystal atoms form a nucleus of critical size it is called homogeneous (Markov 1995). The process of forming a nucleus upon which a crystal can grow depends on the thermodynamic properties of the environment among other factors. One important such variable is the ion concentration product (the product of reactant concentrations raised to their stoichiometric exponents). If this product is above a certain threshold value, the solubility product, then the solution is said to be supersaturated with respect to the solid phase. Thus precipitation can occur according to thermodynamic considerations. Whether or not it will occur, in the time scale of interest, is a more complicated question involving the kinetics of the process.

Modeling crystal formation is an intricate process of nucleation and growth and ripening stages, with surface or diffusion controlled regimes (Markov 1995, Berner 1980) and it has been done to varying degrees of complexity, but as such it will not be covered in this text. The full mechanism of crystal growth is not included in the model used for this thesis. Precipitation for the purpose of our model is reduced to a simplified kinetic reaction with a rate determined by the supersaturation of reactants and by an imposed rate constant. The rate expression as such does not depend on the concentration of the solid phase. This simplified rate represents most closely a nucleation process. A similar consideration is given to the reverse process, namely dissolution of solids back into the porewaters. In dissolution, however, the rate term is a function of the amount of solid phase as well. More details are given in Chapter 3.

2.2.3 Adsorption

Another significant chemical process is adsorption of ions onto solid phases in the sediment. It is important because it changes the distribution of reactive species between the solid and aqueous phases and impacts their reactivity. It is considered as a reversible local equilibrium reaction. It is described by a kinetic term

$$[A_{adsorbed}] = K_{ads}[A_{aq}] \ , \tag{2.28}$$

where the adsorption constant K_{ads} incorporates the parameters governing the adsorption mechanism. The rate of adsorption depends on the available binding sites on solid phases

and thus is a function of the amount of solid material present. Also, since the adsorbing solute is in competition with other ions in solution, such as the hydronium ion ($[H^+]$), it is also a function of pH. Lastly an important variable for the amount of adsorbed species is the concentration of adsorbing solute. The way by which these factors are accounted for the adsorption constant in our model is detailed in the following chapter.

Combining all the expressions given above into a summarizing equation, one obtains a generic digenetic equation for aqueous or solid species.

For aqueous species:

$$\frac{\partial C}{\partial t} = \frac{1}{\phi}\frac{\partial}{\partial x}\Big(\underbrace{\phi D_B \frac{\partial C}{\partial x}}_{\text{Biological Mixing Flux}} + \underbrace{\phi D_{mol} \frac{\partial C}{\partial x}}_{\text{Molecular Diffusion Flux}} \Big) - \frac{1}{\phi}\frac{\partial}{\partial x} \underbrace{(\phi v C)}_{\text{Advection Flux}} - \underbrace{\alpha(C - C_0)}_{\text{Irrigation}} + \underbrace{\sum R}_{\text{Reactions}} \quad \textbf{(2.29)}$$

For solid species:

$$\frac{\partial C}{\partial t} = \frac{1}{(1-\phi)}\frac{\partial}{\partial x}\Big(\underbrace{(1-\phi) D_B \frac{\partial C}{\partial x}}_{\text{Biological Mixing Flux}} \Big) - \frac{1}{(1-\phi)}\partial_x \underbrace{((1-\phi) w C)}_{\text{Advection Flux}} + \underbrace{\sum R}_{\text{Reactions}} \quad \textbf{(2.30)}$$

The chemical reaction rates have been expressed as moles per unit time per porewater volume or dry sediment mass respectively.

2.3 Solution Methodology

2.3.1 Space discretization

Analytical solutions of partial differential equations (PDEs) are often not accessible because the equations can be highly non-linear, as for example due to coupling terms. Solving PDEs then reduces to approximating solutions using numerical methods. There are various numerical avenues one can take to solve one or a system of partial differential equations. These methods consist of approximating the continuous derivative terms of PDEs with local approximations. It consists of expressing space evolution as a truncated Taylor series.

$$C_{x+\Delta x} = C_x + \left.\frac{dC}{dx}\right|_x \Delta x + O(\Delta x^2)$$
$$\therefore \left.\frac{dC}{dx}\right|_x \approx \frac{C_{x+\Delta x} - C_x}{\Delta x} \qquad \textbf{(2.31)}$$

This equation is an example of forward differencing because it is constructed with the forward Taylor series, meaning it propagates the solution from a previous space step forward in space. There is a problem that this scheme is not always stable since, for certain coefficients placed in front of the terms, it can lead to negative or infinite concentrations. An alternative is backward differencing, which uses values at the backward node to approximate the first derivative. However, this scheme is also only first order accurate. Finally, by combining forward and backward differences and taking the average of the

expressions we can arrive at a central difference scheme, which is second order accurate and uses both backward and forward values. However it can be demonstrated that the central difference scheme is also not always stable as in the case of forward differencing. A simple solution to these drawbacks is to use a weighted combination of backward and central differencing, as suggested by Fiadero and Veronis (1977)

$$\frac{dC}{dx} = \frac{(1-\sigma)C_{i+1} + 2\sigma C_i - (1+\sigma)C_{i-1}}{2\Delta x} \quad , \tag{2.32}$$

where

$$\sigma = \coth\left(\frac{v\Delta x}{2D}\right) - \frac{2D}{v\Delta x} \quad . \tag{2.33}$$

This scheme is both second order accurate and numerically stable (at least for the linear case). The term $\frac{v\Delta x}{2D}$ inside the hyperbolic cotangent of the weighting coefficient (σ) is commonly referred to as the grid Peclet number. For very small Peclet numbers σ approaches 0, reducing the expression to a central difference, while for large grid Peclet number σ approaches 1 and the scheme reverts to a backward difference formula. This scheme is particularly useful when the diffusion (D) and advection (v) coefficients are depth dependent, making the grid Peclet number a function of depth.

2.3.2 Time propagation of stiff equations

Like space discretization (equation 2.31), one can express the propagation in time in terms of a forward difference, that is, taking the concentration of the current time step to be the concentration of the previous time step plus the time derivative of the concentration at the previous time step multiplied by the time step. While this is a convenient fully explicit representation of the time evolution of the dependent variable, they may lead to issues of numerical stability (Boudreau 1996a). Another numerical difficulty is in the concept of stiffness. Stiffness occurs in equations where the relevant time scales occur over a large range of values. This is a common characteristic of diagenetic equations which typically include a wide range of chemical reactions which may occur over dramatically different time scales. In such circumstances, one must keep the discretization intervals (Δt) very small in order to avoid oscillating solutions, which makes solving the equations a computationally intensive task.

2.3.2.1 Method of lines

A robust numerical method for solving stiff PDEs is the method of lines (MoL) (Schiesser 1991). The method of lines consists in rewriting the partial differential equations, which are dependent on space and time, as a system of time-dependent ordinary differential equations (ODEs) at fixed depths in the sediment and then solving them with a stiff ODE solver.

Assuming for brevity that ϕ is homogeneous, and ignoring irrigation, the generic diagenetic equation can be written as :

$$\frac{\partial C}{\partial t} = D\frac{\partial^2 C}{\partial x^2} - v\frac{\partial C}{\partial x} + R(C,x) \tag{2.34}$$

Its temporal derivative at a fixed depth i then becomes

$$\frac{dC_i}{dt} = D\frac{(C_{i+1} - 2C_i + C_{i-1})}{\Delta x^2} - v\frac{((1-\sigma)C_{i+1} + 2\sigma C_i - (1+\sigma)C_{i-1})}{2\Delta x} + R(C_i, x_i) \tag{2.35}$$

Combining all the derivatives at all depths (chosen on a grid) throughout the sediment, one gets a set of coupled ordinary differential equations. The large number of such equations for different depth positions, thus defines an array of ODEs approximating the original PDE

$$\begin{aligned}
&\frac{dC_1}{dt} = D\frac{(C_2 - 2C_1 + C_0)}{\Delta x^2} - v\frac{((1-\sigma)C_2 + 2\sigma C_1 - (1+\sigma)C_0)}{2\Delta x} + R(C_1, x_1),\\
&\cdots\\
&\frac{dC_i}{dt} = D\frac{(C_{i+1} - 2C_i + C_{i-1})}{\Delta x^2} - v\frac{((1-\sigma)C_{i+1} + 2\sigma C_i - (1+\sigma)C_{i-1})}{2\Delta x} + R(C_i, x_i),\\
&\cdots\\
&\frac{dC_{n-1}}{dt} = D\frac{(C_N - 2C_{n-1} + C_{n-2})}{\Delta x^2} - v\frac{((1-\sigma)C_N + 2\sigma C_{n-1} - (1+\sigma)C_{n-2})}{2\Delta x} + R(C_{n-1}, x_{n-1}).
\end{aligned} \tag{2.36}$$

The problem thus reduces to solving a large system of coupled, stiff, non-linear ordinary differential equations. This problem is a readily solvable one with prepackaged codes. One

such code, the code used for the present model, is VODE (Brown et. al. 1989). VODE is a linear multistep method and it uses a backward difference formula to handle stiff equations (Byrne and Hindmarsh 1987).

2.3.2.2 Other methods for coupling reaction and transport

As mentioned several times already, the challenge of diagenetic equations comes largely from the coupling of reaction and transport terms, since the two are inter-dependent but occur over different time scales. That is reaction terms affect concentrations which correspondingly influence fluxes.

2.3.2.2.1 Global implicit approach

Conceptually, the simplest way is the global implicit method. It simply considers the transport and reaction terms simultaneously. For example, in the simple case of a reaction diffusion equation, with constant porosity, diffusion coefficient and spatial increments, we can write a fully implicit discretization as

$$\frac{C_i^{t+1} - C_i^t}{\Delta t} = D\frac{C_{i+1}^{t+1} - 2C_i^{t+1} + C_{i-1}^{t+1}}{\Delta x^2} + R(C_i^{t+1}) \quad , \tag{2.37}$$

where the subscripts are depth indexes and the superscripts are time indexes. By rearranging the expression to group the spatio-temporal node terms together we get

$$\underbrace{\left(C_i^t + \Delta t R(C_i^{t+1})\right)}_{d_i} = \underbrace{-\left(\frac{D\Delta t}{\Delta x^2}\right)}_{c_i} C_{i+1}^{t+1} + \underbrace{\left(\frac{2D\Delta t}{\Delta x^2}+1\right)}_{b_i} C_i^{t+1} \underbrace{-\left(\frac{D\Delta t}{\Delta x^2}\right)}_{a_i} C_{i-1}^{t+1} \quad . \tag{2.38}$$

Defining such an equation at every spatial node of a system will yield a matrix of equations

$$\begin{bmatrix} C_1 \\ C_2 \\ \cdots \\ C_{N-1} \\ C_N \end{bmatrix} = \begin{bmatrix} b_1 & c_1 & & & & & \\ a_2 & b_2 & c_2 & & & & \\ & & & \cdots & & & \\ & & & & a_{N-1} & b_{N-1} & c_{N-1} \\ & & & & & a_N & a_N \end{bmatrix}^{-1} \begin{bmatrix} d_1 \\ d_2 \\ \cdots \\ d_{N-1} \\ d_N \end{bmatrix} . \tag{2.39}$$

The coefficient d_i on the right hand side depends implicitly on the concentration of the unknown time step. Such a system can be solved after linearizing the matrix coefficients with respect to concentration and iterating the solution (with, for example, the Newton-Raphson method) until it reaches the desired tolerance level (that is the solution does not change appreciably from one iteration to the next). This method becomes considerably more involved however, once coupling between many species arises via the reaction terms ($R(C_i^{t+1})$). This way the size of the coefficient matrix increases and the corresponding equations are now coupled. Implementing this method would thus require a large amount of computer memory.

2.3.2.2.2 Operator splitting approaches

An alternative to the one step approach is the so called sequential non-iterative approach (SNIA). This method consists of breaking the time step into a transport step

$$\frac{\left(C_i^{trans} - C_i^t\right)}{\Delta t} = L(C_i)^t \quad , \tag{2.40}$$

followed by a reaction step

$$\frac{\left(C_i^{t+1} - C_i^{trans}\right)}{\Delta t} = R_i^{t+1} \quad . \tag{2.41}$$

Here the *trans* superscript indicates a time between time steps t and $t+1$. $L(C_i)$ is used to denote the transport terms, such as the diffusion term of the previous example. The main drawback of this methodology is that it gives equal consideration to the reaction and transport steps. In other words, it assumes that no reaction is taking place until all the reactant has reached the reaction site. One way to improve on this drawback is by imbedding the reaction step between two transport half steps,

$$\begin{aligned}
&\frac{\left(C_i^{trans} - C_i^t\right)}{\Delta t/2} = L(C_i)^t \\
&\frac{\left(C_i^{reacted} - C_i^{trans}\right)}{\Delta t} = R_i^{reacted} \\
&\frac{\left(C_i^{t+1} - C_i^{reacted}\right)}{\Delta t/2} = L(C_i)^{reacted}
\end{aligned} \tag{2.42}$$

a method known as Strang splitting (Steefel et. al. 1996).

Yet another improvement upon the operator splitting method is the sequential iterative approach (SIA), of which there are many implementations. In this method, for each time step, once the reaction term from the previous iteration is used as a source term and then the transport term from the previous iteration is used as a source term. The algorithm iterates, by alternating the source terms until the concentrations computed in each case agree to within some tolerance (Steefel et. al. 1996).

2.3.3 Boundary conditions

In the process of discretizing the differential equations for the description of each layer, information about the layers above and below it are used (such as the spatial derivative terms above demonstrate). Consequently at the spatial boundaries, such as the sediment water interface, we must use boundary conditions to account for layers outside the defined space. The two types of boundary conditions typically considered in diagenetic models, and the ones used in our model are Dirichlet and mixed boundary conditions (Boudreau 1996).

Dirichlet boundary conditions refer to a constant concentration and are used at the SWI boundary. These are appropriate for aqueous species since concentrations at the bottom of water columns are routinely monitored (NERI 2004). Alternatively, other boundary conditions for dissolved species can be given by specifying a diffusion flux across the SWI.

For solid species, given their lesser transport properties, constant diffusive and advective flux boundary conditions at the SWI are more appropriate.

Sufficiently far below the SWI, the species profiles reach somewhat constant values, with creation and destructions reactions either tapering off or balancing exactly. Thus at the boundary far from the SWI diffusive fluxes are taken to be zero.

Chapter 3

Model Specifics

As described in the previous chapter, diagenetic models are comprised of systems of non-linear partial differential equations (see equation 2.1). The model studied in this thesis is a set of 14 such equations which describe the transport and chemical behaviors of 14 solid and solute species in lake sediments. The following is an outline of the specific features of our particular approach for describing the time evolution of the relevant chemical species.

3.1 Extended Model

The model used in this thesis is a subset of a larger model of diagenetic reactions written for the Lake Sediment Structure and Evolution (LSSE) project (Katsev et al. submitted). The extended model encompasses a set of 31 chemical reactions describing the main known diagenetic pathways: primary oxidation reactions (organic matter decomposition), secondary redox reactions (oxidation/reduction of by-products of primary reactions), precipitation/dissolution of solid phases, adsorption/ desorption of aqueous ions onto

solids and acid/base (dissociation) reactions. The expanded model considers the time evolution of a number of chemical species such as organic matter, oxygen, various iron and manganese bearing solids, pH, aqueous and /or adsorbed species (Fe^{2+}, Mn^{2+}, sulfate, phosphate, nitrate, CH_4), as well as total analytical variables such as total aqueous sulfur, total aqueous carbon , total aqueous nitrogen, alkalinity, etc. The model also describes the transport phenomena such as advection (including compaction), diffusion, bioturbation and irrigation.

The reactions of the expanded model were chosen to illustrate the possible chemical mechanisms in lake sediments which were deemed important. These reactions were drawn from a database of diagenesis reactions, dSED, compiled from a wide literature review of lake, marine and groundwater geochemistry (Katsev et al. 2004).

3.2 Phosphorus Model

The model studied in this thesis was constructed as a tool to study the factors influencing phosphorus flux across the sediment water interface (Katsev et al. submitted). It is correspondingly a subset of reactions of the extended model mentioned above. The reactions chosen were those deemed relevant to phosphorus cycling inside the lake sediment. They encompass iron, phosphorus and sulfur transformations in lake sediments as these three cycles are intimately linked (see Chapter 1). As in the extended model, the present phosphorus model also considers primary and secondary redox reactions,

precipitation, adsorption and acid-base dissociations. The set of reactions included in the phosphorus model is given in Table 3.1 (see end of chapter).

R1 – R4 represent organic matter mineralization through oxic respiration, iron and sulfate reduction and methanogenesis. Iron oxidation (R5, R6), sulfide (R7) and iron monosulfide (R8) oxidation were considered as well. The model also accounts for the precipitation (R14, R15, R16) and dissolution (R9, R10, R11) of iron-bearing species, which affect the aqueous iron concentration. Ageing of iron phases (R12, R13) and adsorption of aqueous species (R17, R18) are also incorporated. The above reactions were chosen, because they were deemed to embody, in a minimal set, the main mechanisms of the cycling of iron, sulfur and phosphorus in lake sediments.

Table 3.1 also gives expressions for the reaction rates. The rate expressions for organic matter decomposition (R1 – R4) are described by Monod kinetics, as is common practice in diagenetic modeling (Van Cappellen and Wang 1996), and were explained in Chapter 2. Similarly, since the secondary redox reactions (R5 – R13) are kinetic reactions, their rates were computed as per Chapter 2 as well. As mentioned in the previous chapter, the precipitation rates (R14 – R16) are not expressed with the full complexity of crystal formation. They are formulated as nucleation reactions with a threshold (supersaturation constant) Ω which determines the criteria for the direction of a reaction (precipitation or dissolution). Since the precipitation rates are not expressed as a function of the solid phase concentration, the growth stage of crystal formation is not represented in this model.

The model calculates the time evolution of 14 chemical entities which are given in Table 3.2, along with their boundary conditions for the canonical case. Here 'canonical' refers to a set of representative values assigned to model parameters so as to reflect, at best estimate, a typical generic lake sediment. Since lake environments are quite diverse, as stipulated earlier, these quantities were often selected from wide ranges of possible values. The parameter values for the canonical case were chosen with the help of literature references from the dSED database (Katsev et al. 2004). Aqueous species are given fixed concentration as a boundary condition at the sediment water interface (SWI) while solid species are given fixed flux as a boundary condition at the SWI. At depth, all species are treated as having zero diffusive flux.

Table 3.2: List of dependent variables and their boundary conditions

Symbol	Name/Description	Top Boundary Condition for the canonical case	
OM	Organic Matter	Flux of OM = 5.143×10^{-3}	mol cm^{-2} yr^{-1}
FeHO3	Solid Ferric Oxides	Flux of $Fe(OH)_3$= 7.5×10^{-5}	mol cm^{-2} yr^{-1}
FeS	Iron Monosulfide	Flux of FeS = 0.0	mol cm^{-2} yr^{-1}
CaFeCO3	Siderite–Calcite	Flux of $CaFeCO_3$ = 0.0	mol cm^{-2} yr^{-1}
Viv	Ferrous Phosphates (vivanite)	Flux of $Fe_3(PO_4)_2$ = 0.0	mol cm^{-2} yr^{-1}
FeS2	Pyrite	Flux of FeS_2 = 0.0	mol cm^{-2} yr^{-1}
O2	Oxygen	$[O_2]^0 = 1.0\times10^{-7}$	mol cm^{-3}
SO4	Sulfate	$[SO_4^{2-}]^0 = 0.2\times10^{-6}$	mol cm^{-3}
ZP	Aqueous and adsorbed phosphate		
CH4	Methane	$[CH_4]^0 = 0.0$	mol cm^{-3}
Z1	Aqueous and adsorbed iron		
TC	Total aqueous carbon ($[CO_2] + [HCO_3^-] + [CO_3^{2-}]$)	$[TC]^0 = 2.44\times10^{-6}$	mol cm^{-3}
TS	Total aqueous sulfur ($[H_2S] + [HS^-]$)	$[TS]^0 = 0.0$	mol cm^{-3}
W	Alkalinity ($[HCO_3^-] + 2[CO_3^{2-}] + [HS^-] + F[\text{ads-Fe}] - [H^+] + [OH^-]$)	$[W]^0 = 2.299\times10^{-6}$	mol cm^{-3}

The variable $Fe(OH)_3$ encompasses all reactive ferric iron phases (such as, for example, ferrihydrite and goethite), while vivianite ($Fe_3(PO_4)_2$) represents all ferrous iron

phosphates. OM is used as a generic designation of all organic matter. Thus all organic matter is assumed to have the same resilience to mineralization (i.e. degradation). In our model it is useful to consider total analytical variables incorporating several chemical species, such as total aqueous carbon (TC), total sulfur (TS) or total alkalinity (W), total iron and total phosphate:

$$[TC] = [CO_2] + [HCO_3^-] + [CO_3^{2-}] \ ,$$

$$[TS] = [HS^-] + [H_2S] \ ,$$

$$W = [HCO_3^-] + 2[CO_3^{2-}] + [HS^-] + F[ads\text{-}Fe] - [H^+] + [OH^-] \ ,$$

$$[Z1] = [Fe^{2+}] + F[ads\text{-}Fe] = (1+F \bullet K_{adsFe})[Fe^{2+}] \ ,$$

$$[ZP] = [H_3PO_4] + F[ads\text{-}P] = (1+F \bullet K_{adsP})[H_3PO_4] \ .$$

Where K_{adsP} and K_{adsFe} are effective adsorption constants which will be defined later in the section. Here the conversion factor $F = \rho(1-\varphi)/\varphi$ is used to relate solid and liquid species concentrations. In the model, solid species concentrations are expressed in mol/g of dry sediment and liquid concentrations are expressed in mol/cm^3 of porewater. The term ρ refers to the "grain" density of solid dry sediment (g/cm^3), i.e. not including pores between the solid grains of dry sediment, which is considered constant. The porosity φ was defined in Chapter 2.

The parameters inputted into the model are given in Table 3.3 (at the end of the chapter) along with their canonical values.

3.2.1 Diffusion and reaction rate coefficients

The molecular diffusion coefficients for aqueous species are corrected for porosity according to Archie's law as specified in Chapter 2 and for temperature according to Boudreau (1996a). In our algorithm, diffusive transport of each carbonate (CO_2, HCO_3^-, CO_3^{2-}) and sulfide (H_2S, HS^-) species is characterized by the species proper diffusion coefficient. Thus, the speciation problem, i.e. in which form the carbonate of sulfide species will be present in, must be solved at every time step. This is done straightforwardly from the knowledge of the pH (see section 3.2.4) total aqueous sulfur (TS) and total aqueous carbon (TC):

$$[HS^-]=\frac{TS}{1+[H^+]/K'_{HS}},$$

$$[H_2S]=\frac{TS}{1+K'_{HS}/[H^+]},$$

$$[CO_2]=TC\left[1+\frac{K_{1C}}{[H^+]}+\frac{K_{1C}K_{2C}}{[H^+]^2}\right]^{-1},$$

$$[HCO_3^-]=TC\left[1+\frac{[H^+]}{K_{1C}}+\frac{K_{2C}}{[H^+]}\right]^{-1},$$

$$[HCO_3^-]=TC\left[1+\frac{[H^+]}{K_{1C}}+\frac{K_{2C}}{[H^+]}\right]^{-1},$$

$$[CO_3^{2-}]=TC\left[1+\frac{[H^+]^2}{K_{1C}K_{2C}}+\frac{[H^+]}{K_{2C}}\right]^{-1}.$$

The reaction rate coefficients are similarly corrected for temperature as per Boudreau (1996a). For solid species, molecular diffusion is neglected and only the bioturbation coefficient (D_b) is considered. D_b is expressed as

$$D_b(x) = D_b^0[1\text{-}\tanh(\beta(x\text{-}H))]/[1\text{-}\tanh(-\beta H)] \,, \qquad \textbf{(3.1)}$$

where x is the depth coordinate, D_b^0 is the bioturbation coefficient at the SWI (a constant), H is the characteristic depth where D_b drops drastically, and β defines the sharpness of the drop (Katsev et al., submitted). All of these parameter values are supplied to the model. The bioturbation profile follows a sigmoidal shape with high bioturbation at the top and decreasing toward the bottom.

3.2.2 Porosity, sedimentation rate

The model can compute the equations with a non-uniform porosity. However porosity was set to a constant for the purpose of the investigations which follow. Porosity is also considered constant in time as discussed in Chapter 2. Therefore the advection velocity for solid (w) and liquid (v) species is the same and is equal to the sedimentation rate (u).

3.2.3 Ion adsorption

The present model considers the adsorption of ferrous iron (Fe^{2+}) and phosphate onto solids, which are grouped into iron oxides ($Fe(OH)_3$) and background solids. The

adsorption is modeled as a Langmuir isotherm which is appropriate in the pH range of this model (pH = 6-8). The adsorption expressions are derived as follows. Consider the adsorption equation for a cation (such as Fe^{2+}) with a corresponding dissociation reaction:

Adsorption :	$S{\equiv}H + M^{2+} + HCO_3^- \leftrightarrow S{\equiv}M^+ + CO_2 + H_2O$	eq'm constant K'
Dissociation reaction:	$CO_2 + H_2O \leftrightarrow HCO_3^- + H^+$	eq'm constant K_{1C}
Equivalent reaction:	$S{\equiv}H + M^{2+} \leftrightarrow S{\equiv}M^+ + H^+$	eq'm constant K^*.

Here M^{2+} refers to a divalent cation and S≡ to a solid surface with an occupied adsorption site (the triple line is used to differentiate the adsorption connection from a covalent or ionic bond).

The reaction constants are:

$$K' = [S{\equiv}M^+][CO_2]/[HCO_3^-][M^{2+}][S{\equiv}H]$$
$$K_{1C} = [HCO_3^-][H^+]/[CO_2]$$

Therefore, $$K^* = K'K_{1C} = [S{\equiv}M^+][H^+]/[S{\equiv}H][M^{2+}]. \quad \textbf{(3.2)}$$

Let us label the total concentration (in mol/g dry sediment) of adsorption sites with S_T. We consider two adsorbing surfaces B (background) and FeOX (iron oxyhydroxides); iron oxyhydroxides are treated separately from other adsorbing substrates due to their high affinity for phosphate ions (Boström et al, 1988).

The number of total adsorption sites on each substrate can be expressed as

$$S_T = \Sigma_i (X_i S_{Ti}) \quad , \tag{3.3}$$

where i = FeOX, B and where X_i is the dimensionless weight composition of substrate i (molar mass*[solid]) be it iron oxyhydroxides or background. S_{Ti} is the number of total sites on a given substrate i,

$$S_{Ti} = [S{\equiv}M^+]_i + [S{\equiv}other]_i + S_{fi} \quad , \tag{3.4}$$

where the right hand side terms represent adsorbed iron, other adsorbed cations and remaining free sites respectively. We can approximate that the amount of adsorption sites taken up by competing ions is a linear function of the number of available sites (Balistrieri and Murray, 1981; Van Cappellen and Wang, 1996):

$$[S{\equiv}other]_i = \gamma_i S_{Ti}, \quad \text{where } i = FeOX, B \tag{3.5}$$

Substituting equation 3.4 into 3.3 we get

$$S_T = S_f + [S{\equiv}M^+] + \gamma S_T \tag{3.6}$$

where,

$$S_f = \sum_i X_i S_{fi} \quad ,$$

$$\gamma = \left(\sum_i \gamma_i X_i S_{Ti}\right) / S_T \ ,$$

$$\left[S \equiv M^+\right] = \sum_i \left[S \equiv M^+\right]_i X_i \ , \qquad i = \text{FeOX, Background.}$$

Therefore, from equation 3.2 we can infer that for each substrate:

$$[S{\equiv}M^+]_i = K^*_{Mi}[S{\equiv}H]_i[M^{2+}]/[H^+] = K^*_{Mi}S_{fi}[M^{2+}]/[H^+] \tag{3.7}$$

From equation 3.4 we can express

$$S_{fi} = S_{Ti} - [S \equiv M^+]_i - [S \equiv other]_i$$

$$S_{fi} = (1-\gamma_i)S_{Ti} - \frac{K^*_{Mi}}{[H^+]} S_{fi}[M^{2+}] \tag{3.8}$$

$$\therefore S_{fi} = \frac{S_{Ti}(1-\gamma_i)}{1 + \frac{K^*_{Mi}}{[H^+]}[M^{2+}]} = \frac{[H^+]S_{Ti}(1-\gamma_i)}{[H^+] + K^*_{Mi}[M^{2+}]}$$

Therefore, with the help of equations 3.7 and 3.8 the total adsorbed iron fraction can be expressed as

$$[S-M^+] = \sum_i X_i[S-M^+]_i = \sum_i \left(\frac{X_i K^*_{Mi} S_{Ti}(1-\gamma_i)}{[H^+] + K^*_{Mi}[M^{2+}]}\right)[M^{2+}] \ . \tag{3.9}$$

Comparing equation 3.9 to equation 2.28 from Chapter 2, we see that the effective adsorption constant K_{adsFe} is the summation expression in 3.9. For an anion, like

phosphate, a similar derivation with the adsorption reaction and the corresponding dissociation reaction can be shown to yield a similar expression

$$[S-P_{diss}]=\sum_i X_i[S-P_{diss}]_i=\sum_i\left(\frac{X_i K_{Pi}^{*} S_{Ti}(1-\gamma_i)}{[OH^-]+K_{Pi}^{*}[P_{diss}]}\right)[P_{diss}]\ . \tag{3.10}$$

Here again K_{adsP} is the summation term. In fact the above expression for the adsorption of phosphate can bee seen as an approximation depending on the detailed adsorption mechanism and speciation model used.

3.2.4 pH determination

The acidity (pH) is not an imposed parameter in our model. Rather it is calculated at each time step with a Newton-Raphson root finding algorithm. We solve for the pH by finding the root to the local acid base equilibrium equation and the adsorption relation for iron:

$$\mathbf{F}=\begin{bmatrix}F_1\\F_2\end{bmatrix}=0, \tag{3.11}$$

Where the matrix terms are the expressions for alkalinity and total reduced iron

$$F_1=\frac{[H^+]^2 A_C}{K_{1C}}+[H^+](A_C-TC)+K_{2C}A_C-2TC\cdot K_{2C}=0\,, \tag{3.11a}$$

with A_C=carbonate alkalinity $= W - FK_{adsFe}[Fe^{2+}] - \frac{TS}{1+[H^+]/K'_{HS}} + [H^+] - \frac{K_w}{[H^+]}$, and

$$F_2 = -Z1 + (1+FK_{adsFe})[Fe^{2+}] = 0. \quad \textbf{(3.11b)}$$

The dissociations constants K_{1C}, K_{2C}, K_w, K'_{HS} are defined in Table 3.1. The reader should note that if ammonia and manganese were included, then corresponding terms would appear in equation 3.11.

The Newton-Raphson method then finds the roots X_0 to the above system of equations, given the dependent variables W, TC, TS, Z1 by iteration of the relation

$$F(X) + J(X_0 - X) = 0$$

$$\text{where } J = \begin{bmatrix} \frac{\partial F_1}{\partial [Fe^{2+}]} & \frac{\partial F_1}{\partial [H^+]} \\ \frac{\partial F_2}{\partial [Fe^{2+}]} & \frac{\partial F_2}{\partial [H^+]} \end{bmatrix} \quad \textbf{(3.12)}$$

starting from an initial guess.

The root finding algorithm implemented in the model is taken from subroutine mnewt of Numerical Recipes (Press et. al. 1986), which in turn uses subroutines ludcmp (creates an LU decomposition of the Jacobian matrix) and lubksb (solves the resulting linear system) also from Numerical Recipes. The root finding method thus returns the aqueous iron in the system and the pH ($[H^+]$).

3.3 Numerical approach

As explained earlier, the model consists of a set of non-linear PDEs. In order to solve them, they are spatially discretized on an even depth grid (Δx = L/number of grid nodes, whre L is the sediment depth), resulting in a set of ordinary differential equations (ODEs) foe each concentration at each depth (see Method of Lines Section in Chapter 2). This set is stiff, because the time scales in the equations can be drastically different due to varying reaction rates. The resulting system of ODEs is solved using the code VODE (Brown 1989) as described in Chapter 2. The solutions are propagated to steady state (see below), by running the program for very large times (> 1 000 years), until variations in all the profiles are negligible, within some tolerance limit.

3.4 Stationary solutions

The model allows time-dependent variables (chemical species) to attain a steady state (where profiles no longer change in time or change very slightly), as a way of evaluating the permanent effects of varying model parameters. Although lakes are rarely in steady state, due to, in particular but not exclusively, seasonal variations (see Chapter 1), the comparison of stationary solutions simplifies the interpretation of model outputs (Katsev et al., submitted) and clarifies the role played by each parameter. The model sensitivity to initial conditions was tested and it showed invariable steady state solutions for different initial conditions.

Table 3.1: Model reactions and reaction rates

Rxn #	Reaction	Rate Name	Rate Expression
R1	$(CH_2O)_x(NH3)_y(H_3PO_4)_z + (x+2y)O_2 \rightarrow xCO_2 + yHNO_3 + zH_3PO_4 + (x+y)H_2O$	R_{O2}	$R_{O2} = k_{OM}[OM]f_{O2}$ where $f_{O2} = \frac{[O_2]}{[O_2]+K_{O2}}$
R2	$(CH_2O)_x(NH3)_y(H_3PO_4)_z + 4xFe(OH)_3 + 7xCO_2 \rightarrow 4xFe^{2+} + 8xHCO_3^- + yNH_3 + zH_3PO_4 + 3xH_2O$	$R_{(FeOH)3}$	$R_{FeOH3} = k_{OM}[OM]f_{FeOH3}$ $f_{FeOH3} = \frac{[Fe(OH)_3]}{[Fe(OH)_3]+K_{FeOH2}} \cdot \frac{K_{O2}^{inh}}{[O_2]+K_{O2}^{inh}}$ *
R3	$(CH_2O)_x(NH3)_y(H_3PO_4)_z + \frac{x}{2}SO_4^{2-} \rightarrow xHCO_3^- + \frac{x}{2}H_2S + yNH_3 + zH_3PO_4$	R_{SO4}	$R_{SO4} = k_{OM}[OM]f_{SO4}$ $f_{SO4} = \frac{[SO_4^{2-}]}{[SO_4^{2-}]+K_{SO4}} \cdot \frac{K_{O2}^{inh}}{[O_2]+K_{O2}^{inh}} \cdot \frac{K_{FeOH3}^{inh}}{[Fe(OH)_3]+K_{FeOH3}^{inh}}$
R4	$(CH_2O)_x(NH3)_y(H_3PO_4)_z \rightarrow \frac{x}{2}CH_4 + \frac{x}{2}CO_2 + yNH_3 + zH_3PO_4$	R_{CH4}	$R_{CH4} = k_{OM}[OM]f_{CH4}$ $f_{CH4} = 1 - f_{O2} - f_{FeOH3} - f_{SO4}$
R5	$4Fe^{2+} + O_2 + 8HCO_3^- + 2H_2O \rightarrow 4Fe(OH)_3 + 8CO_2$	R_{FeOX}	$R_{FeOx} = k_{FeOx}[Fe^{2+}][O_2]$
R6	$4S-Fe^+ + O_2 + 4HCO_3^- + 6H_2O \rightarrow 4S-H^0 + 4Fe(OH)_3 + 4CO_2$	R_{surFe}	$R_{surFe} = k_{surFe}[ads-Fe][O_2]$
R7	$H_2S + 2O_2 + 2HCO_3^- \rightarrow SO_4^{2-} + 2CO_2 + 2H_2O$	R_{SOx}	$R_{SOx} = k_{SOx}[TS][O_2]$
R8	$FeS + 2O_2 \rightarrow Fe^{2+} + SO_4^{2-}$	R_{FeSOx}	$R_{FeSOx} = k_{FeSOx}[FeS][O_2]$
R9	$2Fe(OH)_3 + H_2S + 4CO_2 \rightarrow 2Fe^{2+} + S^0 + 4HCO_3^- + 2H_2O$	R_{SFe3}	$R_{SFe3} = k_{SFe3}[TS][Fe(OH)_3]$
R10	$Fe_3(PO_4)_2 + 3H_2S \rightarrow 3FeS + 2H_3PO_4$	R_{sviv}	$R_{sviv} = k_{sviv}[TS][Fe_3(PO_4)_2]$
R11	$FeCO_3 + H_2S \rightarrow FeS + CO_2 + H_2O$	R_{SFeCO3}	$R_{SFeCO3} = k_{SFeCO3}[TS][FeCO_3]$
R12	$FeS + H_2S \rightarrow FeS_2 + H_2$	R_{FeSHS}	$R_{FeSHS} = k_{FeSHS}[FeS][TS]$
R13	$2Fe(OH)_3 + FeS + 6CO_2 \rightarrow 3Fe^{2+} + S^0 + 6HCO_3^-$	R_{FeSFe3}	$R_{FeSFe3} = k_{FeSFe3}[Fe(OH)_3][FeS]$
R14	$Fe^{2+} + HCO_3^- + HS^- \leftrightarrow FeS + CO_2 + H_2O$	R_{FeS}/R'_{FeS}	$R_{FeS} = k_{FeS}(\Omega_{FeS}-1)\delta(\Omega_{FeS}-1)$ $R'_{FeS} = k'_{FeS}[FeS](1-\Omega_{FeS})\delta(1-\Omega_{FeS})$ ** where $\Omega_{FeS} = \frac{[Fe^{2+}_{diss}][HS^-]}{K'_{FeS}[H^+]}$ *** and $[HS^-] = \frac{[TS]}{1+[H^+]/K'_{HS}}$
R15	$3Fe^{2+} + 2H_3PO_4 + 8H_2O \leftrightarrow Fe_3(PO_4)_2 * 8H_2O + 6H^+$	R_{viv}/R'_{viv}	$R_{viv} = k_{viv}(\Omega_{viv}^{\alpha}-1)\delta(\Omega_{viv}-1)$ $R'_{viv} = k'_{viv}[Fe_3(PO_4)_2](1-\Omega_{viv})\delta(1-\Omega_{viv})$ where $\Omega_{viv} = \frac{[Fe^{2+}]^3[P_{diss}]^2}{K'_{viv}}$ *** and $\alpha \approx 1/5$
R16	$xFe^{2+} + (1-x)Ca^{2+} + 2HCO_3^- \leftrightarrow Fe_xCa_{(1-x)}CO_3 + CO_2 + H_2O \quad (x=1)$	R_{FecO3}/R'_{FeCO3}	$R_{FeCO3} = k_{FeCO3}(\Omega_{FeCO3}-1)\delta(\Omega_{FeCO3}-1)$ $R'_{FeCO3} = k'_{FeCO3}[FeCO_3](1-\Omega_{FeCO3})\delta(1-\Omega_{FeCO3})$ where $\Omega_{FeCO3} = \frac{[Fe^{2+}][CO_3^{2-}]}{K'_{FeCO3}}$ ***
R17	$H_3PO_4 \leftrightarrow H_3PO_4(ads)$		see text
R18	$S-H^0 + Fe^{2+} + HCO_3^- \leftrightarrow S-Fe^+ + CO_2 + H_2O$		see text

	Acid Base reactions	Eqm const	Expression
	$CO_{2(aq)} + H_2O \leftrightarrow HCO_3^- + H^+$	K_{1C}	$K_{1C} = \frac{[H^+][HCO_3^-]}{[CO_2]}$
	$HCO_3^- \leftrightarrow CO_3^{2-} + H^+$	K_{2C}	$K_{2C} = \frac{[H^+][CO_3^{2-}]}{[HCO_3^-]}$
	$H_2S \leftrightarrow HS^- + H^+$	K'_{HS}	$K'_{HS} = \frac{[H^+][HS^-]}{[H_2S]}$
	$H_2O \leftrightarrow H^+ + OH^-$	K_W	$K_W = [H^+][OH^-]$

* K_i = Monod constant for species i
K_j^{inh} = inhibition constant from previous (more favorable) electron acceptor j.
** $\delta(x) = 1$ for $x > 0$ and $\delta(x) = 0$ for $x \leq 0$.
***K_X is solubility product

Table 3.3 : Parameters and their canonical values

Parameter	Value	Units	References
L	10	Cm	--
ρ	2.5	g cm^{-3}	
φ	0.8	-	Roden 1997, Boudreau 1997
u	0.2	cm yr^{-1}	
z (P:C)	0.005	-	Hecky 1993
K_{OM}	0.9	yr^{-1}	
K_{O2}	$2.0x10^{-10}$	mol cm^{-3}	Van Cappellen 1996, Dittrich 2004
K_{SO4}	$4.0x10^{-7}$	mol cm^{-3}	Katsev 2004, Van Cappellen 1996
$K_{Fe(OH)3}$	$2.0x10^{-5}$	mol g^{-1}	Katsev 2004, Van Cappellen 1996, Dittrich 2004
k_{FeOx}	$0.35x10^{11}$	cm^3 mol^{-1} yr^{-1}	Van Cappellen 1996
k_{Sox}	$1.6x10^{8}$	cm^3 mol^{-1} yr^{-1}	Van Cappellen 1996
k_{SFe3}	$3.65x10^{7}$	cm^3 mol^{-1} yr^{-1}	Katsev 2004, Wijsman 2002, Fossing 2004, Meysman 2003
k_{sviv}	$1.0x10^{7}$	cm^3 mol^{-1} yr^{-1}	
k_{SFeCO3}	$1.0x10^{7}$	cm^3 mol^{-1} yr^{-1}	
k_{FeSOx}	$2.0x10^{10}$	cm^3 mol^{-1} yr^{-1}	Van Cappellen 1995, Hunter 1998
k_{FeSFe3}	0	g mol^{-1} yr^{-1}	
k_{FeSHS}	$1.0x10^{6}$	cm^3 mol^{-1} yr^{-1}	Meysman 2003 , Rickard 1997
K_{surFe}	$1.25x10^{10}$	cm^3 mol^{-1} yr^{-1}	
k_{FeCO3}	$4.5x10^{-4}$	mol g^{-1} yr^{-1}	Van Cappellen 1996
k'_{FeCO3}	0.25	yr^{-1}	Van Cappellen 1996
K'_{FeCO3}	$4.0x10^{-15}$	$(mol\ cm^{-3})^2$	
k_{viv}	$1.7x10^{-9}$	mol g^{-1} yr^{-1}	Katsev 2004
k'_{viv}	1.0	yr^{-1}	
K'_{viv}	$3.0x10^{-50}$	$(mol\ cm^{-3})^5$	Davison 1993
k_{FeS}	$4.0x10^{-5}$	mol g^{-1} yr^{-1}	Van Cappellen 1996, Hunter 1998
k'_{FeS}	$1.0x10^{-3}$	yr^{-1}	Van Cappellen 1996
K'_{FeS}	$2.51x10^{-6}$	mol cm^{-3}	Morse 1987
K'_{C1}	$8.95x10^{-10}$	mol cm^{-3}	
K'_{C2}	$5.22x10^{-13}$	mol cm^{-3}	
K'_{HS}	$1.5x10^{-10}$	mol cm^{-3}	
K_w	$1.85x10^{-21}$	$(mol\ cm^{-3})^2$	
K^*_{FeonFe}	$4.5x10^{-3}$	-	
K^*_{FeonB}	$1.0x10^{-5}$	-	
K^*_{PonFe}	$6.0x10^{-2}$	-	
K^*_{PonB}	$1.0x10^{-5}$	-	
$S_{TFe}(1-\gamma_{Fe})$	$1.0x10^{-2}$	mol g^{-1}	
$S_{TB}(1-\gamma_B)$	$4.0x10^{-6}$	mol g^{-1}	
D_b^0	10	cm^2 yr^{-1}	Boudreau 1997

Chapter 4

Factorial Tests of Model Parameters

As shown in the previous chapter, the resulting numerical model is a multi-variable system controlled by many parameters. The first goal of the project was to use the model as an exploratory tool to search for the range of behaviors it would predict. We effectively wanted to simulate different hypothetical lake conditions and observe how the chemistry of such hypothetical environments would respond. Thus we performed a coarse scan of the parameter space of our model and looked at the outputs generated.

In order to ascertain the possible range of behaviors, a global sensitivity analysis (Tromp et al., 1995) was performed in parameter space. Nineteen parameters were chosen from the model, their values were varied, and the resulting outputs were recorded. The variations of model parameters was systematic, following a two-level factorial design (Montgomery 2001) as described below. For each realization of the factorial tests, 15 steady state chemical profiles were recorded. These are summarized in Appendix 1. Once the data was collected, some statistical and numerical analysis was performed in order to

extract relationships amongst the chemical profiles as well as between model parameters and the output. These findings are also given in this chapter.

4.1 Factorial Experiment Design

In each complete trial or replication of a factorial design, all possible combinations of factors are investigated. Thus if there are A factors each having B possible values, a full factorial design requires that there be B^A experiments each with a different combination of factor levels. The main effect of a given factor is then assessed by the change in the response produced by a change in the value of the factor.

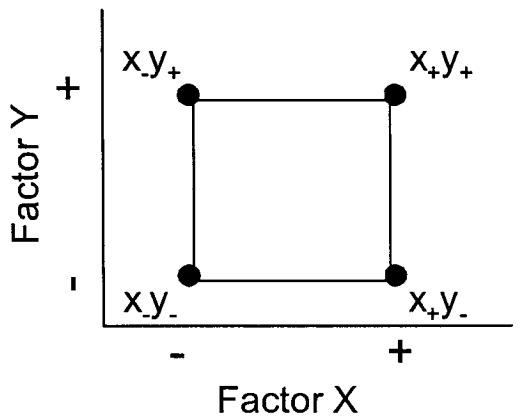

Figure 4.1 – Illustration of 2 level factorial design for 2 parameters X and Y. Four experiments are required, combining the high (+) and low (-) levels of each parameter.

For example, in a simple experiment constituting of two factors (X, Y) each having two levels (+ , -) there are $2^2 = 4$ experiments combining both levels of both factors (see figure 4.1). The effect of factor X can then be expressed as the difference between the average response at the high level of X minus the average response at the low level of X:

$$\text{Effect } (X) = (x_+y_+ + x_+y_-)/2 \; - (x_-y_+ + x_-y_-)/2 \qquad \textbf{(4.1)}$$

and similarly for the effect of Y. In the event of interaction between the factors, the response is different between the levels of one factor for different levels of the other. For example factor X can have a positive effect at low levels of Y but a negative effect at high levels of Y. Here positive effect is defined as an increase in the response function with an increase in the factor value and the reverse for negative effect. In such cases, the measure of the interaction effect can be expressed as the average difference between the effects of one factor at different levels of the other factor:

$$\text{Effect } (XY) = ((x_+y_+ - x_-y_+) - (x_+y_- - x_-y_-))/2 \qquad \textbf{(4.2)}$$

This rationale can be extended to compute interactions between many factors. If multiple realizations of each experiment are made, the average result for each factor combination is taken. For the purposes of the factorial trials used in the course of this project there was one replication of each experiment.

4.2 Summary of Factorial Trials

For the purposes of our investigation, six two-level factorial tests were constructed. We grouped the model parameters being investigated (19 in total) in sets of 6 (or 5). The choice to create multiple groups of fewer parameters was intended for manageability of the data set. Varying all 19 parameters simultaneously would yield a response set too bulky to manage with the statistical software available. In choosing how to organize the groups of parameters, i.e. which parameters to interpermute, the grouping was performed by 'theme'. Each factorial test set combined parameters influencing a particular process in sediments (See Table 4.1). The themes of interest were: parameters affecting iron processes, parameters affecting organic matter, parameters affecting vivianite, parameters affecting sorption and others. Certain model parameters (particularly the boundary conditions) were included in more than one trial either because they influenced more than one process under investigation or for comparison purposes.

The range over which the parameters could vary was estimated based on a recent review of geochemical data (Katsev et. al. submitted). The dSED database (Katsev et al. 2004) was mostly used to identify the range of values reported for process parameters, such as kinetic rate constants. From the set of all values reported for different transport or chemical variables, the highest and lowest were chosen as limiting values. Therefore the high and low levels of a parameter in our tests corresponded to the highest and lowest values reported in the literature for similar environments. These values are given in Table 4.1. Additionally a central set of values, termed the canonical case, was assigned which

Table 4.1: Varied parameter values for factorial experiments

Trial #	Theme	Parameters Varied											
		$Fe(OH)_3$ Flux at SWI (*FluxtopFeOH3*) mol cm-2 yr-1		$[SO_4^{2-}]$ at SWI (*XtopSO4*) mol cm-3		Viv formation rate constant (*Kviv*) mol g-1 yr-1		Viv dissolution rate constant (*K'viv*) yr-1		Vivanite scavenging by Sulfide rate constant (*Ksviv*) cm3 mol-1 yr-1		Siderite scavenging by sulfide rate constant (*KsFeCO3*) cm3 mol-1 yr-1	
	Vivianite	High	Low	High	Low	High	Low	High	Low	High	Low	High	Low
1	formation	7.0E-05	1.3E-05	5.0E-07	1.0E-08	3.0E-09	1.0E-10	1.0E+01	1.0E-01	1.0E+08	0.0E+00	1.0E+08	0.0E+00
		$Fe(OH)_3$ Flux at SWI (*FluxtopFeOH3*) mol cm-2 yr-1		$[O_2]$ at SWI (*XtopO2*) mol cm-3		$[SO_4^{2-}]$ at SWI (*XtopSO4*) mol cm-3		Dissolution of iron oxides by monosulfide rate constant (*KFeSFe3*) g mol-1 yr-1		Bioturbation at the SWI (*Dbmax*) cm2 yr-1		Phosphorus sorption on iron oxides constant (*KPonFe*)	
		High	*Low*	*High*	*Low*	*High*	*Low*	*High*	*Low*	*High*	*Low*	*High*	*Low*
2	Sorption	7.0E-05	1.3E-05	1.5E-07	0.0E+00	5.0E-07	1.0E-08	1.0E+04	0.0E+00	1.0E+01	1.0E+00	1.0E-01	2.0E-02
		Organic Matter Flux at SWI (*FluxtopG*) mol cm-2 yr-1		$Fe(OH)_3$ Flux at SWI (*FluxtoFeOH3*) mol cm-2 yr-1		$[O_2]$ at SWI (*XtopO2*) mol cm-3		$[SO_4^{2-}]$ at SWI (*XtopSO4*) mol cm-3		Organic matter degradation rate constant (*KG*) yr-1			
	Organic	*High*	*Low*	*High*	*Low*	*High*	*Low*	*High*	*Low*	*High*	*Low*		
3	Matter	5.0E-03	1.3E-03	7.0E-05	1.3E-05	1.5E-07	0.0E+00	5.0E-07	1.0E-08	3.0E-01	9.0E-01		
		$Fe(OH)_3$ Flux at SWI (*FluxtopFeOH3*) mol cm-2 yr-1		$[SO_4^{2-}]$ at SWI (*XtopSO4*) mol cm-3		Dissolution of iron oxides by monosulfide rate constant (*KFeSFe3*) g mol-1 yr-1		Dissolution of iron oxides by sulfide rate constant (*KSFe3*) cm3 mol-1 yr-1		Iron sorption on iron oxides constant (*KFeonFe*)		Iron sorption on background constant (*KFeonB*)	
		High	*Low*	*High*	*Low*	*High*	*Low*	*High*	*Low*	*High*	*Low*	*High*	*Low*
4	Iron	7.0E-05	1.3E-05	5.0E-07	1.0E-08	1.0E+04	0.0E+00	3.0E+08	3.0E+02	1.0E-02	5.0E-04	5.0E-05	5.0E-06
		Pyrite formation (*KFeSHS*) cm3 mol-1 yr-1		Vivianite formation rate constant (*Kviv*) mol g-1 yr-1		Bioturbation profile curvature parameter (*DbCurv*) cm		Sedimentation velocity (*U*) cm yr-1		Phosphorus sorption on iron oxides constant (*KPonFe*)		Phosphorus sorption on background constant (*KPonB*)	
	Phosporus sorption and	*High*	*Low*	*High*	*Low*	*High*	*Low*	*High*	*Low*	*High*	*Low*	*High*	*Low*
5	other	1.0E+10	0.0E+00	3.0E-09	1.0E-10	5.0E-01	2.0E-01	3.0E-01	1.0E-01	1.0E-01	2.0E-02	5.0E-05	5.0E-06
		$[O_2]$ at SWI (*XtopO2*) mol cm-3		Pyrite formation (*KFeSHS*) cm3 mol-1 yr-1		Vivianite formation rate constant (*Kviv*) mol g-1 yr-1		Bioturbation at the SWI (*Dbmax*) cm2 yr-1		Sedimentation velocity (*U*) cm yr-1			
		High	*Low*	*High*	*Low*	*High*	*Low*	*High*	*Low*	*High*	*Low*		
6		1.5E-07	0.0E+00	1.0E+10	0.0E+00	3.0E-09	1.0E-10	1.0E+01	1.0E+00	3.0E-01	1.0E-01		

represented typical values of all the model parameters. The canonical case was also constructed from the same database and included values which fall between the high and low level. In some cases the canonical value of a parameter is the same as either the high or low levels, if those were deemed most likely to occur. The canonical values for the model parameters were given in Chapter 3 (Table 3.3).

For each factorial test group of six parameters, their high and low levels were inter-permuted with those of the other parameters in the group (an extrapolation of the combination illustrated in figure 4.1). Thus, each test set comprised $2^6 = 64$ (or $2^5 = 32$) total combinations of parameters, therefore 64 runs and, as such, 64 realizations of each chemical species. For each parameter under investigation, half the test runs (32) included its low level value and half included its high level value. All model parameters which were not specifically investigated were kept at their canonical value throughout the 64 runs.

4.3 Output

4.3.1 Profiles

For each realization, 15 chemical profiles were outputted. There were 6 group tests performed (4 with 6 parameters varied and 2 with 5 parameters varied) leading to a total of 320 steady state realizations. Thus a total of 4800 chemical profiles were generated.

The chemical profiles obtained from all the factorial runs are summarized in Appendix 1. Each factorial test set (as specified in Table 4.1) is displayed individually. For each test set, the output of the 15 different species is shown on 3 pages:

Page 1: Iron bearing species

- aqueous iron (*Fe2+*)
- Iron oxihydroxides (*FeOH3*)
- Iron monosulfide (*FeS*)
- Pyrite (*FeS2*)
- Vivianite (*Viv*)

Page 2: Acidity related species

- Acidity (*pH*)
- Adsorbed phosphate (*adsorbed P*)
- Total aqueous sulfur (*TS*)
- Total carbonate (*TC*)
- Organic matter (*OM*)

Page 3: Other dissolved species

- Oxygen (*O2*)
- Sulfate (*SO4*)
- Dissolved phoshpate (*H3PO4*)
- Nitrate (*NO3*)
- Methane (*CH4*)

In order to meaningfully display the data for each group test, it was deemed pertinent to group the profiles by parameter value. Thus all profiles for a high value of a given parameter are displayed together; all profiles for low value are displayed on a separate adjacent plot. Appendix 1 is thus a complete visual representation of all the results obtained through the factorial analysis of the reaction transport model.

The next step was to visually observe all the profiles and identify the range of their behavior. In many cases, characteristic shapes emerged for a given chemical species. Some species showed little or no variation in behavior (*CH4, NO3, SO4, O2*). Species such as iron hydroxides (*FeOH3*), total carbonate (*TC*), pH, while exhibiting some quantitative variation in profile ranges (shifts in the absolute values of concentrations), did not show any real change in profile shapes. Other chemical species however, varied noticeably in their shape characteristics depending on the imposed parameters. Examples are aqueous iron (*Fe2+*), iron monosulfide (*FeS*), pyrite (*FeS2*), dissolved (*H3PO4*) and adsorbed phosphate (*adsorbed P*), total aqueous sulfur (*TS*) and vivianite (*Viv*). These chemical species could vary both in scale (absolute concentrations) and in shape. Some of these qualitative observations of the factorial test outputs extracted in Appendix 1 are summarized in Table 4.2.

Table 4.2 – Summary of profile characteristics of Appendix 1.

Chemical species	Typical profile characteristics	Qualitative difference(s) between profiles
Dissolved iron	• Peak near the top • Depletion at depth (not always)	• In some cases, continuous accumulation at depth • In some cases, slight depletion • In some cases, drastic depletion to near 0 at depth
Iron oxihydroxides	• Depletion near 0 within top 2 cm of sediment	• In some cases, conc. at SWI higher than others
Iron monosulfide	• Accumulation over in top cm	• In some cases, depletion below 1 cm occurs • In some cases, continued accumulation below 1 cm • In some cases, profile is flat • Below 7 cm some profiles see pronounced increase, others pronounced decrease, others neither
Pyrite		• Some profiles flatten or plateau quickly • Some profiles experience depletion over depth of sediment • Some profiles experience accumulation over depth of sediment
Vivianite	• Monotonous straight profile	• In some cases, accumulation in the top centimeters • In some cases, depletion in bottom half of sediment
Adsorbed phosphate	• Peak in top cm of sediment • Accumulation with depth	• In some cases, partial or total depletion of adsorbed phosphate at depth
pH	• Monotonous profile • pH decreases with depth to a plateau value	• Plateau value varies
Total aqueous sulfur	• Peak near top of sediment	• In some cases, profile plateaus after top few centimeters • In some cases, show partial depletion at depth • In some cases, show total depletion at depth
Total carbonate	• Accumulation in depth to a plateau	• Plateau shifts under different conditions
Organic matter	• Continuous depletion with depth	• SWI concentration varies • Rate of depletion varies
Dissolved Phosphate	• Concentration accumulates with depth until it reaches a plateau	• Some profiles deplete at depth after the initial accumulation • In some cases, depletion is partial • In some cases, depletion is complete
Oxygen	• Depletes quickly below the SWI	• Concentration at the SWI varies
Sulfate	• Concentration depletes at the top centimeters of sediment	• Concentration at the SWI varies
Nitrate	• Depletes quickly below the SWI	• Concentration at the SWI varies
Methane	• Concentration accumulates gradually until a plateau is reached	• Plateau value changes slightly

4.3.2 Statistics and correlations

For a quantitative assessment of the effect of various parameters on chemical profiles to be possible, it was convenient to represent the continuous profiles in the form of a single value, termed a response function (RF). Such response functions can then be used to find statistical relationships between the different profiles as well as between profiles and model parameters (i.e. sedimentary conditions). The choice of response functions is therefore critical in being able to assess the behavior of chemical species, as they represent that behavior. The response functions outlined below were extracted from the factorial tests data for 11 of the 15 chemical species recorded (Appendix 1). Oxygen, sulfate, nitrate and methane profiles were not sampled because their profiles did not show any noticeable or interesting variations. Upon examination of the profiles, three different types of response functions were selected to reflect the profile features we observed:

- **Maximum concentrations (over the depth of the simulated sediment)**: these were chosen to exemplify the scale of the concentration of a given species in the sediment profile. Maximum concentrations would reflect any drastic changes in the presence of chemical species. These response functions were extracted for 11 chemical species, namely all species listed in Appendix 1 except sulfate, methane, nitrate and oxygen.

- **Bottom (or buried) concentrations (i.e. concentrations in the deepest part of the simulated sediment)**: these were chosen to reflect the amount of material

getting buried in the sediment, thus showing the sediment's retention capacity. These response functions were extracted for the same 11 chemical species.

- **Ratio of maximum concentrations within a certain depth interval to buried concentrations**: these were chosen to reflect shape features observed in certain chemical profiles, such as tendencies to accumulate, plateau or deplete throughout the sediment. These were applied to only 3 dissolved chemical species of interest, which exhibited a varied behavior:
  - Aqueous iron: maximum concentration in top 3 cm / bottom concentration
  - Total aqueous sulfur: maximum concentration in top 1.5 cm / bottom concentration
  - Dissolved phosphate: maximum concentration in top 7 cm / bottom concentration

The depth range over which maxima were sampled varied from species to species. These ranges were individually chosen for each chemical species based on the profile characteristics. They were chosen in order to capture features in the profiles such as local maxima which would not have been otherwise registered because of subsequent accumulation in the profile. The shape response functions were chosen to capture the relationship between the presence of a species and its retention. Three possible regimes can be established from such ratios. When the concentration depletes with depth, the ratio is a value larger than one. When the concentration plateaus at depth the ratio is very nearly 1. When there is continued accumulation, the ratio is smaller than 1.

Figure 4.2 gives a summary of the distributions of the first two response functions described above. The distributions are different for the various species and often there is clustering or values and separation between clusters. This may not necessarily be an indication of the presence of forbidden regions for the response function however. The sampling of parameter values was very coarse and the ranges spanned different from parameter to parameter, thus the clustering and segregation observed in the response function histograms could be an artifact of the sampling. Most response functions, with the exception of perhaps pH, did not have a normal distribution (Gaussian). There were some groupings of results with higher frequency of occurrence than others. There may therefore be preferential regimes in the chemical profiles. More complete uniform testing of the parameters would be necessary to confirm that.

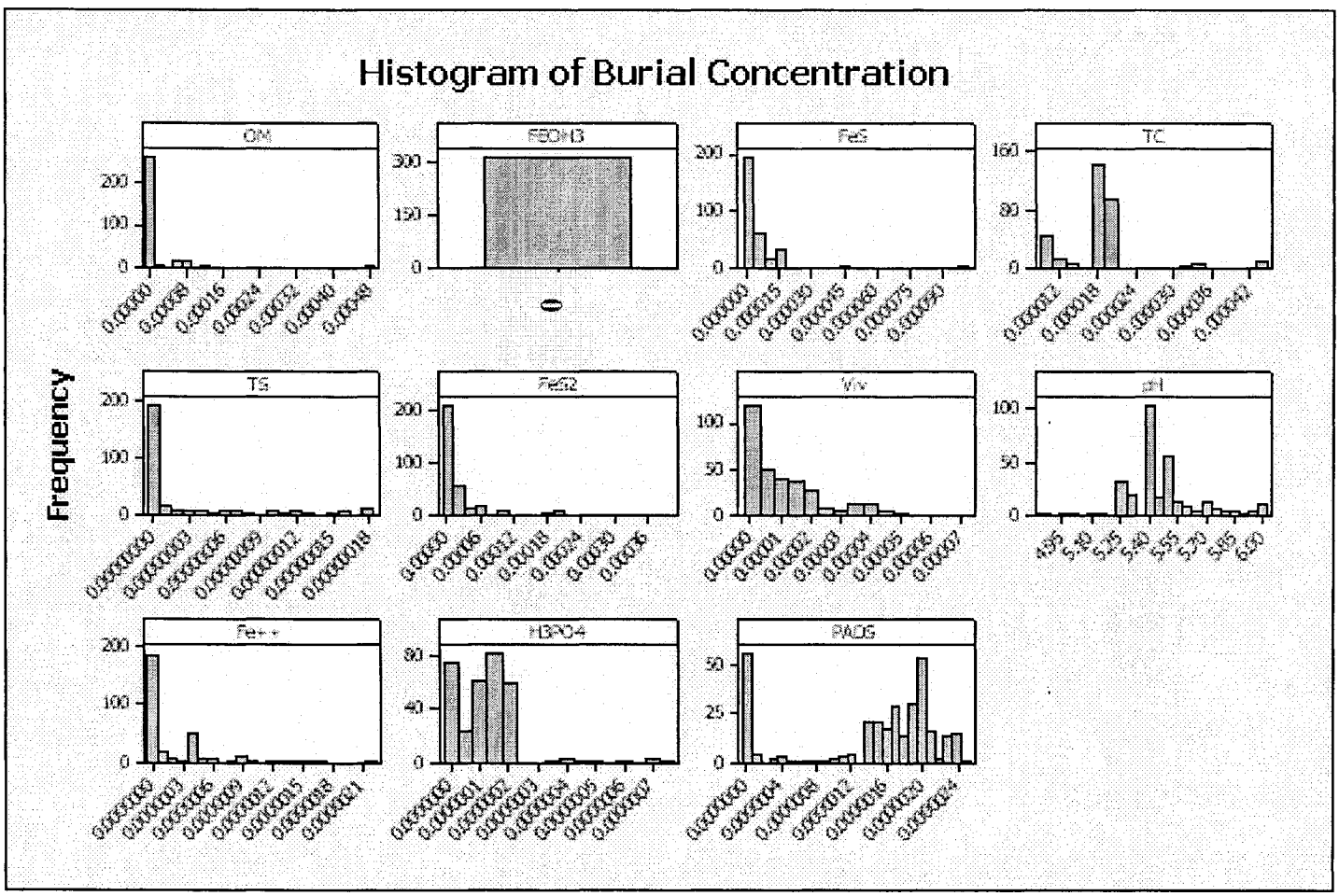
Histogram of Burial Concentration
Frequency
OM
FEOHB
FeS
TC
TS
FeS2
Fe++
HBPO4
PAOS

a)

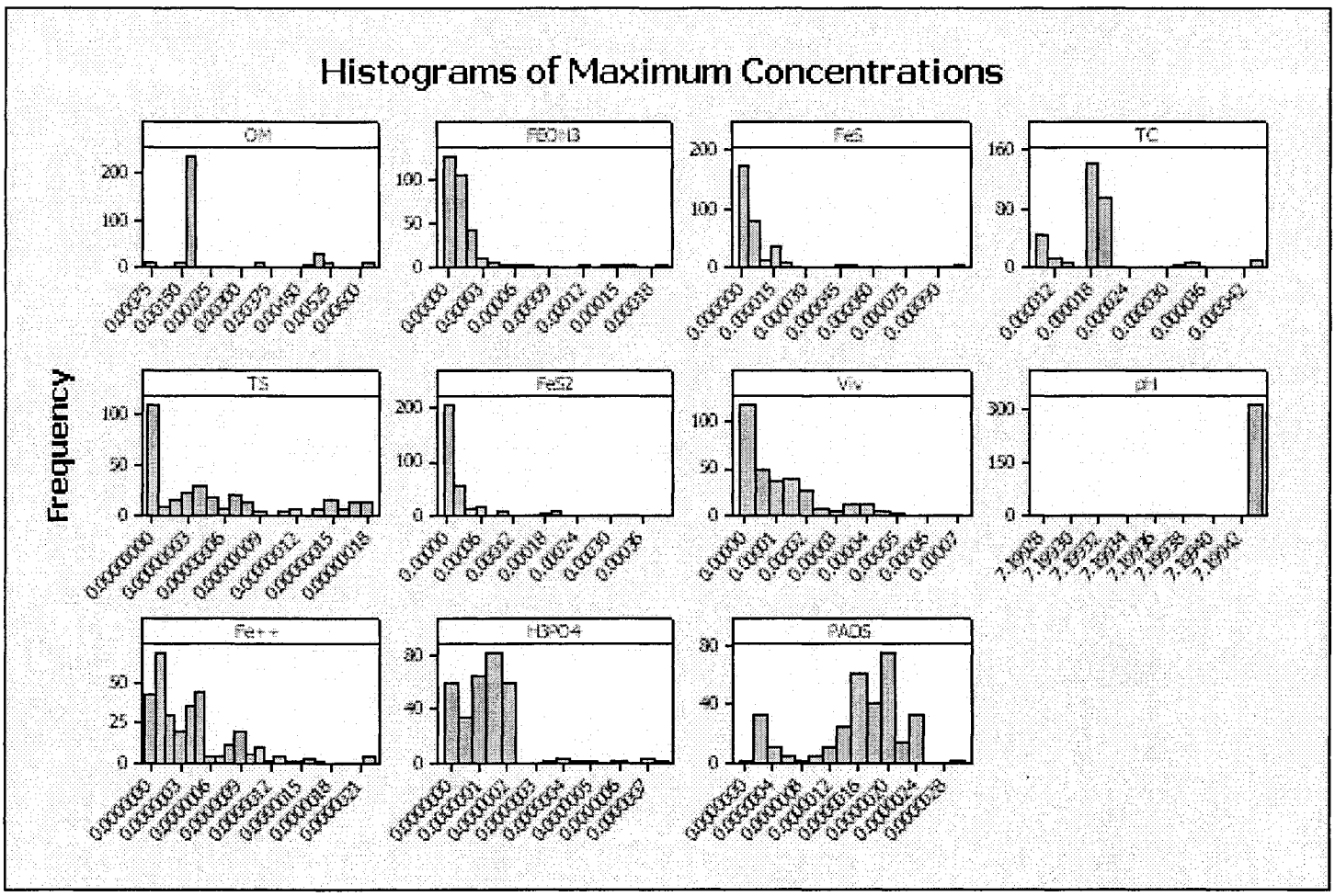

b)

Figure 4.2 – a) Distributions of the burial concentration of various chemical species. b) Distributions of the maximum concentration of chemical species. The units are mol/cm^3_{PW} for dissolved species and mol/g_{DS} for solid species.

In order to test for correlations between the different chemical profiles, covariance tables were calculated for the different groups of response functions. Covariance is a measure of the correlation in fluctuation of two different quantities. It is calculated as the sum over all trials of the deviation of one variable from the mean times the deviation of the other variable form the mean. In the context of our analysis, the covariances themselves are not very useful as they are highly dependent on the variance (spread) of the interacting species (which have a wide range). However, covariances can be normalized to the variance (square root of the standard deviation) of the interacting species. As such, a comparison of normalized covariances indicates which elements are more correlated than others. The covariances, scaled to the variances of the interacting species, for maximum concentrations, burial concentrations and shape response functions are given in Figure 4.3. Also the sign of the covariance gives an indication of the nature of the relationship (competitive or cooperative).

Another effective visual representation of the relationships and/or dependencies between profiles can be made by scatter plots of the same type response functions relative to each other. Figure 4.4 illustrates such scatter plots for the three groups of RFs. Relationships are apparent in several instances. Particularly interesting are the scatter plots of the dissolved concentrations of the species of interest namely dissolved iron, sulfur and phosphorus. There is a relationship between reduced sulfur and iron concentrations, as there is between sulfur and other iron bearing species (FeS, FeS_2, Vivianite). For low values of sulfur concentrations, high concentrations of iron bearing species can be observed, but not so for high values of sulfur and vice versa. There is a similar link

between dissolved iron and phosphorus in the pore water as well as phosphorus and iron bearing solids. Adsorbed phosphorus and sulfur also exhibit a relationship, where low values of adsorbed phosphate are not present for low sulfide concentrations. Notwithstanding a relatively high covariance, dissolved phosphorus and sulfur however, have a random distribution of values relative to each other. These observations seem to hold for both maximum and burial concentrations. It is also noteworthy that the correlation observed between adsorbed phosphate (PADS) and dissolved phosphate (H3PO4) merely reflects the Langmuir adsorption behaviour adopted in our model.

	OM	FEOH3	FeS	TC	TS	FeS2	Viv	Fe++	H3PO4	PADS
OM	1.000	-0.029	-0.022	0.679	-0.032	0.007	0.035	-0.059	0.543	0.167
FEOH3		1.000	-0.007	-0.113	-0.058	-0.040	0.018	0.256	-0.103	-0.173
FeS			1.000	-0.142	-0.135	-0.046	-0.028	0.112	-0.061	-0.151
TC				1.000	0.001	-0.054	0.086	-0.146	0.642	0.341
TS					1.000	-0.105	-0.359	-0.266	0.334	0.286
FeS2						1.000	0.089	0.002	-0.083	-0.050
Viv							1.000	0.315	-0.534	-0.707
Fe++								1.000	-0.364	-0.544
H3PO4									1.000	0.691
PADS										1.000

a)

	OM	FEOH3	FeS	TC	TS	FeS2	Viv	Fe++	H3PO4	PADS
OM	1.000	0.428	0.231	-0.009	0.042	0.067	0.027	-0.061	0.325	0.204
FEOH3		1.000	0.471	-0.304	-0.242	0.132	0.303	0.552	-0.292	-0.113
FeS			1.000	-0.157	0.029	0.002	-0.026	0.070	-0.007	0.121
TC				1.000	0.068	-0.071	0.076	-0.023	0.638	0.210
TS					1.000	-0.028	-0.484	-0.421	0.415	0.334
FeS2						1.000	0.097	0.028	-0.052	0.075
Viv							1.000	0.492	-0.503	-0.645
Fe++								1.000	-0.448	-0.556
H3PO4									1.000	0.625
PADS										1.000

b)

	TS	Fe	H3PO4	pH
TS	1.000	-0.115	0.449	0.104
Fe		1.000	-0.486	-0.410
H3PO4			1.000	0.492
pH				1.000

c)

Figure 4.3 – Covariance between (a) burial, (b) maximum concentrations and (c) shape response functions of chemical species. Values are normalized to the standard deviations of the row and column elements.

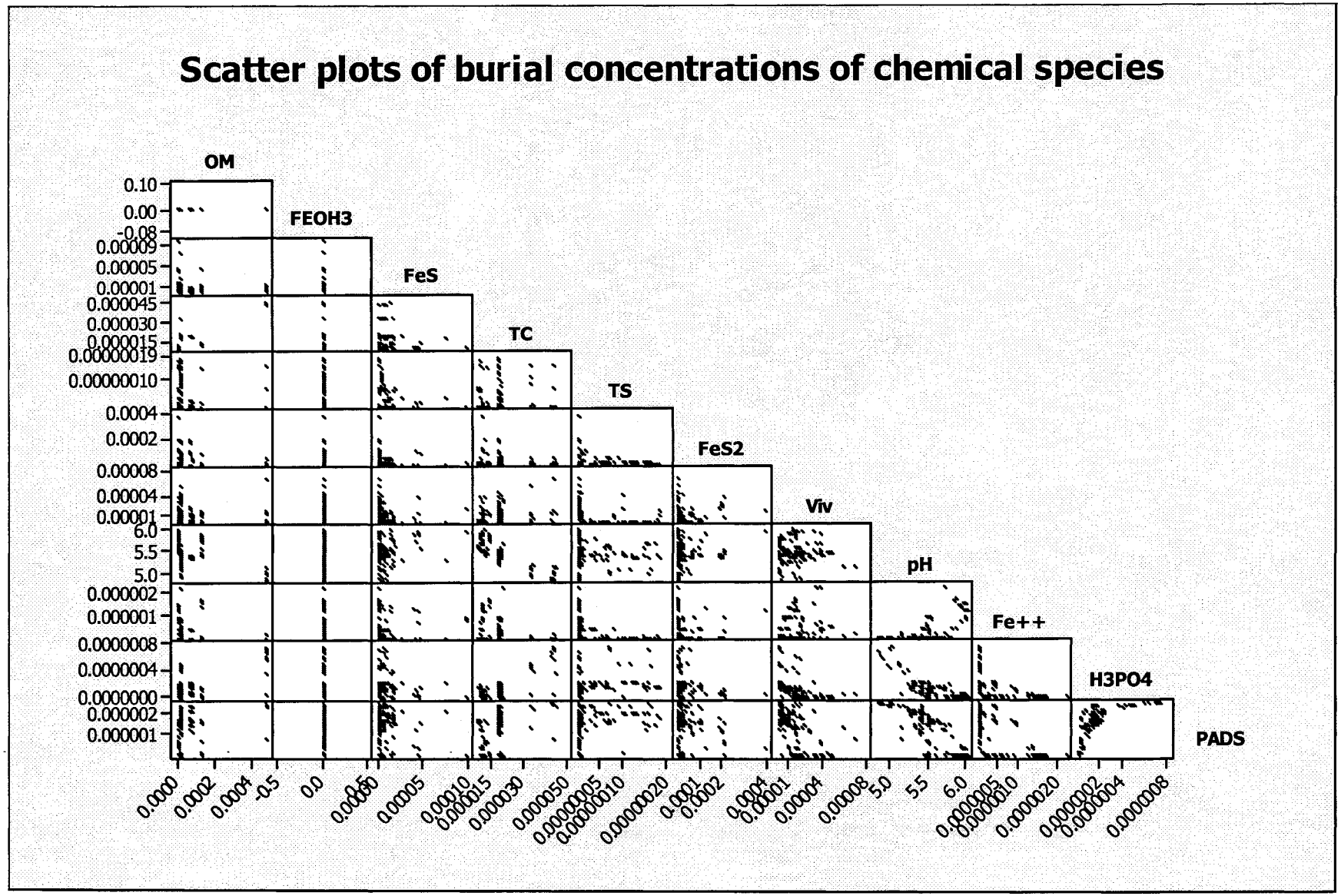
Scatter plots of burial concentrations of chemical species
OM
FEOH3
FeS
TC
TS
FeS2
Viv
pH
Fe++
H3PO4
PADS

a)

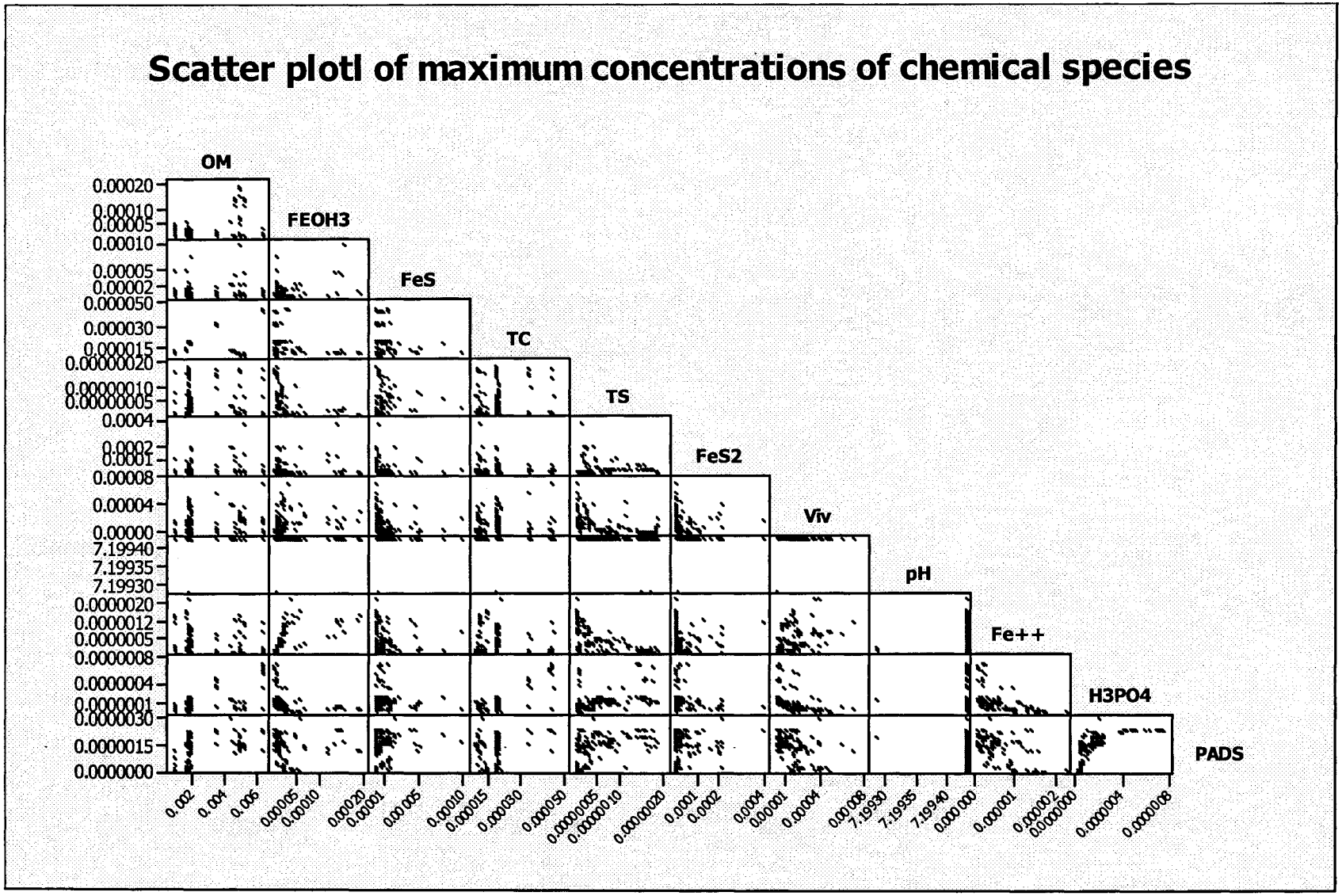
Scatter plotl of maximum concentrations of chemical species
OM
FEOH3
FeS
TC
TS
FeS2
Viv
pH
Fe++
H3PO4
PADS

b)

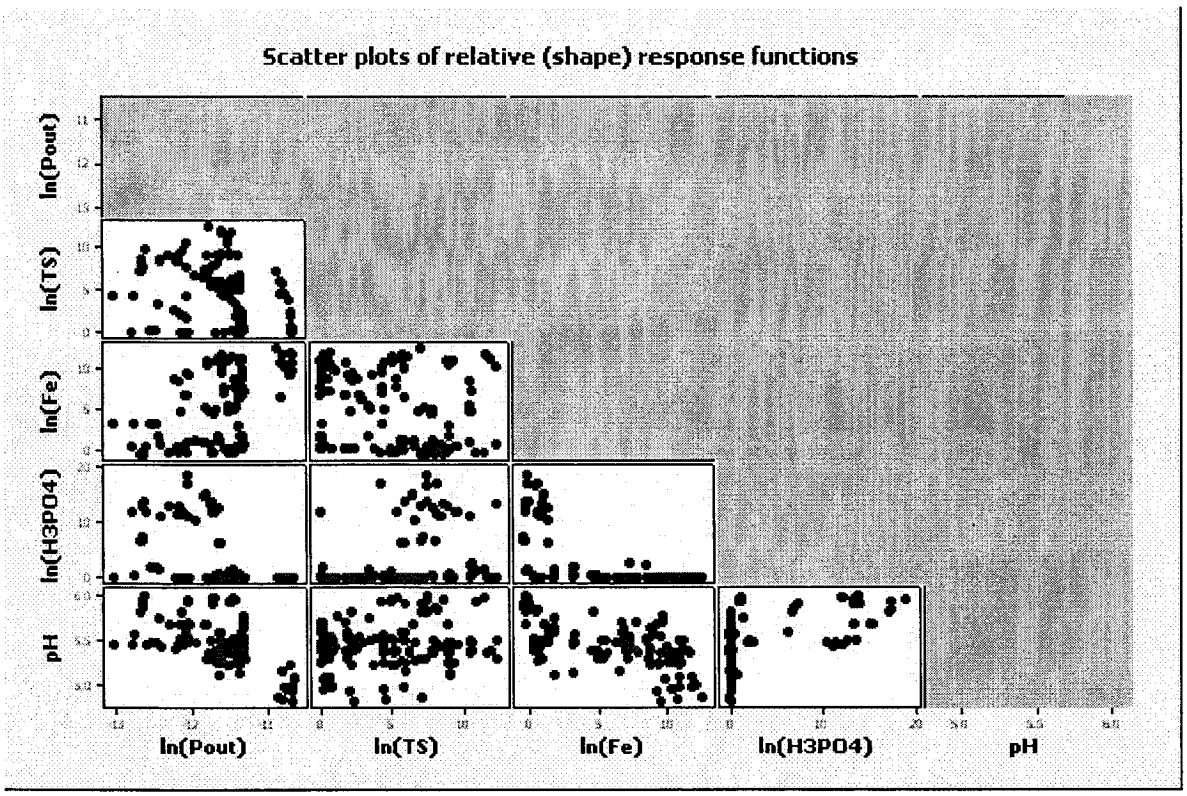

c)

Figure 4.4 – Scatter plots burial concentration response functions (a), maximum concentrations of response functions (b) and shape response functions (c). The shape response function displayed here is the natural logarithm of the shape response function defined earlier in the chapter. The logarithmic form is easier to represent and compare.

4.4 Factorial Analysis Results (Main Effects)

Once relationships between the outputs became apparent, we were led to investigate the relationship between output and model parameters. For that purpose, a factorial analysis was performed on the response functions extracted from the data, as explained above. Figure 4.5 illustrates the main effects of the model parameters from all 6 test groups (as outlined in Table 4.1) combined on the burial concentration and maximum concentration of the solutes of interest (iron, sulfur and phosphorus). The magnitude of the effects on these aqueous concentrations demonstrates the importance of boundary conditions (see chapter 3 for boundary condition definitions). The concentrations and fluxes at the sediment water interface (SWI) had the most significant impact on the concentrations of dissolved nutrients. These results are not surprising as the input of material from the water column (source) is expected to dictate the presence and abundance of major chemical species in our model. Other factors of importance were the rates of organic matter degradation and vivianite precipitation. These are also understandable as the reactions they regulate either generate or deplete the material of interest. The bioturbation parameters and the adsorption constant for phosphate on background solids came out as significant factors influencing these solute profiles as well. Another surprising result is the positive effect oxygen concentration has on the dissolved iron concentration. Oxygen is believed to favor the oxidized form of iron (iron oxihydroxides) which is indeed observed in the factor analysis that follows, yet it concurrently also increases reduced iron concentrations (*Fe2+*). This effect is investigated further in the following chapter.

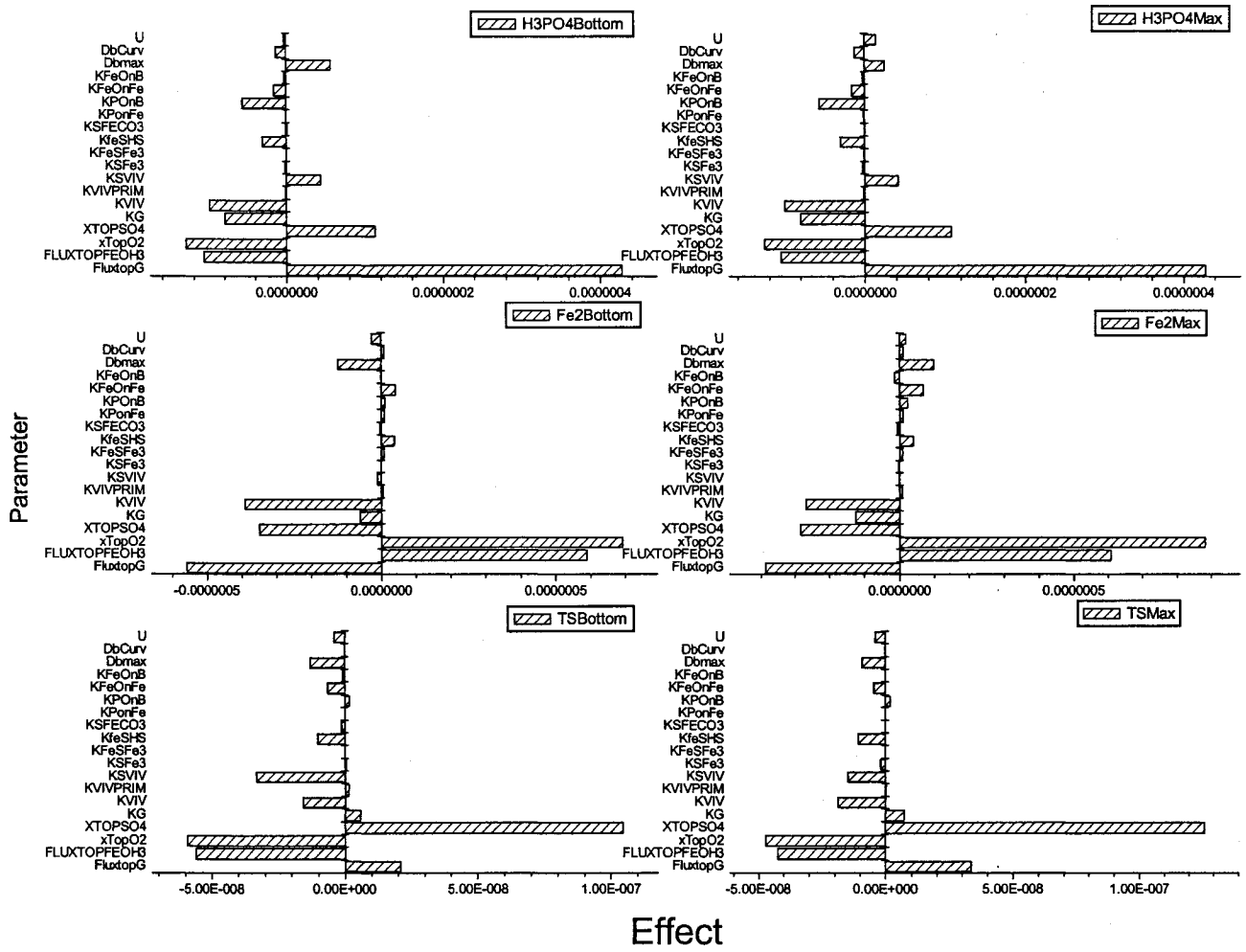

Figure 4.5 – First order (main) effects of model parameters on aqueous nutrient concentrations – dissolved Phosphate (*H3PO4*), dissolved Iron (*Fe2*) and dissolved Sulfide (*TS*). Left hand side plots represent effects on burial concentrations (denoted with Bottom suffix); right hand side plots represent effects on maximum concentrations (denoted with Max suffix). The units of the effect are the units of the species concentration.

Legend:

U – advection velocity
DbCurv – curvature of the bioturbation profile
DbMax – Bioturbation at the SWI
KFeOnB – adsorption constant for Iron on background solids
KFeOnFe – adsorption constant for Iron on Iron Oxihydroxides
KPOnB – adsorption constant for Phosphate on background solids
KPOnFe– adsorption constant for phosphate on Iron oxihydroxides
KSFeCO3 – dissolution of siderite by sulfide rate constant
KFeSHS – pyrite formation rate constant
KFeSFe3 – dissolution or Iron oxides by iron monosulfide rate
KSFe3 – dissolution of Iron oxides by sulfide rate constant
Ksviv – vivianite scavenging by sulfide rate constant
KvivPrim – dissolution of vivianite rate constant
Kviv – vivianite formation rate constant
KG – overall organic matter degradation rate constant
xtopSO4 – sulfate concentration at the SWI
xtopO2 – oxygen concentration at the SWI
fluxtopFeOH3 – flux of Iron oxihydroxides at the SWI
fluxtopG – flux of organic matter at the SWI

Figure 4.6 illustrates the main effects of the parameter on the solid iron-bearing species. Once again, the boundary conditions come out as the dominant factors. It is interesting however, that the effect of oxygen concentration at the SWI has an effect opposite from the expected one on the concentrations of vivianite and iron sulfides; oxygen increase is expected to induce a higher oxidized iron phase (ferrihydrite) and less reduced iron phases, but the observed effect of oxygen on reduced iron is different, although the effect on $Fe(OH)_3$ is indeed positive. For higher levels of oxygen, lower levels of reduced iron would be expected, thus reduced iron species are not thought to precipitate as much. This is potentially linked to the fact that an increase in oxygen has the effect of increasing the dissolved iron in the pore water as mentioned above. Finding the mechanism which causes oxygen to increase dissolved iron concentrations might explain the vivianite and iron sulfides behaviors as well since these species are dependent on aqueous iron through their respective precipitations reactions. Also the effect of the organic matter degradation rate (KG) is not well understood. These effects are examined in more detail in the following chapter. The reaction rates which seem dominant (among those tested) for this grouping of profiles are vivianite formation, vivianite scavenging by sulfide and pyrite formation. Once again, the transport parameters, namely advection velocity and bioturbation come out as significant factors, even more so than for dissolved species.

Figure 4.7 presents the effects on chemical concentrations of the remaining species, those related to acidity. The effects shown in this figure are those expected from the model reactions. The boundary conditions are again dominant. However, the importance of bioturbation comes through as in the previous cases.

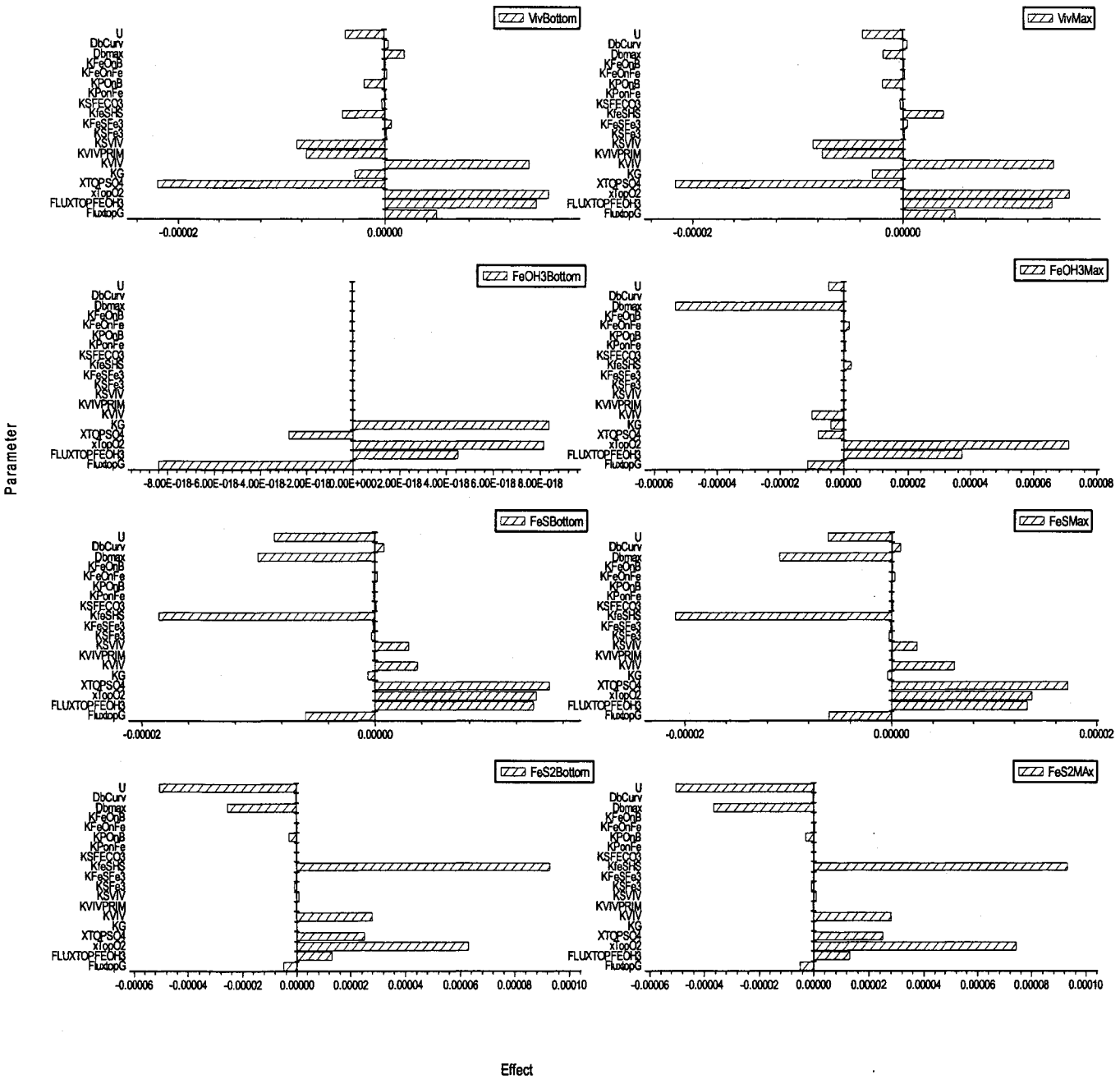

Figure 4.6 – First order (main) effects of model parameters on solid iron species concentrations – Vivianite (Viv), Iron Oxihydroxides (FeOH3), Iron Mononsulfide (FeS) and Pyrite (FeS2). Left hand side plots represent effects on burial concentrations (denoted with Bottom suffix); right hand side plots represent effects on maximum concentrations (denoted with Max suffix). Effect is in untis of species.

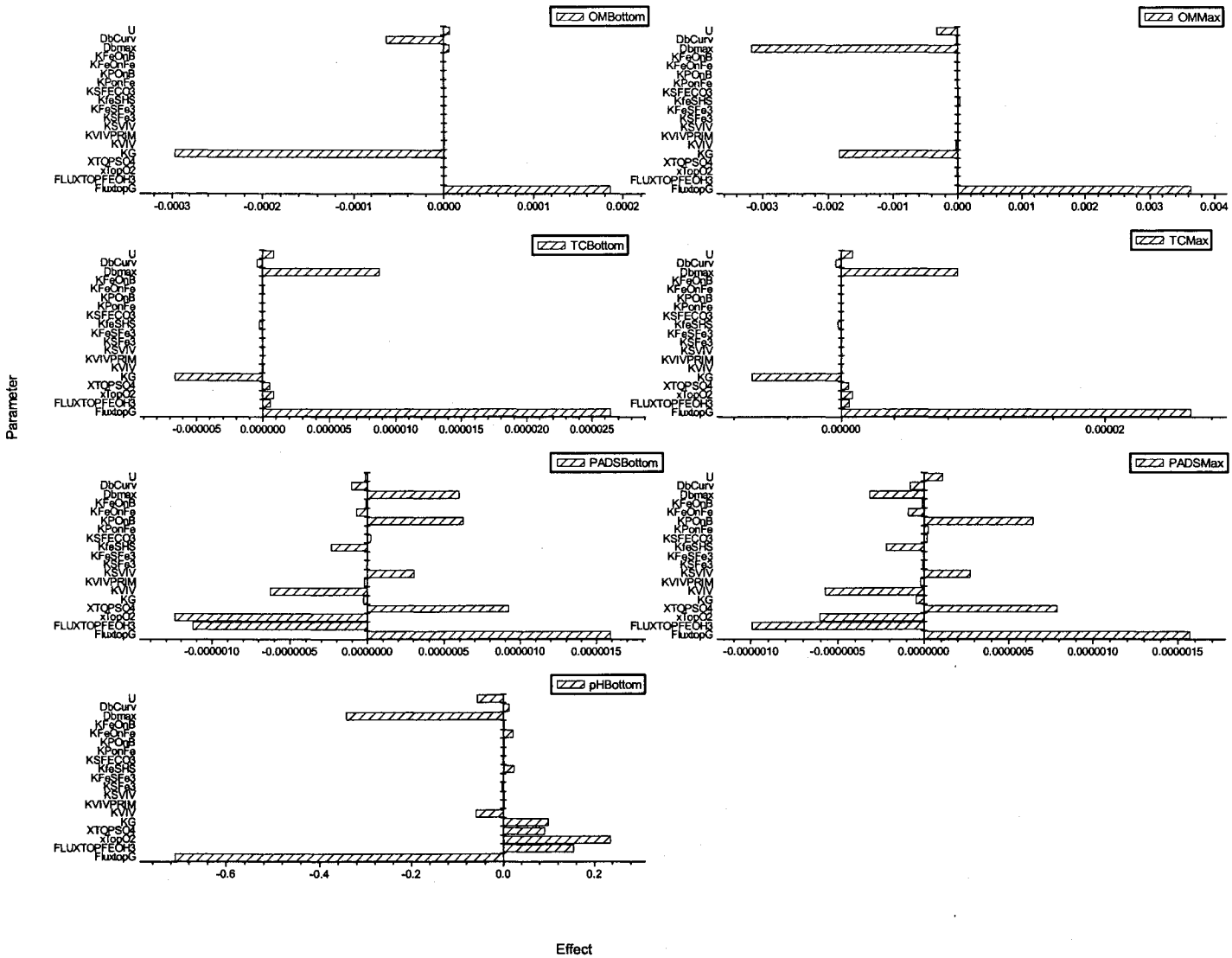

Figure 4.7 – First order (main) effects of model parameters on species concentrations – organic matter (OM), total carbonate species (TC), adsorbed Phosphate (PADS) and pH. Left hand side plots represent effects on burial concentrations (denoted with Bottom suffix); right hand side plots represent effects on maximum concentrations (denoted with Max suffix). Individual units depend on the chemical species in question, as in the previous figures.

Finally, Figure 4.8 illustrates the parameter effects on the shape response functions for the dissolved nutrient species (ratios between maximum and buried concentrations). While the boundary conditions are still very important, other parameter effects are comparable in magnitude, particularly the rates of vivianite precipitation and scavenging by sulfide and pyrite formation. Once again bioturbation and advection are shown to induce noticeable effects in the response functions.

The above findings point to a small group of parameters which consistently play an important role in shaping the chemical profiles in our hypothetical model sediments. The boundary conditions, but also bioturbation, advection and rate constants such as that for vivianite precipitation and vivianite dissolution by sulfide are important in determining the profiles characteristics of iron, sulfur and phosphorus. These reactions thus come across as the major link between the cycling of these three elements.

The factorial tests have thus given some insights into which parameters significantly influence the chemical behavior of sediments. In some cases the factors which came out as important are interesting such as the transport (bioturbation and advection) and adsorption (particularly of phosphate ions on background solids). They illustrate the importance of modeling physical and transport processes in sedimentary diagenesis, in addition to chemical inter-conversions. Some reactions did not show much influence over chemical concentrations but a select few, such as vivianite precipitation and scavenging, as well as pyrite formation were often significant. The intricacies of how such reactions interact to create the effects observed cannot be determined from the factorial tests.

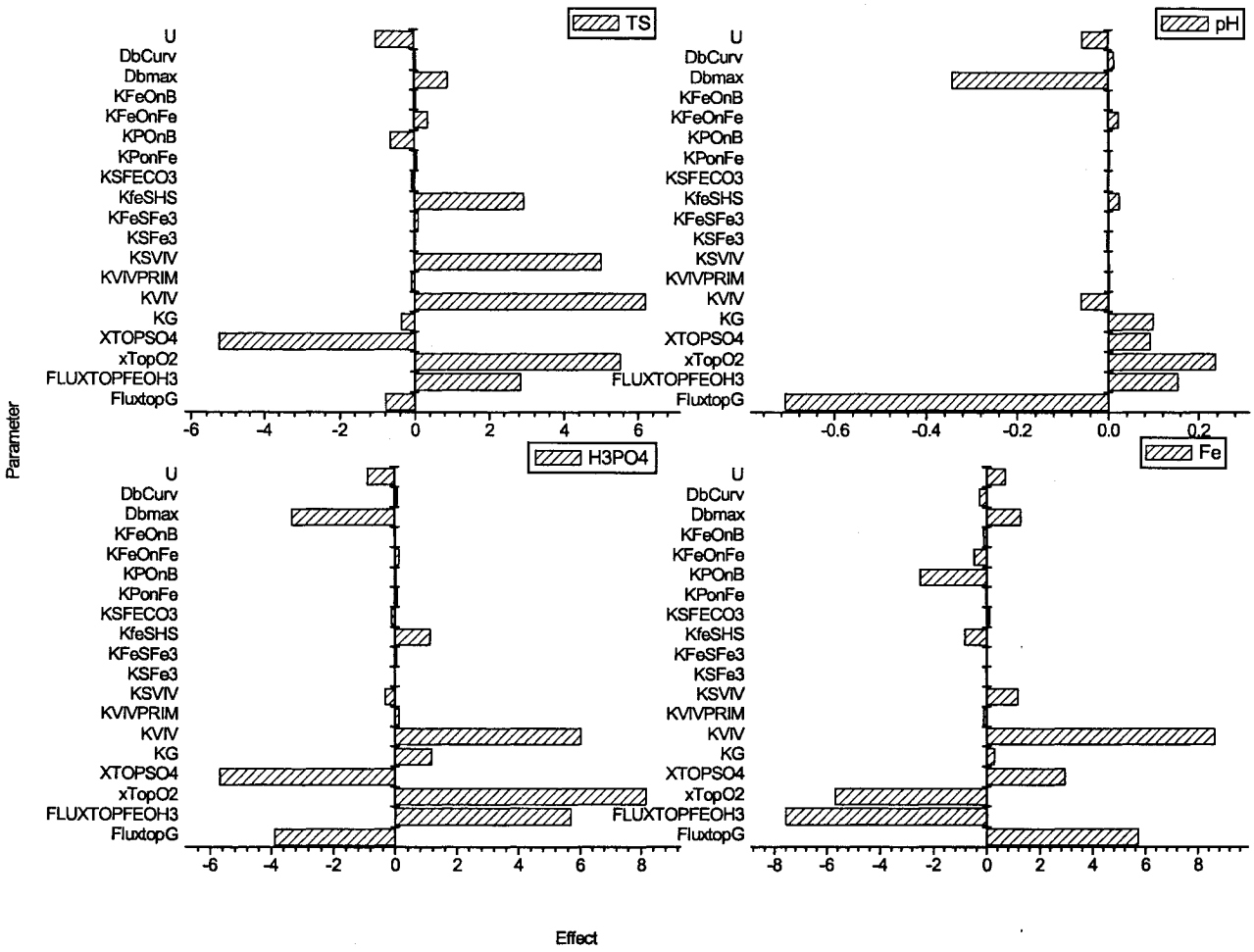

Figure 4.8 – First order (main) effects of model parameters on shape response functions (natural logarithm of the ratio between maximum and burial concentrations) for dissolved Sulfur (*TS*), pH, Dissolved phosphate (*H3PO4*) and dissolved Iron (*Fe*) concentrations. Again, effects are expressed in units corresponding to the chemical species in question.

Table 4.3 summarizes the factor effects on chemical concentrations and points to some of the interesting effects which require further elaboration. To ascertain those details of the model workings, one must take a closer look at the mechanisms at play and their interdependence. This is done in the next chapter. The factorial analysis has nevertheless given very useful information as to where to look in deconstructing the mechanisms at play. The above summarized results imply that a small group of reactions, though not necessarily the expected ones, plays a pivotal role in generating the chemical profiles observed. Thus a statistical overview of the data has given information about the chemistry and physical processes of sediments.

Table 4.3 – Summary of factor effects on maximum and burial concentrations.

RF	Fe2+		H3PO4		TS		FeO H3	FeS		FeS2		Viv		OM		TC	pH
Parameter	Max	Bur	Max	Bur	Max	Bur	Max	Max	Bur	Max	Bur	Max	Bur	Max	Bur	Max/ Bur	Bur
U	+	-	+	-	-	-	-	-	-	-	-	-	-	-	+	+	-
DbCurv	+	+	-	-	-	-	+	+	+	-	-	+	+	-	-	-	+
DbMax	+	-	+	+	-	-	-	-	-	-	-	-	+	-	+	+	-
KFeOnB	-	-	-	-	-	-	+	+	+	+	+	+	+	0	0	+	+
KFeOnFe	+	+	-	-	-	-	+	+	+	+	+	+	+	0	0	+	+
KPOnB	+	+	-	-	+	+	+	-	-	-	-	-	-	0	0	+	+
KPOnFe	+	+	-	-	+	+	+	-	-	-	-	-	+	+	-	+	+
KSFeCO3	-	-	+	+	-	-	-	+	+	+	+	-	-	-	-	-	-
KFeSHS	+	+	-	-	-	-	+	-	-	+	+	+	-	+	-	-	+
KFeSFe3	+	+	-	-	-	+	+	-	-	-	-	+	+	+	-	+	+
KSFe3	-	+	-	-	-	+	-	-	-	-	-	+	+	0	0	-	-
Ksviv	+	-	+	+	-	-	+	+	+	+	+	-	-	-	-	+	+
KvivPrim	+	+	-	-	+	+	+	-	-	-	-	-	-	-	-	+	+
Kviv	-	-	-	-	-	-	-	+	+	+	+	+	+	-	-	+	-
KG	~	~	~	~	≠	≠	~	~	~	≠	≠	~	~	-	-	-	+
xtopSO4	-	-	+	+	+	+	-	+	+	+	+	-	-	-	-	+	+
xtopO2	≠	≠	-	-	-	-	+	≠	≠	≠	≠	≠	≠	-	-	+	+
fluxtopFeOH3	+	+	-	-	-	-	+	+	+	+	+	+	+	≠	≠	+	+
fluxtopG	-	-	+	+	+	+	-	-	-	-	-	+	+	+	+	+	-

Note: The table shows the sign of the effects only. Entries highlighted in shadow represent difference in effect of the same factor on the maximum and burial concentrations of the same species. The italicized entries are interesting (not obvious) effects which warrant closer observation. Some of those effects will be examined further in the next chapter.

Chapter 5

Chemical Species: Depth Profiles and Formation Mechanisms

In the course of the systematic factorial runs outlined in Chapter 4 and illustrated in Appendix 1, it became noticeable that many chemical species had depth profiles with features which remained constant across the trials. In other words, even though the concentration distributions with depth for a given chemical species could vary quantitatively, they retained a similar behavior as the model parameters were varied. However, this was not always the case; in some instances a variation in input parameters would generate a qualitative change (also termed a regime change) in the depth profile. Most notably, some profiles would switch from accumulation of concentration at depth to depletion or vice versa. It was therefore interesting to examine some chemical profiles more specifically with respect to the parameters which factorial analysis suggested are likely to govern them. As a consequence of such an investigation, the reaction mechanisms which give rise to typical shapes of depth profiles could be determined. Also the critical points in parameter space which could affect the regime of a species could be identified.

As the chemical cycles considered through this model are mainly those of phosphorus, iron and sulfur, it was deemed useful to look at representative aqueous species of these elements (namely dissolved phosphate, dissolved iron and total aqueous sulfur) as indicators of chemical behavior.

In order to examine more closely the mechanisms from which profiles arise, i.e. the effects of reactions and species on profiles, a number of tests were performed whereby selected parameters were altered (individually) with respect to the canonical case defined in Chapter 3, to see their effect on the behavior of a particular chemical species. The factorial trials of the previous chapter were useful indicators of which model parameters were likely to have significant effects. Thus the parameters selected for testing in this chapter were the six or seven greatest effects demonstrated in the previous chapter. Each factor deemed important for a given chemical species, was varied (with it's high and low values the same as those of the factorial trials) individually in order to eliminate the interaction effects with other factors, alluded to earlier, which can mask or enhance the effect of individual parameters. The chemical profile resulting from the canonical case, as well as from each variation of the selected parameters were all plotted together to show the comparative effects of different factors.

In addition to these tests, and based on the information they provided, some additional mechanistic tests were performed. These involved turning chemical reactions in the model on or off to see how those reactions impact chemical profiles. These test runs were not systematic as in the factorial trials case. Rather they were chosen based on

speculation (guessing) as to which reactions were likely to be of influence. As such they will be detailed along with the results, where pertinent. For each chemical species under investigation, all reactions which produce or create that species were tested, by changing the reaction rate coefficients, to see the effect on its profile. Additionally, the depth distributions of the reaction rates were extracted as well, which proved useful in deciphering their influence on profiles. Often, features in the chemical profile of a given species could be linked to a reaction occurring at the corresponding depth or to another chemical species appearing or disappearing. Sometimes there was an interplay observed between several mechanisms which combined to give an observed effect, but often an individual dominant mechanism could be assigned as the driving force behind a particular feature.

The sediment depth, for many of the runs reported here was changed to 18 cm as opposed to 10 cm which was the case for the factorial trials reported in the previous chapter. An 18 cm depth further ensures a zero diffusive flux at the bottom boundary, which ensures no distortion of the profile shapes. While most chemical species can reach a constant (or very nearly constant) concentration by 10 cm of depth, and this depth is not very computationally expensive, the runs performed for this chapter were not as numerous as for the previous chapter. Thus, a deeper sediment could be modeled (i.e. longer simulations). Given the numerical constraints, a depth of 18 cm was found to be optimal, since most chemical species were equilibrated by that depth and computation time was not greatly affected. Some tests were performed to compare the depth profiles at 10cm ,

18 cm, 20 cm, and 40 cm deep sediments without great variations in the scales and profile shapes.

In this chapter the term "representative profiles" refers to those generated by the canonical set of parameters as outlined in Chapter 3. Whenever qualitative deviations from the representative profiles occur, they are noted along with the factors correlated to that change.

5.1 Phosphate

5.1.1 Morphology of profiles

The profiles generated from the canonical case are given in Figure 5.1. In the canonical case, the concentration of dissolved phosphate is near zero at the top of the sedimentary column, and accumulates gradually throughout the sediment until about half way though the column, where it reaches a plateau. The lack of dissolved phosphate just below the SWI, is due mostly to the species being adsorbed at the top of the sediment. The high adsorption of phosphate near the SWI is due to the presence of iron oxihydroxides, which have a high affinity for phosphate (see figure 5.1). Adsorbed phosphate also increases with depth; it has a local maximum just below the SWI, then drops in concentration following which, the adsorbed phosphate continues to accumulate in parallel to the dissolved profile. The two profiles grow essentially in parallel since they are both driven by the same source reactions. The partition between dissolved and adsorbed phases, is

governed initially by the amount of substrate to adsorb onto, as well as the amount of dissolved phosphate available. The first peak in adsorbed phosphate corresponds in location to the depth over which there is still much ferrihydrite in the sediment. As ferrihydrite becomes less available due to dissolution, less phosphate is adsorbed and more remains in the pore water (this is where the PADS profile begins to deplete and the H3PO4 profile begins to increase).

The effect of pH is generally not seen in the phosphate profiles. As pH decreases with depth, hydroxide ions, which compete with phosphate for binding sites, decrease, thus there should be an increased affinity for phosphate binding. This effect may be another reason why adsorbed phosphate is initially increasing just below the SWI (where it has a local maximum), in addition to the high iron oxide availability (one way to test the extent of pH effect on adsorbed phosphate would be to eliminate the pH term in the adsorption isotherm and redo these same tests). However, once iron oxides are depleted, and whereas pH is still decreasing, there is a local decrease in adsorbed phosphate (see feature in top cm of PADS profile). Therefore one can conclude that the effect of available solid material is predominant over the effect of varying pH.

Throughout the many tests, the profiles of dissolved phosphate have a well defined range of behavior such as the ones shown in Figure 5.2 (and throughout Appendix 1). The dissolved phosphate profiles can be grouped into three categories: those which accumulate until reaching a plateau (the majority), those which accumulate to a peak halfway through the sediment, and those which reach a peak higher in the sediment (top

quarter) and deplete to concentrations near zero (see Appendix 1 – Data 1 for representations of all three regimes). One additional feature in the dissolved phosphate profile is an inflection point approximately halfway down the sediment. That feature is postulated to be caused by the bioturbation curvature parameter which induces a similar inflection in the organic matter profile (See Appendix - 1 Data 5 for illustration). Overall, the adsorbed phosphate profiles follow the dissolved phosphate with the additional feature of a local maximum near the top of the sediment.

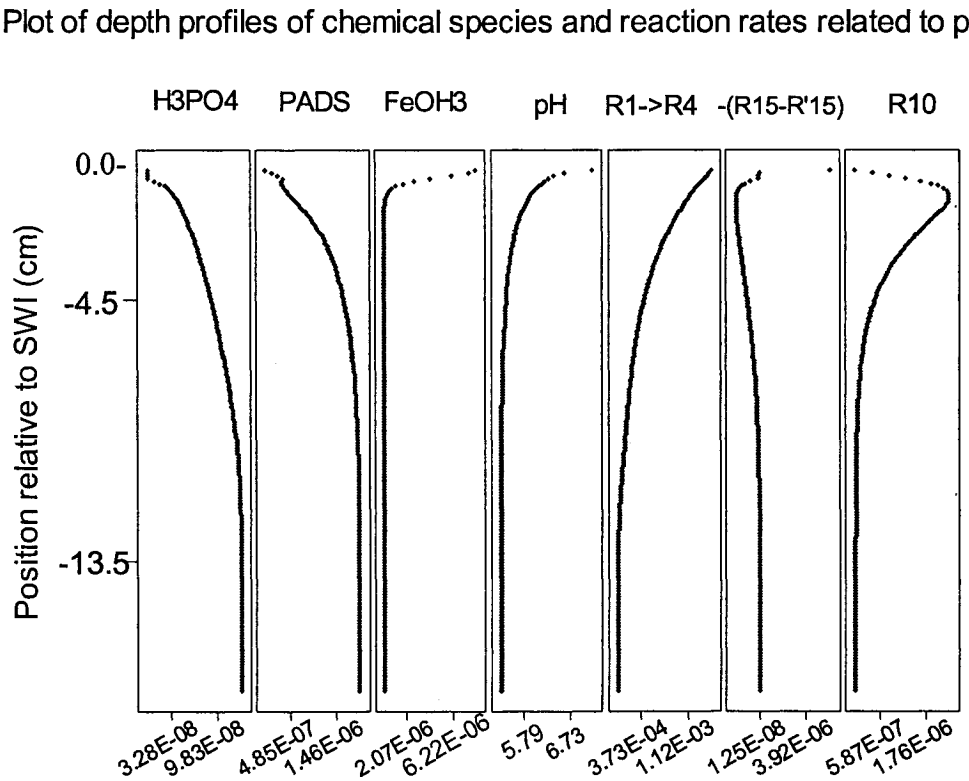

a)

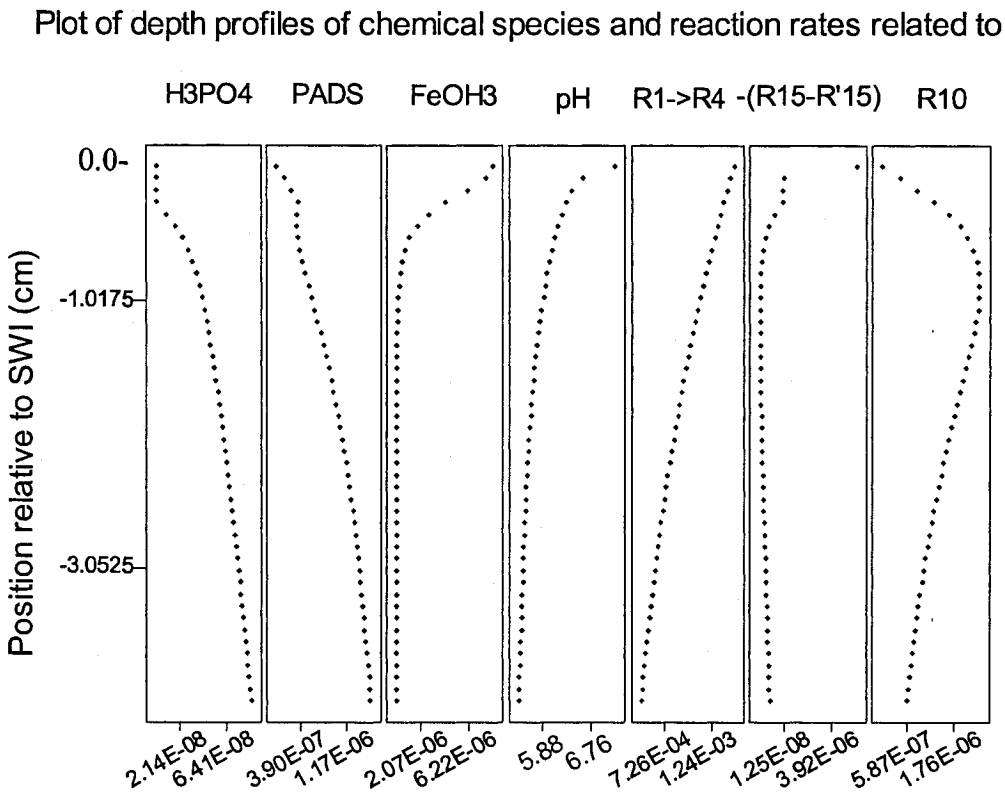

b)

Figure 5.1 - Plots of the (a) depth profiles over 18 cm and (b) close ups (4cm) of phosphate and related species and reactions for the canonical case (see Chapter 3). Units for dissolved chemical species are in mol/cm^3_{PW} and for solid species in mol/g_{DS} as specified in Chapter 3. Units for reaction rates are in mol/g_{SD}/yr also according to Tables 3.1 and 3.3 of Chapter 3.

5.1.2 Mechanisms

H_3PO_4 can be produced from three classes of reactions, namely OM degradation (R1 to R4), vivianite dissolution (R'15)[1] and scavenging of vivianite through hydrogen sulfide (R10). Tests were performed where the reaction rate constants of relevant reactions (R1 to R4, R10, R15, R'15) were reduced, increased or turned off, while other parameters were kept at their canonical values, to examine the effects. The depth distributions of the reaction rates for the reactions in question are given, for the canonical case only, in Figure 5.1. The observed effects of reaction rates on phosphate profiles are summarized below; quantitative results are not given here (as only qualitative effects on the profile shape were sought).

In the cases near canonical parameter values, OM degradation is found to be the predominant producer of phosphate with a rate an order of magnitude higher than the other reactions (see Figure 5.1). As expected, where OM degradation rates are high the amount of phosphate, free or bound to solids, is large. Increasing the rate of sulfide induced - vivianite dissolution (R10) has negligible or no effect on the profile. Decreasing the rate of vivianite formation has the effect of increasing the amounts of both aqueous phosphate and adsorbed phosphate. The two profiles grow simultaneously such that the partition between aqueous and adsorbed phosphate is not significantly influenced.

---

[1] Please note that primes are used with respect to precipitation reactions only (R14, R15 and R16). The prime refers to the reverse of a precipitation reaction, that is the dissolution process when the solution is undersaturated with respect to the mineral phase.

The fate of dissolved phosphate, is either to stay in the pore water as dissolved phosphate, adsorb onto solids (R17), or precipitate as vivianite (R15). The proportion is higher for the adsorbed phase near the top. Upon testing the effect of vivanite production on the phosphate profile, it was found that, for an increase in vivanite formation, the associated dissolution by sulfide (R10) increases correspondingly and releases some of the precipitated phosphate, thus quenching the effect of vivianite formation on the phosphate profiles. This compensation is not perfect however and it is possible, given the right combination of parameters, to create profiles of depletion of phosphate at depth by adjusting the rate of vivianite formation.

As H_3PO_4 is being produced near the sediment water interface (SWI), it initially nearly all adsorbs onto solids because, in the top layer of sediment, iron oxyhidroxides are still abundant. As $Fe(OH)_3$ gets reductively dissolved (R9) or mineralized (R2), the availability of sorption sites decreases. Thus soluble H_3PO_4 increases in the porewater. Once the concentration of H_3PO_4 in the porewater becomes high however, this stimulates further adsorption and the adsorbed phosphate profile continues to grow in response to the dissolved phosphate.

5.1.3 Influential factors

The main factors shown to affect phosphate determined in Chapter 4 were: OM flux from the water column, oxygen at the SWI, sulfate at the SWI, iron oxide depositional flux from the water column, rate of vivianite formation, rate of OM degradation and the

adsorption of phosphate on background solids (See figure 5.2). From the range of dissolved profiles displayed, we see that high oxygen and high iron flux induce profiles with little dissolved phosphate. A possible mechanism for such occurences could be that the high oxygen and iron flux create an increase in the ferrihydrite concentration in the sediment thus increasing the fraction of adsorbed phosphate and decreasing the dissolved fraction (corroborated by Figure 5.2b).

A low rate of vivianite formation can produce a peak in the phosphate profile. The effect of high oxygen and iron on the phosphate profiles could also be linked to vivianite formation, as the vivianite profile for both those cases is increasing with depth (observed but not shown here). Similarly, for a slow rate of vivianite formation, the decrease in phosphate is correlated to a corresponding increase in the vivianite profile (meaning that when the vivianite rate constant is low, precipitation occurs deeper in the sediment, thus affecting the lower part of the phosphate profiles).

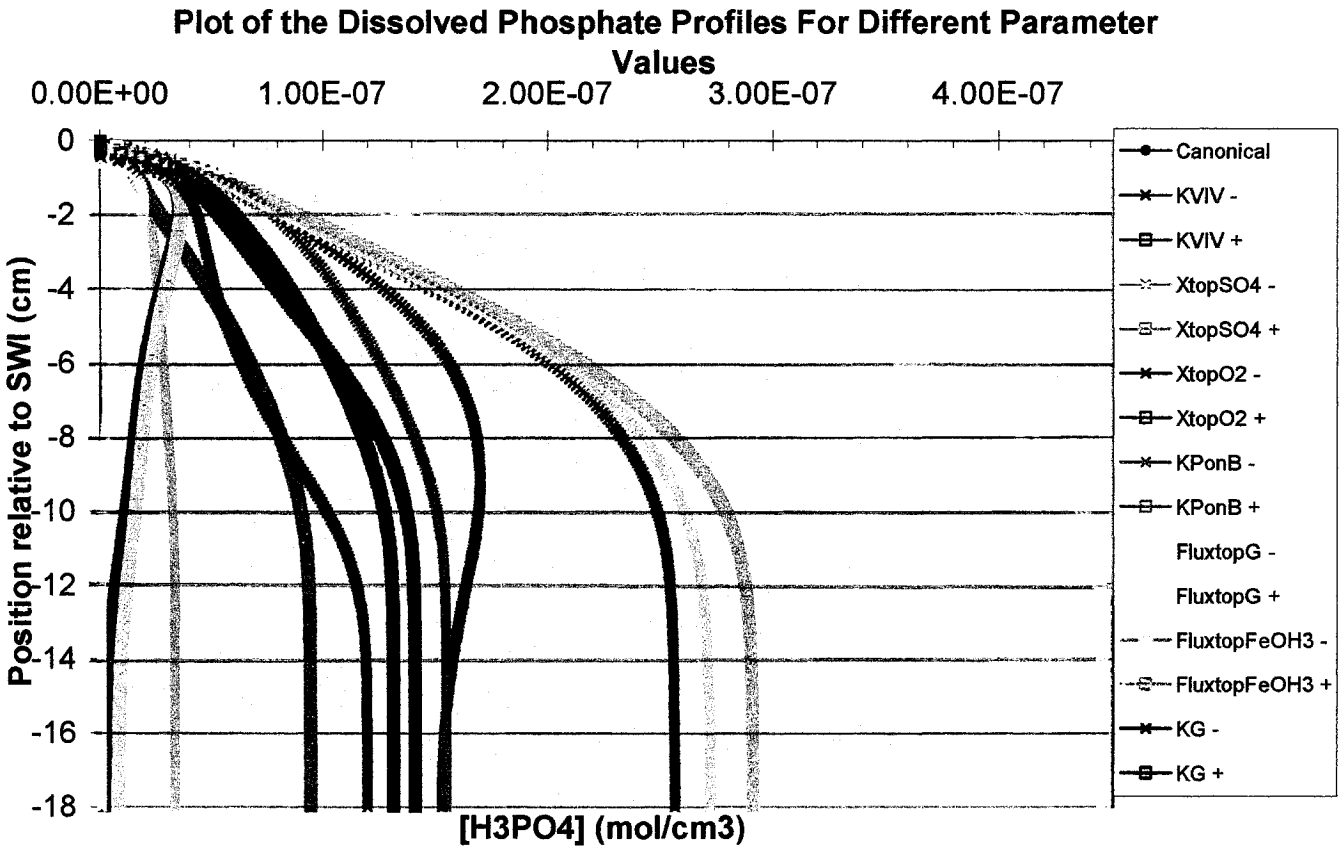
Plot of the Dissolved Phosphate Profiles For Different Parameter Values
0.00E+00
1.00E-07
2.00E-07
3.00E-07
4.00E-07
0
-2
-4
-6
-8
-10
-12
-14
-16
-18
Position relative to SWI (cm)
[H3PO4] (mol/cm3)
Canonical
KVlV -
KVlV +
XtopSO4 -
XtopSO4 +
XtopO2 -
XtopO2 +
KPonB -
KPonB +
FluxtopG -
FluxtopG +
FluxtopFeOH3 -
FluxtopFeOH3 +
KG -
KG +

a)

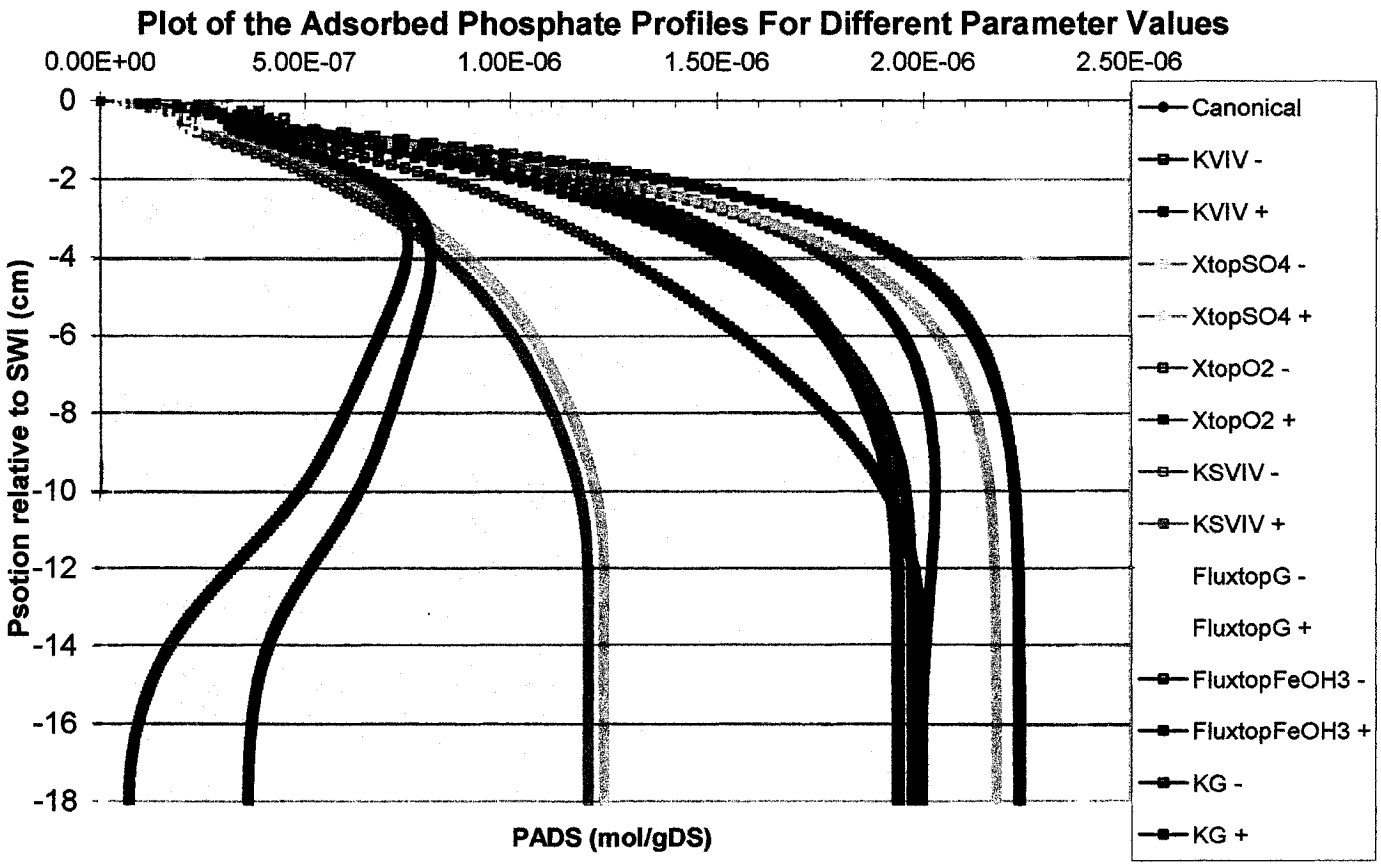

b)

Figure 5.2 - Plot of a) dissolved and b) adsorbed phosphate profiles as a function of depth for the high and low limits (as specified in Chapter 4) of the main factors identified for phosphate.

Legend: Kviv – rate constant for vivianite precipitation
xtopSO4 – $[SO_4]$ at SWI
xtopO2 – $[O_2]$ at SWI
KPonB – Adsorption constant for phosphate on background solids
FluxtopG – Flux of organic matter
FluxtopFeOH3 – Flux of iron oxides
Ksviv – rate constant for vivianite dissolution by sulfide
KG – rate constant for OM degradation

5.2 Reduced Iron

5.2.1 Morphology of profiles

Throughout the factorial tests reported in the previous chapter, the aqueous iron profile displayed a well-defined range of behaviours. A typical profile, that of the canonical case, is shown in Figure 5.3. The concentration of aqueous iron is zero at the sediment water interface (this is a result of its boundary condition). Aqueous iron concentration then increases with depth quickly. Further into the sediment, the profile depletes slowly until it reaches a constant concentration in the lowest third of the sediment. The significant variation in iron profiles is in the degree to which aqueous iron depletes in the bottom half of the sediment; in some cases, nearly all the dissolved iron can get consumed while in others it accumulates, thus it remains in the pore water (refer to Appendix 1 for examples). This difference can be categorized by two regimes, namely one where iron profile has a peak, and one where the peak is simply a plateau (see Figure 5.4). However, there are many intermediate profiles between these extreme cases (again examples are available in Appendix 1).

Plot of depth profiles of chemical species and reaction rates related to iron

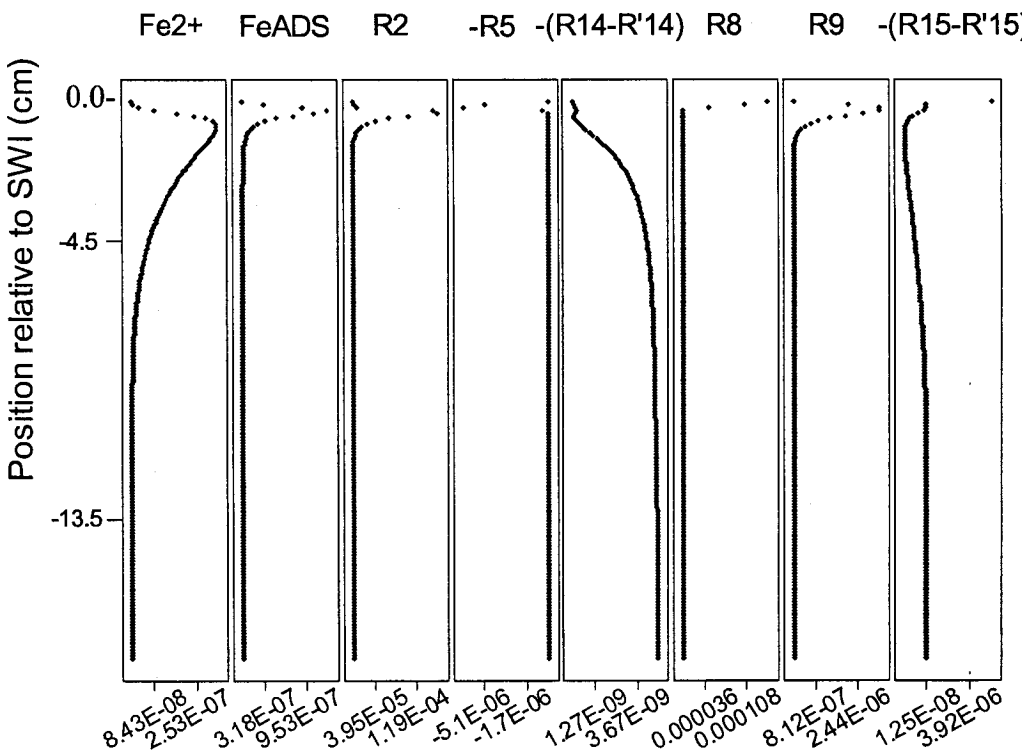

a)

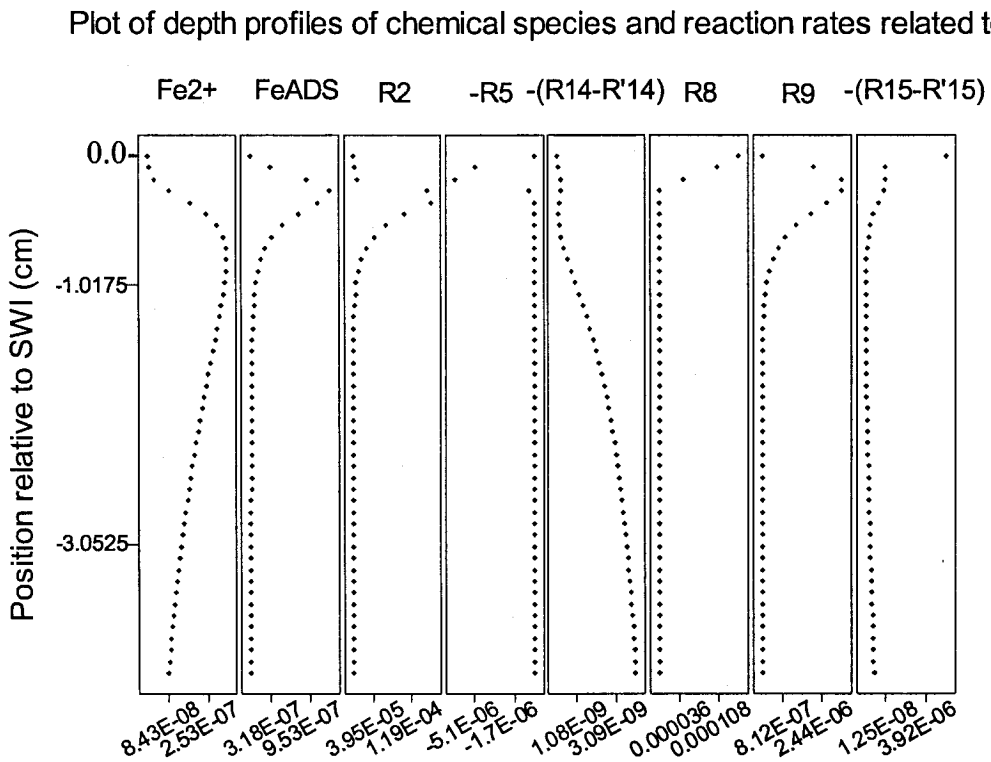

b)

Figure 5.3 – Plots of the (a) depth profiles over 18 cm and (b) close ups (4cm) of iron and related species and reactions for the canonical case. Units for solids are in mol/gDS and for dissolved species in mol/cm^3_{PW}, while reaction rates are in $mol/g_{DS}/yr$.

5.2.2 Mechanisms

Aqueous iron is produced by three reactions in the model: R2, R8, R9. It is consumed by the precipitations reactions R14, R15, R16 and by the oxidation reaction R5. The depth profiles of the rates of these reactions, for the canonical case, are given in Figure 5.3, except R16 which does not occur under the canonical conditions. These profiles help in the interpretation of mechanisms contributing to the iron profile. To test the impact of iron relevant reactions on the dissolved iron profile, the kinetic rate constants of these reactions were varied both below and above the canonical values. These reactions were also turned off individually and their effect on the dissolved iron profile was observed (the details of these tests are not given here, only the observations from these tests, along with reaction rate profiles, are summarized herein). R2 has the largest contribution to the production of ferrous iron, though the rate of R8 is comparable in scale inside the oxic zone (see Figure 5.3). All three ferrous iron producing reactions occur almost entirely in the top centimeter of sediment, at least for parameters near the canonical case. Thus they combine to generate the peak of aqueous iron around 1cm. Below that depth, only aqueous iron depletion occurs (though R'14 generates some relatively small quantities of $[Fe^{2+}]$ as shown in Figure 5.3). Except for the reaction involving adsorbed iron, depletion of iron occurs via reactions R5, R14, R15 and R16, the last one being very rare. R5 occurs in the top centimeter of sediment along with all the production reactions (see figure 5.3), thus its effect on the deeper profile is not noticeable. The absence of iron directly below the SWI is due to sorption, but this ceases shortly below the SWI due to depletion of ferrihydrite. At higher depths, vivianite formation (R15) consumes iron. The

rate of vivanite formation can thus influence the amount of iron in the pore water at depth, with high kinetic rates resulting in near zero concentrations of aqueous and

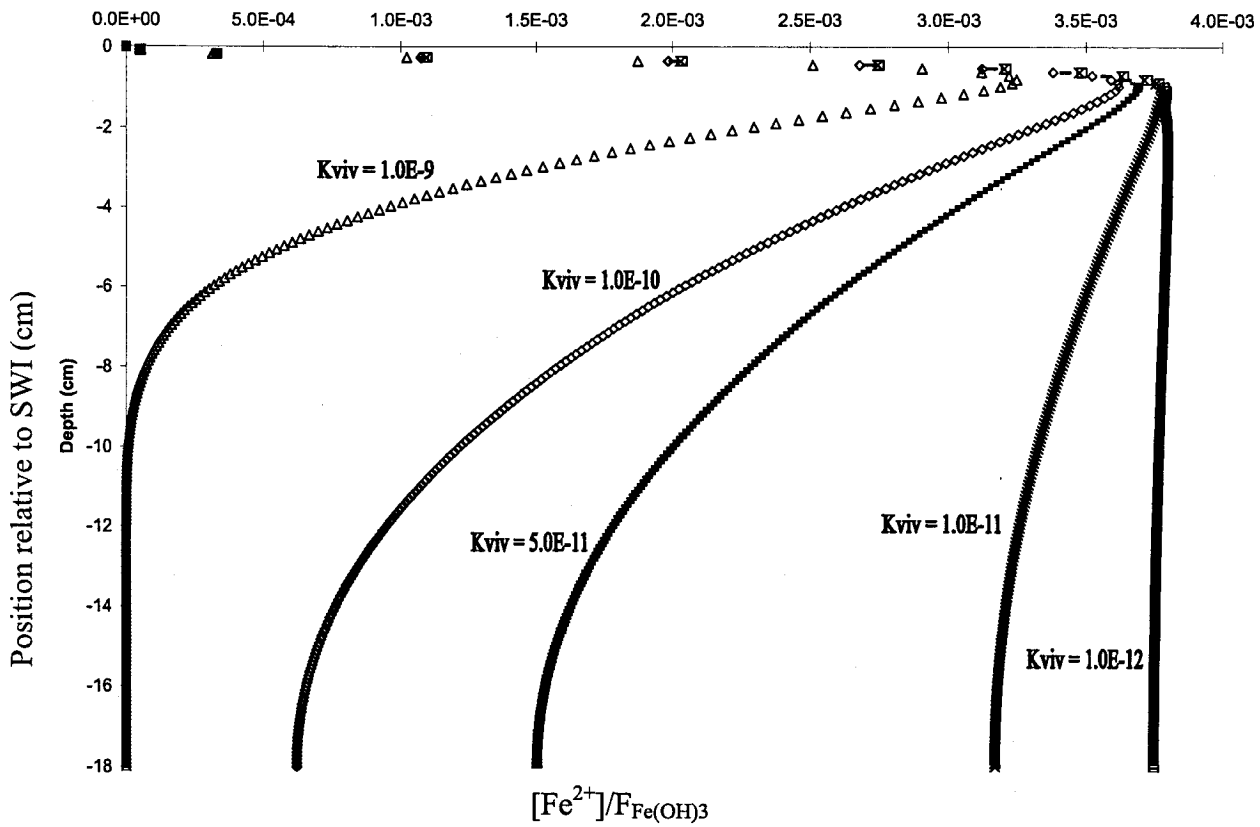

a)

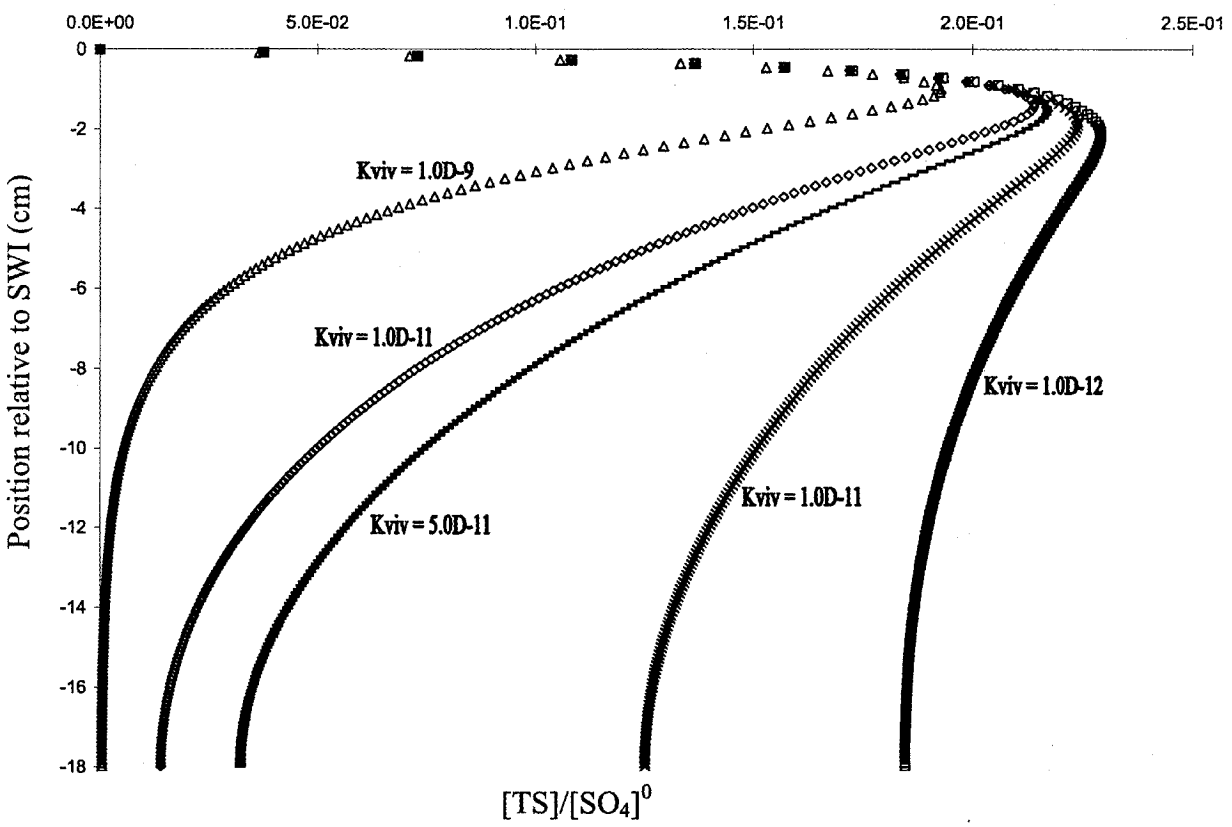

b)

Figure 5.4: Effects of rate of vivianite formation on (a) dissolved iron and (b) total aqueous sulfur. The iron concentrations were normalized to the ferrihydrite influx, thus they are in units of cm^2_{sed} yr / g_{DW}. The sulfur concentrations were normalized to the sulfate concentration at the SWI, thus they are dimensionless.

adsorbed iron near the bottom; Figure 5.4 demonstrates the span of the vivianite formation effect.

The [Fe^{2+}] that is not consumed, will partition between aqueous and adsorbed fractions according to the corresponding adsorption constant (see Chapter 3, Eq. 3.11). Like phosphate, the iron adsorption depends on the availability of solids (like $Fe(OH)_3$), pH and the amount of aqueous iron. Near the sediment water interface (SWI), where iron hydroxides are present, pH is high (6.5 - 7) and iron is readily produced, the adsorbed iron fraction is very high (Fig. 5.3); it is an order of magnitude higher than aqueous iron. As pH drops below 6.5, adsorption of cations (like [Fe2+]) is hindered. This combined with the progressive disappearance of iron solids due to reductive dissolution (R2), plus the consumption of dissolved iron by precipitation causes noticeable decrease in the adsorbed iron profile.

It is noteworthy to mention that, if vivianite precipitation (R15) is low at the bottom, the aqueous iron profile still retains some concentration at depth comparable to its peak value, but adsorbed iron at depth is significantly less than its peak value. This is likely due to the fact that further into the sediment there are fewer iron solids to adsorb onto and the pH is more unfavorable causing a larger fraction of iron to remain in the porewater. Thus whereas the major fraction of iron is adsorbed near the SWI, at depth, most of the iron remains dissolved.

Another useful juxtaposition is that of aqueous iron with other solid iron-bearing phases in sediments. This allows us to see how iron is partitioned between dissolved and precipitated fractions (Figure 5.5). It can thus be seen that more iron is in a solid phase than is dissolved.

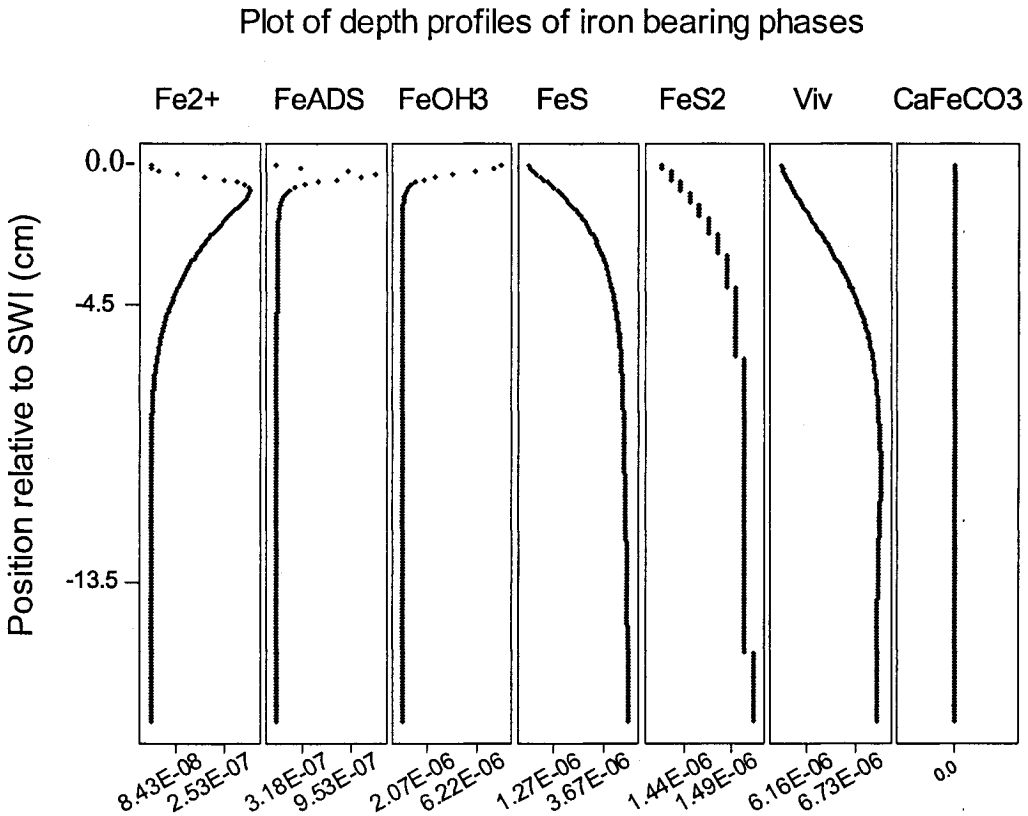

Figure 5.5 – Iron bearing phases profiles for the case of canonical parameters. The solid species concentrations are in mol/g_{DS} while the aqueous concentration is in mol/cm^3_{PW}.

5.2.3 Influential factors

As demonstrated in the previous chapter, the main factors in our model influencing the iron profile were: oxygen concentration in the water column, flux of ferrihydrite into the sediment, flux of organic matter, concentration of sulfate in the water column, bioturbation and rate of organic matter degradation. The individual effect of each of these factors on the dissolved iron profile is given in Figure 5.6. The profiles in the figure are consistent with the factorial analysis results. That is, increasing oxygen at the SWI increases the scale of the dissolved iron profile; this effect of oxygen on different iron phases is studied further later in this chapter. Increasing the flux of iron into the sediment induces more pore water iron, which is easily understood; introducing more source material gives rise to more dissolved iron. The flux of organic matter and its rate of degradation both have a negative effect on the porewater concentrations of iron. The effect of OM degradations is also given some further attention later in the chapter. Increases in sulfate concentrations at the SWI as well as vivianite formation both cause a decline in the dissolved iron profiles. These are attributed to the rate of formation of FeS by R14 coupled with the precipitation of vivianite which deplete the iron ions dissolved in the porewater.

The interesting effect here is that of bioturbation. According to the factorial analysis of the previous chapter, Dbmax should have a positive effect on the maximum iron concentration. The positive effect on the maximum of iron is seen in the plot of Figure 5.6 between low and high levels of Dbmax, however both those profiles fall below the

canonical profile. So the effect of bioturbation on dissolved iron is both positive, for some range of values and negative for another range of values.

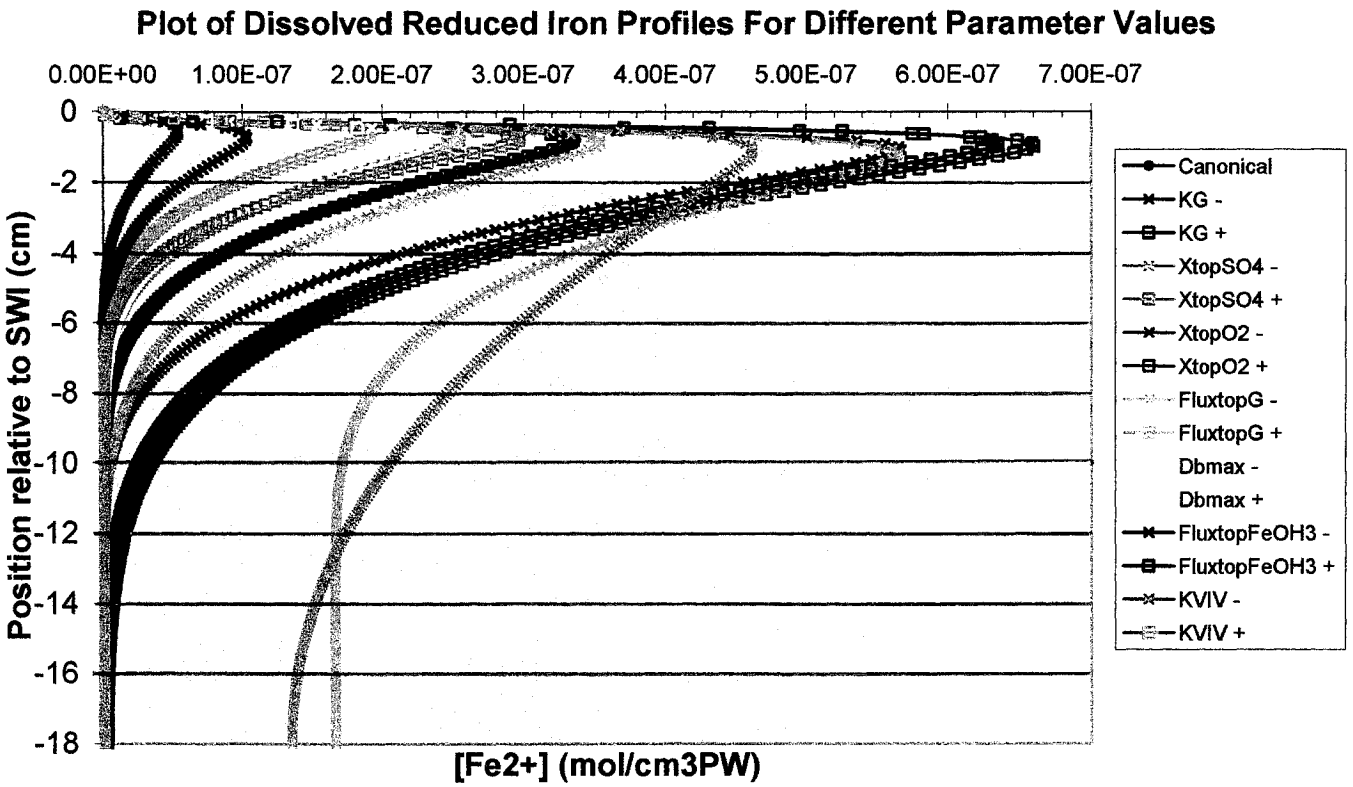

Figure 5.6 - Plot of dissolved reduced iron profiles as a function of depth for the high and low limits of the main factors identified for iron.

Legend: Kviv – rate constant for vivianite precipitation
xtopSO4 – $[SO_4]$ at SWI
xtopO2 – $[O_2]$ at SWI
Dbmax – Bioturbation at the SWI
FluxtopG – Flux of organic matter
FluxtopFeOH3 – Flux of iron oxides
KG – rate constant for OM degradation

5.3 Sulfur

5.3.1 Morphology of profiles

Total aqueous sulfur (TS) here is understood to mean [H_2S] and [HS^-] in the porewater. The general dissolved sulfur profile outputted by our model has a recurring shape. It is characterized by an accumulation of aqueous sulfur in the top cm below the SWI and a subsequent depletion of sulfur progressively at depth (the accumulation curve being sharper than the depletion curve), as illustrated in Figure 5.7 and throughout Appendix 1. Depending on the parameter values, the depletion can be drastic and sulfur can be nearly completely consumed within the top 5 cm or it may equilibrate to a smaller concentration at depth (see Figure 5.4b for an illustration of the effect of the rate constant of vivianite precipitation (Kviv) on TS). This set of features (or profile regimes) is very similar to the morphology of dissolved iron, and is also correlated to vivanite precipitation. The effect here however is indirect; vivianite precipitation does not directly deplete sulfur, but it induces a corresponding hike in vivianite dissolution by sulfide (R10), as alluded to in section 5.2.2, which consumes H_2S, thus depleting the TS profile.

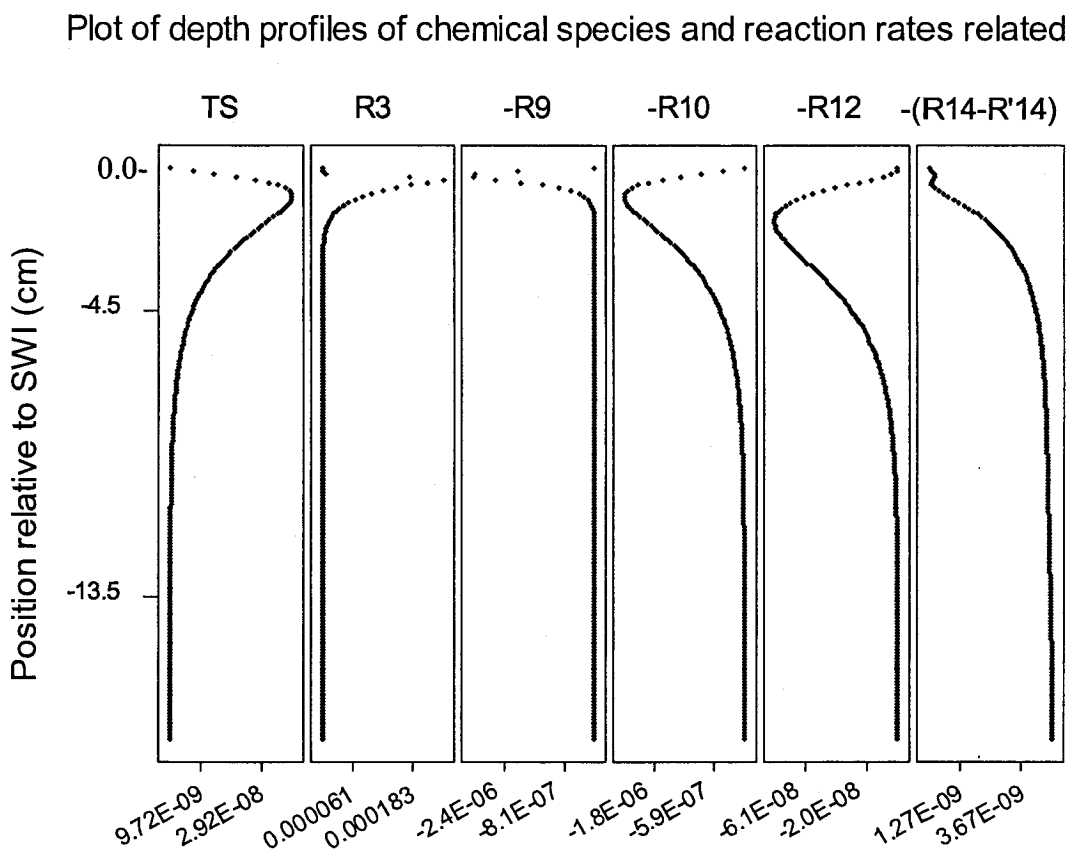
Plot of depth profiles of chemical species and reaction rates related to sulfur
TS
R3
-R9
-R10
-R12
-(R14-R'14)
Position relative to SWI (cm)
0.0
-4.5
-13.5
9.72E-09
2.92E-08
0.000061
0.000183
-2.4E-06
-8.1E-07
-1.8E-06
-5.9E-07
-6.1E-08
-2.0E-08
1.27E-09
3.67E-09

a)

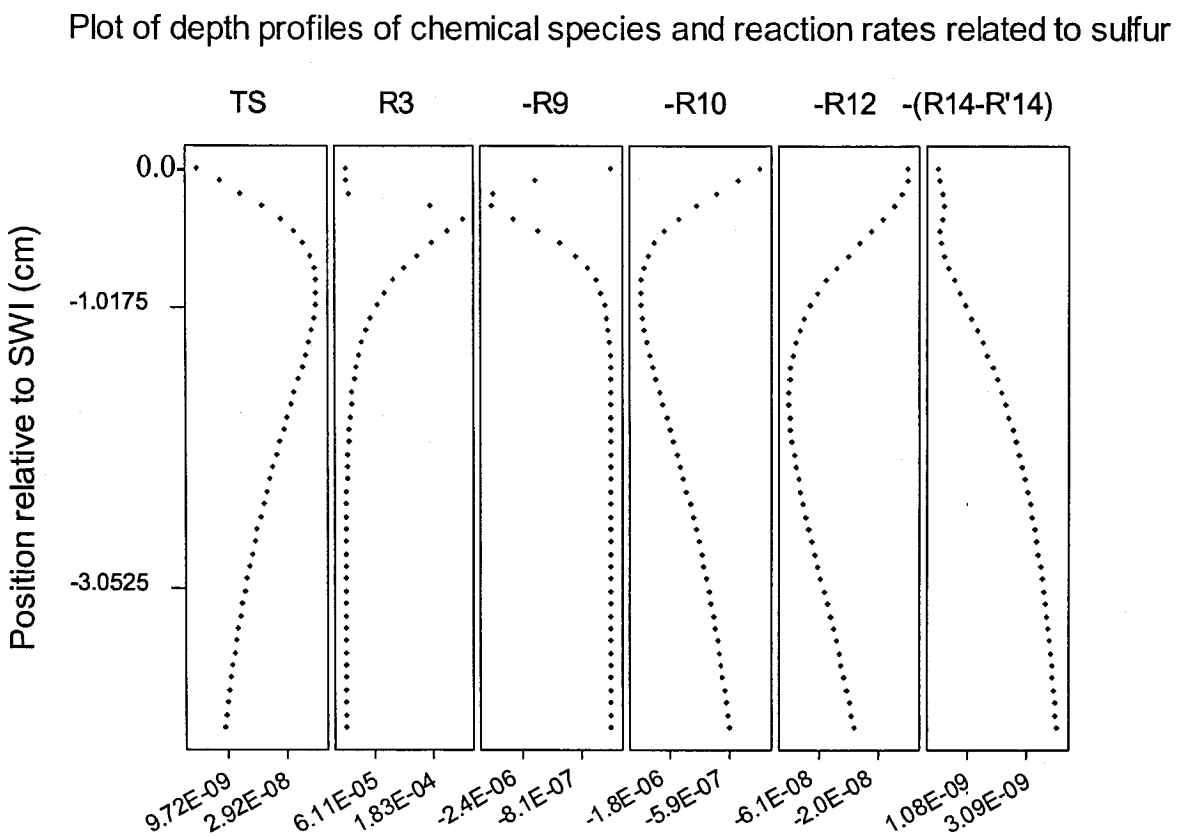

b)

Figure 5.7 – Plots of the (a) depth profiles over 18 cm and (b) close ups (4cm) of species and reactions related to sulfur for the canonical case. The concentration of TS is in mol/cm^3_{PW} and the rates are in $mol/g_{DS}/yr$.

5.3.2 Mechanisms

Similarly to the phosphorus and dissolved iron profiles, rate constant for the reactions pertinent to sulfur were turned on or off (or varied) individually and the resulting profiles compared. The depth profiles for the reaction rates were also outputted. This information was examined and the resulting observations are given herein. The reactions which produce sulfur are R3 and R'14 (however the rate of R'14 is typically 5 orders of magnitude smaller than the rate of R3, as illustrated in Figure 5.7). The reactions which consume sulfide are R7, R9, R10, R11, R12, R14. However, the production reaction (R3) has a rate (for parameters near the canonical case) at least two orders of magnitude higher than any other reaction rate. Sulfate reduction (R3) peaks near the top 0.5 cm and total aqueous sulfur peaks just below that (see Figure 5.7). Once the sulfur accumulation has tapered off depletion reactions consume the accumulated sulfur. The primary consumption comes from iron monosulfide precipitation (R14), vivianite dissolution by H_2S (R10) and pyrite formation by H_2S (R12), the other reactions having rates small in magnitude in comparison. The dissolution reactions (R10, R12) both persist at depth. Again, vivianite comes out as an important player in the shape of the sulfur profile as well, due to the fact that vivianite precipitation occurs at depth. Any sulfur released by the dissolution of FeS (R'14) is not sufficient to change the effects of the contributions from other reactions.

5.3.3 Influential factors

The main factors influencing the dissolved sulfur concentration are: concentration of sulfate at the SWI, concentration of oxygen in the water column, flux of iron oxides into the sediment, flux of organic matter into the sediment, rate constant for vivianite precipitation, rate constant for vivianite dissolution by sulfide and rate constant for pyrite formation. These factors, and their effects are summarized in Figure 5.8. The effects observed in Figure 5.8 are consistent with the factorial test results of the previous chapter and their hierarchy (order of importance) as well. The effect of vivanite formation on TS is easily understood through the scavenging reaction (R10); the effect of the rate constant for the scavenging reaction (K_{sviv}) confirms that (see Figure 5.8). SWI sulfate has an expected high impact on the total dissolved sulfur in sediment. Oxygen has a negative effect on the reduced sulfur, which is understandable since it favors the oxidized form of sulfur (sulfate) over the reduced form (sulfide) through R7. It is also understandable that pyrite formation (K_{FeSHS}) should deplete porewater sulfide. Iron flux decreases sulfide, again due to vivianite precipitation and subsequent scavenging by sulfide which increases FeS and pyrite concentrations and decreases TS. Finally increasing the organic matter degradation constant increases total sulfide in the sediment, most likely by inducing sulfate reduction.

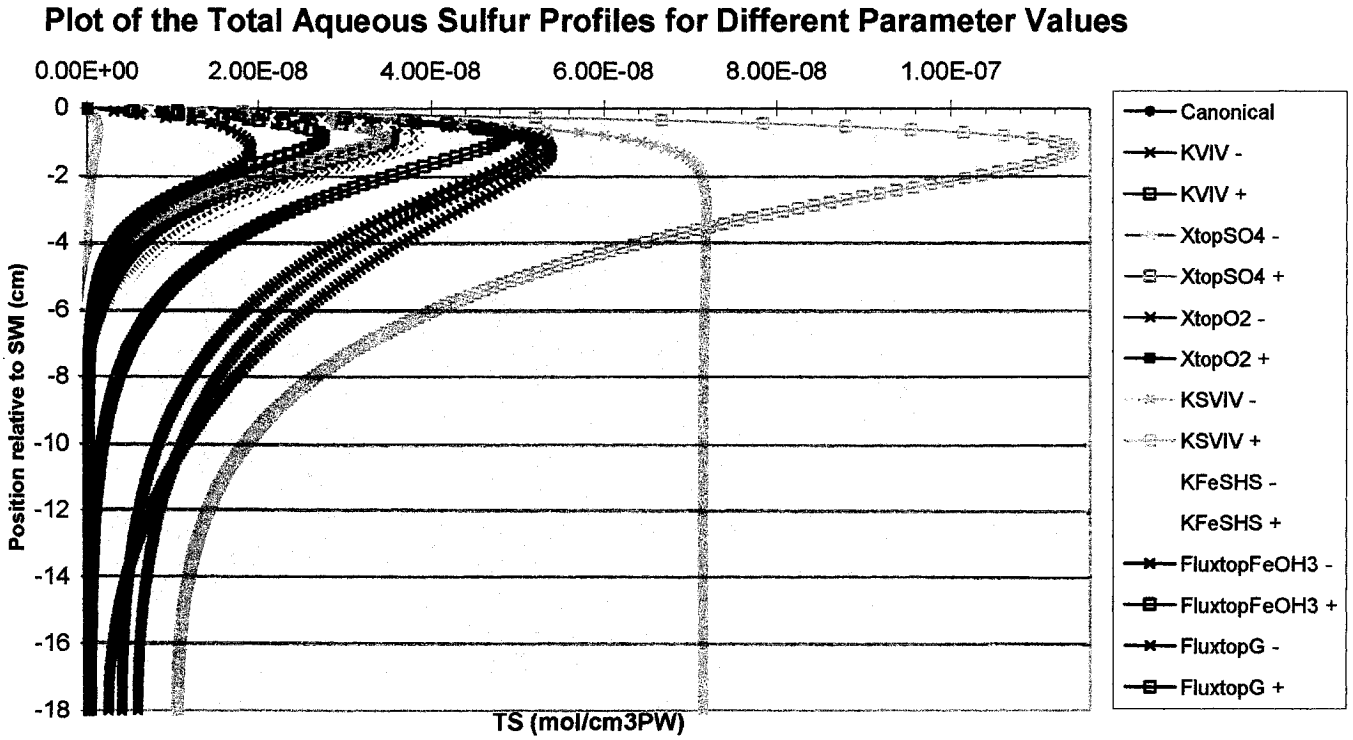

Figure 5.8 - Plot of total aqueous sulfur profiles as a function of depth for the high and low limits of the main factors identified for iron.

Legend: xtopSO4 – $[SO_4^{2-}]$ at SWI
xtopO2 – $[O_2]$ at SWI
Ksviv – rate constant for vivianite dissolution by sulfide
FluxtopG – Flux of organic matter
FluxtopFeOH3 – Flux of iron oxides
KFeSHS – rate constant for pyrite formation
Kviv – rate constant for vivianite formation

It is important to note here there is room for discrepancies between the effects of parameters as per the factorial runs and those from individual variations of the parameters. In many cases, the effect noted is consistent with the factorial test results. In some cases however it can be different than expected. This is not an error in the data processing, but rather due to the way the effect is calculated in the factorial test formula. By averaging the effect of one parameter over a range or other factors, we are including the effects of those other factors in the statistics. Thus the net effect is dependent on which factors were varied simultaneously. When one factor has a strong individual effect on a chemical species, its effect will predominate across many tests and remain consistent with inter-permutations of other parameter. However, if the main effect of a factor is smaller, or there are significant interaction effects with other factors, which outweigh the main effect of a factor, the results will be greatly influenced by the variation in other factors. Thus factorial tests are important to use as a screening tool, keeping in mind that the results may not translate exactly into the individual effects of a parameter.

5.4 Effect of Oxygen and Organic Matter Degradation on Iron Species

As mentioned in the previous chapter, oxygen has an interesting positive effect on both oxidized and reduced iron species. To study that further, some tests were performed, looking at the integrated total iron concentration (including aqueous iron, adsorbed iron and all solid iron bearing phases) throughout the sediment as function of the oxygen concentration at the sediment water interface. Figure 5.9 shows the total iron concentration vertically integrated over depth (in $cm_{sed}mol/cm^3_{PW}$) vs. oxygen

concentration at the SWI. It is interesting to note that for the traditionally used boundary conditions (used in the factorial tests), where the sediment is not explicitly coupled to the water column dynamics, and where the dissolved iron profile has a gradient due to a zero concentration boundary condition, the total accumulated iron in the sediment is significantly lower than the amount suggested by the influx of ferrihydrite if no diagenesis were to occur. The amount expected to accumulate throughout the sediment (when diagenesis does not occur) is simply the influx of ferrihydrite ($mol/cm^2_{sed}yr$) divided by the sedimentation velocity (cm_{sed}/yr) and by the porosity (cm^3_{PW}/cm^3_{sed}) and multiplied by the sediment depth (cm_{sed}) and is indicated by the horizontal lines in the top of Figure 5.9.

Also the integrated iron vs. oxygen decreases from anoxia to oxic conditions until it reaches a minimum (near $[O_2]$ =1.5E-8 mol/cm^3) and then increases again with oxygen. The total integrated iron is in fact higher at the high level of oxygen than at anoxia (taken as the low level of oxygen in our trials) which is consistent with the positive effect observed in the factorial trials.

The overall level of integrated iron implies a loss of iron from the sediment, with respect to the case where no diagenesis occurs. Upon further investigation, this loss was attributed to the boundary conditions for iron bearing species at the SWI and the absence of coupling to the water column dynamics. As the dissolved iron profile increases sharply near the SWI it induces a high diffusive flux of reduced iron back to the water column. Additionally, the concentration gradients of the solid iron bearing species,

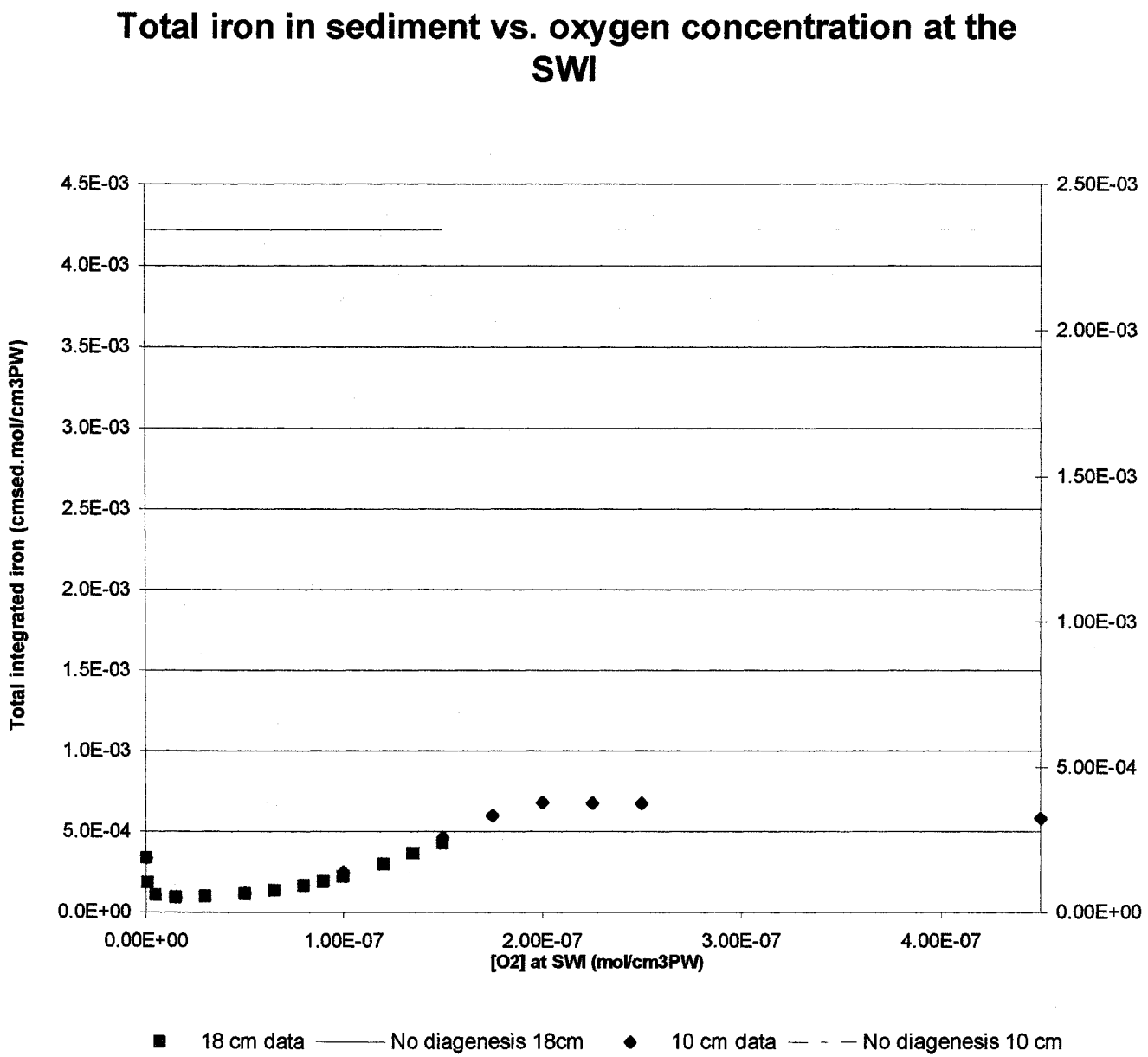

Figure 5.9 – Plot of total iron in sediment as function of oxygen at the water boundary for different sediment depths and recycling conditions.

created by the shape of these profiles (please see Figure 5.5 for illustration), also induce a bioturbative flux out of the sediment and into the water column. The bioturbative and diffusive fluxed out of the sediment at the SWI were calculated for the canonical case. They were found to represent 77% of the influx of iron into the sediment. Thus the major fraction of iron put into the sediment re-escapes into the water column in the form of dissolved and solid iron species. As there is no explicit coupling between the water column dynamics and the sediment, this iron is not re-oxidized and recycled back into the sediment and therefore it is lost to the overlying water. For this scenario, the oxygen concentration at the boundary had a noticeable effect on the total iron profile. For very high oxygenation of the water column however, there is a saturation effect as seen in Figure 5.9. The total integrated iron is never equal to the amount estimated by the influx of ferrihydrite (in the case where no diagenesis occurs), thus there is a net loss of iron from the sediment, induced by the diagenetic reactions, at steady state.

When examining the distribution of iron among the various iron species (Figure 5.10), we see that the increase of iron increase near anoxia is due to increased storage in the form of pyrite, whereas as the oxygen at the boundary increases there is increased storage in the form of vivianite. Thus pyrite appears favored under more reducing conditions (consistent with common knowledge), while vivianite prevails in a more oxidized environment. The effect on vivianite can be rationalized by remarking that high oxygen creates conditions for which sulfur favoured in its oxidized form (sulfate) thus the rate of reaction R10 decreases, and so more vivianite remains in the sediment. To verify this mechanism a test was performed where sulfur content in the sediment was reduced (by

reducing the sulfate boundary condition), which indeed caused an increase in the vivianite concentration. Where the two distributions (vivianite and pyrite) intersect in Figure 5.10 is approximately where the minimum of the total iron function lies, accounting for the shape of the curve. Figure 5.11 shows the shape of the total iron profile with depth.

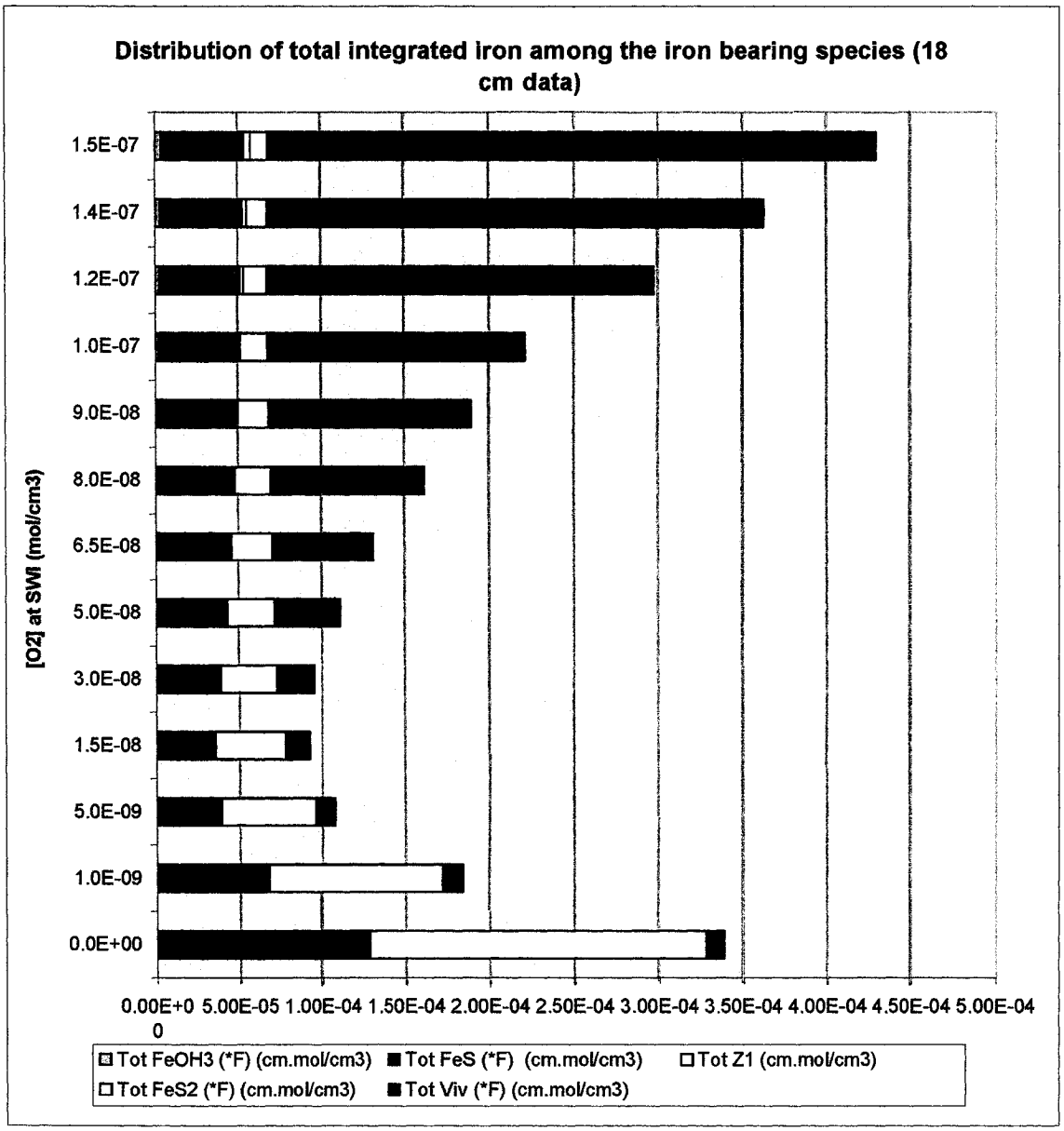

Figure 5.10 – Plot of total integrated iron in sediment, grouped by species as a function of the oxygen at the water boundary when there is no recycling from the water column. The concentrations are expressed in $cm_{sed}.mol/cm^3_{PW}$.

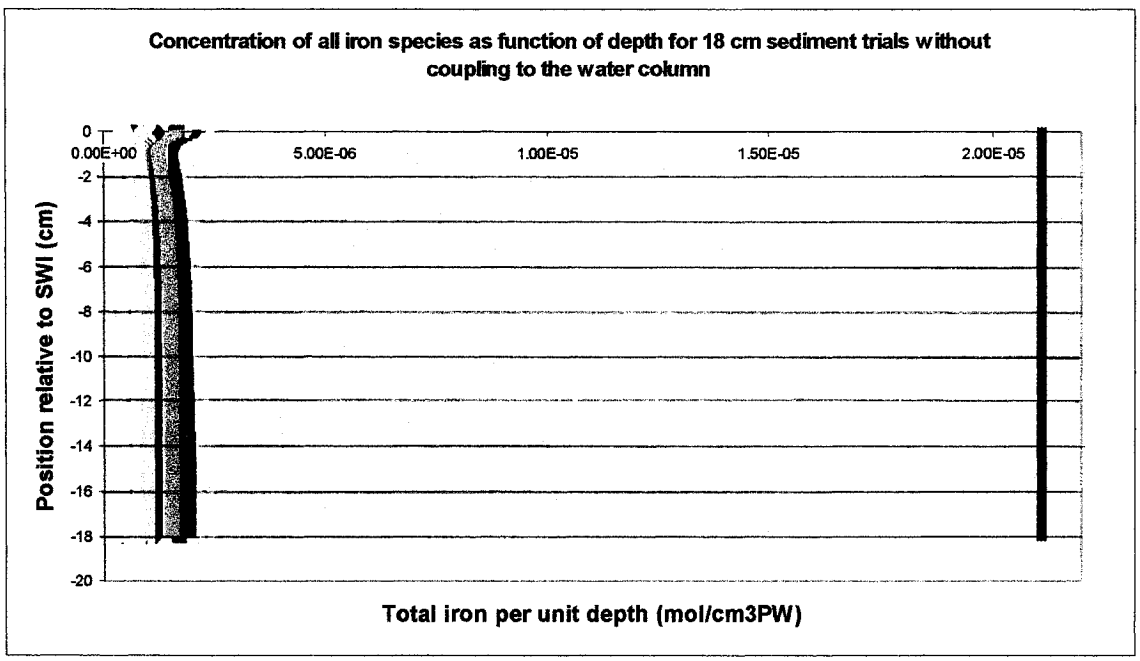

Figure 5.11 – Plots of the total iron (sum of all iron-bearing species) profiles for an 18 cm sediment for varying oxygen concentrations at the SWI (the oxygen concentrations depicted in Figure 5.9). The different curves correspond to the different realizations of sediment iron concentrations for varying oxygen at the SWI (as reported in Fig. 5.9). The line on the far right represents the profile of total iron in the case where no diagenetic reactions occur (then all iron accumulates in the form of ferrihydrite).

Figure 5.12 illustrates also the effect of oxygen on the maximum and burial concentrations of total iron. The two quantities are very similar due to the shape of the total iron profile (Figure 5.11) where the concentration of iron-bearing species is high at depth. Both values have very nearly the same sensitivity to oxygen and it is the same sensitivity as total integrated iron has to oxygen.

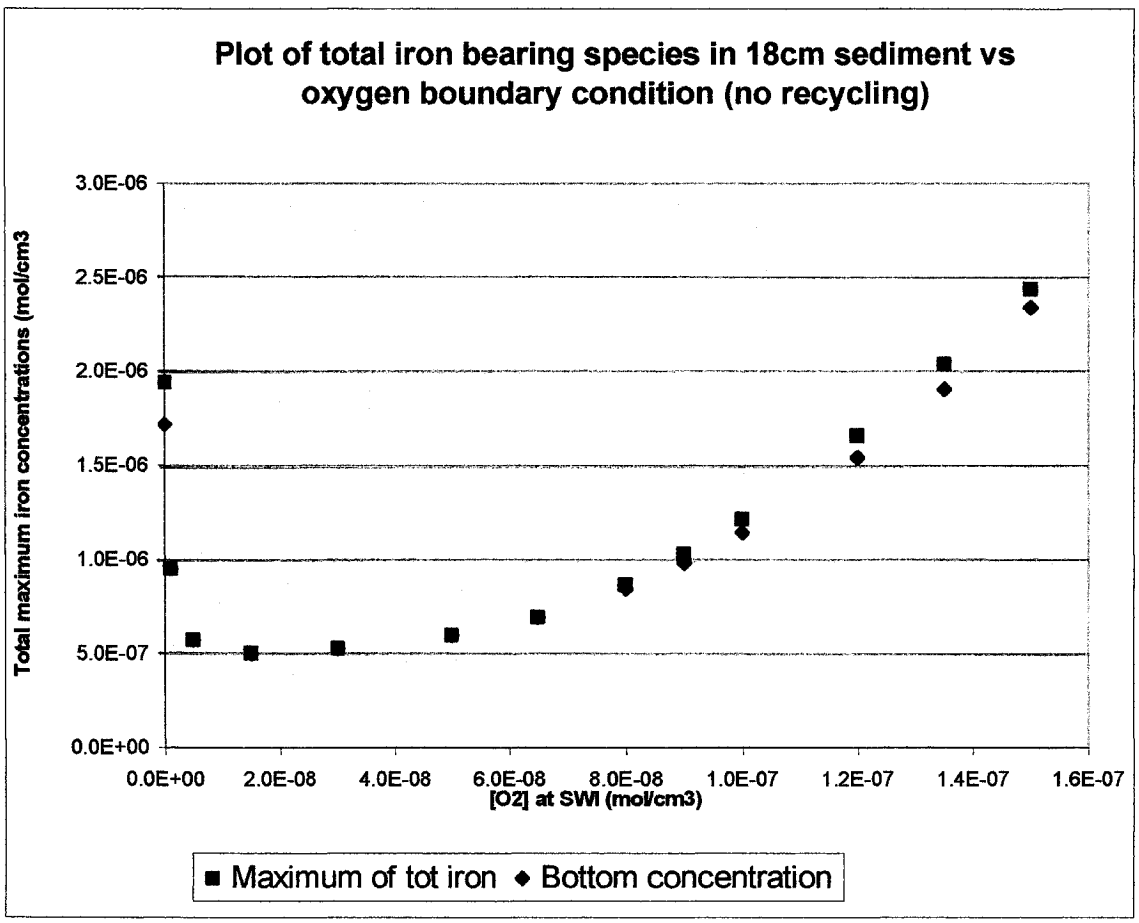

Figure 5.12 – Effect of oxygen concentration at the SWI on maximum and burial concentrations of total iron. Both axes are expressed in units of mol/cm^3_{PW}.

Finally, tests of the effect of organic matter degradation, expressed by the overall degradation constant KG (see figure 5.13) showed that the higher the amount of degradation, the lower the total iron retained in the sediment. This drop in total integrated iron is due primarily to the decrease of storage in the form of vivianite (Figure 5.13b). There is a slight increase in the pyrite formed but this effect is negligible compared to the decrease in the vivianite phase. One possible explanation is that increasing the degradation rate has the effect of reducing iron higher up in the sediment, where vivianite precipitation does not occur. Also increasing sulfide production scavenges more vivianite (this would be consistent with higher pyrite levels observed), thereby reducing the amount of that phase.

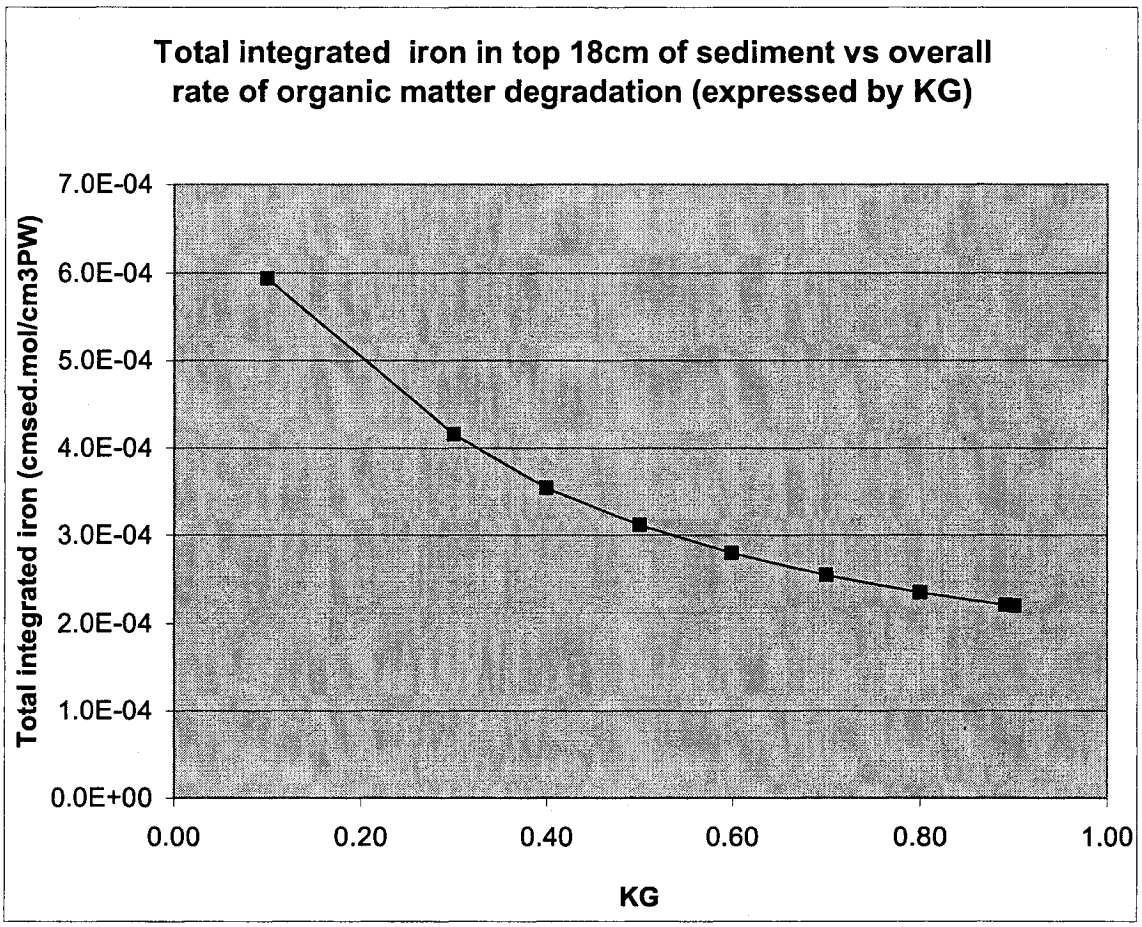
Total integrated iron in top 18cm of sediment vs overall rate of organic matter degradation (expressed by KG)
Total integrated iron (cmsed.mol/cm3PW)
7.0E-04
6.0E-04
5.0E-04
4.0E-04
3.0E-04
2.0E-04
1.0E-04
0.0E+00
0.00
0.20
0.40
0.60
0.80
1.00
KG

a)

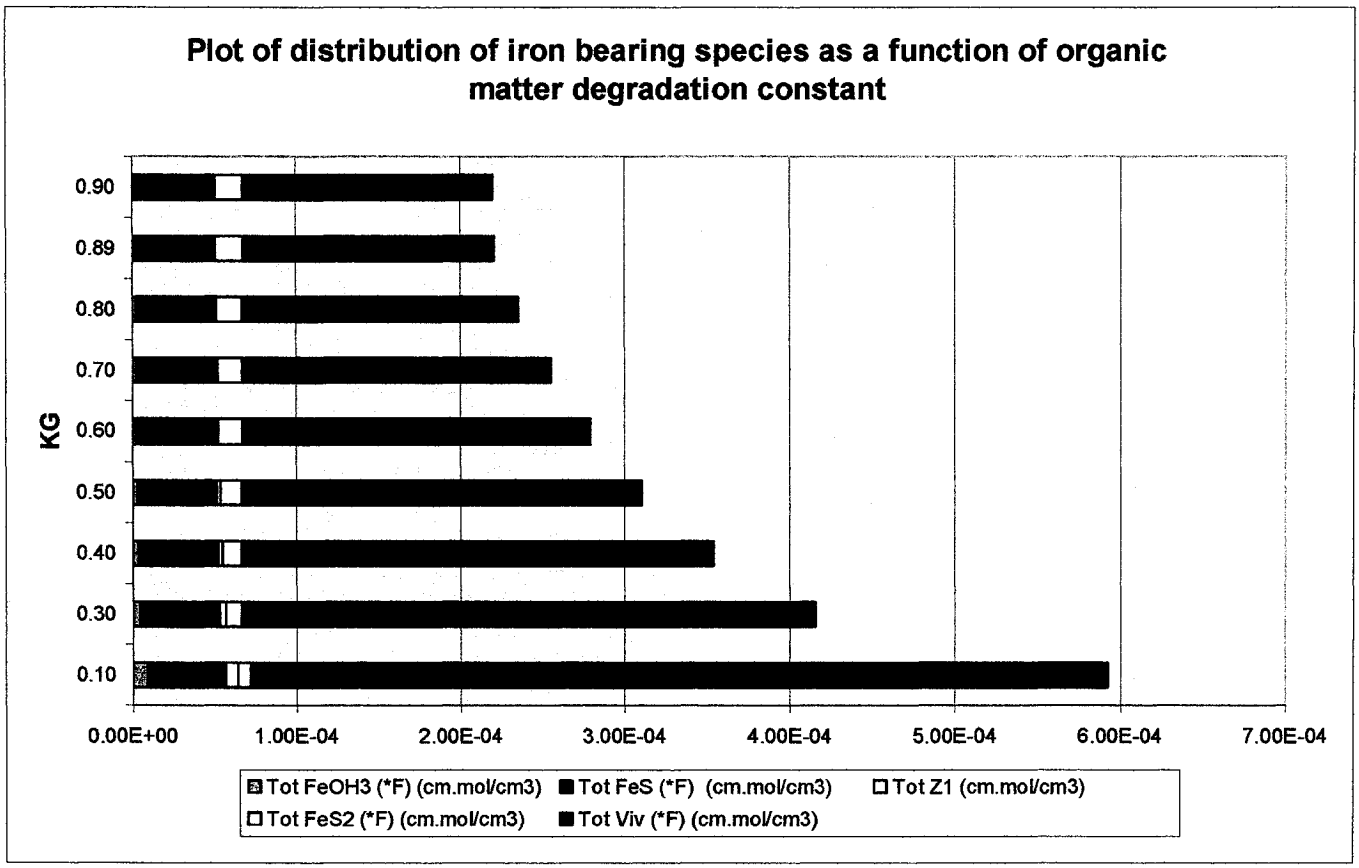

b)

Figure 5.13 – Plot of (a) total integrated iron and (b) total integrated iron distributed by species as a function of the rate of organic matter degradation. The concentrations are expressed in units of $cm_{sed}.mol/cm^3_{PW}$.

Conclusions

This thesis reports on an examination of the chemical cycling of iron, sulphur and phosphorus in lake sediments, using a numerical reaction transport model for sediment early diagenesis.

A scan of the parameter space of the model was performed, based on the range of observed values in the literature. The results of the parameter space examination were illustrated fully in Appendix 1 and summarized in Table 4.2. The most interesting trend to emerge from the range of behaviours displayed was that in several dissolved species, namely dissolved iron, sulphur and phosphate (and correspondingly in adsorbed phosphate as well), there was a regime change observed in the profile shapes. One group of profiles accumulated concentration over the depth of the sediment while in another the species was consumed at depth. Also in some cases there was a noticeable change of scale of the profiles (i.e. the concentrations throughout the sediment were significantly different from the majority of other profiles for the same species).

Some chemical species did not show variation in their profile shapes, for any combination of parameters tested. Such species as $[H^+]$ (pH), total carbonate, oxygen, sulphate, nitrate and methane remained consistent throughout the trials.

Maximum and burial concentrations of the chemical profiles, were extracted from the set of profiles generated by the scan of parameter space (maximum, minimum and canonical values of model parameters). The maximum or burial concentrations of different chemical species were not normally distributed across the many trials. Also, calculated covariances between chemical species showed strong correlations between iron bearing species and sulphide, as well as iron bearing species and phosphate. This is an expected result given how these chemical cycles are linked in the model. The correlation calculations also showed that sulfur and phosphorus are correlated to each other. The latter result was later identified to be due to the precipitation and dissolution mechanisms of vivianite.

For the statistical analysis done on response functions defined as the maximum or burial concentrations of chemical profiles, the main conclusions are that, among the many factors (i.e. model parameters) tested, the precipitation of vivianite, where it occurs, the boundary conditions (i.e. characteristics of the water column), organic matter degradation, bioturbation and advection consistently emerge as influential to the chemical profiles. The effects of these factors are expressed as follows:

- The boundary conditions proved more significant for dissolved than for solid species:
    - Dissolved phosphate was impacted primarily by OM influx and secondly, to a lesser degree, by oxygen in the water column.

- Dissolved iron was impacted mostly by the oxygen concentration in the water column, while influx of iron and OM were close second effects.
- Dissolved sulphide was modulated primarily by the sulphate concentration of the water column.

The most significant observation among the dissolved species is that oxygen impacts iron concentration even more than the iron bearing material (ferrihydrite) influx.

- Solid iron bearing species were also influenced significantly by boundary conditions, particularly oxygen concentration at the SWI and iron influx.
- Among the other factors, the only consistently noticeable effects were for transport parameters for bioturbation and advection velocity. The only reaction rate constant to consistently appear as influential to the majority of chemical profiles was the rate of vivianite precipitation (or dissolution).
- In individual cases, other parameters, were significant, however these results are often trivial (i.e. obvious considering the model construction). For example, in the case of sulphur bearing species (TS, FeS, FeS_2) only, dissolution of vivianite by sulphide (R10) and pyrite formation (R12) emerge as important reactions. Also, organic mater parameters were paramount for carbon bearing species.

Correspondingly, one important finding of the parameter space scan was that many of the factors investigated did not show an impact on the chemical profiles. Some reaction rate constants tested (namely R16, R12, R13, R9) did not show neither significant nor consistent effects on profiles, with the exception of R12 which was influential primarily

on iron monosulfide and pyrite profiles. Adsorption parameters were not found to be significant, with the exception of the adsorption constant for phosphate on background solids which came out as the most influential adsorption parameter (of the four considered in our tests) with respect to some chemical species.

Chapter 5, in turn, elaborated on the findings of the factorial analysis, by looking for mechanisms explaining the numerical chemical profiles for three relevant dissolved species (Fe^{2+}, TS, H_3PO_4). The mechanisms found for profile shapes confirmed the factorial analysis results given in chapter 4.

- Organic matter degradation is the primary mechanisms determining the phosphate profile. Vivianite precipitation (R15) has some effect on the profile shape (under the right conditions) while vivianite dissolution by sulphide (R10) has negligible effect.
- Organic matter degradation is the most important cause of reduced iron. Most noticeable impact on the iron profile is from vivianite precipitation which can change the profile regime (from accumulation to depletion at depth). High rates of vivianite precipitation deplete the dissolved iron at depth.
- Sulfide is mostly contributed by organic matter degradation. Vivianite has the most pronounced impact on total sulphur profile shape, through the scavenging reaction (R10) which is stimulated by the production of vivianite. Increases in vivianite production (R15) and increases in the corresponding scavenging reaction (R10) will both cause a depletion of sulphur at depth.

In the second part of Chapter 5, two interesting effects of the factorial analysis were examined in more detail. Most importantly, it was found that the total accumulated iron in the sediment is significantly lower than the amount expected based on the influx of ferrihydrite into a non-diagenetic sediment. In order to examine this effect the fluxes of all iron bearing species were calculated. It was found that the diffusive and bioturbative outfluxes of iron solids, dissolved iron and adsorbed iron constitute a significant portion of the influx of ferrihydrite (approximately 77%). Thus, due to the nature of the boundary conditions and the concentration gradients of chemical profiles near the SWI, there is a simulated significant efflux (and corresponding loss) of iron back into the water column.

Tests on the effect of organic matter degradation rate on total iron showed the effect to be linked to storage in the form of vivianite.

Future work

Although several self-consistency checks have already been performed successfully on the model, including some mass balance checks, other verifications can be done as well. For example, it would be useful to calculate the sum of all incoming and outgoing fluxes of iron (and other species) to the sediment to see if they balance at steady state. Additionally, it would be meaningful to verify mass balance across all unit volumes of sediment to ensure that no significant mass loss occurs (some mass loss can be expected due to the discretization process which uses truncated Taylor polynomials to express the derivatives).

One of the main future improvements to modeling sediment diagenesis should be looking at coupling the sediment to the dynamics of the water column. The effect of the water column is great because it sets the boundary conditions of the sediment and thus can significantly affect the profiles. Specifically implementing complete or partial recycling of material effluxed into the water column may prove beneficial in expressing realistic conditions. In natural environments material is constantly lost from the sediment to the water column. However it is assumed that at least after some time some or all of this material will resettle back to the sediment (in some form) thus effectively being recycled. Modeling the nature (and time scale) of that recycling will help improve the realism of sedimentary models.

Another useful improvement would be to expand on how the solid phases of the sediment are modeled. It may be useful to increase the complexity of the described precipitation and dissolution processes (ex: including a growth and ripening stages), particularly when the precipitation reactions prove important. In some natural environments which are supersaturated with respect to a solid phase (ex.: vivianite), that phase is not observed. This is either because the kinetics of the solid phase are too slow or the solid phase is not stable in that environment. Accounting for those factors by modeling the kinetics in more detail or accounting for the stability of a solid phase before precipitating it may change solid species profiles and, with them, other profiles.

Adding other chemical cycles such as those of nitrogen, manganese and others is another logical extension of this study. With more chemical species and reactions combined together new interconnecting mechanisms may arise which will complement the results of this study. Another extension would include considering the biota population (bacteria) as a model variable through both bioturbation and for biologically mediated reactions (like OM degradation). As such, reaction rates in the sediment will be coupled to the environmental conditions, such as oxygen presence, and reflect more realistic behaviours. Looking at different phases of organic matter with differing resiliencies inside the sediment may also add useful complexity to the model by introducing organic material deeper into the sediment and stimulating some reactions to occur at depth.

References

Aguilera, D. R., Jourabchi, P., Spitery, C., Regnier, P., (2005) A knowledge-based reactive transport approach for the simulation of biogeochemical dynamics in Earth systems, *Geochemistry Geophysics Geosystems*, **6**.

Aller, R.C. (1982) The effects of macrobenthos on chemical properties of marine sediment and overlying water. In: *Animal-sediment relations*, McCall, P.L. and Tevesz, M.J.S. (eds), Plenum, New York, 53-102.

Balistrieri, L.S. and Murray, J.W. (1981). The surface chemistry of δMnO_2 in major ion seawater. *Geochim. & Cosmochim. Acta* **46**, 1041-1052.

Bandstra, L.M. (2000) Beloit College, Beloit, WI 53511, unpublished data.

Bharmal, S.M. and F.L. Laurent (2004) "Nutrient assessment from sediment pore waters at Kigoma Bay, Lake Tanganyika" *Nyanza Project course report.* (http://www.geo.arizona.edu/nyanza/past.html)

Beck M. B., (1987) Water quality modeling: A review of the analysis of uncertainty, *Water Resources Research*, **23**, 1393-1442.

Berner, Robert (1980) *Early Diagenesis A Theoretical Approach*, Princeton University Press, New Jersey.

Berner, R. A, (1970) Sedimentary pyrite formation. *American Journal of Science* **268,** 1-23.

Boudreau, Bernard P. (1996a) *Diagenetic Models and Their Implementation: Modeling Transport and Reactions in Aquatic Sediments*, Springer, Berlin.

Boudreau, Bernard P. (1996b) A method-of-lines code for carbon and nutrient diagenesis in aquatic sediments, *Computers & Geosciences*, **22**, 479-496.

Boström B., Andersen J. M., Fleischer S., and Jansson M. (1988) Exchange of phosphorus across the sediment-water interface. *Hydrobiologia* **170**, 229-244.

Brown, Peter N., Byrne, George D. and Alan C. Hindmarsh (1989) VODE: A Variable-Coefficient ODE Solver, *J. Sci. Stat. Comput.*, **10**, 1038-1051.

Brun R., Reichert P., and Kunsch H. R., (2001) Practical indentifiability analysis of large environmental simulation models, *Water Resources Research*, **37**, 1015 – 1030.

Byrne, G., and A. Hindmarsh (1987) Stiff ODE Solvers: A review of current and coming attractions, *Journal of Computational Physics*, **70**, 1-62.

Carignan R. and Tessier A. (1988). The co-diagenesis of sulfur and iron in acid lake sediments of southwestern Quebec, *Geochim. Cosmochim. Acta* **52**, 1179-1188.

Curtis P.J. (1989). Effects of hydrogen ion and sulphate on the phosphorus cycle of a Precambrian Shield lake. *Nature* **337**, 156-158.

Davison, W., Lishman, J. P., and Hilton, J. (1985) Formation of pyrite in freshwater sediments: implications for C/S ratios, *Geochimica and Cosmochimica Acta*, **149**, 1615-1620.

Davison, W., (1993) Iron and Manganese in lakes. *Earth-Science Reviews.* **34,** 119-163.

Dittrich M., Wehrli B., and Reichert P. (2004). Lake sediment modeling over different time scales, in press.

Einstein, A. (1905) On the motion of small particles suspended in liquids at rest required by the molecular kinetic theory of heat, *Annalen Der Physik*, **17**, 549-560.

Elrod, Virginia A., William M. Berelson, Kenneth H. Coale, and Kenneth S. Johnson (2004) The flux of iron from continental shelf sediments: A missing source for global budgets, *Geophysical Research Letters*, **31**.

Emerson, S. (1985) Early diagenesis in anaerobic lake sediments. II Thermodynamics and kinetics controlling the formation of iron phosphate. *Geochimica et Cosmochimica Acta.* **42**, 1307 – 1316.

Fiadero, M.E. and Veronis, G. (1977) On weighted-mean schemes for the finite-difference approximation to the advection-diffusion equation. *Tellus* **29**.

Fossing H., Berg P., Thamdrup B., Rysgaard S., Sorensen H.M., and Nielsen K. (2004). A model set-up for an oxygen and nutrient flux model for Aarhus Bay (Denmark). *NERI Technical Report*, No. **483**.

Froelich P.N., Klinkhammer G.P., Bender M.L., Luedtke G.R., Heath G.R., Cullen D., Dauphin P. (1979). Early oxidation of organic matter in pelagic sediments of the eastern equatorial Atlantic: suboxic diagenesis. *Geochim. Cosmochim. Acta* **43**, 1075-1090.

Fürrer and Wehrli (1996). Microbial reactions, chemical speciation, and multicomponent diffusion in porewaters of a eutropic lake, *Geochim. Cosmochim. Acta* **60,** 2333-2346.

Haese, R., (2000) The reactivity of Iron, in *Marine Geochemistry*, Eds.: H.D. Schulz and M. Zabel, Springer-Verlag, Berlin, 233 – 261.

Hansel, C. et. al., (2003) Secondary mineralization pathways induced by dissimilatory iron reduction of ferrihydrite under advective flow, *Geochimica et Cosmochimica Acta*, **67**, 2977-2992.

Hecky R. E., Campbell P., and Hendzel L. L. (1993) The stoichiometry of carbon, nitrogen, and phosphorus in particulate matter of lakes and oceans. *Limnol. Oceanogr.* **38**, 709-724.

Heide N. Schulz[1*] and Horst D. Schulz[2] (2005) Large Sulfur Bacteria and the Formation of Phosphorite, *Science*, **307**, 416-418.

Hunter, K.S., Wang, Y., and Van Cappellen, P. (1998). Kinetic modeling of microbially driven redox chemistry of subsurface environments: coupling transport, microbial metabolism and geochemistry. *J. Hydrol.* **209**, 53-80.

Hupfer, M., Fischer, P. and K. Freses (1998) Phosphorus Retention mechanisms in the sediment of an eutrophic mining lake. *Water, Air, and Soil Pollution.* **108**, 341-352.

Kainz, Martin, Marc Lucotte, and Christopher C. Parrish, (2003) Relationships between organic matter composition and methyl mercury content of offshore and carbon-rich littoral sediments in an oligotrophic lake, NRC Canada Report. (http://web.uvic.ca/water/publications/)

Kalff, J. (2002) Iron, Manganese, and Sulfur in Limnology*: Inland Water Ecosystems.* Prentice Hall, NJ, 384 – 291.

Katsev S., Rancourt D.G., and L'Heureux I. (2004). dSED: A database tool for modeling sediment early diagenesis, *Computers and Geosciences* **30**, 959-967

Katsev, S., Tsandev, I., L'Heureux I., and D. G. Rancourt (submitted to GCA 2005) Factors Controlling Long Term Phosphorus Efflux in lake sediments: Exploratory reaction-transport modeling.

Konhauser, K. O. (1998) Diversity of bacterial iron mineralization. *Earth Science Reviews.* **43**, 91-121.

Laksov, C., Amelung, W. and Pfeiffer, S. (2002) Organic Matter Preservation in the Sediment of an Acidic Mining Lake. *Env. Sci. and Technol.* **36**, 4218 – 4223.

Langmuir, D. (1997) *Aqueous Environmental Geochemistry*, Prentice Hall, NJ.

Lerman, A. D., Imboden, J. and J. Gat eds. (1978) *Physics and Chemistry of Lakes.* Springer-Verlag, NY.

Loveley, Derek R., (1987) Organic Matter Mineralization with the Reduction of Ferric Iron: A Review, *Geomicrobiology Journal.* **5**, 375 – 399.

Maassen ,Sebastian, Dietrich Uhlmann and Isolde Ro (2005) Sediment and pore water composition as a basis for the trophic evaluation of standing waters, *Hydrobiologia*, **543**, 55–70.

Manheim, F. T. (1970) Diffusion of iorns in unconsolidated sediments, *Earth and Planetary Science Letters*, **9**, 307.

Manning P.G., Murphy T.P. and Prepas E.E. (1991) Intensive formation of vivianite in the bottom sediments of mesotrophic Narrow Lake, Alberta. *Can. Mineral.* **29**, 77-85.

Markov I. (1995) *Crystal Growth for Beginners*, World Scientific.

Meysman, F. (2001) Modelling the Influence of Ecological Interactions on Reactive Transport Processes in Sediments, PhD Thesis, Ghent University (Belgium).

Meysman F.J.R., Boudreau B.P., and Middelburg J.J. (2004). Why does biological mixing resemble Fickian diffusion? *J. Mar. Res.,* in press.

Montgomery D.C. (1997) *Design and analysis of experiments*, John Wiley & Sons, New York.

Morel, Francois M. M. and Janet G. Hering, (1993) *Principles and Applications of Aquatic Chemistry,* Wiley Inter-Science, NY.

Morse, J., W. (1999) Sulphides in Sandy sediments: New Insights on the reactions responsible for sedimentary pyrite, *Aquatic Geochemistry* **5**, 75-85.

Morse J. W., Millero F.J., Cornwell J.C., and Rickard D. (1987). The chemistry of the hydrogen sulfide and iron sulfide systems in natural waters. *Earth-Sci. Rev.* **24**, 1-42.

Murray, T. (1995) The correlation between iron sulfide precipitation and hypolimnetic phosphorus accumulation during one summer in a soft water lake, *Can. J. Fish. Aquat. Sci.* **52**, 1190-1194.

Nedwell, D. B., (1982) The cycling of Sulphur in Marine and Freshwater Sediments, in *Sediment Microbiology*, Nedwell, D. B. and Brown, C. M., eds. Academic Press, London, 73 - 106.

Omlin M., Brun R., and Reichert P. (2001) Biogeochemical model of lake Zurich: Sensitivity, identifiability and uncertainty analysis. *Ecological Modelling* **141**, 105-123.

Press, William H., Teukolsky, Saul A., Vetterling, William T. and Brian P. Flannery (1986) *Numerical Recipes in Fortran 90*, University of Cambridge Press, Cambridge.

Pyzik, A. J., and Sheldon E. Sommer, (1981) Sedimentary iron monosulphides: kinetics and mechanism of formation. *Geochimica et Cosmochimica Acta.* **45**, 687 – 698.

Rickard D. (1997). Kinetics of pyrite formation by the H_2S oxidation of iron (II) monosulfide in aqueous solutions between 25 and 125 C: The rate equation. *Geochim. Cosmochim. Acta* **61**, 115-134.

Roden E. E. and Edmonds J. W. (1997) Phosphate mobilization in iron-rich anaerobic sediments: microbial Fe(III) oxide reduction versus iron-sulfide formation. *Arch. Hydrobiol.* **139**, 347-378.

Rudd, J. W. M., Kelly, C. A., and Furutani, A. (1986) Role of sulphate reduction in long term accumulation of organic and inorganic sulphur in lake sediments. *Limnology and Oceanography.* **31**, 1281-1291.

Saltelli, A., S. Tarantola, and K. Chan (1999) A quantitative, model independent method for global sensitivity analysis of model output, *Technometrics*, **41** (1), 39-56.

Santana-Casiano, J. M., Gonzalez-Davila, M., Rodriguez M. J., and Millero, F. (2000) The effect of organic compounds in the oxidation kinetics of Fe(II). *Marine Chemistry.* **70**, 211 – 222.

Schiesser, W. E., (1991) *The Numerical Method of Lines: Integration of Partial Differential Equations*, Academic Press, San Diego.

Soetaert K., Herman P. M. J., and J. J. Middelburg, (1996) A model of early diagenetic processes from the shelf to abyssal depths, *Geochimica et Cosmochimica Acta*, **60**, 1019-1040.

Steefel, C.I. and K.T.B MacQuarrie, (1996) Approaches to Modeling Reactive Transport in porous Media, In: *Reactive Transport in Porous Media*, Lichter, P.C., Steefel, C.I. and E.H. Oelkers eds., In: *Reviews in Mineralogy*, **34**, Mineralogical Society of America.

Talbot, M.R and P.A. Allen, (1996) Lakes, in *Sedimentary Environments: Processes, Facies and Stratigraphy*, Reading, H.G., ed., Blackwell Science, 83 – 124.

Tromp T.K., Van Cappellen P., Key R.M. (1995). A global model for the early diagenesis of organic carbon and organic phosphorus in marine sediments. *Geochimica Cosmochimica Acta* **59**, 1259-1284.

Urban, N. R., (1994) Retention of Sulphur in Lake sediments, in *Environmental Chemistry of Lakes and Reservoirs*, Baker, L. A., ed. American Chemical Society, Washington D.C., 323 – 369.

Van Cappellen, P. and Y. Wang (1996) Cycling of iron and manganese in surface sediments: a general theory for the coupled transport and reaction of carbon, oxygen, nitrogen, sulfur, iron and manganese, *American Journal of Science*, **296**, 197-243.

Van Cappellen P. and Y. Wang (1995) Metal cycling in surface sediments: modeling the interplay between transport and reaction; in Metal Speciation and Contamination of Aquatic Sediments (Allen, H.E., ed), Ann Arbor Press, 21-64.

Van Cappellen P., Gaillard J.-F. and C. Rabouille, (1993) Biogeochemical transformations in sediments: Kinetic models of early diagenesis, *NATO ASI Series*, **14**, 401-445.

Wersin , Paul, Patrick Hohener, Rudolf Giovanoli and Werner Stumm, (1991), Early Diagenetic Influences on Iron Transformations in Fresh-Water Lake Sediment, Chemical Geology, **90**, 233-252.

Wetzel, R. (1983) *Limnology*, Saunders, Philadelphia.

Wetzel, R. and G. Likens (2000) *Limnological Analyses*, Springer, NY.

Wijsman J.W.M., Herman, P.M.J., Middelburg, J.J. and Soetaert, K. (2002). A model for early diagenesis processes in sediments of the continental shelf of the Black Sea. *Estuarine, Coastal and Shelf Science* **54**, 403-421.

Appendix

DATA I

Vivianite Parameters Factorial Test

Legend: Chemical Species:

Designation		Species: { Chemical Formula }
[Fe2+]	–	Aqueous Iron : { $[Fe^{2+}]$ }
FeOH3	–	Iron oxyhydroxide : { $Fe(OH)_3$ }
FeS	–	Iron monosulfide : { FeS }
FeS2	–	Pyrite : { FeS_2 }
Viv	–	Vivianite : { $Fe_2(PO_4)_3$ }
pH	–	Acidity : { $[H^+]$ }
adsorbed P	–	Adsorbed Phosphate : { Solid≡P }
TS	–	Total aqueous Sulphur: { $[HS^-] + [H_2S]$ }
TC	–	Total aqueous Carbon: { $[CO_3^{2-}]+[HCO_3^-]+[H_2CO_3]$ }
OM	–	Organic matter : { CH_2O }
[O2]	–	Oxygen : { $[O_2]$ }
[SO4]	–	Dissolvaed Sulphate : { $[SO_4^{2-}]$ }
[H3PO4]	–	Dissolved Phosphate : { $[H_3PO_4]$ }
[NO3]	–	Dissolved Nitrate : { $[NO_3]$ }
[CH4]	–	Dissolved Methane : { $[CH_4]$ }

Parameters:

Name	Description	Low Value	High Value
$Fe(OH)_3$ flux	*Iron hydroxide flux at the SWI*	1.25×10^{-5} mol·cm2/yr	7.0×10^{-5} mol·cm2/yr
$[SO4]_{top}$	*Concentration of sulfate at the SWI*	1.0×10^{-8} mol/cm^3	0.5×10^{-6} mol/cm^3
Rviv	*Rate of vivianite formation*	Kviv = 1.0×10^{-10} mol/g·yr	Kviv = 3.0×10^{-9} mol/g·yr
R'viv	*Rate of vivianite dissolution*	K'viv = 0.1 1/yr	K'viv = 10 1/yr
Rsviv	*Rate of viviatine dissolution by sulphide (H_2S)*	Ksviv = 0.0 cm^3/mol·yr	Ksviv=1.0×10^8 cm^3/mol·yr
RsFeCO3	*Rate of siderite dissolution by sulphide (H_2S)*	$KsFeCO_3$ = 0.0 cm^3/mol·yr	$KsFeCO_3$= 1.0×10^8cm^3/mol·yr

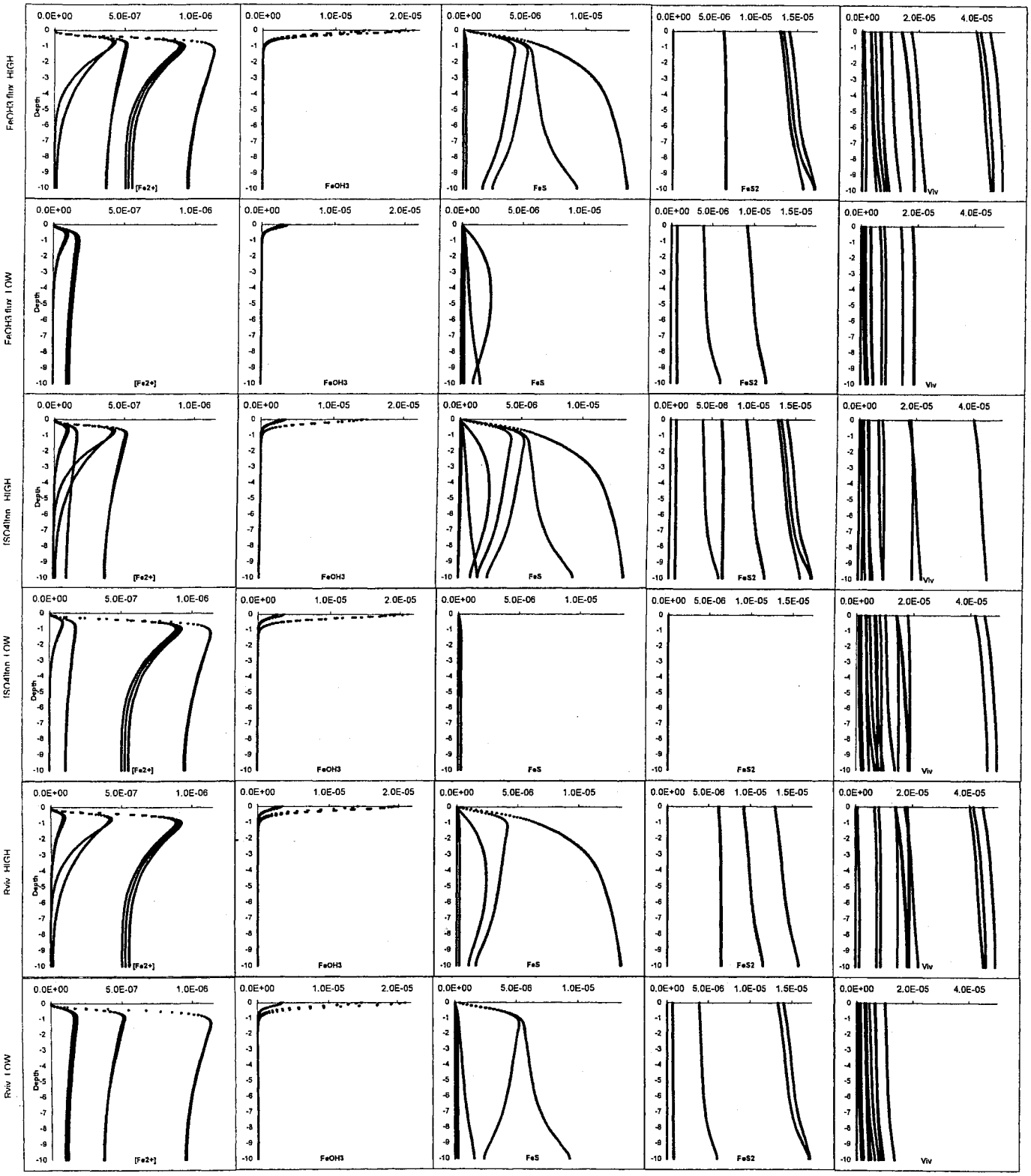
FeOH3 flux HIGH
FeOH3 flux LOW
fSO4flux HIGH
fSO4flux LOW
Rviv HIGH
Rviv LOW
Depth
[Fe2+]
FeOH3
FeS
FeS2
Viv
0.0E+00
5.0E-07
1.0E-06
1.0E-05
2.0E-05
5.0E-06
1.5E-05
4.0E-05


Rviv HIGH
Rviv LOW
Rsviv HIGH
Rsviv LOW
RsFeCO3 HIGH
RsFeCO3 LOW
Depth
[Fe2+]
FeOH3
FeS
FeS2
Viv
0.0E+00
5.0E-07
1.0E-06
1.0E-05
2.0E-05
5.0E-06
1.5E-05
4.0E-05

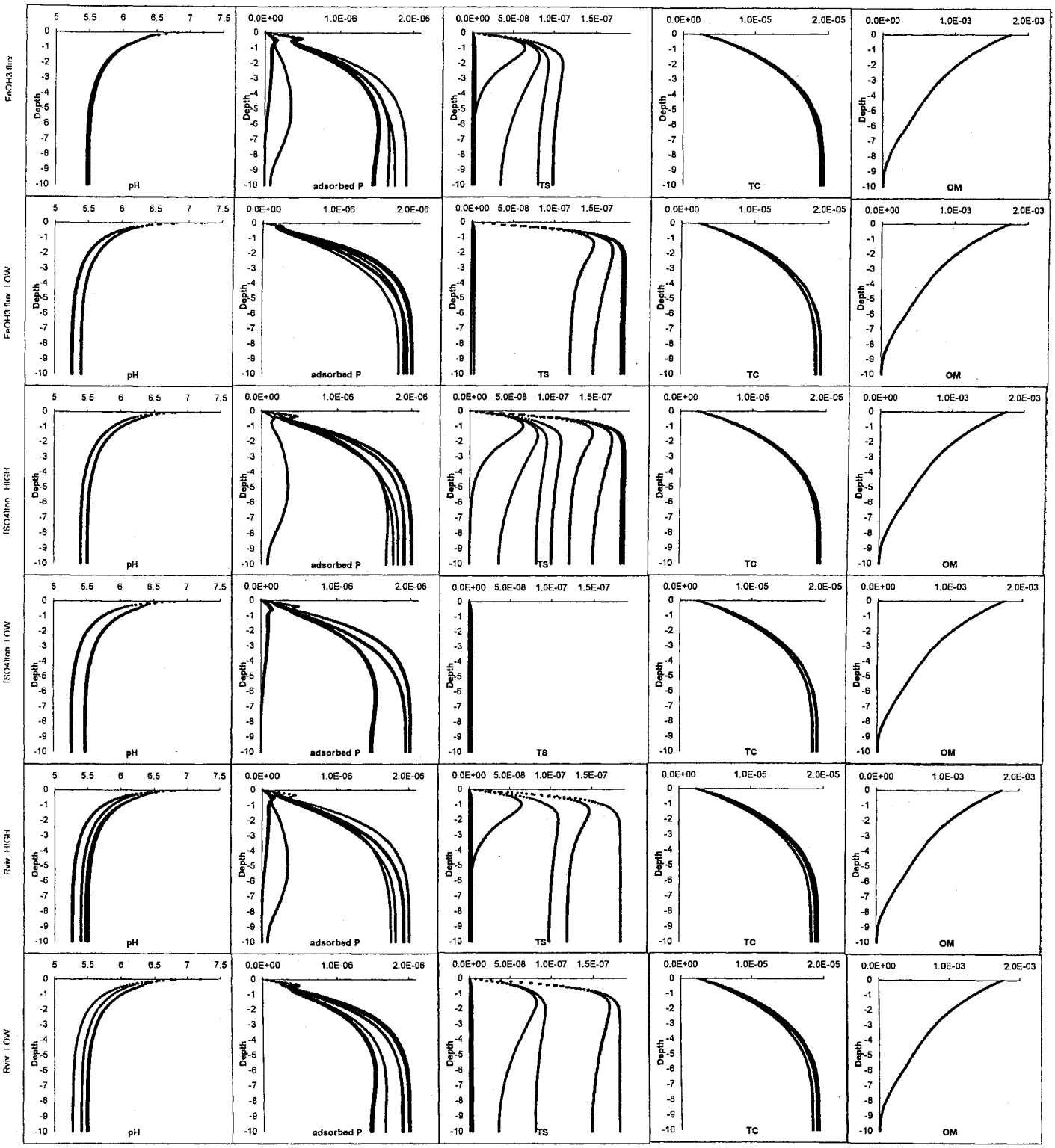
FeOH3 flux
FeOH3 flux LOW
SO4 flux HIGH
SO4 flux LOW
Riv HIGH
Riv LOW
Depth
pH
adsorbed P
TS
TC
OM

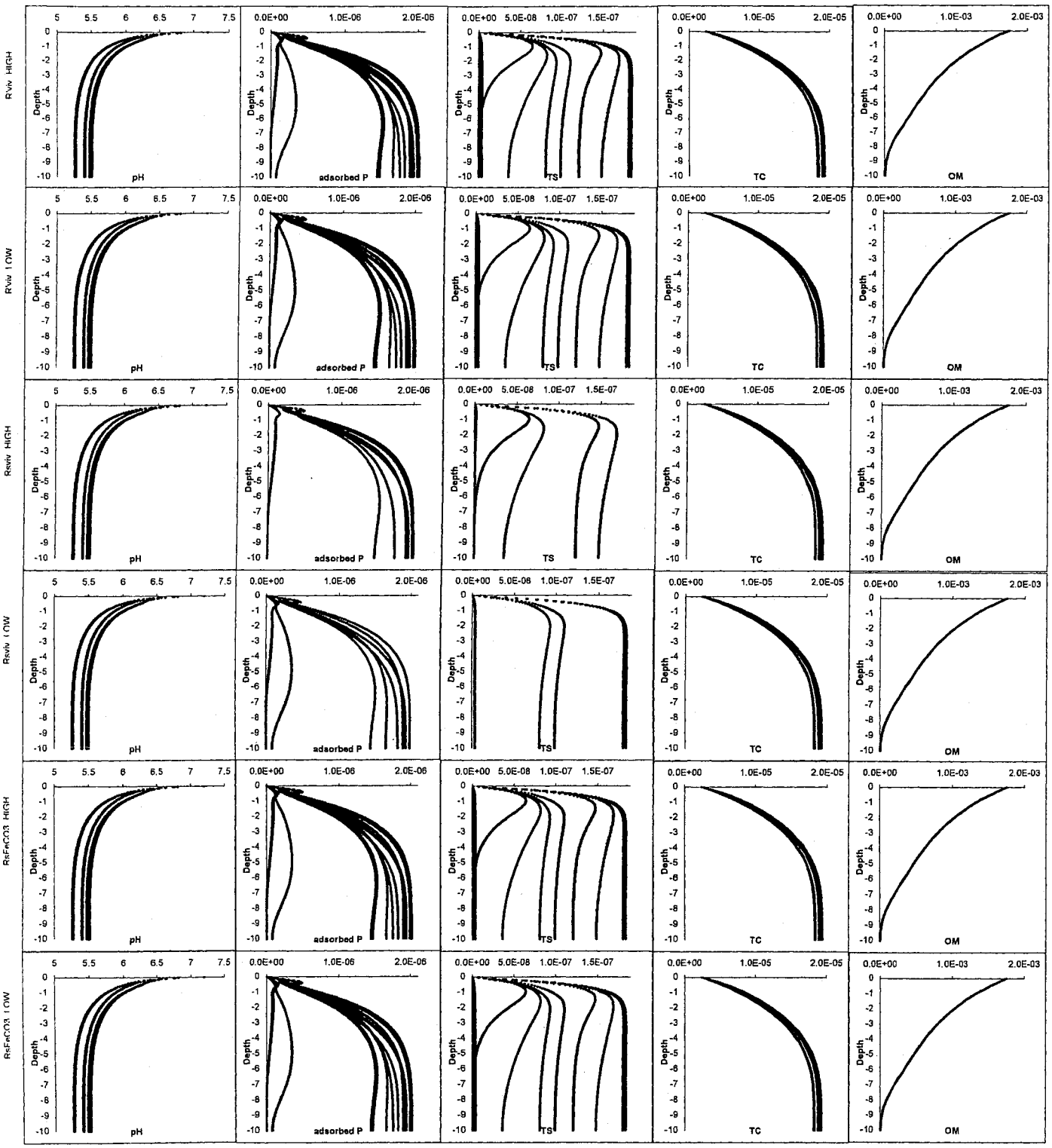
Rviv HIGH
Rviv LOW
Rviv HIGH
Rviv LOW
RsFeCO3 HIGH
RsFeCO3 LOW
pH
adsorbed P
TS
TC
OM
Depth

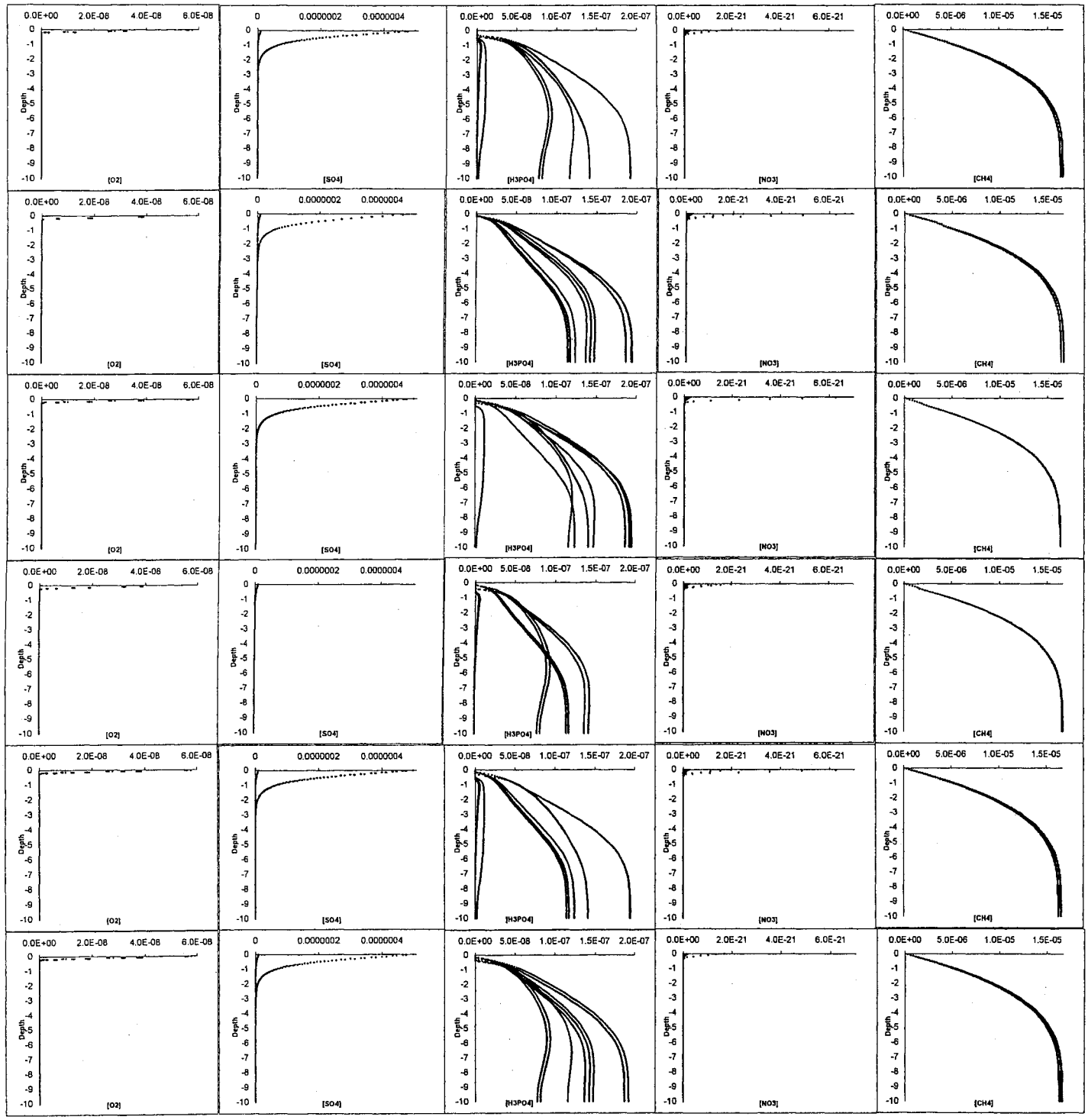
Fe(OH)3 flux HIGH
Fe(OH)3 flux LOW
ISO4dmn HIGH
ISO4dmn LOW
Rxiv HIGH
Rxiv LOW
[O2]
[SO4]
[H3PO4]
[NO3]
[CH4]
Depth

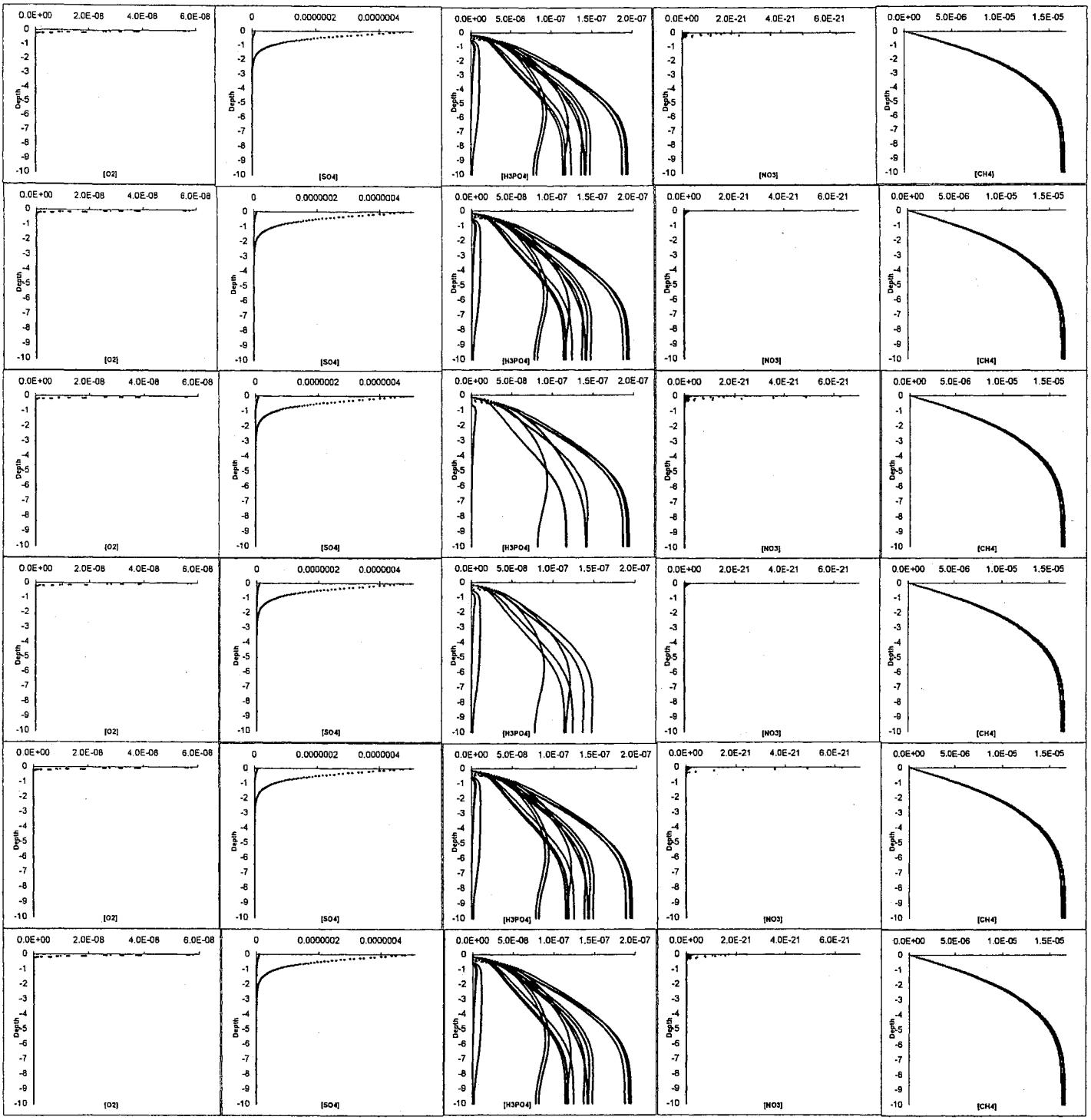
Revu HIGH
Revu LOW
Revu HIGH
Revu LOW
ReFeOx HIGH
ReFeOx LOW
Depth
[O2]
[SO4]
[H3PO4]
[NO3]
[CH4]

DATA 2

Sorption parameters

Legend: Species:

Designation		Species : { Chemical Formula }
[Fe2+]	–	Aqueous Iron : { $[Fe^{2+}]$ }
FeOH3	–	Iron oxyhydroxide : { $Fe(OH)_3$ }
FeS	–	Iron monosulfide : { FeS }
FeS2	–	Pyrite : { FeS_2 }
Viv	–	Vivianite : { $Fe_2(PO_4)_3$ }
pH	–	Acidity : { $[H^+]$ }
adsorbed P	–	Adsorbed phosphate : { Solid≡P }
TS	–	Total aqueous sulphur: { $[HS^-] + [H_2S]$ }
TC	–	Total aqueous carbon: { $[CO_3^{2-}]+[HCO_3^-]+[H_2CO_3]$ }
OM	–	Organic matter : { CH_2O }
[O2]	–	Oxygen : { O_2 }
[SO4]	–	Dissolvaed Sulfate : { $[SO_4^{2-}]$ }
[H3PO4]	–	Dissolved Phosphate : { $[H_3PO_4]$ }
[NO3]	–	Dissolved Nitrate : { $[NO_3]$ }
[CH4]	–	Dissolved Methane : { $[CH_4]$ }

Parameters:

Name	Description	Low Value	High Value
KPonFe	*Adsorption constant for phosphate on iron oxides*	KPonFe = 2.0×10^{-2}	KPonFe = 1.0×10^{-1}
$Fe(OH)_3$ flux	*Flux of iron oxides at the SWI*	1.25×10^{-5} mol·cm^2/yr	7.0×10^{-5} mol·cm^2/yr
$[O_2]$ top	*Concentration of oxygen at the SWI*	0.0 mol cm^{-3}	1.5×10^{-7} mol cm^{-3}
$[SO_4]$ top	*Concentration of sulfate at the SWI*	1.0×10^{-8} mol cm^{-3}	0.5×10^{-6} mol cm^{-3}
RFeSFe3	*Rate of dissolution of iron oxide by FeS*	KFeSFe3 = 0.0 g / mol·yr	KFeSFe3= 1.0×10^4 g / mol·yr
DBmax	*Maximum bioturbation*	DBmax = 1.0 cm^{2}yr^{-1}	DBmax = 10.0 cm^{2}yr^{-1}

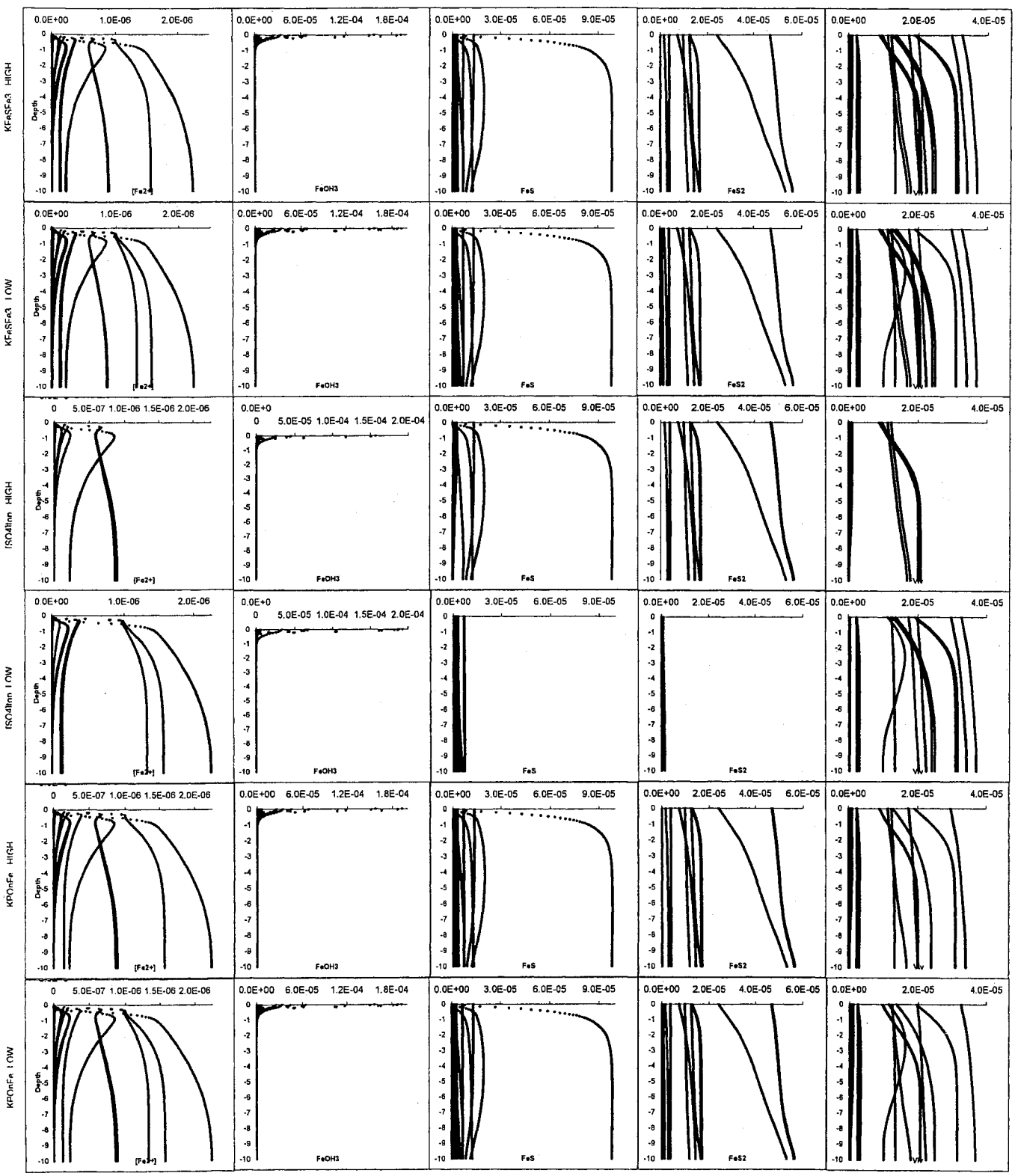
KFeSFe3 HIGH
KFeSFe3 LOW
ISO4flux HIGH
ISO4flux LOW
KPOnFe HIGH
KPOnFe LOW
Depth
[Fe2+]
FeOH3
FeS
FeS2

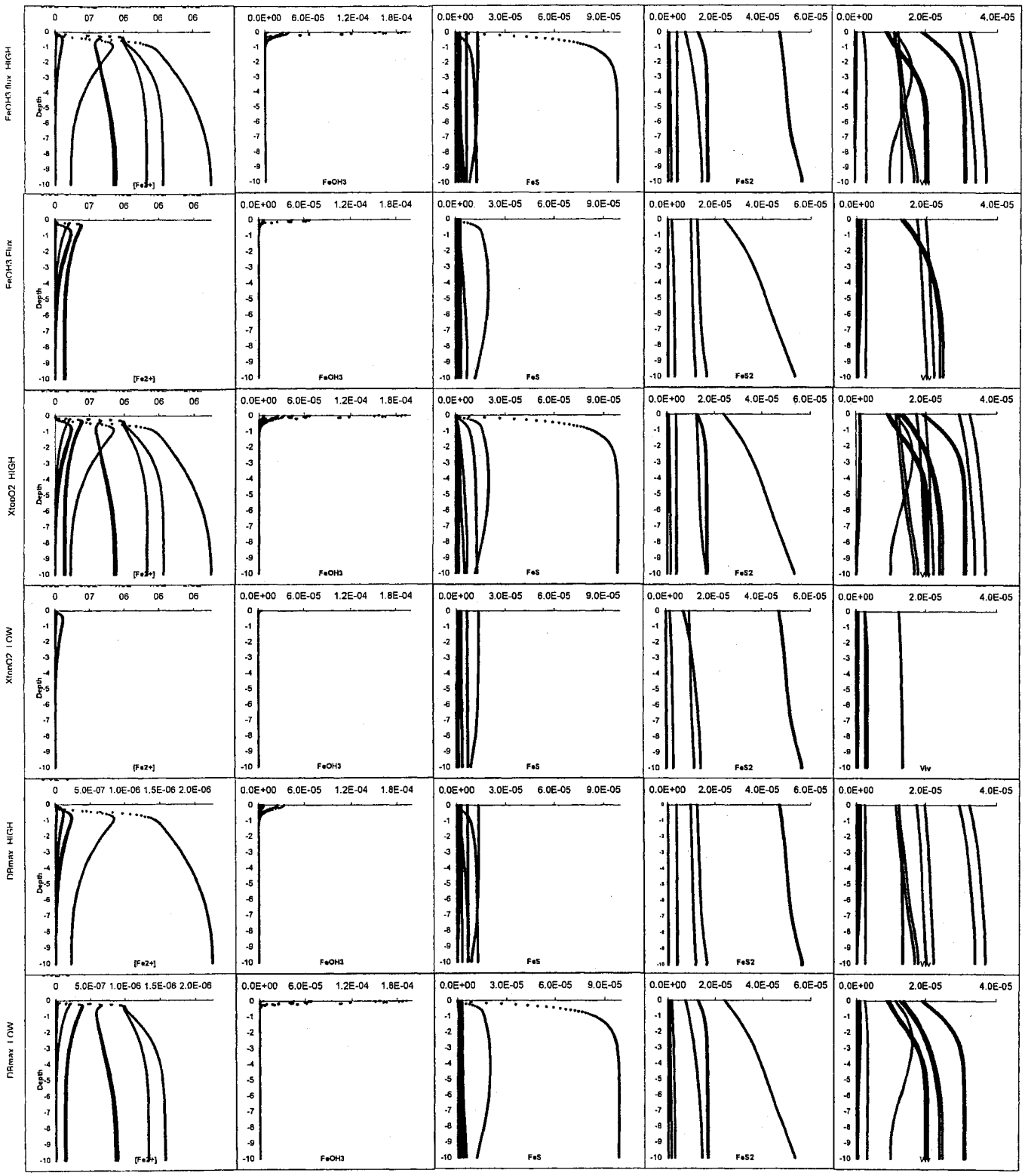
FeOH3 flux HIGH
FeOH3 Flux
XtotO2 HIGH
XtotO2 LOW
DRmax HIGH
DRmax LOW
Depth
[Fe2+]
FeOH3
FeS
FeS2
Viv

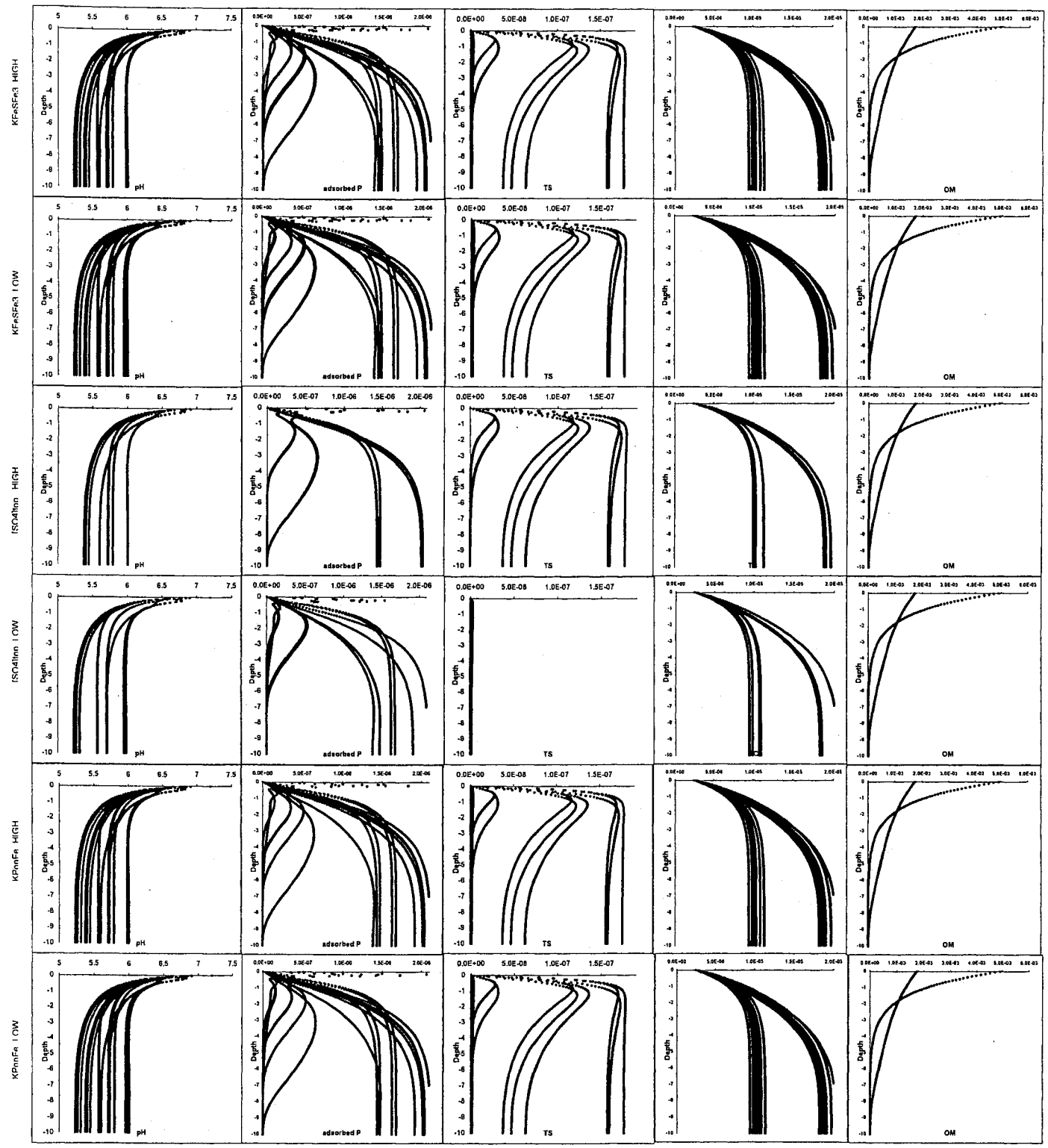
KFeSFe3 HIGH
KFeSFe3 LOW
MSO4Mn HIGH
MSO4Mn LOW
KPmFe HIGH
KPmFe LOW
pH
adsorbed P
TS
OM
Depth

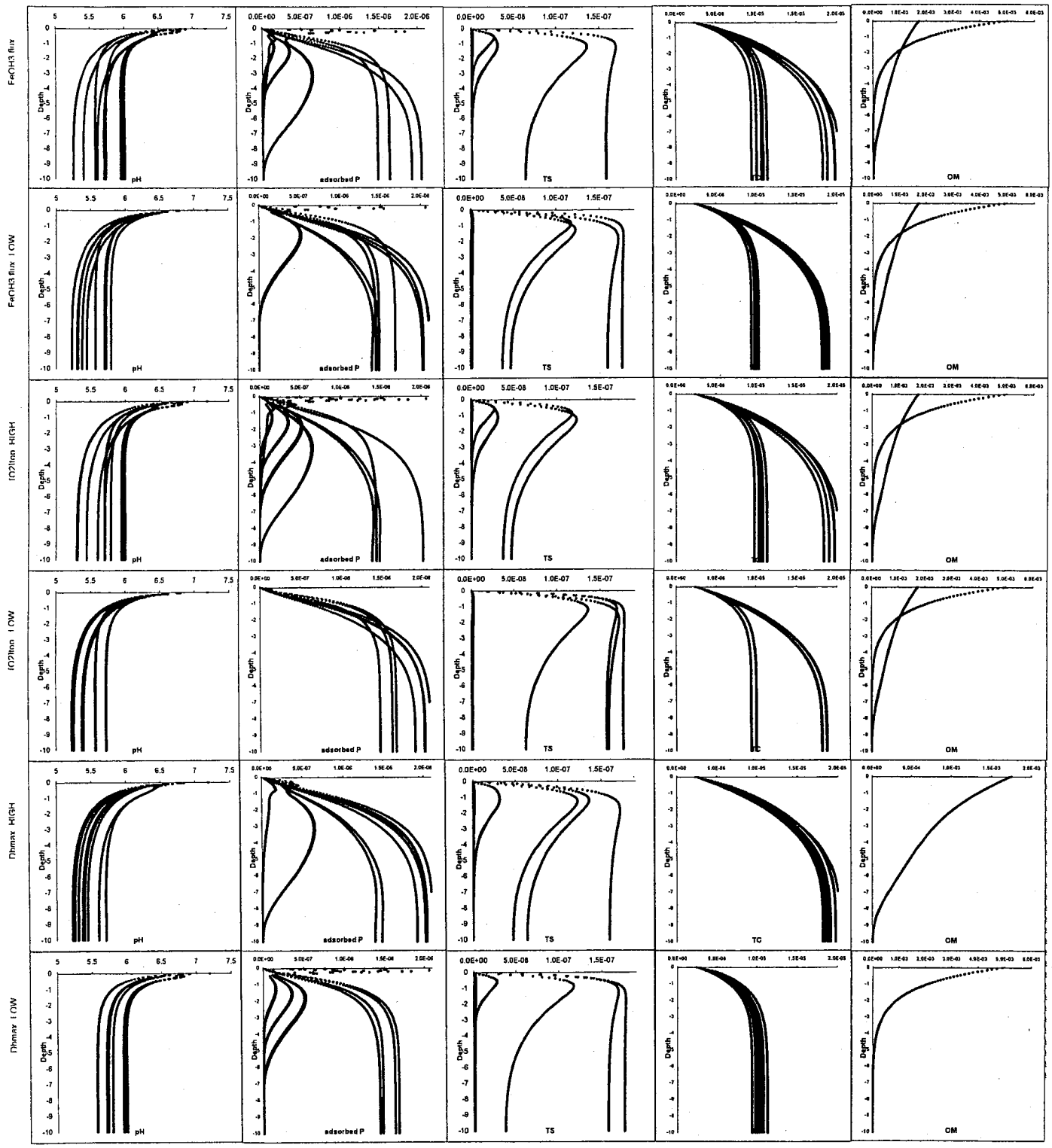
FeOH3 flux
FeOH3 flux LOW
Diffusion HIGH
Diffusion LOW
Dbmax HIGH
Dbmax LOW
pH
adsorbed P
TS
TC
OM
Depth

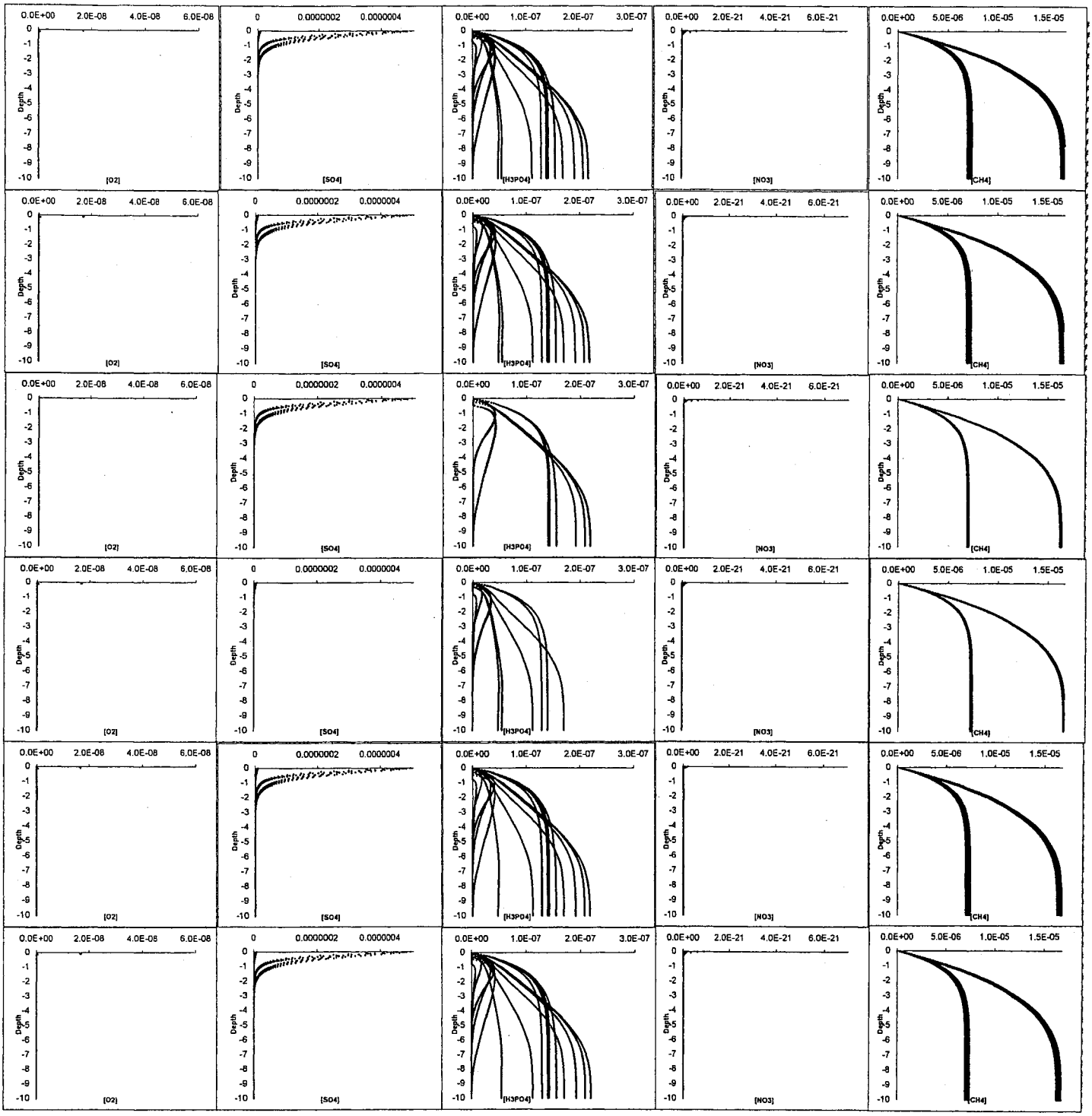
KFeSFe3 HIGH
KFeSFe3 LOW
KMnMn HIGH
KMnMn LOW
KFeFe HIGH
KFeFe LOW
Depth
[O2]
[SO4]
[H3PO4]
[NO3]
[CH4]

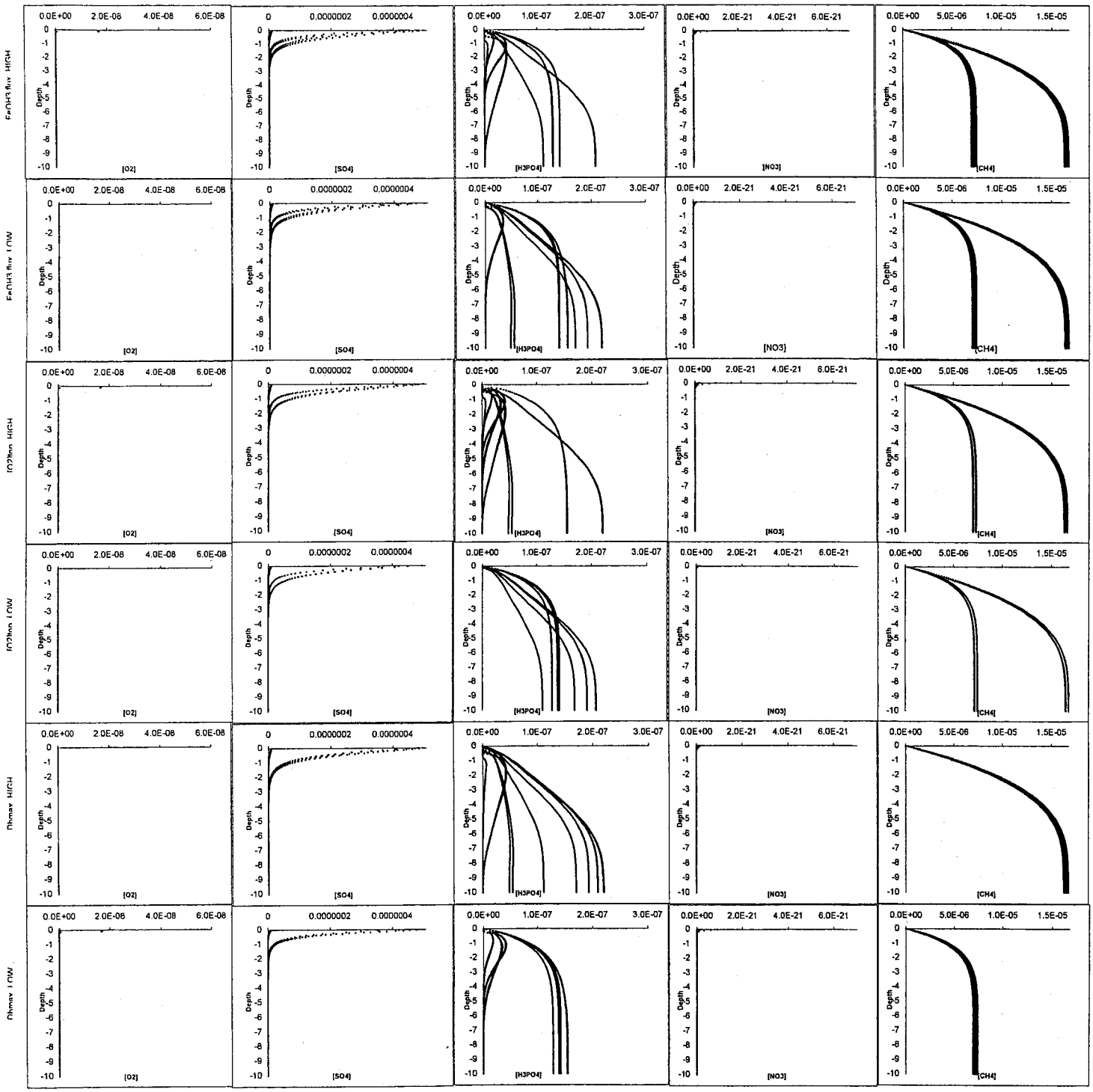
FeOH3 flux HIGH
FeOH3 flux LOW
Oxygen HIGH
Oxygen LOW
Dmax HIGH
Dmax LOW
Depth
[O2]
[SO4]
[H3PO4]
[NO3]
[CH4]

DATA 3

Sorption parameters

Legend: Species:

Designation		Species : { Chemical Formula }
[Fe2+]	–	Aqueous Iron : { $[Fe^{2+}]$ }
FeOH3	–	Iron oxyhydroxide : { $Fe(OH)_3$ }
FeS	–	Iron monosulfide : { FeS }
FeS2	–	Pyrite : { FeS_2 }
Viv	–	Vivianite : { $Fe_2(PO_4)_3$ }
pH	–	Acidity : { $[H^+]$ }
adsorbed P	–	Adsorbed phosphate : { Solid≡P }
TS	–	Total aqueous sulphur: { $[HS^-] + [H_2S]$ }
TC	–	Total aqueous carbon: { $[CO_3^{2-}]+[HCO_3^-]+[H_2CO_3]$ }
OM	–	Organic matter : { CH_2O }
[O2]	–	Oxygen : { O_2 }
[SO4]	–	Dissolvaed Sulfate : { $[SO_4^{2-}]$ }
[H3PO4]	–	Dissolved Phosphate : { $[H_3PO_4]$ }
[NO3]	–	Dissolved Nitrate : { $[NO_3]$ }
[CH4]	–	Dissolved Methane : { $[CH_4]$ }

Parameters:

Name	Description	Low Value	High Value
OM flux	*Flux of organic matter at the SWI*	1.25×10^{-3} mol·cm^2/yr	5.0×10^{-3} mol·cm^2/yr
$Fe(OH)_3$ flux	*Flux of iron oxides at the SWI*	1.25×10^{-5} mol·cm^2/yr	7.0×10^{-5} mol·cm^2/yr
$[O_2]$ top	*Concentration of oxygen at the SWI*	0.0 mol cm^{-3}	1.5×10^{-7} mol cm^{-3}
$[SO_4]$ top	*Concentration of sulfate at the SWI*	1.0×10^{-8} mol cm^{-3}	0.5×10^{-6} mol cm^{-3}
KG	*Rate of organic matter respiration*	KG = 0.3 mol cm^2/yr	KG = 0.9 mol cm^2/yr

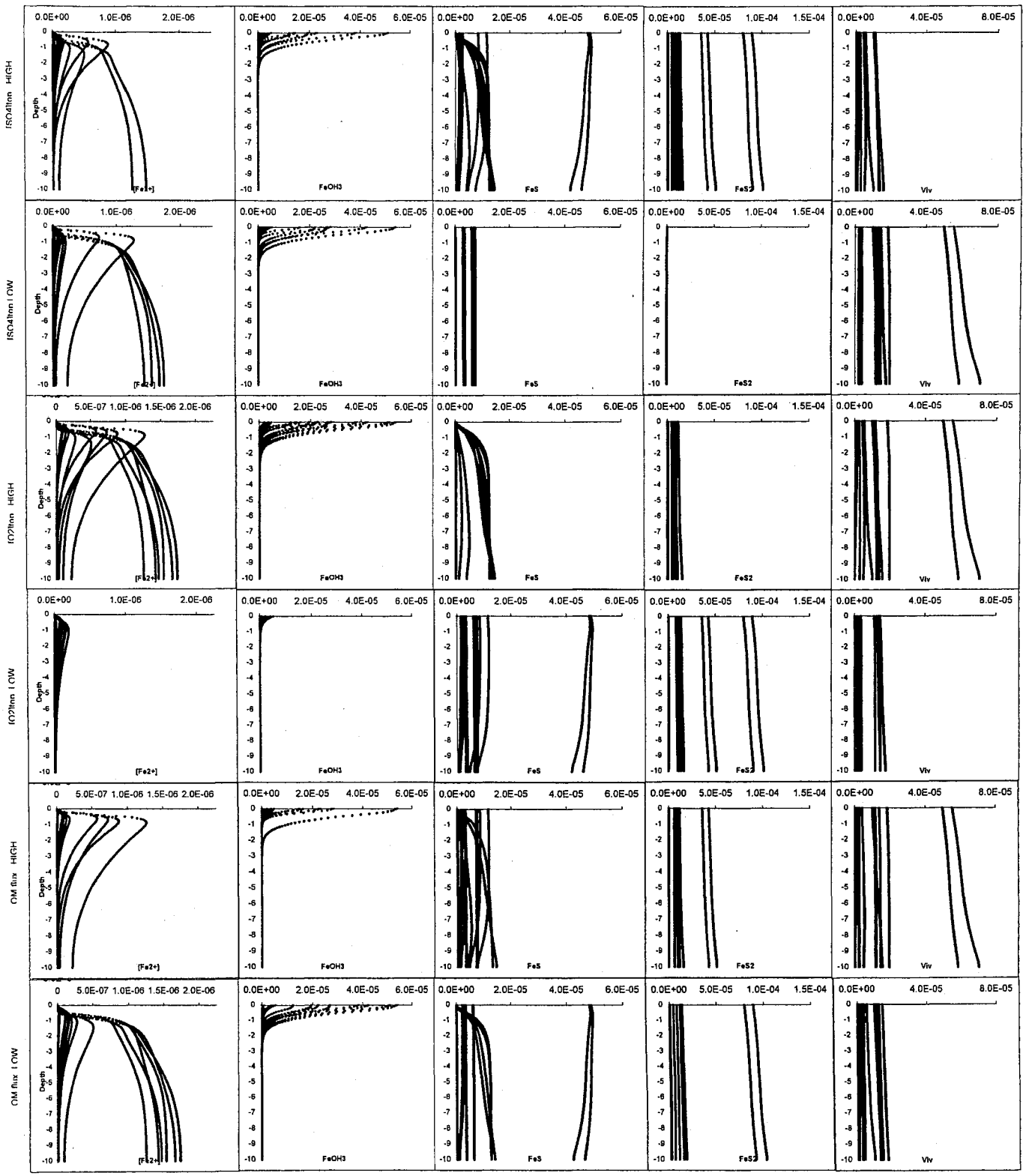
Isolation HIGH
Isolation LOW
OM flux HIGH
OM flux LOW
Depth
[Fe2+]
FeOH3
FeS
FeS2
Viv

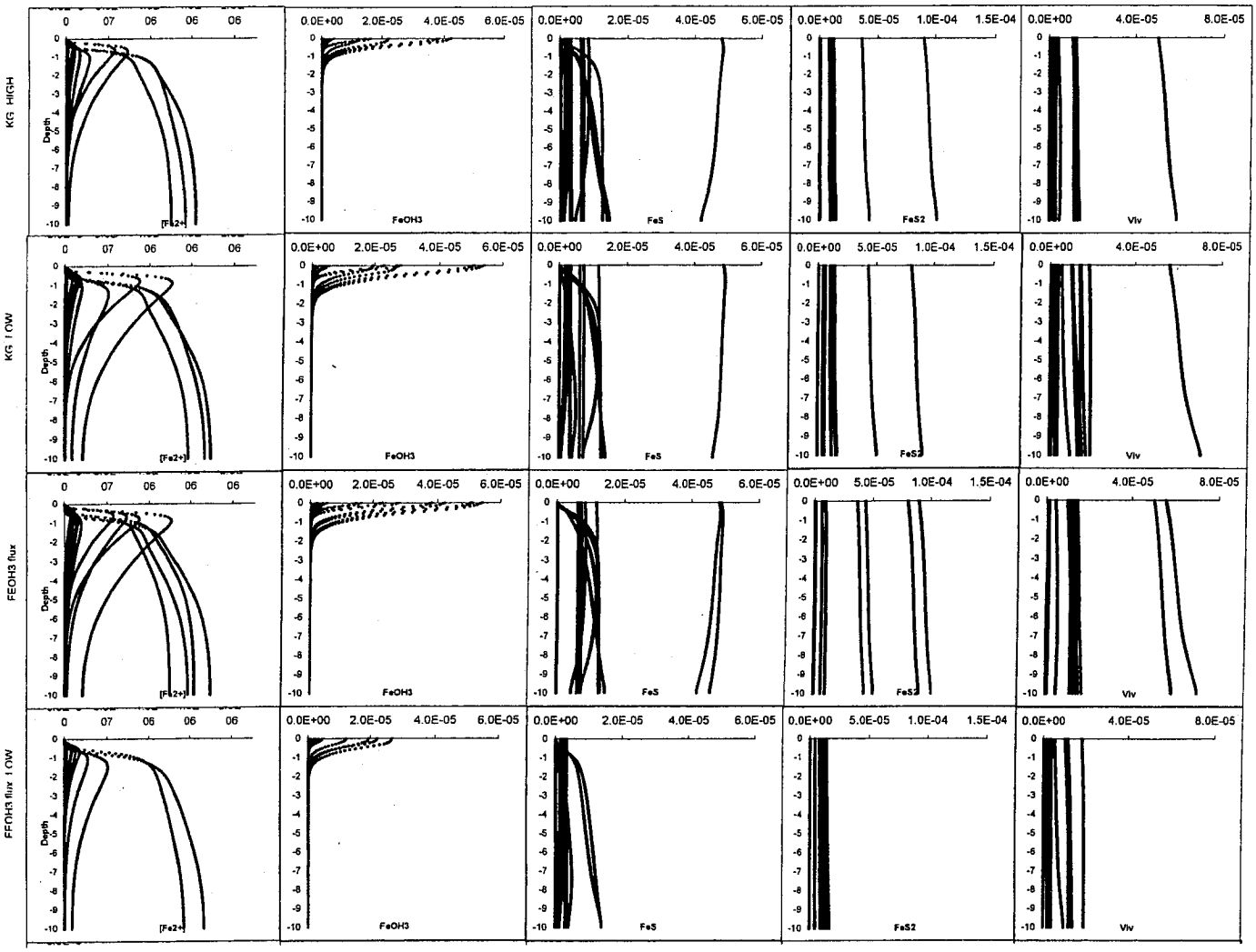
KG HIGH
KG LOW
FEOH3 flux
FEOH3 flux LOW
Depth
[Fe2+]
FeOH3
FeS
FeS2
Viv
0 07 06 06 06
0.0E+00 2.0E-05 4.0E-05 6.0E-05
0.0E+00 5.0E-05 1.0E-04 1.5E-04
0.0E+00 4.0E-05 8.0E-05

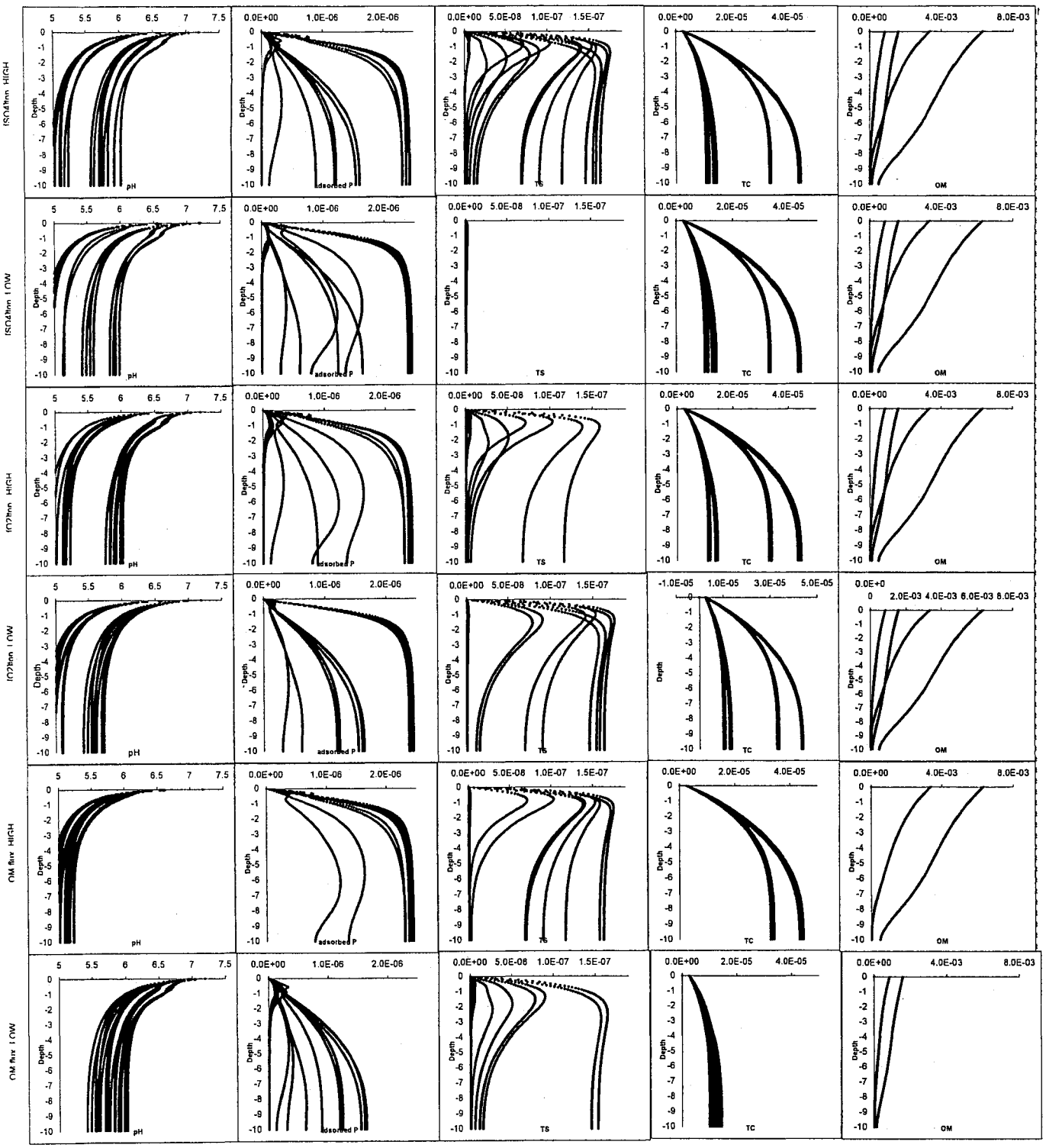
ISOAtm HIGH
ISOAtm LOW
ISOAtm HIGH
ISOAtm LOW
OM flux HIGH
OM flux LOW
pH
adsorbed P
TS
TC
OM
Depth

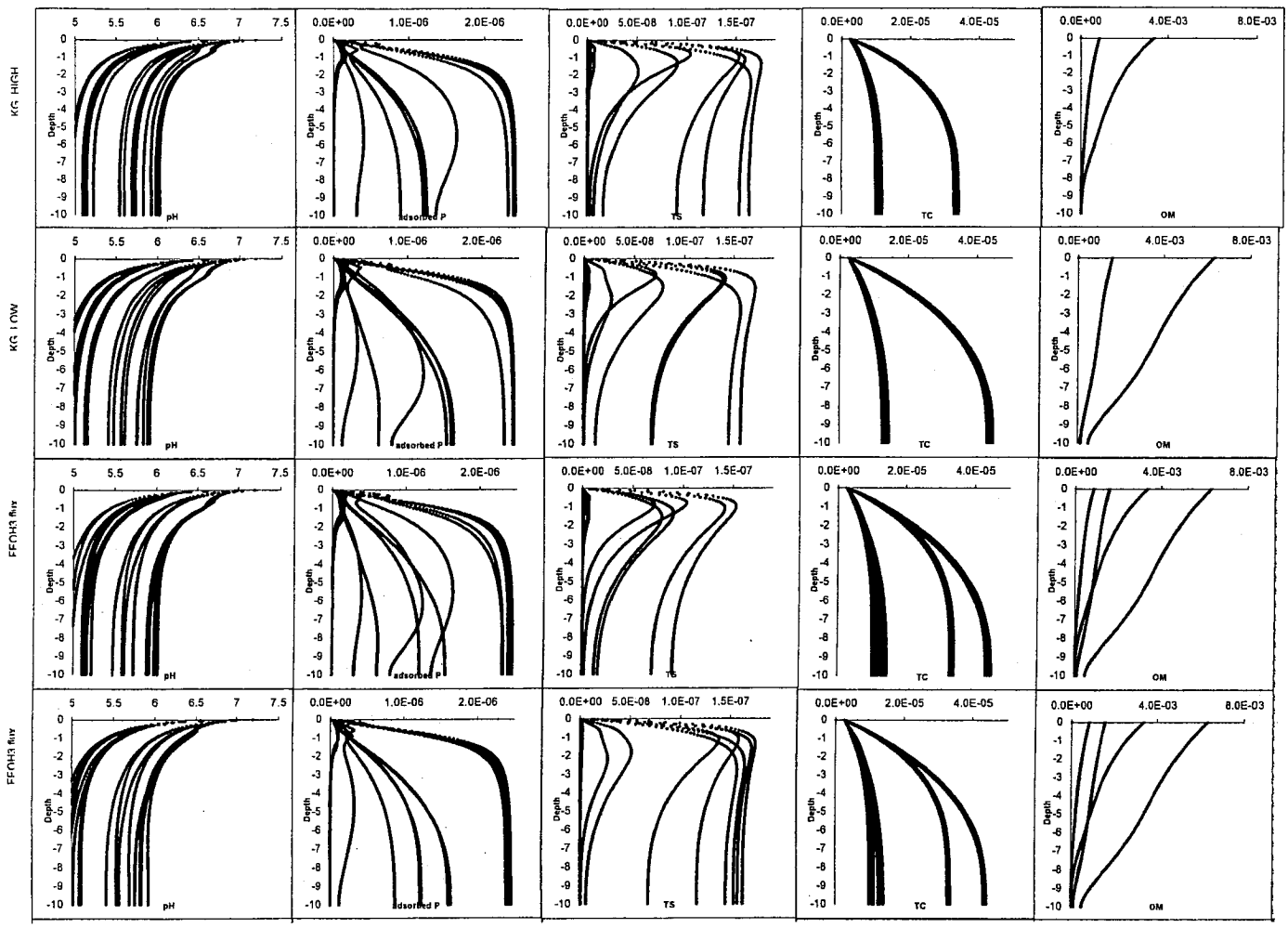
KG HIGH
KG LOW
FEOH3 fix
FEOH3 fix
pH
adsorbed P
TS
TC
OM
Depth

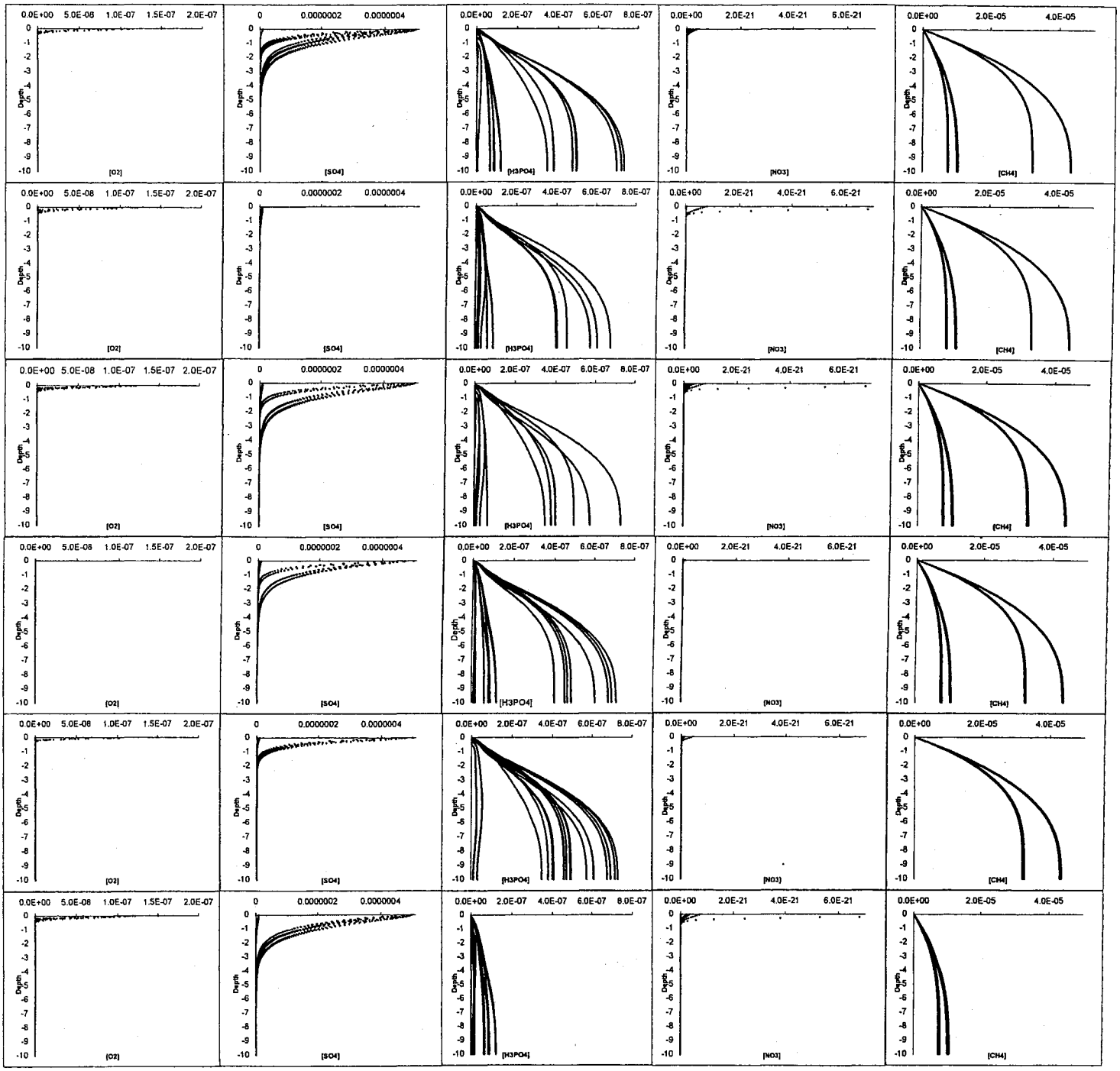
[O2]
[SO4]
[H3PO4]
[NO3]
[CH4]
Depth

DATA 3

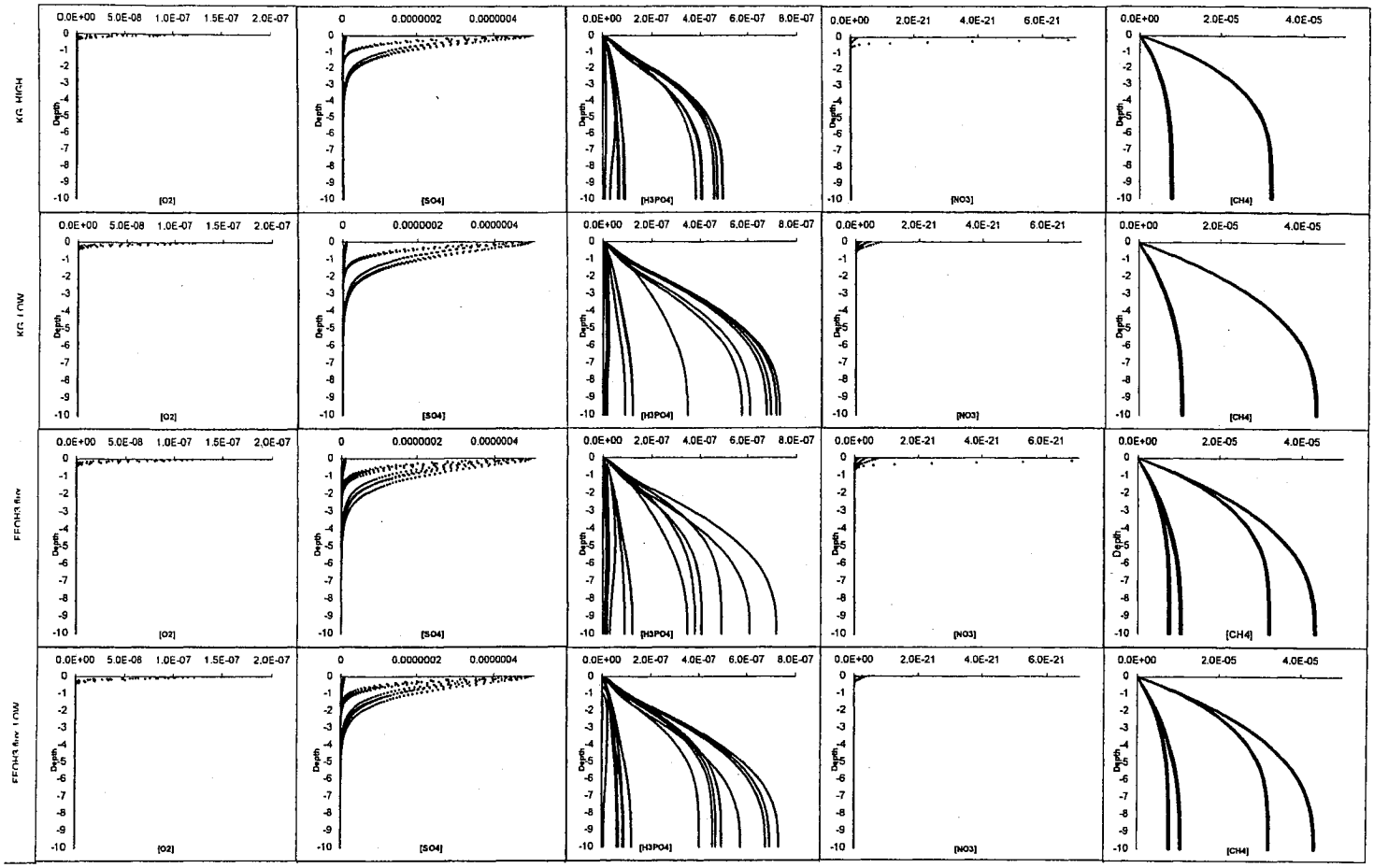
Kz HIGH
Kz LOW
FEHR flux
FEHR flux LOW
Depth
[O2]
[SO4]
[H3PO4]
[NO3]
[CH4]

DATA 4

Iron parameters

Legend: Species:

Designation		Species : { Chemical Formula }
[Fe2+]	–	Aqueous Iron : { $[Fe^{2+}]$ }
FeOH3	–	Iron oxyhydroxide : { $Fe(OH)_3$ }
FeS	–	Iron monosulfide : { FeS }
FeS2	–	Pyrite : { FeS_2 }
Viv	–	Vivianite : { $Fe_2(PO_4)_3$ }
pH	–	Acidity : { $[H^+]$ }
adsorbed P	–	Adsorbed phosphate : { Solid≡P }
TS	–	Total aqueous sulphur: { $[HS^-] + [H_2S]$ }
TC	–	Total aqueous carbon: { $[CO_3^{2-}]+[HCO_3^-]+[H_2CO_3]$ }
OM	–	Organic matter : { CH_2O }
[O2]	–	Oxygen : { O_2 }
[SO4]	–	Dissolvaed Sulfate : { $[SO_4^{2-}]$ }
[H3PO4]	–	Dissolved Phosphate : { $[H_3PO_4]$ }
[NO3]	–	Dissolved Nitrate : { $[NO_3]$ }
[CH4]	–	Dissolved Methane : { $[CH_4]$ }

Parameters:

Name	Description	Low Value	High Value
KFeOnFe	*Adsorption constant for iron on iron oxides*	5.0×10^{-4}	1.0×10^{-2}
KFeOnB	*Adsorption constant for iron on background solids*	5.0×10^{-6}	5.0×10^{-5}
$Fe(OH)_3$ flux	*Flux of iron oxides at the SWI*	1.25×10^{-5} mol cm^2/yr	7.0×10^{-5} mol cm^2/yr
RsFe3	*Dissolution of iron oxide by sulfide*	KsFe3 = 3.0×10^2 $cm^3 mol^{-1} yr^{-1}$	KsFe3= 3.0×10^8 $cm^3 mol^{-1} yr^{-1}$
$[SO_4]$ top	*Concentration of sulfate at the SWI*	1.0×10^{-8} mol cm^{-3}	0.5×10^{-6} mol cm^{-3}
RFeSFe3	*Dissolution of iron oxide by FeS*	KFeSFe3 = 0.0 g $mol^{-1} yr^{-1}$	KFeSFe3=1.0×10^{-4} g $mol^{-1} yr^{-1}$

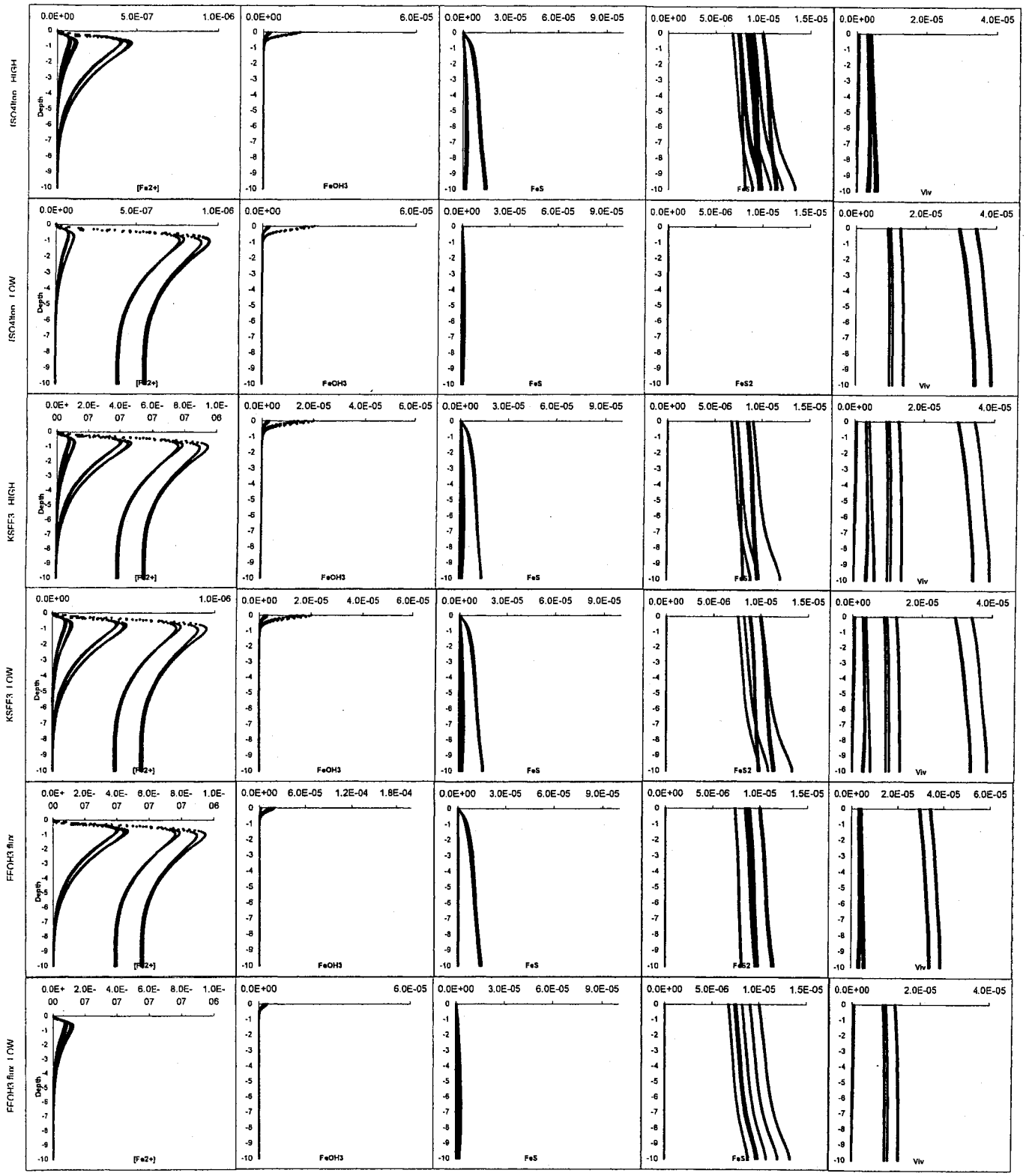
ISOAtion HIGH
ISOAtion LOW
KSFF3 HIGH
KSFF3 LOW
FEOH3 flux
FEOH3 flux LOW
Depth
[Fe2+]
FeOH3
FeS
FeS2
Viv

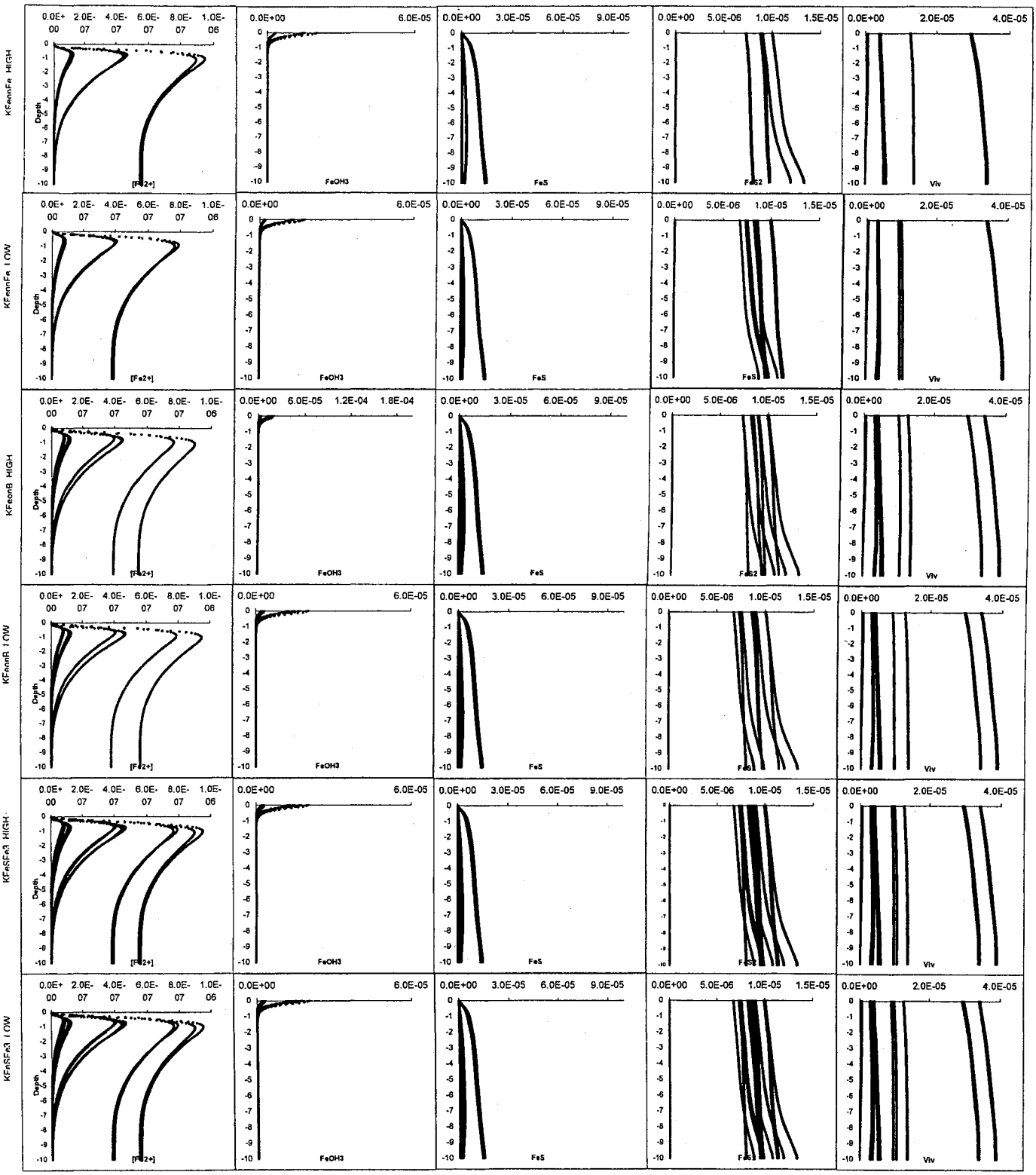
KFeonFe HIGH
KFeonFe LOW
KFeonB HIGH
KFeonB LOW
KFeSFe3 HIGH
KFeSFe3 LOW
Depth
[Fe2+]
FeOH3
FeS
FeS2
Viv

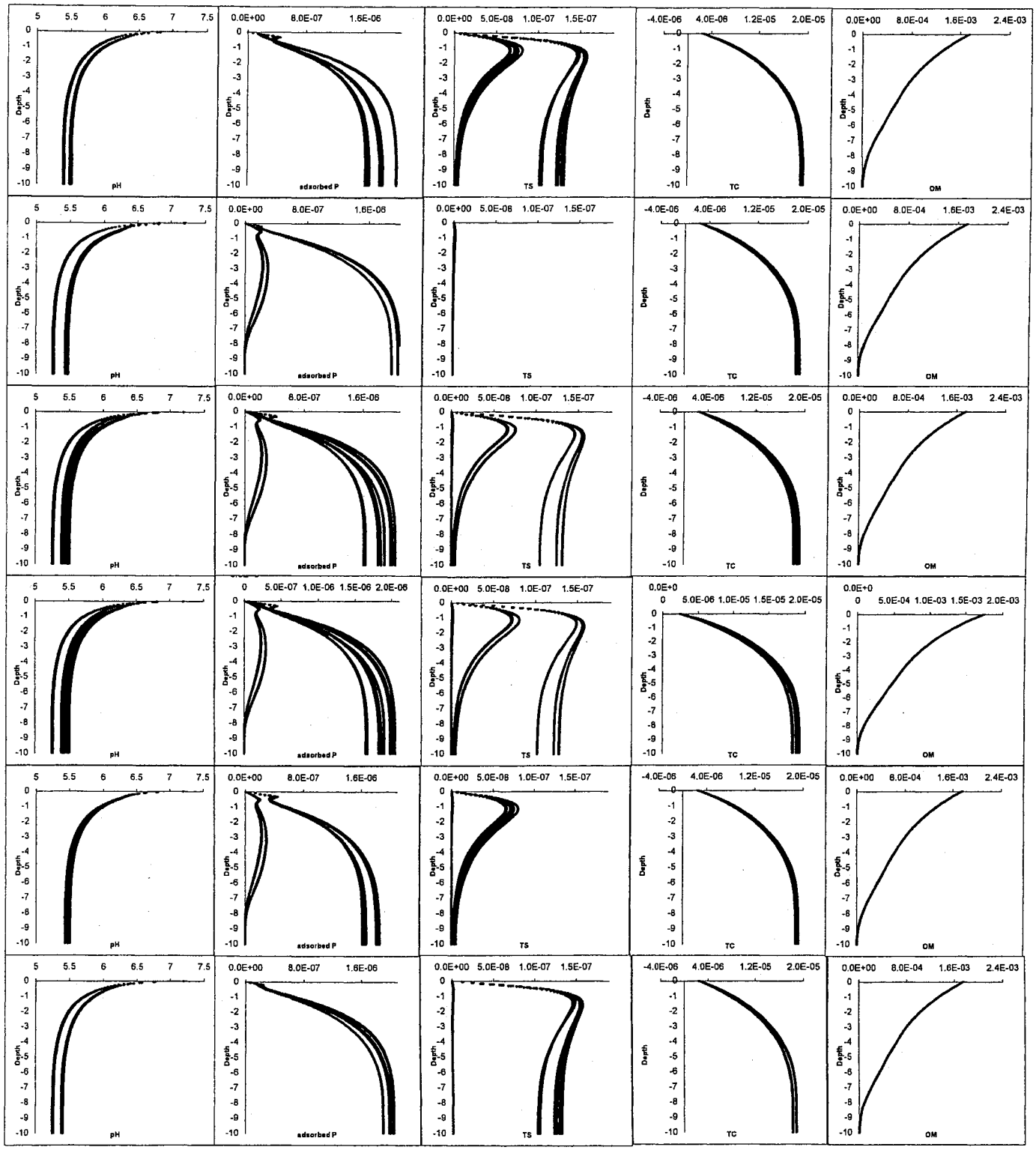
fSO4flnn HIGH
fSO4flnn LOW
KSFF3 HIGH
KSFF3 LOW
FeOH3 flux
FeOH3 flux LOW
pH
adsorbed P
TS
TC
OM
Depth

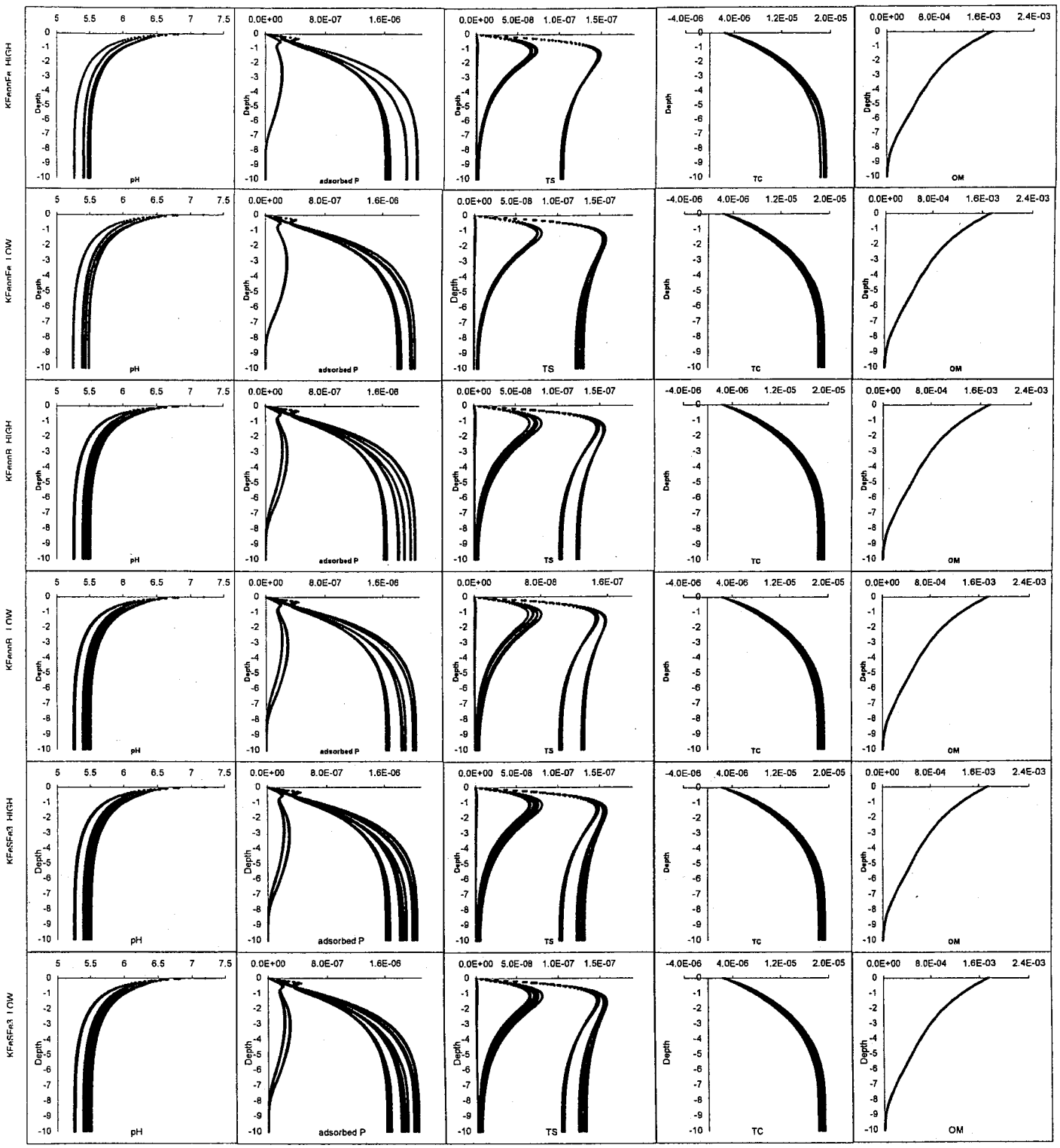
KFeonFe HIGH
KFeonFe LOW
KFeonR HIGH
KFeonR LOW
KFeSFe3 HIGH
KFeSFe3 LOW
pH
adsorbed P
TS
TC
OM
Depth

DATA 4

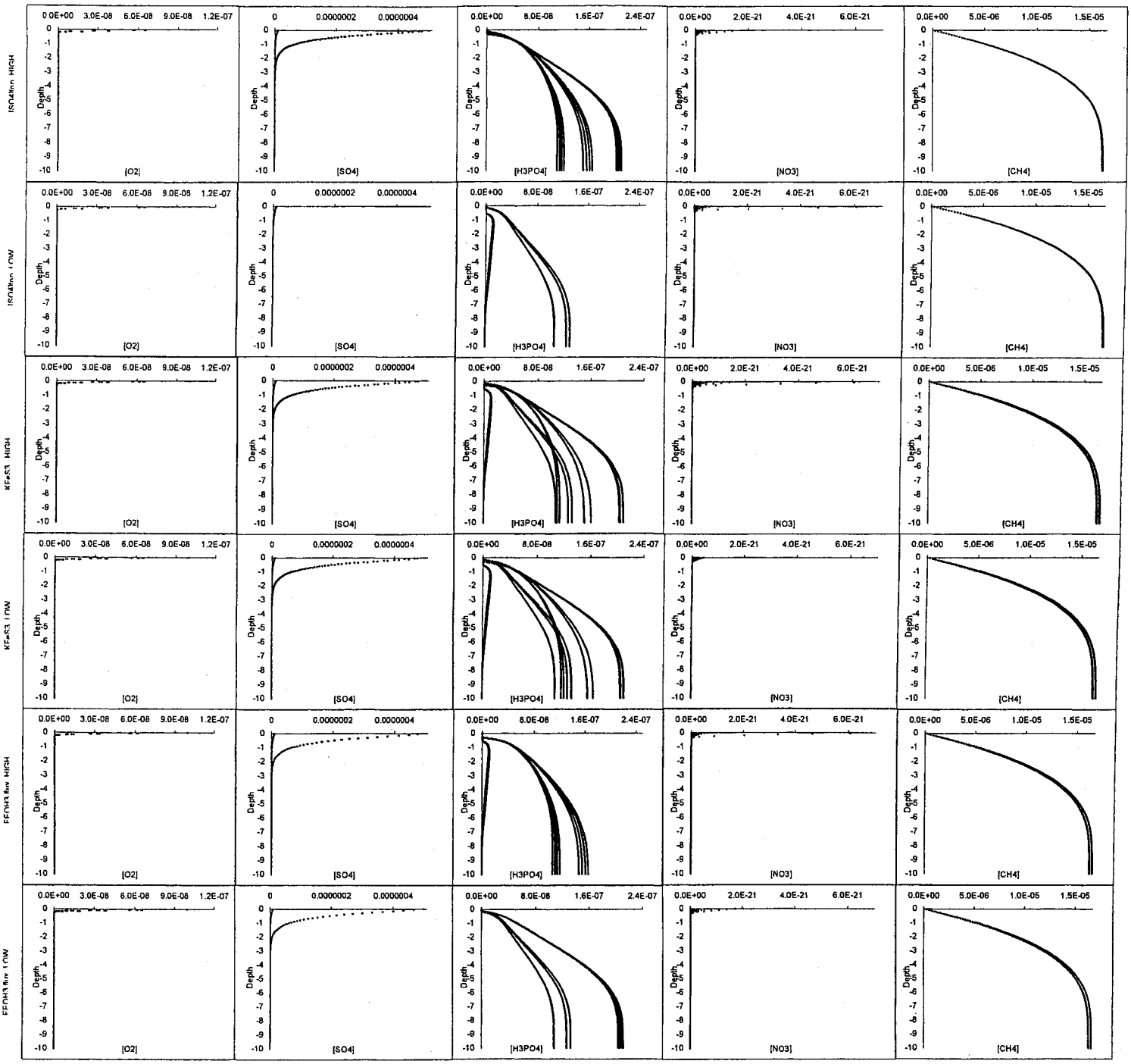

DATA 4

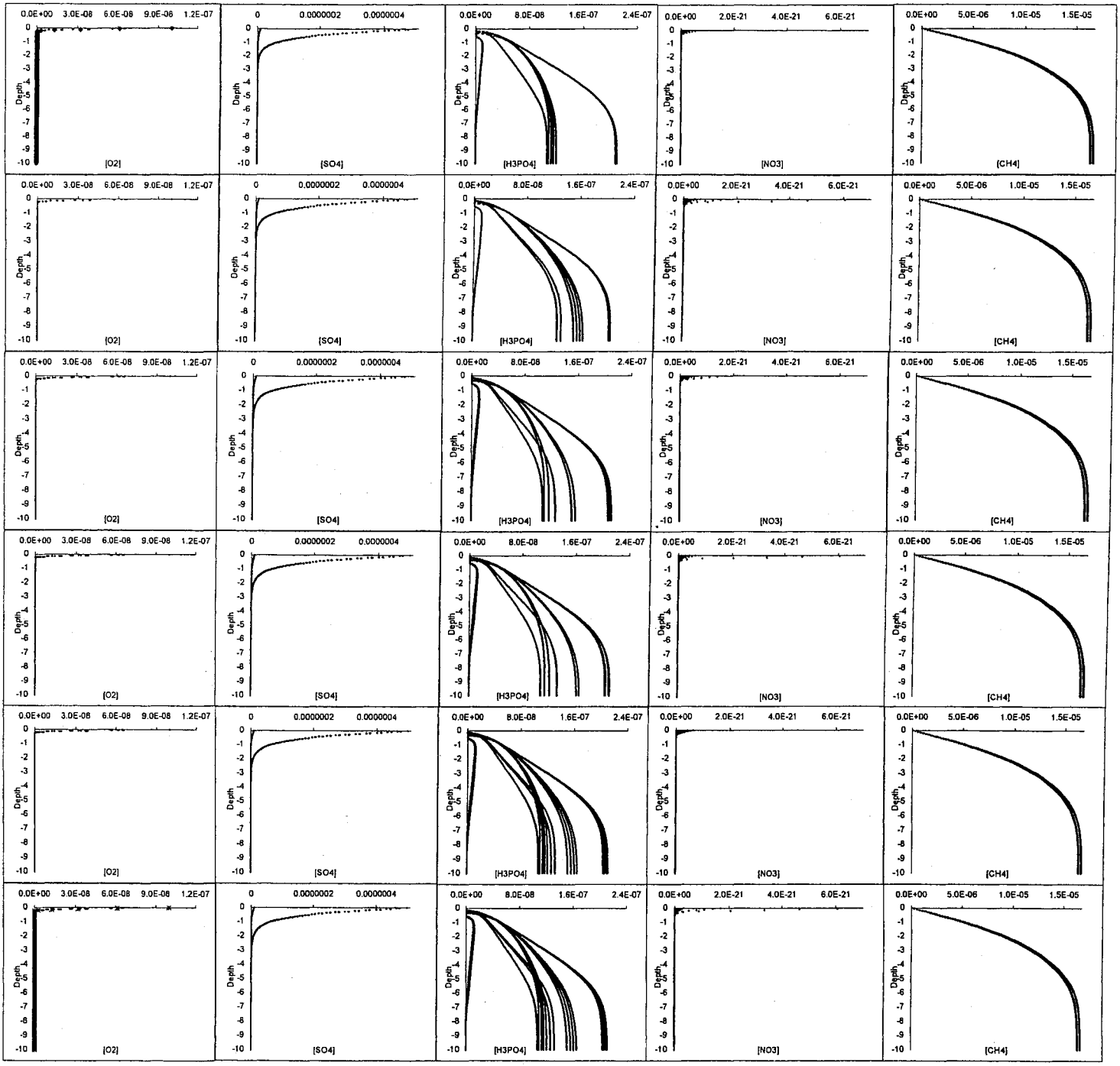
KFeonFe HIGH
KFeonFe LOW
KFeonR HIGH
KFeonR LOW
KFeSFe3 HIGH
KFeSFe3 LOW
[O2]
[SO4]
[H3PO4]
[NO3]
[CH4]
Depth

DATA 5

Phosphate sorption and other parameters

Legend: Species:

Designation		Species : { Chemical Formula }
[Fe2+]	–	Aqueous Iron : { $[Fe^{2+}]$ }
FeOH3	–	Iron oxyhydroxide : { $Fe(OH)_3$ }
FeS	–	Iron monosulfide : { FeS }
FeS2	–	Pyrite : { FeS_2 }
Viv	–	Vivianite : { $Fe_2(PO_4)_3$ }
pH	–	Acidity : { $[H^+]$ }
adsorbed P	–	Adsorbed phosphate : { Solid≡P }
TS	–	Total aqueous sulphur: { $[HS^-] + [H_2S]$ }
TC	–	Total aqueous carbon: { $[CO_3^{2-}]+[HCO_3^-]+[H_2CO_3]$ }
OM	–	Organic matter : { CH_2O }
[O2]	–	Oxygen : { O_2 }
[SO4]	–	Dissolvaed Sulfate : { $[SO_4^{2-}]$ }
[H3PO4]	–	Dissolved Phosphate : { $[H_3PO_4]$ }
[NO3]	–	Dissolved Nitrate : { $[NO_3]$ }
[CH4]	–	Dissolved Methane : { $[CH_4]$ }

Parameters:

Name	Description	Low Value	High Value
KPOnFe	*Adsorption constant for phosphate on iron oxides*	2.0×10^{-2}	1.0×10^{-1}
KPOnB	*Adsorption constant for phosphate on background solids*	5.0×10^{-6}	5.0×10^{-5}
DBcurvature	*Curvature of the bioturbation profile*	0.2	0.5
RFeSHS	*Formation of pyrite*	KFeSHS = 0.0 $cm^3 mol^{-1} yr^{-1}$	KFeSHS=$1.0 \times 10^{10} cm^3 mol^{-1} yr^{-1}$
U	*Sedimentation rate*	0.1 cm yr^{-1}	0.3 cm yr^{-1}
Rviv	*Rate of vivianite formation*	KVIV = 1.0E-10 mol/g·yr	KVIV = 3.0E-9 mol/g·yr

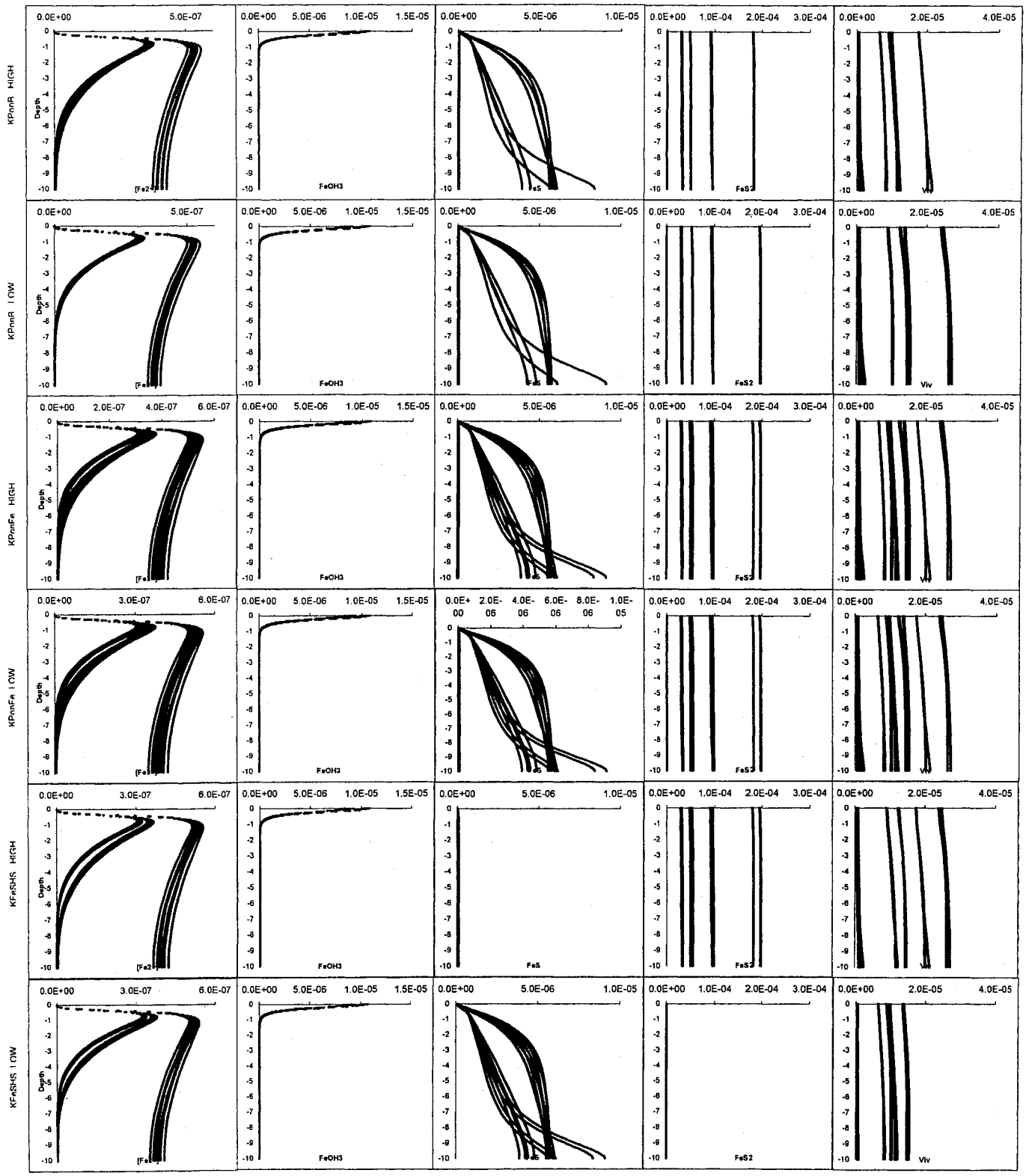
KPmnR HIGH
KPmnR LOW
KPmnFe HIGH
KPmnFe LOW
KFeSHS HIGH
KFeSHS LOW
Depth
FeOH3
FeS
FeS2
Viv

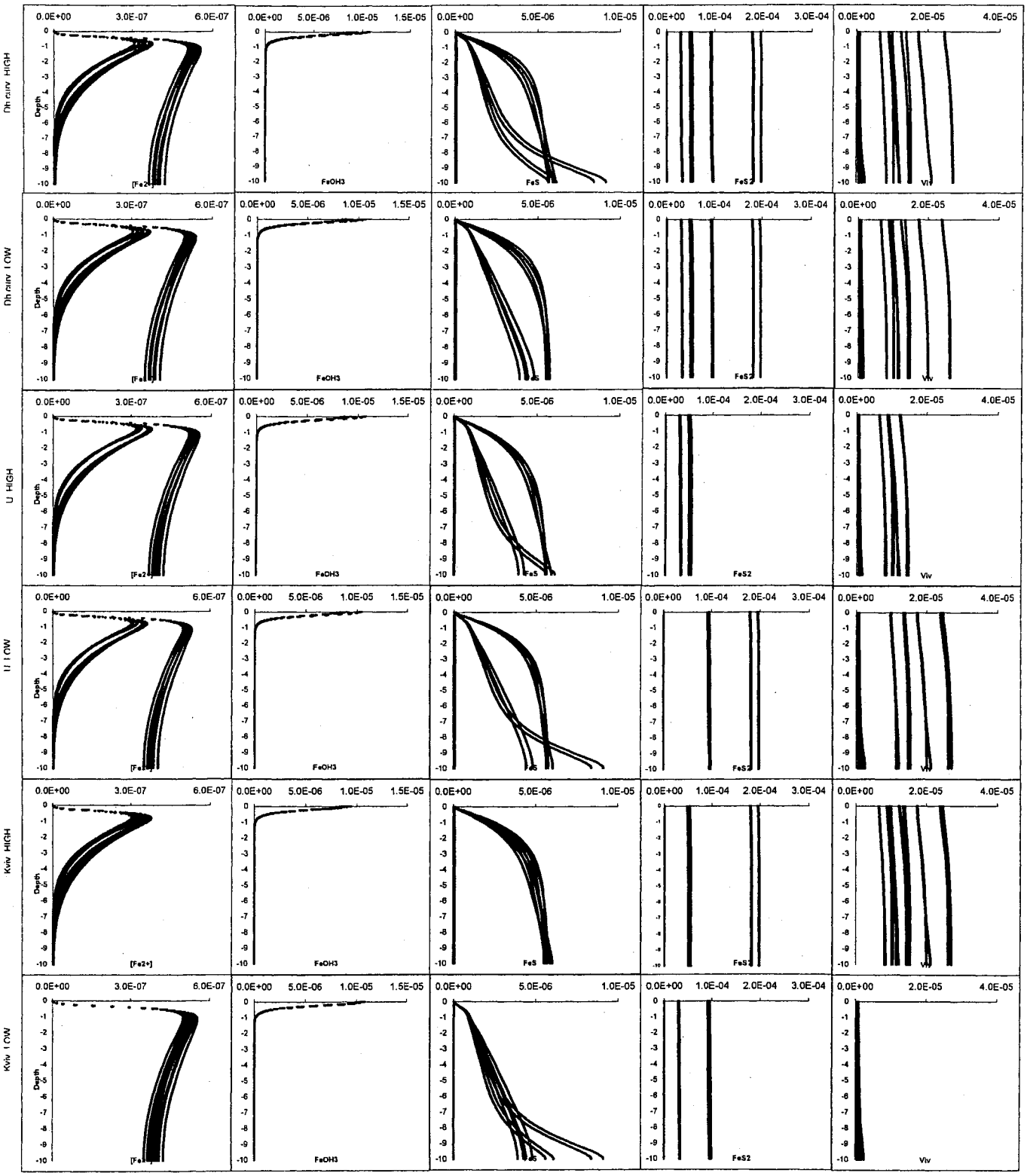
Dh.cav HIGH
Dh.cav LOW
U HIGH
U LOW
Kviv HIGH
Kviv LOW
Depth
[Fe2+]
FeOH3
FeS
FeS2
Viv

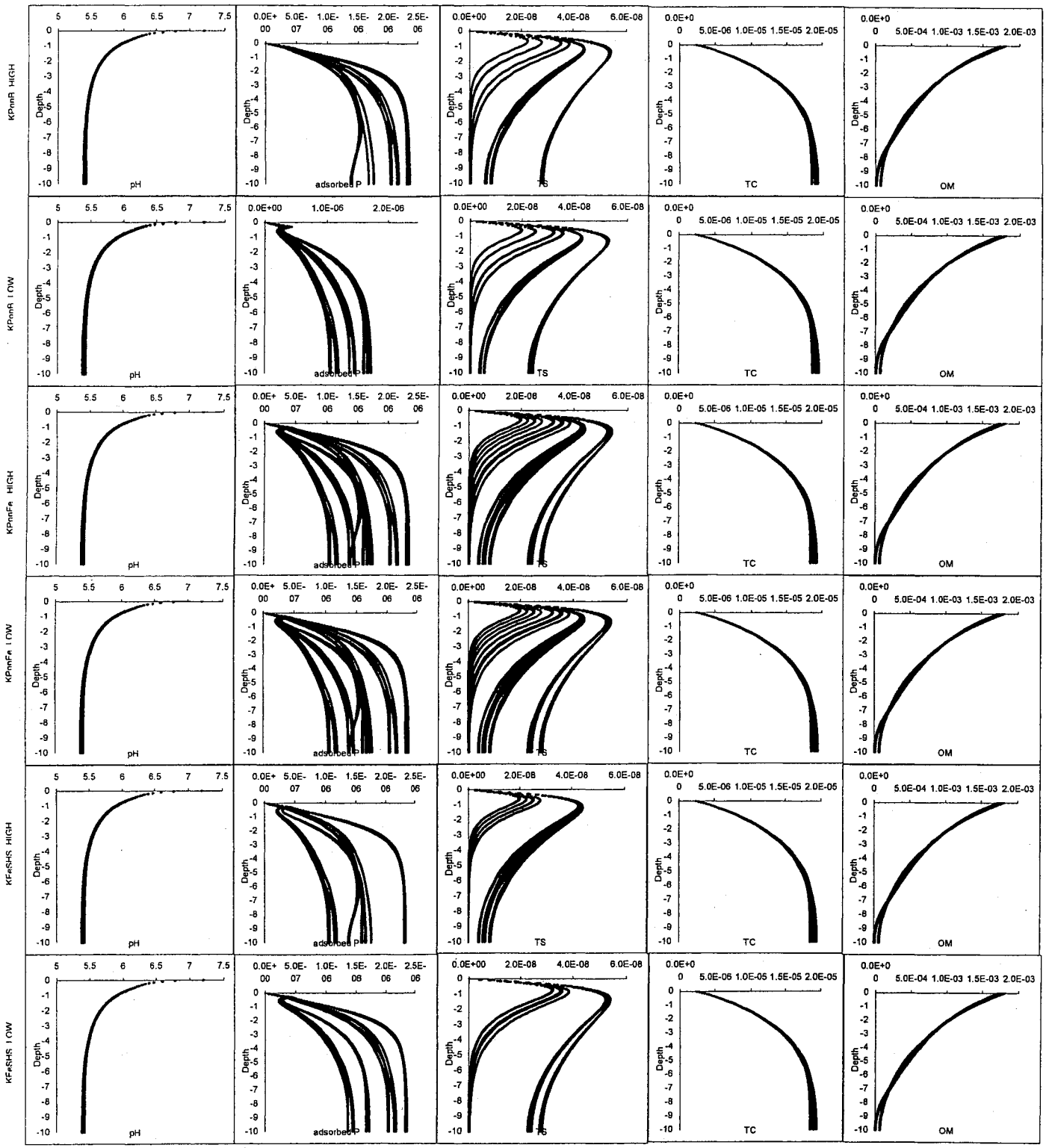
KPnnR HIGH
KPnnR LOW
KPnnFe HIGH
KPnnFe LOW
KFeSHS HIGH
KFeSHS LOW
pH
adsorbed P
TS
TC
OM
Depth

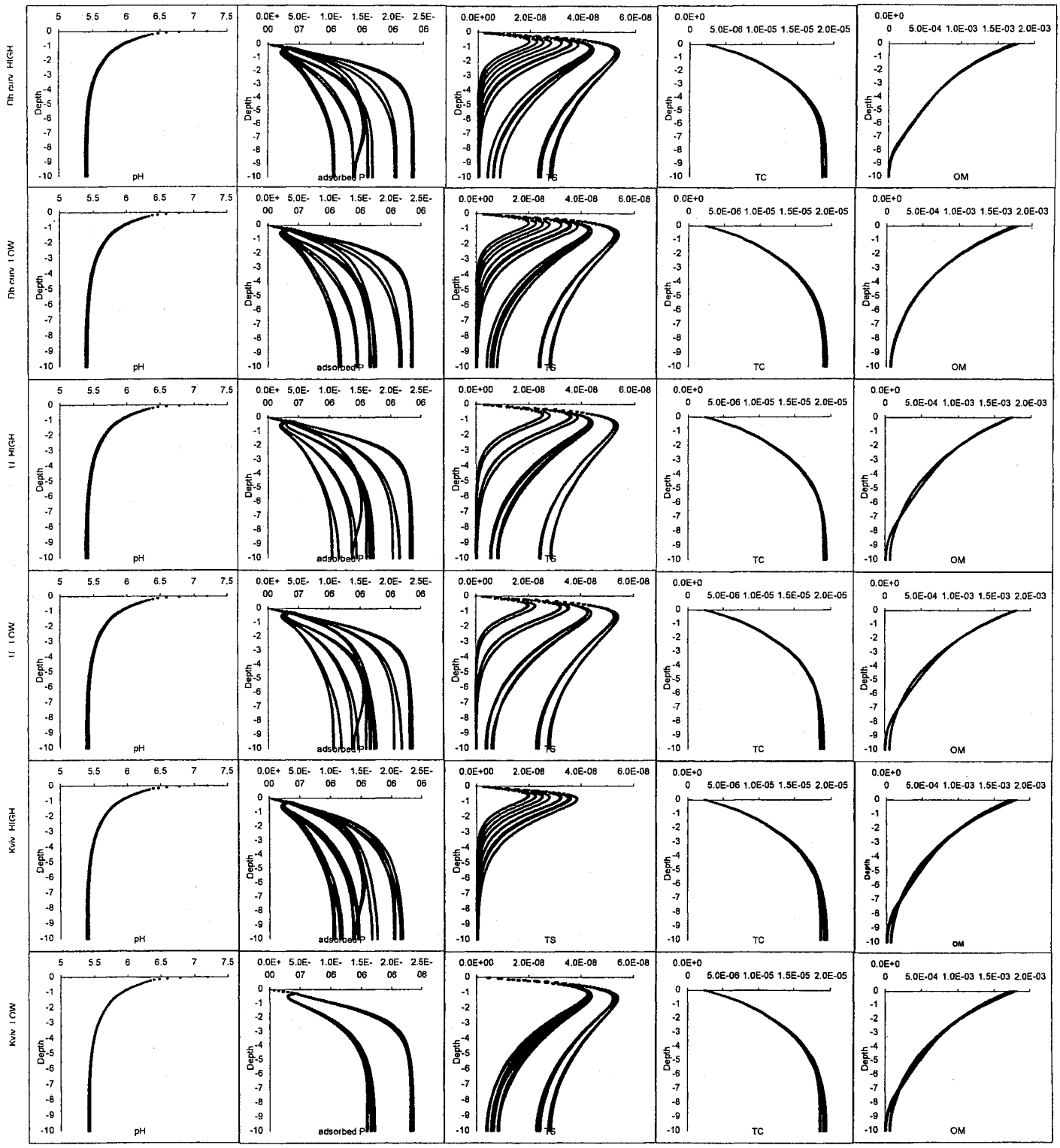
Ph curv HIGH
Ph curv LOW
Kd HIGH
Kd LOW
Kviv HIGH
Kviv LOW
Depth
pH
adsorbed P
TS
TC
OM

DATA 5

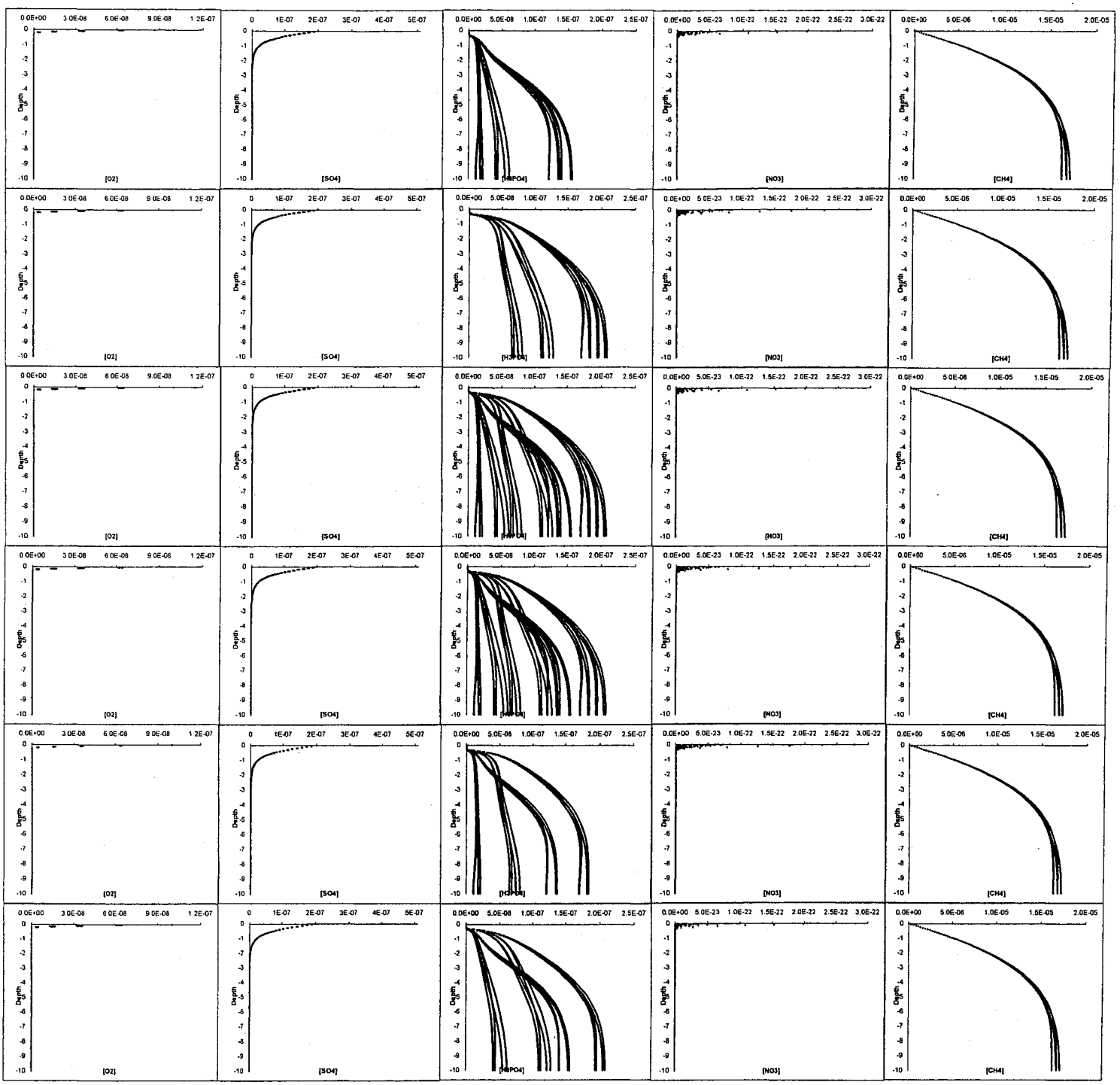
KPmnR HIGH
KPmnR LOW
KPmnFe HIGH
KPmnFe LOW
KFeSHS HIGH
KFeSHS LOW
[O2]
[SO4]
[H3PO4]
[NO3]
[CH4]
Depth

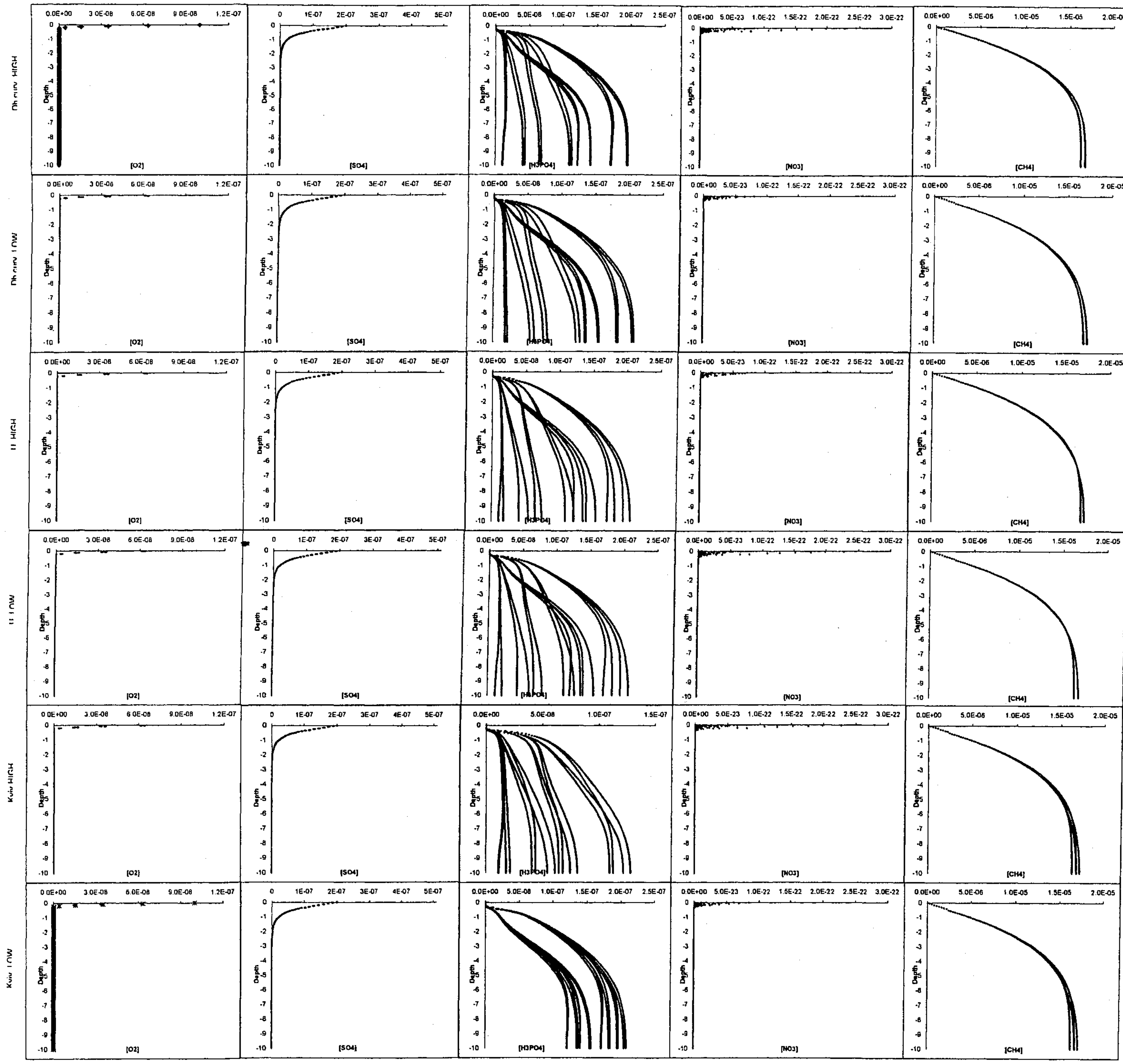
[O2]
[SO4]
[H3PO4]
[NO3]
[CH4]
Depth
0.0E+00 3.0E-08 6.0E-08 9.0E-08 1.2E-07
0 1E-07 2E-07 3E-07 4E-07 5E-07
0.0E+00 5.0E-08 1.0E-07 1.5E-07 2.0E-07 2.5E-07
0.0E+00 5.0E-23 1.0E-22 1.5E-22 2.0E-22 2.5E-22 3.0E-22
0.0E+00 5.0E-06 1.0E-05 1.5E-05 2.0E-05

DATA 6

Remaining parameters

Legend: Species:

Designation		Species : { Chemical Formula }
[Fe2+]	–	Aqueous Iron : { $[Fe^{2+}]$ }
FeOH3	–	Iron oxyhydroxide : { $Fe(OH)_3$ }
FeS	–	Iron monosulfide : { FeS }
FeS2	–	Pyrite : { FeS_2 }
Viv	–	Vivianite : { $Fe_2(PO_4)_3$ }
pH	–	Acidity : { $[H^+]$ }
adsorbed P	–	Adsorbed phosphate : { Solid≡P }
TS	–	Total aqueous sulphur: { $[HS^-] + [H_2S]$ }
TC	–	Total aqueous carbon: { $[CO_3^{2-}]+[HCO_3^-]+[H_2CO_3]$ }
OM	–	Organic matter : { CH_2O }
[O2]	–	Oxygen : { O_2 }
[SO4]	–	Dissolvaed Sulfate : { $[SO_4^{2-}]$ }
[H3PO4]	–	Dissolved Phosphate : { $[H_3PO_4]$ }
[NO3]	–	Dissolved Nitrate : { $[NO_3]$ }
[CH4]	–	Dissolved Methane : { $[CH_4]$ }

Parameters:

Name	Description	Low Value	High Value
KFeSHS	*Formation of pyrite*	0.0 $cm^3mol^{-1}yr^{-1}$	1.0E10 $cm^3mol^{-1}yr^{-1}$
DBmax	*Maximum of the bioturbation profile*	1.0 cm^2yr^{-1}	10.0 cm^2yr^{-1}
$[O_2]$ top	*Concentration of oxygen at the SWI*	0.0 mol cm^{-3}	1.5E-7 mol cm^{-3}
U	*Sedimentation rate*	0.1 cm yr^{-1}	0.3 cm yr^{-1}
Rviv	*Rate of vivianite formation*	KVIV = 1.0D-10 mol/g·yr	KVIV = 3.0D-9 mol/g·yr

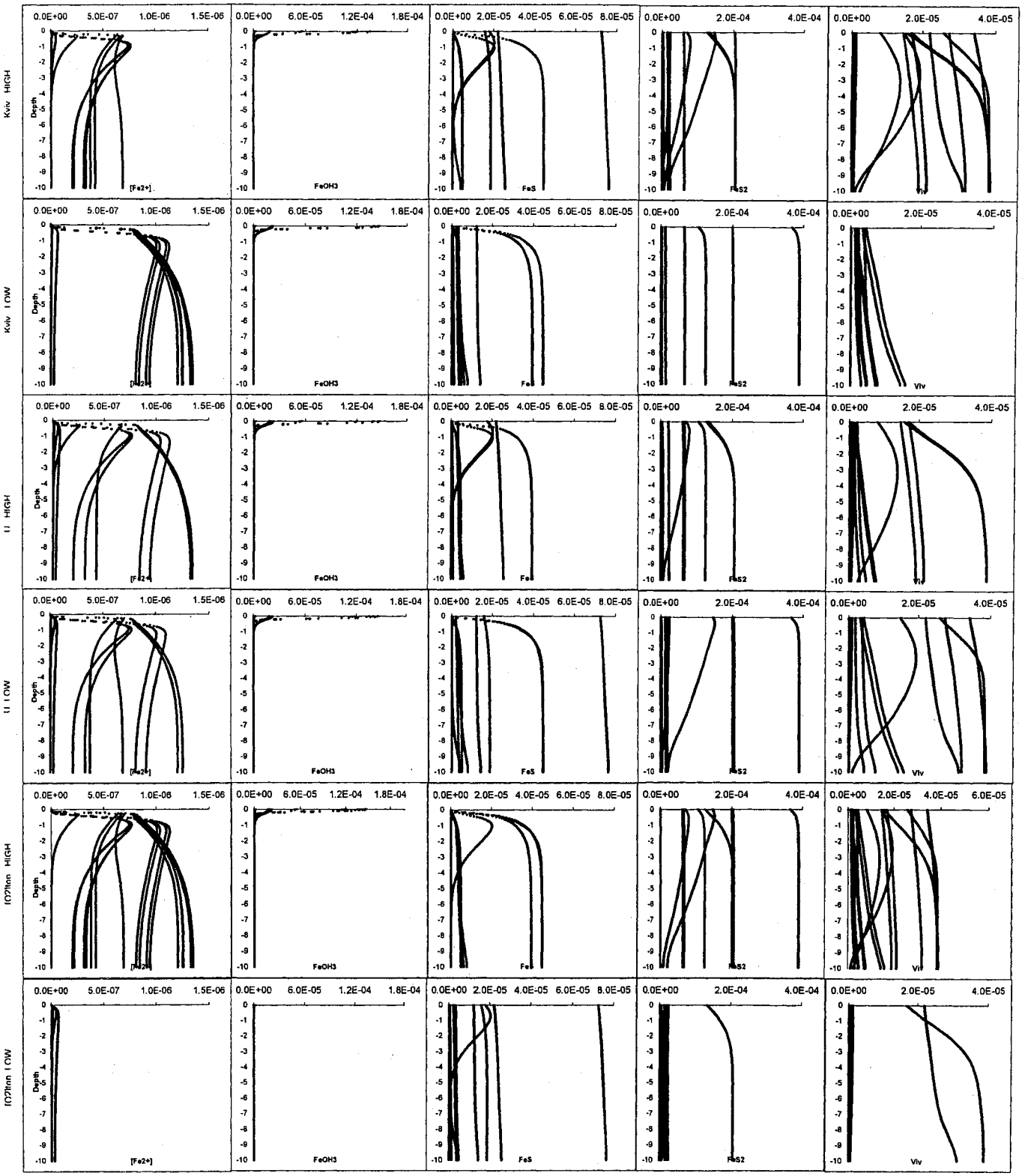
Kviv HIGH
Kviv LOW
O2flux HIGH
O2flux LOW
[Fe2+]
FeOH3
FeS
FeS2
Viv
Depth

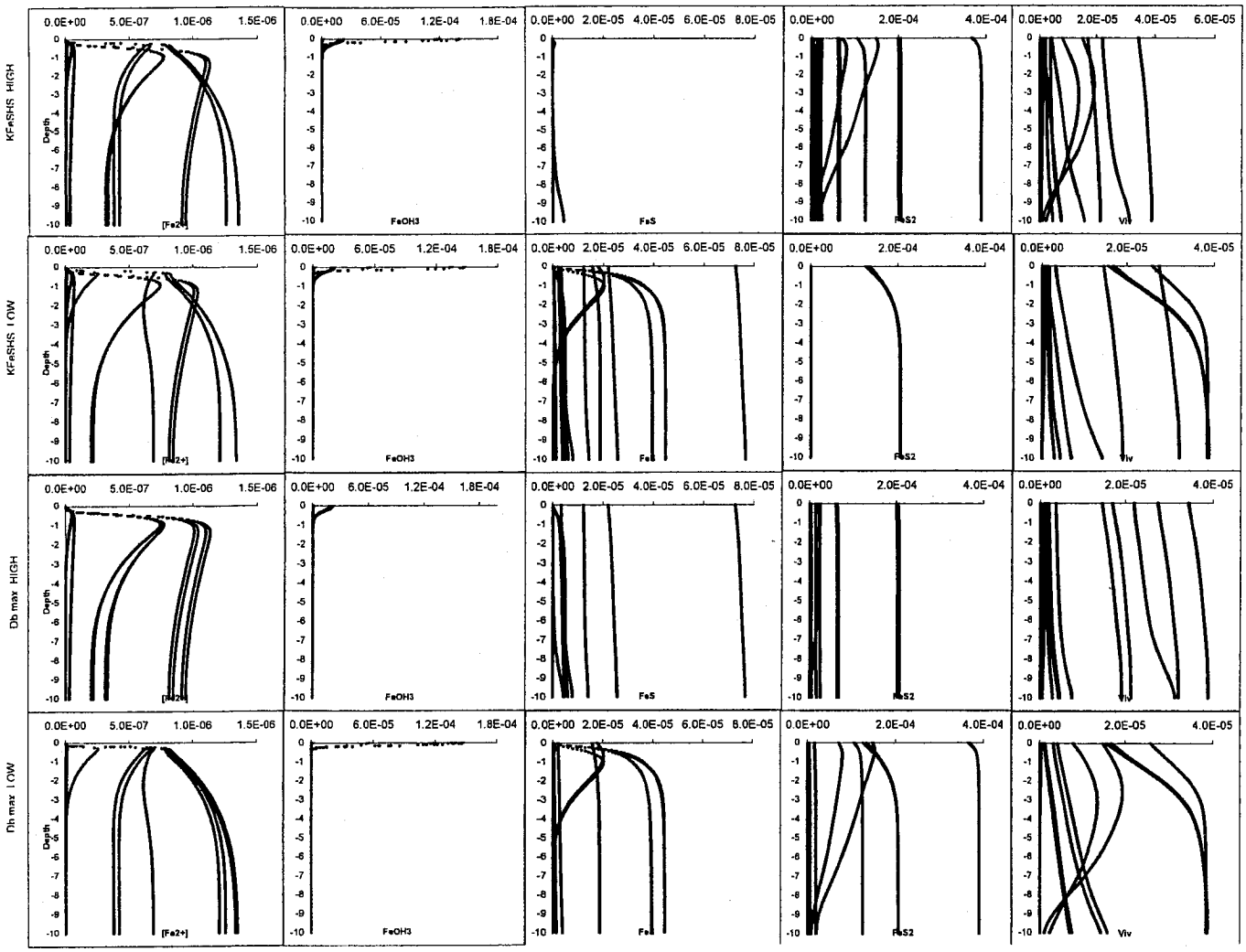
KFeSHS HIGH
KFeSHS LOW
Db max HIGH
Db max LOW
Depth
[Fe2+]
FeOH3
FeS
FeS2
Viv
0.0E+00
5.0E-07
1.0E-06
1.5E-06
6.0E-05
1.2E-04
1.8E-04
2.0E-05
4.0E-05
6.0E-05
8.0E-05
2.0E-04
4.0E-04

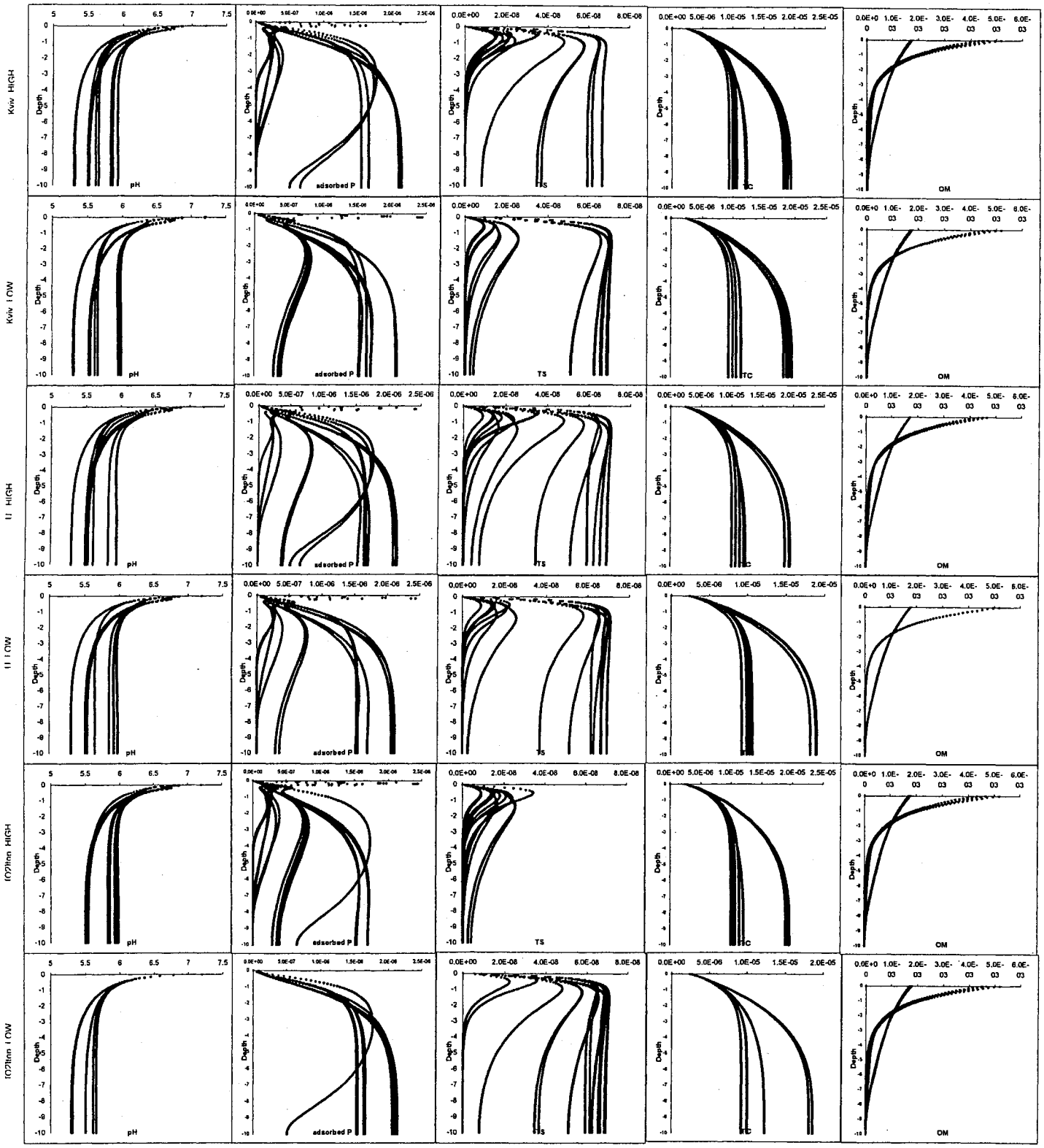
Kviv HIGH
Kviv LOW
II HIGH
II LOW
Poltava HIGH
Poltava LOW
pH
adsorbed P
TS
TC
OM
Depth

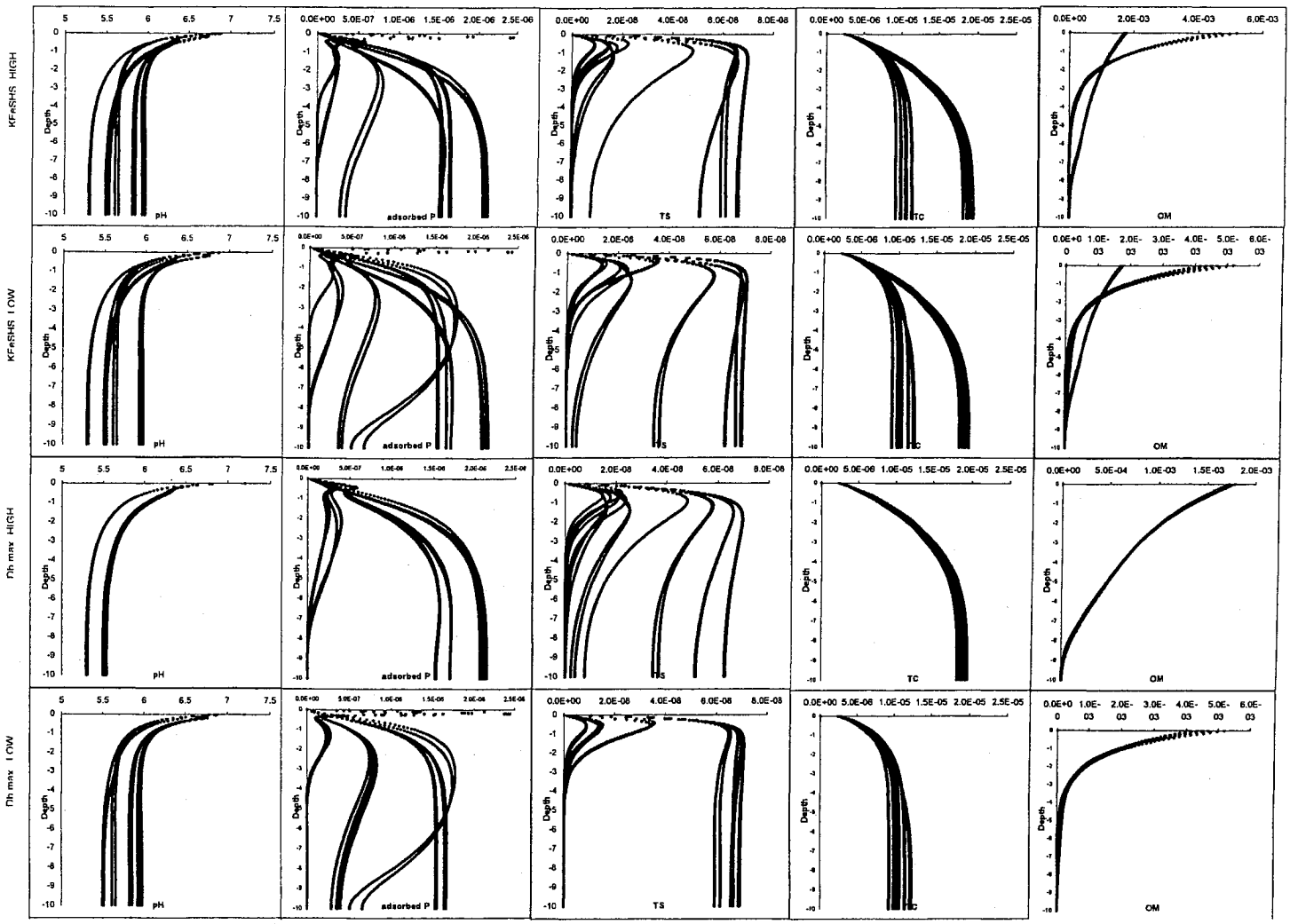
KFeSHS HIGH
KFeSHS LOW
Dh max HIGH
Dh max LOW
pH
adsorbed P
TS
TC
OM
Depth

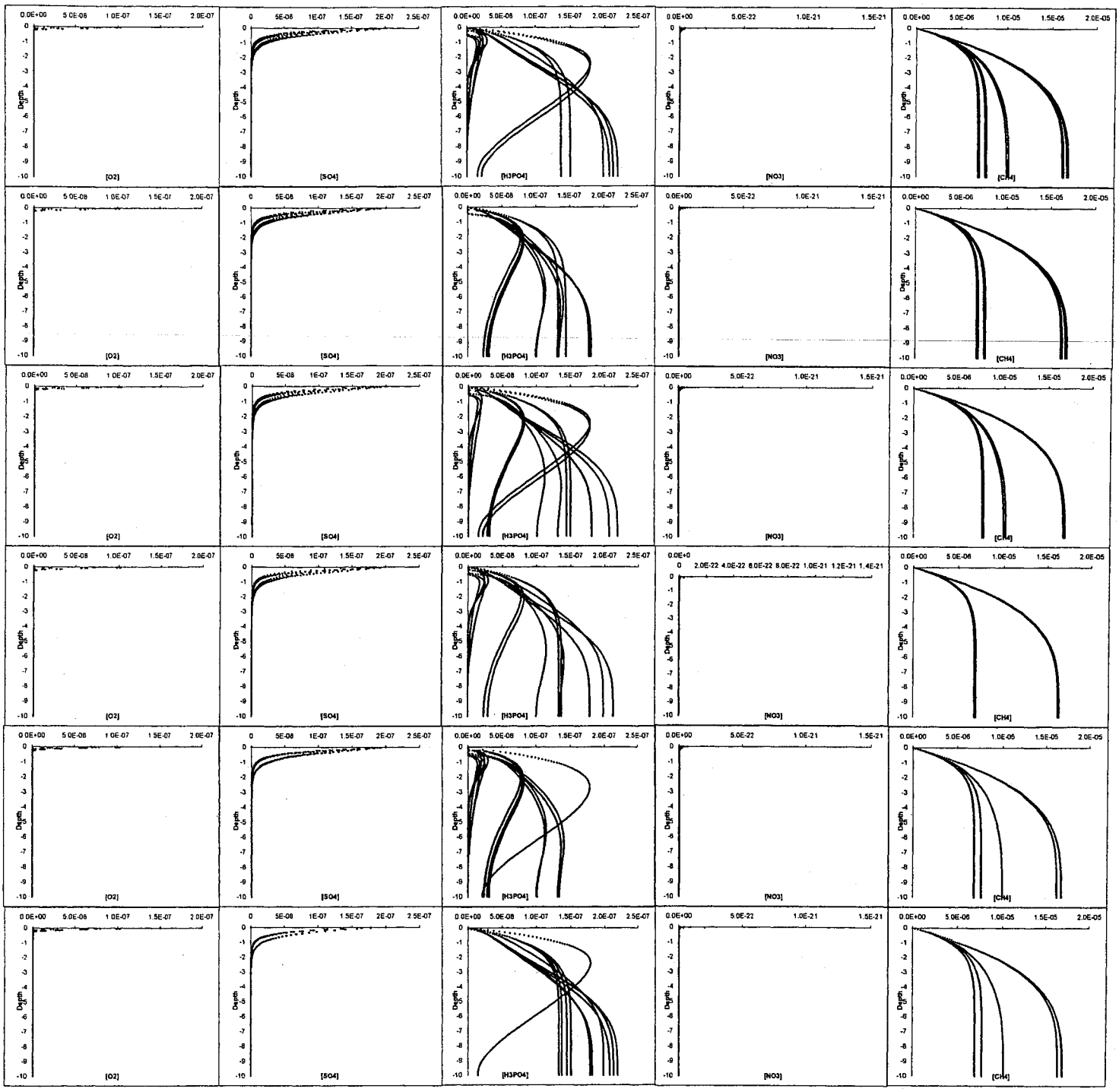
Kviv HIGH
Kviv LOW
U HIGH
U LOW
[O2]top HIGH
[O2]top LOW
Depth
[O2]
[SO4]
[H3PO4]
[NO3]
[CH4]

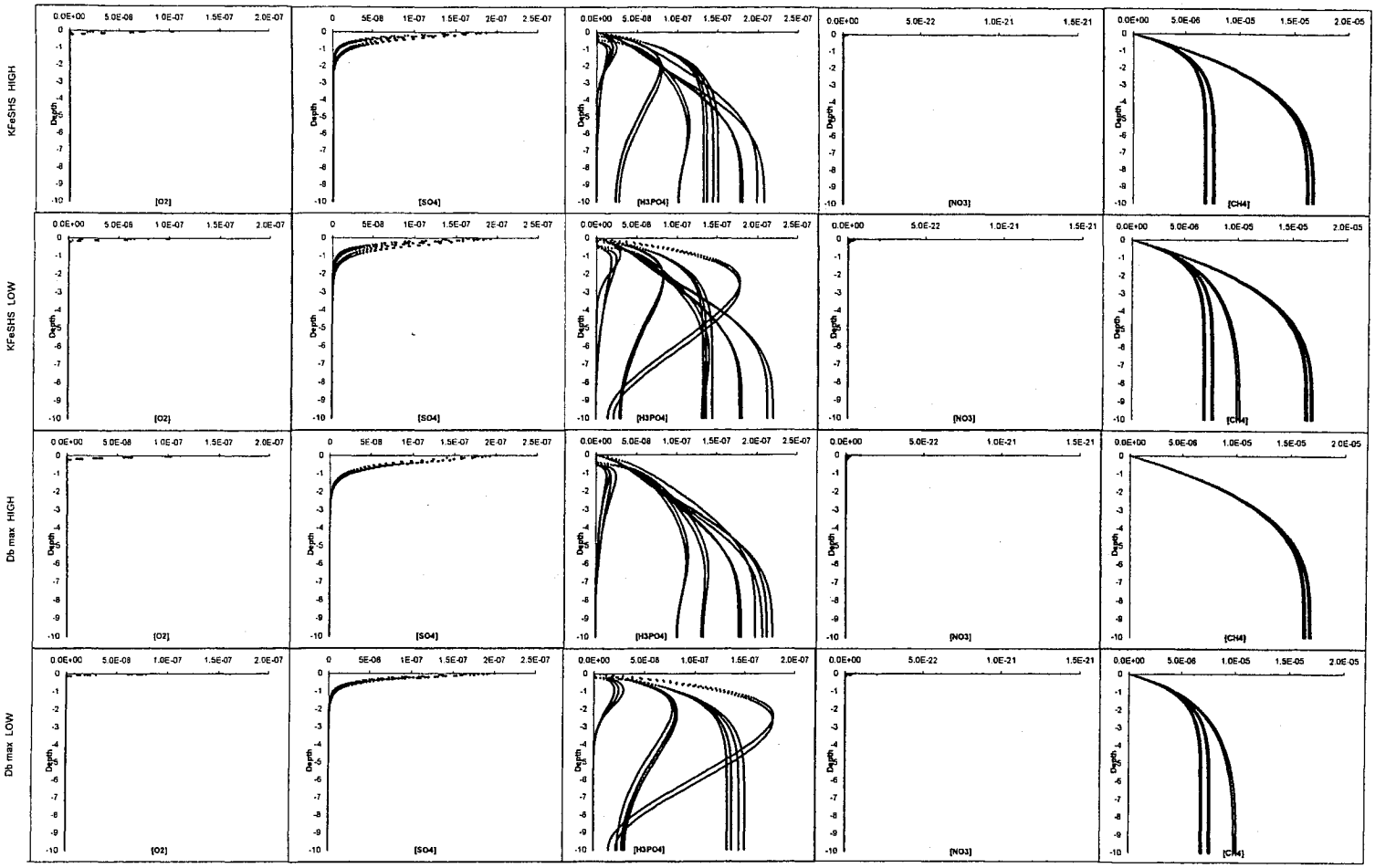
KFeSHS HIGH
KFeSHS LOW
Db max HIGH
Db max LOW
[O2]
[SO4]
[H3PO4]
[NO3]
[CH4]
Depth